Sorbonne Université

Ecole doctorale 515 Complexité du Vivant

UMR 8227 (SU – CNRS) Laboratoire de Biologie Intégrative des Modèles Marins /

Equipe de recherche « Morphogenesis of Macroalgae »

Biophysical and cellular mechanisms of tip-growth in the brown alga *Ectocarpus sp*.

Par Hervé Rabillé

Thèse de doctorat de Biologie

Dirigée par Dr. Bénédicte Charrier

Présentée et soutenue publiquement le 3 décembre 2018

Devant un jury composé de :

M. Arezki Boudaoud, Professeur de l'ENS de Lyon, France : Rapporteur

Mme. Siobhan Braybrook, Project Investigator at the University California Los Angeles, USA : Rapporteuse

M. Benedikt Kost, Professeur de l'Université Friedrich Alexander Universität, Erlangen, Allemagne : Examinateur

M. Bernard Kloareg, Professeur de Sorbonne Université de Paris, France : Examinateur

Mme Bénédicte Charrier, Directrice de Recherche CNRS : Directrice de thèse

Except where otherwise noted, this work is licensed under
http://creativecommons.org/licenses/by-nc-nd/3.0/

Sorbonne Université

Ecole doctorale 515 Complexité du Vivant

UMR 8227 (SU – CNRS) Laboratoire de Biologie Intégrative des Modèles Marins /

Equipe de recherche « Morphogenesis of Macroalgae »

Biophysical and cellular mechanisms of tip-growth in the brown alga *Ectocarpus sp*.

Par Hervé Rabillé

Thèse de doctorat de Biologie

Dirigée par Dr. Bénédicte Charrier

Présentée et soutenue publiquement le 3 décembre 2018

Devant un jury composé de :

M. Arezki Boudaoud, Professeur de l'ENS de Lyon, France : Rapporteur

Mme. Siobhan Braybrook, Project Investigator at the University California Los Angeles, USA : Rapporteuse

M. Benedikt Kost, Professeur de l'Université Friedrich Alexander Universität, Erlangen, Allemagne : Examinateur

M. Bernard Kloareg, Professeur de Sorbonne Université de Paris, France : Examinateur

Mme Bénédicte Charrier, Directrice de Recherche CNRS : Directrice de thèse

Except where otherwise noted, this work is licensed under
http://creativecommons.org/licenses/by-nc-nd/3.0/

Preamble

Contribution

This thesis project is by no means the only product of my own work, but is instead the fruit of the collective work of many people. The contribution of each is detailed below. At first, the project has involved the effort of all the members of the Morphogenesis of MacroAlgae research team. **Dr Bénédicte Charrier**, researcher in plant biology, performed a substantial part of the cytology experiments and data analysis. **Dr Bernard Billoud**, lecturer in bioinformatics, contributed to the analysis of some quantitative data and carried out all the computational work related to the mechanical modelling of *Ectocarpus* tip-growth. **Élodie Rolland**, research technician in tissue culture, performed most of the algae cultivation tasks, especially the preparation of the parthenosporophytes of *Ectocarpus* grown on glass coverslips, which were essential for most of the experiments.

The staining of the actin cytoskeleton using the phalloidin-based probe has been performed in collaboration with **Pr. Christos Katsaros** and his PhD student **Maria Koutalianou**, both from the National and Kapodistrian University of Athens (Greece).

Actin and tubulin immunolocalisation experiments have been carried out with **Dr. Adeel Nasir** (Friedrich Alexander Universität, Erlangen-Nurnberg, Germany), who supplied us with an alternative protocol for cytoskeleton staining during a short visit.

All the observations of cell ultrastructure by Transmission Electronic Microscopy (TEM) have been conducted by **Dr. Sophie Le Panse**, from the “MerImage” microscopy plateform at the Roscoff Marine Biology Station.

The AFM data that are briefly presented and discussed in this report have been acquired by **Benoit Tesson** (Scripps Institution of Oceanography, University of California, San Diego, USA).

The identification of the causal mutation in the mutant *étoile* (*etl*) and the bioinformatic analysis (with the help of **B. Billoud**) of the candidate *ETOILE* gene which is briefly discussed in this report, is mostly the work of **Zofia Nehr** (former PhD student in the team). I performed the final completion of her substantial work with the help of the L2 student **Quentin Rochas**, whom I supervised.

Finally, the results presented on the effect of drugs depolymerizing the cytoskeleton on the growth and morphogenesis of the apical cell were from time-lapse pictures of *Ectocarpus* filaments grown by **Carole Duchêne**, a former L3 internship in our team.

Articles

The **Part 1** (Introduction section) of the report contains a large chapter reviewing the biomechanical models of tip-growth across the tree of life. It will be submitted as a review for an annual series or a book (Rabillé & Charrier, in preparation). The **Part 1** also comprises an Opinion paper discussing the extent to which the cell wall composition and its intrinsic mechanics impact growth (Charrier, Rabillé & Billoud, in press in Trends in Plant Science).

The **Part 2 deals with** the biomechanics of tip-growth and of the cell wall. It contains two Original Research papers. The first article (**Part 2.1**) presents a visco-elastic model accounting for the tip growth in *Ectocarpus*, highlighting the role of the cell wall thickness

(Rabillé et al., in revision in *PLoS Biology*). The second one (**Part 2.2**) reports the role of alginates in the mechanics of the cell wall along the filament of *Ectocarpus* (Rabillé et al., in preparation).

Acknowledgements

First I must thank the two organisms that have funded my PhD: **The Presidency of the former Université Pierre and Marie Curie** (now fused with Sorbonne Université) and the **Brittany Region**. I am also indebted to the Phycomorph Network (EC funded COST Action FA1406) for having funding my Short-Term Scientific Mission from the 12th to the 29th of October, 2016, in the laboratory of Pr. Christos Katsaros (see below).

I thank warmly **Dr Bénédicte Charrier**, head of the Morphogenesis of MacroAlgae (MMA) team and my PhD supervisor, for having given me the opportunity to do work on such an exciting research project, at the very forefront of the current knowledge in cellular and developmental biology. Thank also you a lot for all the time you have dedicated to supervising my thesis, for all the (often very long) theoretical discussions about the mechanisms of cell growth, and especially on wall expansion mechanisms, the very hot topic that repeatedly came at the center of our thoughts in the course of these three years. Also, thank you for founding the very last weeks of this thesis project.

In the same vein, I have to thank you a lot, **Dr Bernard Billoud**, for your dedication into the project, and for the HUGE work for the numerical modelling of *Ectocarpus* tip-growth. Thank you also for, again, all the theoretical discussions mentioned above, and for you many informed, enlightened, and often stated loud and clear, points of view on the numerous hot technical and theoretical issues this research project has given rise to. More generally, I would like to tell all my gratitude to both **B. Charrier** and **B. Billoud**, for the overwhelming work that was the redaction and formatting of the two original papers which drafts are included in this report, in which I have only played a small part.

I also would like to thank **Dr Catherine Boyen** for having funded one extra month and a half of my thesis, that have allowed me to have time to write my report (extra time that I have largely abused).

I would also like to thanks all the member of my thesis committee, for their GREAT patience and indulgence (my apologies, again, for the almost 2 hours' lateness at the second meeting, and my complete lack of professionalism), for their interest in the project and their kind pieces of advice. So thanks to **Pr Bruno De Reviers**, **Dr Hayat Bouteau**, **Dr Thierry Comtet**. Thank also to **Dr Arezki Boudaoud** and **Dr. B. Billoud** for attending the first meeting in February 2017.

I thank also all the members of my thesis comitee, that have kindly accepted to attend and evaluate my future thesis defence, that is to take place on the 3rd of December 2018. So thank you **Dr Siobhan Braybrook**, **Dr Arezki Boudaoud**, **Dr Bernard Kloareg** and **Dr Benedikt Kost**. Many thanks especially for two former for tackling the task of evaluating this huge report.

Here and now, I would like to thanks all the other people that have got involved in the thesis project, and without whom nothing, or so few, would have been possible. First I would like to thanks **Élodie Rolland**, research technician in the team, for preparing loads of *Ectocarpus* cultures necessary for virtually all the experiments. Also thanks a lot to **Dr Sophie Le Panse** for the massive TEM work. Thank a lot to **Pr Christos Katsaros** and to (future Dr) **Maria Koutalianou**, for your dedication and help with the actin fluorescent staining. Also thank you very much, **Dr Adeel Nasir**, for your charitable help with actin staining, and providing us with some very good complementary results regarding this delicate. I have also to thanks to the two internship students, whose works have contributed to this project: first **Carole Duchêne**, L3 internship, for all her time-lapses of *Ectocarpus* growth and

development in presence of various drug, that I used to measure the impact of LatB on the morphogenesis of the apical cell. Secondly, thank to **Quentin Rochas**, L2 internship, for all his molecular biology work (much better than mine) to complete the positional cloning of *étoile*. Regarding this task (that is not addressed in this report), I have also to thank **Dr Zofia Nehr** for her help, especially regarding the use of the GeneMapper software. Finally, thanks to **Dr Thomas Torode**, **Dr Cécile Hervé** and **Pr. Paul Knox** for providing the anti-alginate monoclonal antibodies (BAMs) and, at last, thanks to **Murielle Jam,** for having prepared and furnished the stock solution of the G-specific alginate-lyase (AlyA1, designated as AlyG in this report), that was central in our work on the links between the alginates and wall mechanics.

Now I must thank all my mates (students and young doctors), three years, for the soirées, restaurant sessions, coffee breaks, and fun and moral support in general, that have enlightened these three harsh years (especially the last one). Thanks first to **Dr Maria Matard-Mann**, **Laure Mignerot**, **Dr Adèle James** (A.K.A "Miss l'Oréal"), **Anaïs Naretto**, and **Eugénie Grigorian**, that all experience (or have experienced recently) the ups and downs of the thesis. Thanks also to **Elodie Rolland**, **Dr Jonathan Dorival** (*ouai, c'est pas faux !!!!*), **Dr Yacine Badis**, **Dung Nguyen Thi Ngoc**, **Dr Zofia Nehr**, and **Émilie Guilloud**. Thank you, all of you, for your kindness, your good mood, and more simply for having being there!

Special thanks to **Maria**, for your kindness, cheerfulness, and your constant support and numerous pieces of advice. Please never change the way you are! And thank you also for the anti-stress essential oils! Special thanks to **Yacine**, too, just for being that crazy, for the political discussion and for having taught me the rudiments of boxing. And special thanks to, you **Eugénie**.

Also thanks to my two office neighbours, **Ludovic Delage** and **Gaëlle Correc**, for your general kindness, happiness, and jokes. Thank you for having endured my antisocial, and sometimes grumpy, temperament.

To finish, I wish to thanks my few friends and my family members, that have been shield against my loneliness, even though we have stayed in contact through social networks (Roscoff is so damn far from the rest of France!). So thank you very much to **Emmanuel Daoud-Hoareau**, **Mathieu Pierre** and **Gwendoline Birot**, my master best friends, members of the RDP team (you know what I mean)! Thank you, **Mathieu David** and **Conrad Hillairet**, my only friends from the "Classe Préparatoire". We are far from one another, and have somewhat lost touch each other, but I never forgot you. Thank you to you, **mummy** and **daddy**, and to **Armelle** and **Gwenaëlle**, my two sisters to which I am so close. Without all of you, the World would be much darker than it is.

Table of content

1. Introduction ... 15

1.1. "The mechanics of tip-growth: an overview over the Tree of Life" ... 17

1.1.1. Introduction ... 17
1.1.2. General concepts of biomechanics of cell morphogenesis and tip-growth ... 19
1.1.3. The cytoskeleton as the main mechanical factor of the growth patterning ... 25
1.1.4. The cell wall as the main mechanical factor of growth patterning ... 34
1.1.5. Turgor and associated hydrodynamic flows as the main mechanical factor of the growth patterning ... 58
1.1.6. Conclusion and perspectives ... 62

1.2. Brown algae: an ideal and stimulating groups for discovering alternative morphogenetic mechanisms ... 67

1.2.1. General overview of brown algae ... 67
1.2.2. Morphological diversity and morphogenetic pathways in brown algae ... 69
1.2.3. Physical constraints on the development and morphogenesis of brown algae ... 72
1.2.4. Cellular peculiarities ... 73

1.3. About the transposition of canonical mechanical models of cell wall expansion to brown algae 79

1.3.1. Abstract ... 79
1.3.2. Cell wall expansion: does the known matter really matter? ... 79
1.3.3. Uncoupling cell wall growth from the intrinsic properties of the wall ... 80
1.3.1. Cell wall growth: demystifying polysaccharide chemistry ... 83
1.3.2. Concluding remarks and future prospects ... 91
1.3.3. Glossary ... 92

1.4. *Ectocarpus* as a model system to study cellular morphogenesis in brown algae ... 93

1.4.1. A model species for the brown algae ... 93
1.4.2. Ectocarpus (partheno)sporophytes are ideal for the study of cell morphogenesis ... 94
1.4.3. Cellular morphogenesis and tip-growth in prostrate filaments ... 94
1.4.4. étoile: a tip-growth mutant of Ectocarpus ... 97

1.5. Thesis objectives ... 98

2. Biomechanics of the apical cells and biomechanical strategy of the apical cell tip-growth ... 99

2.1. A mechanical model of *Ectocarpus* tip-growth ... 99

2.1.1. Abstract ... 99
2.1.2. Author summary ... 100
2.1.3. Introduction ... 100
2.1.4. Results ... 102
2.1.1. Discussion ... 113
2.1.2. Materials and Methods ... 121

2.2. The mechanical role of alginates in *Ectocarpus* cell walls ... 127

2.2.1. Introduction ... 127
2.2.2. Results ... 129
2.2.3. Discussion ... 146
2.2.4. Materials and Methods ... 150

3. Molecular underpinning of apical cell tip-growth: the role of the (actin) cytoskeleton 155

3.1. Background ... 155

3.2. Organization of the microtubules (MTs) in the apical cell 156

3.3. Role of the actin cytoskeleton in tip-growth of *Ectocarpus* 156

3.3.1. Organization of the actin in the apical cell 156

3.3.2. Impact of depolymerization of F-actin on apical cell organisation and growth 162

4. General discussion and perspectives 173

4.1.1. Cell wall thickness gradient as a mechanical patterning factor in tip-growth 173

4.1.2. How to generate a stable thickness gradient? 176

4.2. The importance of wall mechanics in tip-growth of *Ectocarpus* apical cells.....178

4.2.1. Mechanical features of the cell wall in the apical cell 178

4.2.2. In muro molecular determinism of wall mechanical properties 182

4.2.3. Cytoplasmic determinism of wall mechanical properties: direct mechanical role of the actin cytoskeleton?..... 184

4.2.4. Conclusion: differential role of the cytoskeleton and of the wall chemistry and mechanics in the control of growth 186

5. Material and Methods.....191

6. Cited references.....201

List of Figures

Part 1 – Introduction

Figure 1.1	Basic characteristic of a tip-growing cell	p. 21
Figure 1.2	Mechanisms of amoeboid locomotion	p. 27
Figure 1.3	Classification of the different mechanical "strategies" observed or envisioned for tip-growing cells	p. 64
Figure 1.4	Phylogenetic positions of brown algae (Phaeophyceae)	p. 68
Figure 1.5	Overview of the diversity of thallus construction modes in brown algae	p. 70
Figure 1.6	Cell wall mechanical properties involved in cell wall expansion	p. 81
Figure 1.7	Comparison of the cell wall chemical composition and structure in land plants and brown algae	p. 86
Figure 1.8	*Ectocarpus* general morphology and early pattern of growth	p. 96

Part 2 – Biophysics of tip-growth in *Ectocarpus*

Figure 2.1	Diversity of tip-growth in the Eukaryotic tree	p. 103
Figure 2.2	Position and direction of cell wall expansion during growth	p. 105
Figure 2.3	Viscoplastic model of tip growth	p. 107
Figure 2.4	Turgor and curvature of the apical cells.	p. 108
Figure 2.5	Cell-wall thickness of the apical cell	p. 111
Figure 2.6	Schemes summarizing the biophysical properties of two tip growing cells: *Ectocarpus* filament apical cell and tobacco pollen tube	p. 112
Figure 2.7	Contribution of the cell wall biophysical parameters in *Ectocarpus* and pollen tube tip growth	p. 116

Figure 2.8	Impact of yield threshold (σ_y) and extensibility (Φ) variations on *Ectocarpus* tip growth	p. 118
Figure 2.9	Impact of the cell wall thickness gradient and pattern of cell wall biosynthesis	p. 120
Figure 2.10	Filament organisation and cell morphologies observed by scanning electronic microscopy	p. 133
Figure 2.11	Mannuronan-rich alginate blocks labelled with BAM6 antibody	p. 134
Figure 2.12	Mannuronan-Guluronan alginate blocks labelled with BAM7 antibody	p. 135
Figure 2.13	Guluronan-rich alginate blocks labelled with BAM10 antibody	p. 136
Figure 2.14	Summary of alginate mapping along the filament of *Ectocarpus*	p. 137
Figure 2.15	Cell wall thickness and structure along the filament	p. 139
Figure 2.16	Wall stress along the filament	p. 140
Figure 2.17	Alginate location in response to a hypotonic shock	p. 142
Figure 2.18	Alginate location in response to a hypertonic shock	p. 145
Figure 2.19	Stiffness in the dome by dilatation/retractation	p. 146

Part 3 – Molecular basis of tip-growth: the role of actin cytoskeleton

Figure 3.1	Organization of microtubules in the apical cells of the WT and *étoile*, revealed by immunofluorescence microscopy	p. 159
Figure 3.2	Distribution and organization of the actin cytoskeleton in the apical cells of WT and *étoile*, revealed by (immuno)fluorescence microscopy	p. 160
Figure 3.3	Summary of the general organization of the actin and microtubule cytoskeleton in the *Ectocarpus* prostrate filaments of the apical cell	p. 163
Figure 3.4	LatB effectively depolymerizes the AFs in the apical cells of Ectocarpus prostrate filaments	p. 165

Figure 3.5	AF depolymerization of LatB abolish tip-growth but not surface expansion in apical cells, and zonal organization of the apical cells according to the dependence of the shape upon the presence of AFs	p. 166
Figure 3.6	AF depolymerization by LatB reduces cell wall deformability after ~19h of treatment	p. 170
Figure 3.7	AFs depolymerization by LatB does not inhibit wall deposition but alter its structure	p. 171
Figure 3.8	AFs depolymerization by LatB enhances cellulose deposition in the wall of the apical cell	p.172

Part 4 – General discussion

Figure 4.1	Global overview of the results on the integrated mechanism of tip-growth in the apical cell of *Ectocarpus* sporophytic vegetative filaments	p. 190

List of Tables

Part 1 – Introduction

Table 1.1	Techniques employed for the study of cell wall mechanics during expansion.	p. 84
Table 1.2	Cell wall components of land plants and brown algal cell walls	p. 88

Part 2 – Biophysics of tip-growth in *Ectocarpus*

Table 2.1	Elastic Modulus E of the four virtual cell wall layers L1-4 inferred from the force curves obtained by atomic force microscopy.	p. 150

1. Introduction

In order to carry out this pioneering study about the biomechanical mechanism of tip-growth in *Ectocarpus*, a considerable analysis of the literature has been necessary to put our results in the context of research and theories about cell growth and morphogenesis. In this introductory session, the huge literature about the biomechanics of tip-growth, especially in walled-cell organisms (land plants, all fungal or fungal-like organisms, algae, and bacteria to a lesser extent) is critically reviewed in a first part (**1.1**, a review paper in preparation). In this chapter the main mechanical models are presented, with their advantages and pitfalls, and the diversity of models is discussed in the context of the origin and the evolution of tip-growth.

In a second part (**1.2**), the general characteristic of brown algae in term of phylogeny, ecology, morphogenesis and cellular characteristics (cytoskeleton and cell wall) are reviewed, in order to expose the particularly exciting challenges and opportunities that this special group offers to study alternative cellular and tissular morphogenetic mechanisms.

In a third part (**1.3**), the problem of wall expansion and its molecular control during walled cell growth and morphogenesis is tackled, in the form of an Opinion Paper that is in press in the journal *Trends in Plant Science.* In this part, the traditional methods and concepts pertaining to the mechanism of wall expansion, developed mainly for terrestrial plants, are questioned. A detailed comparison of cell wall structure and chemical composition between land plants and brown algae is presented, to show that the mechanisms at play during cell growth must be radically different between the two groups. The latter must be studied anew, without *a priori* hypothesis drawn from the land plant literature, in order to discover novel mechanisms of cell wall expansion, and their link with cell and tissue morphogenesis.

In a fourth part (**1.4**), the brown algal model species to study cell morphogenesis and tip-growth, *Ectocarpus sp.*, is described, with the current knowledge about its development.

Finally, the specific objectives of this thesis project are presented in a fifth part (**1.5**).

1.1. "The mechanics of tip-growth: an overview over the Tree of Life"

In preparation (this part is to be published as a book chapter).

1.1.1. Introduction

From the sub-cellular to the organism levels, growth and morphogenesis are fundamental mechanical processes, and the developing organisms have to comply with the rules of the physical world to acquire their final form and size (Boudaoud, 2010; Mirabet *et al.*, 2011; Ali *et al.*, 2014). One of the most fundamental issue in the field of evolutionary developmental biology (evo-devo) is to decipher how living things adapted to make use of the inescapable physical laws to achieve functional morphologies essential to their fitness, and how those mechanisms have emerged and evolved afterwards. Evolution works mainly at the genomic level, while growth and morphogenesis result from the physical transformation of living structures that imply in part (but not only) their mechanical deformations (Niklas, 2000; Ali *et al.*, 2014). Thus, an outstanding issue is to understand to what extent the evolution of "macroscopic" biomechanical processes at play during morphogenesis have been constrained by i) the genes and the molecular machinery behind the metabolic networks, that build the cell structural components, and that control the cell spatial organization and dynamics, and ii) by the "physical world", including the cytomechanical properties (resulting from the composition and structure of cellular components) and those of the external abiotic environment (Hamant and Traas, 2010; Mirabet *et al.*, 2011; Ali *et al.*, 2014). Different trade-off between these factors could have resulted in the range of morphogenetic strategies observed in today's living organisms.

The study of morphogenesis of isolated cell types not embedded into a multicellular tissue is a good approach for this aim, because these cells are easily accessible for experimental manipulations and microscopic observations, have a limited number of interacting physical components and thereby represent simplified systems for modelling (Harold, 1990; Niklas, 2000; Geitmann, 2006*a*; Geitmann and Ortega, 2009). In this respect, tip-growth represents an ideal case, because it is extremely polarised, yet simple and robust (see an overview of the general characteristics of tip-growing cells in **Fig 1.1**). Tip-growing cells are generally "invading cells" exploring external environments and thus are easily isolated and cultivated in laboratory for *in-vivo* studies. Tip (or apical) growth is one of the most common polarised cell elongation form in the living world (Heath, 1990), and is encountered in a large range of taxonomic groups, both in prokaryotes (actinomycetes, Prosser, 1990) and in eukaryotes (land plants, metazoans, eumycetes, oomycetes, the three major groups of macroalgae and several minor algal clades, Heath, 1990). Its wide phylogenetic occurrence is a testament to the large adaptive advantage it provides to the organisms, such as the exploration and colonization of vast surfaces or the invasion of hard solid media like soils or living tissues. Extremely elongated filaments insure critical functions as diverse as colonization, anchorage, water and nutriment uptake or delivery of particular cargos or chemical signals between distant spots in the organism, to cite just a few (Money *et al.*, 2004; Harris, 2011; Sanati Nezhad and Geitmann, 2013; Bezanilla *et al.*, 2015). It represents a unique chance for evo-devo studies of basic cellular morphogenetic phenomena spanning many branches of the tree of life, and for digging into its deepest evolutionary roots. In this context, the most important question is

whether such a distinctive polarized growth form could have been generated by different biomechanical morphogenetic strategies. This would allow deciphering the degree to which the "physical world" carries weight on the mechanisms of tip growth. In addition, exploring in parallel the molecular aspect of tip-growth functioning would indicate to what extent the variations of biomechanical mechanisms are correlated to variations in the set of available molecular regulators and pathways in different groups.

Until now, it is not clear whether tip-growth has emerged repeatedly in the course of evolution, or if it only appeared once and has thereafter been conserved in the various diverging lineages. From a molecular point of view, the invasive growth processes in Eukaryotes (at least in land plants, fungi and metazoans) are thought to be controlled by a common, evolutionary conserved molecular "toolkit" (Vaškovičová et al., 2013). This molecular toolkit involves the actin cytoskeleton, cellular trafficking, the exocyst, some molecular pathways including Rho-GTPases and lipid signalling. The evolutionary distance between land plants, metazoans and eumycetes suggests that the molecular toolkit was already present in the Last Eukaryotes Common Ancestor (LECA), so any eukaryotic taxa may have had the opportunity to inherit it. However, even if these molecular players are homologous, it is still possible that the regulatory network they built emerged from convergent evolution, rather than having a unique origin (Vaškovičová et al., 2013). In the future, the involvement and degree of conservation of such core toolkit remains to be investigated in more details, including other, underexplored phylogenetic groups. The scarce data existing about underexplored groups, like brown algae (Coelho *et al.*, 2002; Fowler *et al.*, 2004; Hable and Kropf, 2005; Bogaert *et al.*, 2013; Muzzy and Hable, 2013; Hable, 2014) and oomycetes (Jackson and Heath, 1989; Garrill *et al.*, 1993) suggest that at least some of these molecular factors are again involved in tip growth in these distant clades, belonging to the Stramenopiles "kingdom", further supporting the hypothesis of a conserved molecular toolbox. Although some molecular players are also found in polarly growing prokaryotes (Zhang *et al.*, 2010), those involved in tip-growing Actinomycetes seem specific to them (Flärdh, 2003, 2010; Flärdh *et al.*, 2012), suggesting independent evolutionary roots for tip-growth between the major domains of the tree of life. However, more research will be needed in the future before concluding about the degree of conservation and divergence of the molecular factors involved in tip-growth regulation, and about their effect on tip growth biomechanics.

At a physical level, cellular growth and morphogenesis result from the combined action of "protruding" forces generated by the protoplast to expand the cell surface at localized areas, and of "resisting" forces, that tend to oppose the firsts. The latter are those generated in reaction by either the cellular envelope (cell membrane and extracellular matrix, Mirabet *et al.*, 2011) and by the external medium in which the cell is growing (Money, 1999; Sanati Nezhad and Geitmann, 2013, **Fig 1.1**). Thus, it would be sensible that only few, or maybe a unique, biomechanical strategy, could account for such a robust, conserved cellular morphogenesis as tip-growth. Nonetheless, for more than one century of research, a surprising plethora of alternative biomechanical models of tip-growth have been imagined and put forward by different authors. However, most of the putative mechanisms are, for now, only theoretical, and some models lack clear experimental support. Should such diversity turn out to be real, it would be interesting to test whether it is more correlated to the phylogenetic position or to the abiotic environment of the organism, or to the particular physical conditions encountered by apically-growing cell types. At least, because of the fundamental difference in cell size and structure between eukaryotes and prokaryotes, tip-growth mechanisms are likely to be completely different between the two domains (Prosser, 1990). In the eukaryotes, an interesting modelling paper by Campàs and colleagues (2012) pointed toward a disparity in the physiological and biophysical strategies adopted by land plants (Archaeplastida) and

hyphal eumycetes (Opistokontes) on the one hand, and by fungi-like oomycetes (Stramenopiles) on the other hand. In prokaryotes, some Actinomycetes also form hyphae very similar to eumycetes and oomycetes; all the three groups form complex mycelial networks able to invade host tissues or soils (Prosser, 1990; Flärdh, 2010; Cameron *et al.*, 2015). Yet, these three groups do not share any close phylogenetic ancestor and evolved completely independently. This simple noticing suggests that tip-growth has emerged multiple times by convergent evolution, always leading to the same final, reproducible morphology.

Unfortunately, the current literature on tip-growth lacks of a broad view on the emergence and evolution of tip-growth across the tree of life. A large majority of studies have indeed focused only on some favoured taxonomic groups, i.e. the angiosperms, eumycetes and metazoans, each only represented by a small set of model species. The few papers offering an evo-devo comparison of tip-growth mechanisms generally remained focused on these few groups (Vaškovičová *et al.*, 2013; Honkanen and Dolan, 2016; Honkanen *et al.*, 2016; Rensing, 2016) while other taxonomic groups are still largely neglected. Deciphering if, and how, the physical constraints and the genomic baggage of an organism have influenced the biomechanical strategies to produce tip-growing cells will require more work in the future, and need to encompass understudied taxa, and to cross-correlate the biomechanical processes and their regulators into single, integrated models.

The aim of the present review is to browse the current knowledge about the diversity of biomechanical strategies of tip-growth drawn from both experimental evidences (cell mechanics, ultrastructure and chemistry) and theoretical models. A first chapter will briefly present the basic characteristics of tip-growing cells, in term of growth kinetics and mechanics (**Part 1.1.2**). The various biomechanical models will then be presented and classified according to the main cellular component or physical parameters involved. Those mechanical players, namely the cytoskeleton (**Part 1.1.3**), the cell wall (**Part 1.1.4**) and the turgor pressure (**Part 1.1.5**) are thus successively described as the main "mechanical patterning factor" of tip-growth. The models are critically evaluated to uncover their strength and limits. For the sake of conciseness, the various experimental approaches and details about the implementation of mathematical and computational models are left apart. We rather focus on the concepts, theories and ideas that have been supported or validated by experimental data. When possible, the reader is redirected toward the relevant papers for more information.

1.1.2. General concepts of biomechanics of cell morphogenesis and tip-growth

1.1.2.1. Diversity of tip-growing cell shapes

All tip-growing cell type share the same basic architecture: an elongated, generally stable tubular region terminated by a differentiated apical region, where the expansion of the cell envelope ─ a cell membrane completed with the internal cortical cytoplasm and the outer extracellular materials ─ is restricted (Heath, 1990; Martin *et al.*, 2001; **Fig 1.1**). The restriction of the surface expansion to the apex implies that the tubular regions become increasingly older as the distance from the tip increases. These non-growing regions are

defined as being "distal" to the apex that is generally designated as the proximal pole. This terminology can be sometimes confusing as the growing tip is generally the farthest extremity of a cellular projection that emerged from a basal cell body, like the pollen tube emerging from the pollen grain or the root hair from a root epidermal cell (Gilroy and Jones, 2000; Rounds and Bezanilla, 2013), and thus should rather be designated as the distal pole. By commodity, we will keep the traditional terminology used by authors working on tip-growing cells, that is, the apex being the proximal pole.

Tip-growing walled cells are generally considered as perfectly axisymmetric shells. From the extreme tip of the cell (the apical pole *per se*), meridians can be drawn toward the distal directions, more or less parallel to the longitudinal axis of the cell. This direction is called the meridional direction. The orthogonal direction to the meridional one is called the hoop, transversal or circumferential direction. Because of the axial symmetry of the cell, most molecular, physiological and physical parameters occurring at the cell surface during tip-growth (like cell wall deposition, ion flux, membrane and *in muro* enzymatic activities) can be comprehensively quantified only as a function of the meridional position. However, some geometrical, structural and kinetics parameters (at least surface curvature and strain rates) can be anisotropic, i.e. can be different between the meridional and circumferential directions. Thus, those properties must be, at any point of the cell surface, quantified in both meridional and circumferential directions (**Fig. 1.1**).

The tubular region below the apical growth site is traditionally designated as the "shanks" or the "shaft", and has generally the basic form of an isodiametric elongated cylinder. In some cases low residual growth can still occur in subapical regions, generally contributing to a slight and gradual increase in diameter, for example in *Medicago truncatula* root hair (Shaw *et al.*, 2000) or in *Saprolegnia ferax* hyphae (Jackson and Heath, 1990). Beyond this basic and highly conserved shape, a large diversity of diameters is found between taxa, ranging from the narrow hyphae of Actinomycetes (less than 1 µm in diameter; Prosser, 1990; Goriely and Tabor, 2003*a*), to the wide giant cells (several hundreds of µm) of the sporangiophore of *Phycomyces* (Castle, 1958) and the giant siphonous cell of the alga *Vaucheria* (Xanthophyceae; Mine and Okuda, 2003; Mine *et al.*, 2008).

In contrast to the tubular shanks, the growing apices show a large diversity of shapes. In the non-walled axon of metazoan neurons, it grows as a cone, a highly complex motile device projecting numerous filipodia in all directions (Heidemann, 1990; Franze and Guck, 2010). This is in striking contrast to walled cell organisms, which the vast majority of tip-growing cells belongs to, where the growing apical region is much simpler and generally takes the form of a demi-spheroid or a prolate demi-ellipsoid dome (**Fig 1.1**). However, the dome shape usually appears significantly divergent from a truly ellipsoid shape, as in the *M. truncatula* root hair, (Shaw *et al.*, 2000; Dumais *et al.*, 2004) and the *Phycomyces* sporangiophore (Castle, 1958). Thus, even among walled cell organisms, a large diversity of dome shapes exists between distantly related taxa, and this has been pinpointed as the sign of fundamentally different biomechanical strategies between distantly related groups (Campàs and Mahadevan, 2009; Campàs *et al.*, 2012). To wholly quantified the shape and the wall strain of tip-growing cells, both the circumferential and meridional curvatures must be quantified as a function of the meridional distance from the apical pole (see for examples Chen, 1973; Hejnowicz *et al.*, 1977; Dumais *et al.*, 2004).

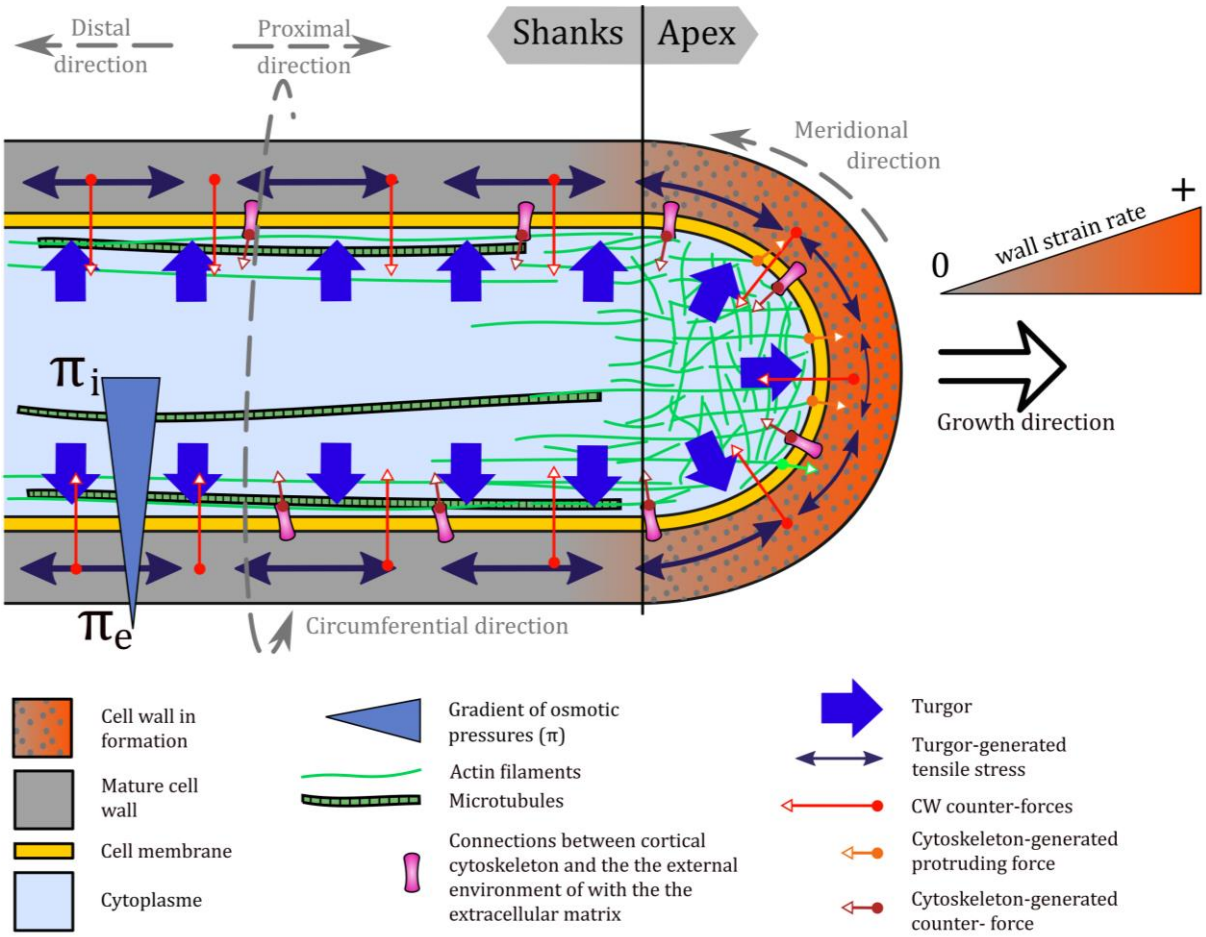

Figure 1.1 - General organisation of a tip-growing cell

The schema represents a walled cell tip-growing cell (such as found in land plants, fungi or algae) with a strong turgor pressure, but the same principles apply to animal cells, that have fairly only a cell membrane. In this situation, turgor pressure is still present but with much lower values (maximum some hundreds of Pa). The cell is organised into an apical region and tubular shanks. Growth activity, i.e. deposition and expansion of the cellular envelope, is restricted to the apical tip, especially for walled cells, where cell wall does are stabilized at the base of the dome, and no more expansive growth occurs in the shank. The turgor results from a difference of osmotic pressure between the internal and the external medium (π_i and π_e, respectively). The cytoskeleton is particularly abundant, with often long microtubules (MTs) and actin filaments (AFs) more or less parallel to the longitudinal axis in the shanks, and a complex network of AFs in the apical region. Expansive growth at the apex (apical dome for walled cell organism) results from a local unbalance between the outward directed "protruding" mechanical forces that tend to expand the cell envelope surface and volume, and "resisting forces" that opposes the firsts. The "protruding" forces are generated by the cytoskeleton or the turgor pressure. The resisting forces are primarily exerted by the cell envelope, namely the cortical cytoskeleton and / or the cell wall when present. The external medium in which the cell is growing can also exert significant mechanical impedance on the growing apex. In walled cells, the resistance of the external wall to the turgor generates a high tensile stress in the wall, that is generally thought to provide most of the work of wall expansion. However, in cases where the cell wall has a constant thickness across the cell surface, the tensile stress is lower in the apical dome because of local curvature, making it *a priori* unfavourable to restrict growth in this area.

1.1.2.2. Diversity of cell envelopes in tip-growing cells

Tip-growth implies that the expansion of the cell envelope is essentially restricted to the apical region, while the sub-apical region adopts a stable tubular shape. In plant and fungal organisms, the envelope includes a cell wall that is the key element to be deformed to actuate tip-growth (Hamant and Traas, 2010; Mirabet *et al.*, 2011; Chebli and Geitmann, 2017). The presence of such extracellular compartment is paralled by the presence of a high internal hydrostatic pressure, called turgor. The internal hydrostatic pressure in cell results from the difference of osmotic pressure between the cytoplasm (π_i) and the external medium (π_o), the former being more concentrated in osmotically active solutes than the second. Higher internal osmolarity lower the water potential of the cytoplasm compared to that of the external environment (**Fig 1.1**). The water thence permanently tends to flow inside the protoplast, developing a hydrostatic pressure. At any given point on the inner face of the cell envelope, it generates a constant outward directed force orthogonal to the tangent to the cell surface at this point. The cytoplasm is traditionally conceptualised as an aqueous fluid and, because of the water incompressibility, the turgor is thought to be a scalar, not a vectorial (i.e. oriented) force, meaning that it is constant throughout the cytoplasm (Winship *et al.*, 2010), and thus exert the same protrusive force at any point of the cell surface. In principle, turgor alone cannot, then, generate a cell shape different than a purely spherical cell (Hamant and Traas, 2010; note, however, that this is not entirely true, see for example Boudaoud, 2003; Bigan, 2015).

However, for the sake of mechanical equilibrium, the outward-directed protrusive force of the turgor is contained by the cell wall, in which a huge tensile stress that builds up in the outer cell envelope, until a mechanical equilibrium is reached. As the cell wall has a certain thickness, not negligible compared to the cell radius, the turgor-generated tensile force is, at any point of the cell surface, distributed on a cross-section of wall. The tensile force per unit cross-sectional area of wall is called the **tensile stress** and is equivalent to a pressure (Pa; **Fig 1.1**). The wall tensile stress that build in response to turgor is even larger than the turgor itself, because of the thinness of the cell wall compared to the cell radius (Castle, 1937) and provides the mechanical energy necessary to stretch the wall (Geitmann and Ortega, 2009; Guerriero *et al.*, 2014). At any point of the cell surface, the tensile stress will depend on mainly 4 factors: 1) the turgor pressure (MPa), 2) the local cell surface shape, represented by the curvature measured in a least two, perpendicular directions (m^{-1}) and 3) the local cell wall thickness (m) that effectively bears the tensile stress (Dumais et al., 2006). The tensile stress is positively correlated with turgor but negatively regulated by the others two parameters, and all could be locally modified to control the local expansion of cell surface at sub-cellular scales, underlying heterotropic growth like tip-growth (Green, 1965, 1969; Geitmann and Ortega, 2009). In the cylindrical part of a tip-growing cells, the circumferential stress is twice as large as the meridional stress. In the apical dome, if the wall thickness is considered constant, the tensile stress progressively decreases toward the apical pole in both the circumferential direction because of the increasing curvature, and both components gradually converge to the same value at the extreme pole (Hejnowicz *et al.*, 1977; Dumais *et al.*, 2004). This, indeed, represents the main paradox of tip-growth in walled cell organisms: surface expansion is restricted to the apical dome, where the tensile stress that make the work of expansion is the lowest in the whole cell! Most of the experimental and theoretical models dedicated to the biomechanic of tip-growth have indeed aimed to solve this conundrum (Harold, 2002; Geitmann, 2006*b*; Kroeger and Geitmann, 2012*b*).

In non-walled cells, the outer layer of the cell envelope is the cell membrane, that is a fluid layer of phospholipids and proteins (even though the existence of lipid rafts and the complex topographies of cell membrane greatly restrict the mobility of the constituting

molecules in the plane of the membrane; Janmey, 1995; Adler *et al.*, 2010; Levental and Veatch, 2016). In this case, the cell "surface", even if deposited in specific areas, can flow laterally, preferentially toward the site of active expansion. Such processes most likely occur in the animal migrating cells (Lauffenburger and Horwitz, 1996), growing axons (Franze and Guck, 2010), and the amoebas (Taylor and Condeelis, 1979; Grębecki, 1994). In these cell types, the "cell envelope" includes the cortical actomyosin that is connected to the extracellular medium (see **Part 1.3** below). Yet, the same mechanical principles apply to the cell membrane and cortical cytoskeleton in those kinds of cell. The cell membrane is under more or less tension because of the protrusive forces exerted by the weak hydrostatic pressure or the cytoskeleton, and those forces regulates the shape, motility, migration, and finally morphogenesis, of the cell (Houk *et al.*, 2012; Diz-Muñoz *et al.*, 2013; Lieber *et al.*, 2013; Kim *et al.*, 2015).

1.1.2.3. Biomechanical theories of growth and morphogenesis control in walled cell organisms

A vast majority of tip-growing cell types occurs in walled organisms, like plants, fungi, and algae (Heath, 1990). As stated above, it is the cell wall that must be stretched at the growing tip to expand forward the cell, and this mechanical work is thought to be done by the tensile stress that is built in this compartment in reaction to the turgor pressure inside the protoplast (see above). In this context, several biophysical theories have been developed to explain growth and morphogenesis in walled cell (Cleland, 1971, page 19; Cosgrove, 1986; Geitmann and Dumais, 2009; Mirabet *et al.*, 2011). For a proper understanding of the mechanical models that will be developed in the rest of the review, these two theories are briefly exposed here.

1.1.2.3.1. The canonical theory of Lockhart

The canonical biophysical theory of plant cell growth established by Lockhart (Lockhart, 1965) and further extended by Ortega and other authors (Ortega, 1985; Passioura et al., 1992; Geitmann and Ortega, 2009), stated that the turgor prevents the water from entering the cell. As a consequence, the cell growth can occur only when the turgor is decreased (Winship et al., 2010, 2011). Turgor cannot be regulated directly, though; rather, it is decreased by stress relaxation mechanisms into the cell wall, pointing toward this compartment as the major mechanical patterning agent involved in walled-cell organisms (Cleland, 1971; Cosgrove, 2016; see Part IV). In this theory, the cell wall expansion is considered as the flowing of a viscous material put under tensile stress generated by the differences in internal and external hydrostatic pressures (i.e, turgor). The cell wall will, however, only yield if the tensile stress is above a limit tensile stress value called the **yield-threshold**. As the wall expansion is irreversible, the deformation is considered plastic in nature, and traditionally represented as a purely plastic flows. The rate of viscous extension is proportional to the difference between the tensile stress and the yield-threshold, by a coefficient called the cell wall **extensibility coefficient**, that is equivalent to the inverse of the viscosity (the higher the viscosity of the cell wall, the lower the extensibility). When the tensile stress is below the yield-threshold, there is no plastic extension and the cell wall is only elastically stretched. The yield-threshold and the extensibility coefficient therefore represent two mechanical parameters relevant for plant cell growth, and the Lockhart model has been widely accepted both by plant biologists

and mycologists (Harold, 2002; Geitmann and Ortega, 2009). As plastic deformations occur when tensile stress rises above the yield-threshold only, the Lockhart's mathematical formalism has been further developed to integrate the impact of elastic deformation on the "plastic" stretching of the wall (Ortega, 1985; 2017; Cosgrove, 1986). The plant cell growth is a steady-state process, but for a proper understanding it can be discretised by an abstract series of iterative events described as follow: 1) The cell wall tensile stress is relaxed (i.e. dissipated) in part, by plastic modification of the wall (polymers or cross-links breakage); 2) The turgor pressure thus decreases, resulting in a decrease of the cell water potential. 3) The decreased water potential generates a water uptake from the external medium, thus re-increasing the turgor and enlarging the cell volume by wall expansion. Only at this stage the wall polymers are separated and creep against each over. 4) The re-established turgor re-increases the cell wall tensile stress. Continual, steady-state growth of the cell can then be assimilated by a continued repetition of this cycle, the turgor being maintained constant by continual synthesis or uptake of osmotically active solutes into the cytoplasm (Cosgrove, 1993a,b, 1997; Szymanski and Cosgrove, 2009).

1.1.2.3.2. The alternative theory of the Loss of Stability.

The LOS theory derives from the Leonhard Euler's mathematical theory of structural instability. The cell wall is modelled as a closed vessel containing an incompressible fluid under pressure that gets destabilised when the tensile stress reaches a critical value (P_{CR}; Wei and Lintilhac, 2003). This destabilization results in a small volume increment that relax tension. As water is incompressible, the small increment is cell volume quickly reduces the turgor so that it passes down the P_{CR} and growth is blocked (Wei and Lintilhac, 2003; Lintilhac, 2014). The cell expansion is thus controlled by a kind of "binary switch" process. The critical value depends on the cell geometry, including the ratio between the cell wall thickness and the cell radius and local surface curvatures, and on some simple intrinsic mechanical properties of the cell wall, that are the elastic moduli (E) and the Poisson's ratio (ν). Higher stiffness (higher E) or thickness increases P_{CR}, and so negatively impacts on the growth rate, while higher cell radius or Poisson's ratio decreases P_{CR} and so promotes local growth. At any time, growth by LOS only occurs at the point of the cell surface where P_{CR} is the lowest, resulting in a "pixelated growth" that shimmers over more or less extended area on the cell (Wei and Lintilhac, 2003). By spatially regulating any of the above-mentioned geometrical or mechanical parameters, the cell could easily determine where growth is to occur, and so the theory offers an elegant mechanism to achieve heterotropic plant cell enlargement processes like tip-growth. Growth directionality can further be achieved by generating cell wall with anisotropic stiffness, in which case elongation happens only in the direction of minimum stiffness (Wei and Lintilhac, 2003). Therefore, the theory entails that the regulation of the turgor pressure by the cell could be a way to promote growth (by increasing the osmolarity of the cytoplasm). However, the authors argue that, for proper regulation of cell morphogenesis, the cell would more conveniently regulate the local critical value of the cell wall, that depends on some mechanical properties of the wall (Wei and Lintilhac, 2007; Schopfer et al., 2008).

1.1.3. The cytoskeleton as the main mechanical factor of the growth patterning

In non-walled cell organisms like amoebas, animals and some crawling spores of red macroalgae (Pickett-Heaps *et al.*, 2001) and fungi (Trevithick and Galsworthy, 1977), the cytoskeleton is the main determinant of the cellular shape and mechanics (Torralba *et al.*, 1998). It confers the cell with several mechanical properties relevant to the cell function, like the strength (resistance to deformation) and the viscoelasticity (Ingber, 1997; Durand-Smet *et al.*, 2014). Moreover, in growing or migrating cells, the generation of forces necessary to expand the cell outer envelope and to penetrate into the external medium is also insured by the cytoskeleton. This fundamental component of the cell is thus far from being a simple, static scaffold supporting the cell architecture. The work of force generation in non-walled cells is mainly insured by the actin cytoskeleton (known as microfilaments or actin filaments, AFs), and sometimes the associated motor proteins of the myosin family (Condeelis, 1993; Insall and Machesky, 2009; Krause and Gautreau, 2014). Polymerisation of AFs at their "barbed end" can generate a protruding force against the cell membrane, making it expand in a specific direction, to form specialized structures such as filipodia, lobopodia and lamellipodia (Condeelis, 1993; Peskin *et al.*, 1993; Mitchison and Cramer, 1996). Myosin-mediated extensions or contractions of AFs networks in specific areas of the cell also generate forces on the cell membrane and/or the external medium, contributing to cell expansion and migration (Condeelis, 1993; Peskin *et al.*, 1993; Mitchison and Cramer, 1996; Krause and Gautreau, 2014). Extended acto-myosin networks lying behind the cell membrane (cortical cytoplasm) can drive extensive and oriented flows of envelope material over the whole surface or in restricted areas (Stossel, 1982). This process is fundamental to many growth and locomotion mechanisms in non-walled cells, and seems to be evolutionary ancestral and conserved, as it is common to distantly related organisms (Bray and White, 1988; Grębecki, 1994). The precise mechanochemical functioning of such processes is far too complex to be addressed here in details, and the reader is directed to the above-cited reviews for more information.

1.1.3.1. Cytoskeleton-driven tip-growth in non-walled cell organisms

The cytoskeleton provides an easy, convenient machinery to drive a localized, highly directional cell extension phenomenon like tip-growth, as the mechanical forces it exerts can be easily oriented in specific directions, as observed in filipodia containing thick bundles of parallel AFs polymerizing in a single direction (Condeelis, 1993; Mitchison and Cramer, 1996). Meanwhile, the tubular shaft left behind the "growing tip", that naturally results from the membrane stretching, like a floppy rubber balloon tugged at one point in a particular direction, can be further stabilised by other, more static components of the cytoskeleton networks, possibly involving AFs but also microtubules (MTs) and intermediate filaments (IFs). In non-walled organism, such biomechanical strategy is by far the most plausible to insure proper tip-growth or tip-growth-like directed migration.

1.1.3.1.1. Tip-growth in amoebas

Cellular processes during amoeba migration. Amebozoas constitute a group of unicellular protists close to Opisthokonts (Baldauf, 2008). This clade shows many forms,

traditionally designated as "amoebas", which have no rigid extracellular matrix and migrate into their surrounding environment by what is known as the "amoeboid locomotion". In such a process, a part of or the whole cell assumes the form of a giant pseudopodium, that is roughly a protoplasmic cylinder advancing along its longitudinal axis (Bray and White, 1988; Grębecki, 1994). The leading extremity has a rounded ellipsoidal shape, so the pseudopodium shape is reminiscent of the typical tip-growing plant and fungal cells (Steer, 1990; see **Part 1.1.2** and below). In monotactic forms like *Amoeba proteus* (Grębecki, 1984), the whole cell is advancing in a single direction, so that all the cytoplasm is dragged forward behind the leading tip. In that case, the rear of the cell appears as a retracted, rumpled "uroid" region that is passively dragged by the locomotive anterior part of the cell (Hellewell and Taylor, 1979; Taylor and Fechheimer, 1982). The cytoplasm is divided into a cortical, gelated, contractile layer (ectoplasm) and an internal, solated (i.e. near-fluid) region (endoplasm), and the whole is constantly cycling as the cell is progressing forward (Taylor and Condeelis, 1979), with the ectoplasm permanently contracting backward while the endoplasm flows forward, toward the leading front. In the latter, most of the cytoplasm returns from the endoplasm to the ectoplasm and reverts its direction of flowing into a typical fountain motion (Steer, 1990; Grębecki, 1994). The remaining part of the endoplasmic material "fills" the apical region, pushing the apical boundary forward. Alternatively, the whole endoplasm can be integrated back into the ectoplasm, and only pushes on a frontal hyalin cap, a static, giant vacuole that itself pushes on the apical membrane, while maintaining the apex rounded shape (Hellewell and Taylor, 1979; Grębecki, 1994). As the cell membrane is considered a "fluid mosaic", new cell membrane are supposed to be mainly provided by lateral, "in-plane" diffusion of phospholipids towards the leading front (Grębecki, 1994), making amoeboid locomotion less dependent upon massive exocytosis at the growing tip compared to "typical" tip-growth forms in walled cells.

Biomechanical models of amoeboid locomotion. The cellular and physical bases of amoeboid locomotion has been the object of intense research for almost a century, with many conflicting models being proposed (Allen, 1973; Grębecki, 1984, 1994; Taylor and Condeelis, 1979). The most recent mechanical models predicate that AFs and associated Myosin II or I motor proteins generate the contraction forces in the ectoplasm (**Fig 1.2**). The contractile forces have varying intensities, creating gradient of surface tension over the cell surface resulting in the cortical flow phenomenon, a widespread mechanism of cell morphogenesis and motility in non-walled cell (Bray and White, 1988). In giant amoebas the contraction force is constant all along the shanks, but these patterns still drive the rearward contraction of the ectoplasm (Grębecki, 1984, 1994; Bray and White, 1988). Adhesion of cortical AFs to the substratum on the flanks is probably mediated by transmembrane complexes containing spectrin-like proteins and other linker proteins, like alpha-actinin, talin, vinculin, and also some less-known, low-molecular weight linker proteins (Pollard, 1984; Choi and Jeon, 1989, 1992; Grębecki, 1994). These adhesions are necessary for the contracting ectoplasm to pull on the external medium, making the contracting posterior region advance forward (Grębecki, 1984; **Fig 1.2**).

From this model it appears that the prime pushing force responsible for tip-growth-like protrusion of the leading tip is only indirectly generated by the contracting actomyosin meshwork of the ectoplasm (Condeelis, 1993; Yanai *et al.*, 1996; Pollard and Borisy, 2003). Actually, according to the solation-contraction hypothesis, tip protrusion results rather from a coupling between the cytoskeletal network and the hydrostatic pressure (Taylor and Fechheimer, 1982; Janson and Taylor, 1993). Cortex contraction occurs everywhere except at the apical dome where the actomyosin is depolymerised; this contraction pattern would create a negative gradient of hydrostatic pressure from the rear of the cell to the leading front, generating the forward flow of cytosol. Thus, in giant amoeboid cells, AFs and associated

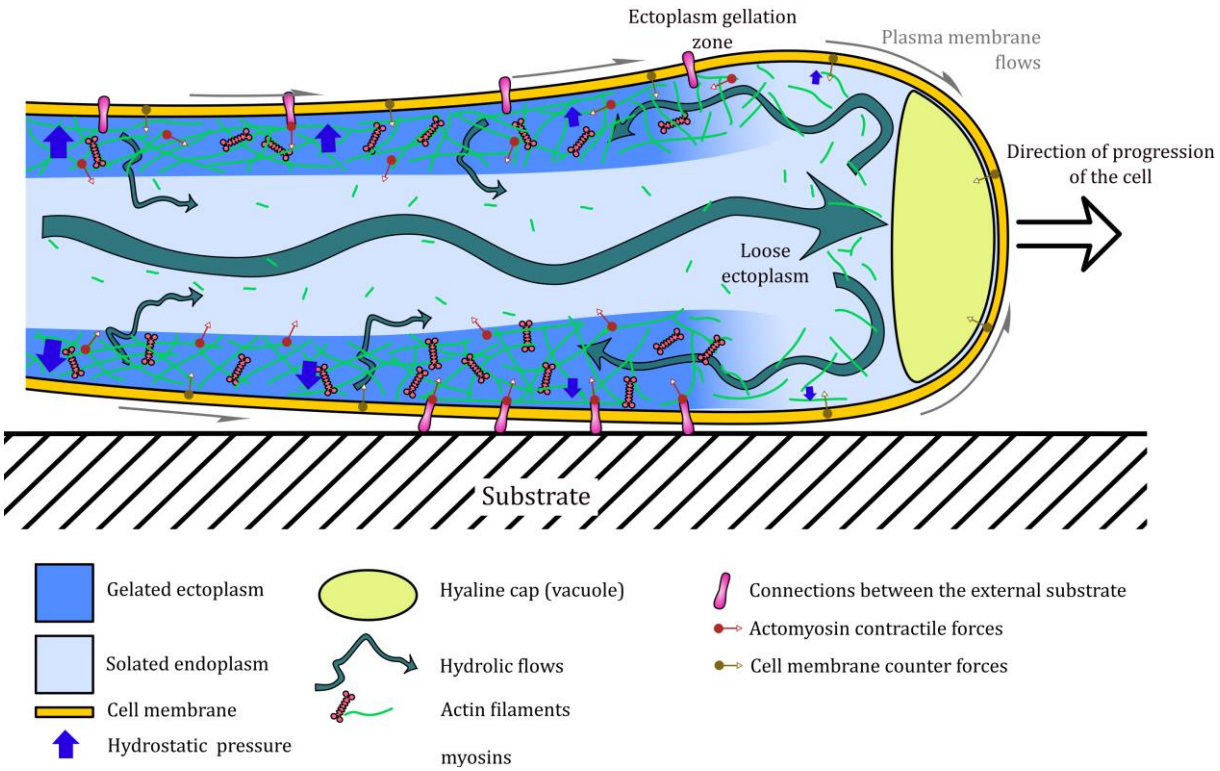

Figure 1.2 - Mechanisms of the amoeboid locomotion

Schematic representation of tip-growth-like locomotion of amoebas, according to the "cortical contraction" hypothesis (Grębecki, 1994). The "protrusive force" corresponds to the forward flow of the solated endoplasm, generated by contraction of the actomyosin cortex (gelated ectoplasm) in every part of the cell except at the apical leading front. In this particular location the AFs are lowly polymerised and barely cross-linked with myosins (this region is se designated as "loose" ectoplasm in this schema). Water flows then pass through the depolymerizing actomyosin cortex to "fill" the leading front. In some instance a "hyaline cap", corresponding to a giant vacuole, occupies the apical cytoplasm, and the water forward flow only pushes on this cap to make the apical cap progress forward. Most of water flows backward in the forming ectoplasm, where AFs polymerisation is active and the actomyosin network is reconstructed. In the shank, the activity of myosin generates a general, uniform contracting force that pressurizes the cell. When the cortical cytoskeleton is connected to the external medium by transmembrane connections, this general contraction of the actomyosin cortex pulls on distal part of the cell, dragging them forward. As the phospholipids constituting the cell membrane are not rigidly bound to the actomyosin cortex, this compartment flows passively forward because of the double effect of cell contraction at the rear of the cell and protrusion at the leading front.

myosins motors do not control growth by generating a direct, pushing force on the cell membrane toward the direction of growth by polymerizing or gliding AFs. Nevertheless, the cytoskeleton remains both the primary motor of cell elongation and the mechanical patterning agent that establishes the cell shape and the directional growth. Meanwhile, the hydrodynamical flow toward the tip is curiously reminiscent of the active role that turgor pressure plays in most tip-growing plant cells (see **Part 1.1.2**, **1.1.4** and **1.1.5**), thus supporting the theory of tip-growth in walled cells as being derived from an ancestral amoeboid locomotion (Steer and Steer, 1989; Steer, 1990; Heath and Steinberg, 1999; Pickett-Heaps and Klein, 1998, see **Part 1.1.3.2** below).

1.1.3.1.2. Tip growth in animal axon

In metazoans, tip growth is not a commonplace mode of cell morphogenesis, but it is found in the neuron that displays by far the most dramatic cell morphology among all animal cell types, which is fundamental for its function (Heidemann, 1996). The neuron cell body (soma) deploys several thin, elongated processes, namely the axons (rather called neurites in culture) and dendrites (Heidemann, 1990, 1996), that both elongate into the extracellular matrix by a tip-growth-like process, although recent data have suggested that the surface expansion is not always restricted to the leading tip (cf **Part 1.1.2**). Here we will discuss only axon tip-growth, which is by far the most studied case.

Cellular processes at play during axon polarized growth. Axons, that can be several meters long in large animals, elongate by the motile activity of a specialized device at the tip of the axon, called the growth cone, that leads the progression of the axon until it reaches its target (another neuron or a non-neuronal cell) and differentiates into a synapse (Landis, 1983; Franze and Guck, 2010). It is a highly specialised, complex motile device, with the double purpose of powering and directing the elongation of the axon into the complex, tight 3D extracellular environment of the nervous system. In cultured neurons the growth cone appears as a flat, enlarged region at the distal extremity of the axon, that further deploys numerous, thin filipodia in several directions. These filipodia are permanently extending and retracting and are thought to play a critical role in “sensing” the external environment, both chemically and physically, in search for directional cues (Bray, 1987; Suter and Forscher, 2000). Lamellipodia extend between the filipodia, and the rest of the cytoplasmic content of the growth cone is then “pulled” into the lamellipodia. The complete process of growing cone thus closely resembles the typical “crawling” mechanism found in other locomotive animal cells (Heidemann, 1990, 1996; Heidemann and Buxbaum, 1998).

The cytoskeleton is abundant everywhere in the axon and is essential for the growth cone motility. As in amoeboid locomotion and any other form of animal cell migration, the actomyosin cortex is the prime motor of growth cone motility and thus of axon elongation (Bray and White, 1988; Heidemann, 1990; Dent and Gertler, 2003; all the other reviews cited here). In the long, extended tubular shaft of the axon, long AFs, MTs and IFs (intermediate filaments, also called “neurofilaments” in axons) are found always more or less longitudinally oriented. The AFs are mainly located in the cortical region just underneath the axonal cell membrane (axolemma), while MTs and IFs are more abundant in the central region of the axoplasm (Heidemann, 1990). Although the complete set of molecular factors and mechanisms involved in the process are not entirely known, these cytoskeletal elements must be involved in the massive, rapid transport of cytoplasmic and membranous components toward the growing tip (a typical feature of tip-growth; Heidemann, 1996). In contrast, few MTs and IFs are found in the apical growth cone (except in the central region, where they are

thought to polymerize), while AFs and myosin chains still form a dense cortical layer. The latter drive the complex motility of the growth cone, including filipodia extension and retraction, lamellipodia spreading and ruffling coupled to rearward flow of membrane toward the base of the growth cone and, finally, the progression of the whole growth cone (Landis, 1983; Heidemann, 1990, 1996).

Biophysical models of axons growth. The detailed biomechanical functioning of axon elongation has been extensively studied for more than 50 years, and several models, sometimes irreconcilable, have been proposed by different authors (Bray, 1973; Landis, 1983; Heidemann, 1990; Dent and Gertler, 2003; Betz *et al.*, 2006; Betz *et al.*, 2009; O'Toole *et al.*, 2008; Franze and Guck, 2010). Only the two main adversary models will be briefly discussed here, and the reader is sent to the above-mentioned reviews for more information about the details of both and other variations around these themes. The first and simplest model of axon elongation postulated that the AF polymerisation at the leading edge of the lamellipodia, powered by actin cytoskeleton, is by itself the prime mechanism of the elongation of the whole axon (Aletta and Greene, 1988). The whole cytoplasm would then move forward in bulk into the thin lamellipodia, along with additional membranous material by "in-plane" diffusion, resulting in enlargement. This mechanism is basically that of "crawling" migrating animal cells (Mitchison and Cramer, 1996). In parallel, regions of the cell cortex passively left behind the leading edge would naturally acquire a rough tubular shape by the slight meridional tensile stress generated by the advance of the leading front. Those region would get thinner and consolidated by underlying cytoskeleton coupled or not to the extracellular substrate via transmembrane connexions, finally resulting in the tubular shaft of the axon (Aletta and Greene, 1988; Heidemann, 1990).

However, while this model can apply to some types of neurons, it cannot account for several features found in most of elongating axons in specific conditions (Bray, 1987), for example the constriction of the distal part (rear) of the growth cone, leading to a much thinner, straight axon shaft. In most case, the growth cone as a whole behaves as a complete locomotive cell, actively pulling on the axon like a "leukocyte on a leash" (Heidemann, 1990), as it progresses into the external environment (Bray, 1979, 1987; Lamoureux *et al.*, 1989; Heidemann, 1990). The current biomechanical model of axon tip-growth is thus the following. In the growth cone, the cell membrane is permanently flowing backward due to a gradient of contraction of the underlying cortical acto-myosin meshwork, centred on the distal region (close to the junction with the axon shaft), the so-called "cortical flow" (Bray, 1973; Bray and White, 1988). When connexions between the AFs and the extracellular space are created by "molecular clutches" (likely containing adhesion proteins like cadherin or spectrin), the cortex cannot flow backward any more, and instead mechanically pulls on the external environment (Heidemann and Buxbaum, 1998; Suter *et al.*, 1998; Suter and Forscher, 2000; Wang, 2007; Franze and Guck, 2010) and propels the cytoplasmic content forward, making the whole growth cone advance. The locomotive growth cone then actively pulls on the axon and stretches it out (Bray, 1979; Buxbaum and Heidemann, 1988; Lamoureux *et al.*, 1989; Dennerll *et al.*, 1989). The molecular connections into the growth cone also serve as mechanical anchorage for the AFs meshwork that expand at the leading edge of the lamellipodia, and to propel the vesicles and other cytoplasmic content forward (Heidemann and Buxbaum, 1998).

This "pulling model" also gives an elegant simple way to generate the thin straight tubular shape of the axon shaft: this form will naturally result from the mechanical stretching of the somewhat elongated portion of cell left behind the advancing growth cone (the tubular form is the one that minimizes the surface tension compared to more complex forms). However, this mechanism cannot explain the long-term maintenance of the tubular shaft,

especially when the growth cone stops pulling. As mentioned before, the axon shaft is rich in longitudinally aligned cytoskeleton elements, and there are evidences that show that these elements plays an essential role in mechanically maintaining the shape of the axon (Heidemann, 1990, 1996; Franze and Guck, 2010). The exact mechanism of that maintenance is complex and counterintuitive for biologists not familiar with thermodynamic concepts, and involves the concept of "tensegrity" ("tensional integrity", Ingber, 1997). In short, the cortical actomyosin network puts the axon shaft under tension and tends to contract it, as evidenced when the axon is cut or pulled away from the substrate (Shaw and Bray, 1977; Bray, 1979; Dennerll *et al.*, 1988; Heidemann, 1990). In opposition, the polymerisation and tethering of MTs and neurofilaments in the central area of the axon decrease their free energy, that promotes the "surface compression" of this central meshwork and the polymerisation of MTs and neurofilaments. As a consequence, those cytoskeletal elements elongate and align, generating a force that counteracts the contraction force of actomyosin (Dennerll *et al.*, 1988; Buxbaum and Heidemann, 1988; Heidemann, 1990). In addition, the external medium, pulled backward by the actomyosin cortex through transmembrane connections, would also add another resisting force in addition to that of MTs and neurofilaments. According to the tensegrity concept, all these opposing mechanical forces would contribute to stabilizing the elongated tubular shaft of the axon (Heidemann, 1990; Franze and Guck, 2010).

To conclude, in the frame of the latter model, the tip-growth of axon is highly derived and specific to this unique cell type, in which the growing tip is highly differentiated into a specialised "crawling machine" with a highly modified, dynamic shape, cumulating the functions of cell surface material (plasma membrane) supply and expansion, and of anchorage to and pulling on the external medium to promote the establishment and elongation of the long, thin axon shaft (Bray, 1987; Franze and Guck, 2010). This specialized device probably emerged as a necessary adaptation to the very complex and mechanically soft environment of the nervous system of metazoans (Franze and Guck, 2010). Axon tip-growth has indeed few in common with the "traditional" amoeboid locomotion mechanism in which these functions are not restricted to a small zone of the cell and its evolutionary origin is probably independent from that of other tip-growing forms in other taxa.

1.1.3.2. Amoeboid-like models of tip-growth in walled-cells

1.1.3.2.1. Evidences in favour of an ameboid-locomotion like apparatus conserved in walled cell taxa

Contrary to the "naked" cells of amebozoans and metazoans, land plant, algal and fungal cells have all in common the presence of a stiff cell wall surrounding the whole protoplast, and a high internal turgor pressure (see **Part 1.1.2**). The cell wall is a complex extracellular matrix made mainly of various matrix and cable-like polysaccharides, mixed with some amount of proteins (Carpita and MCann, 2000; Popper *et al.*, 2011*a*). The high turgor is built up in the protoplast by a large gradient of osmotic pressure between the internal and the external media, and it is widely accepted among botanists and mycologists that high turgor is necessary to mechanically expand the stiff cell wall, and as such make cells grow (Geitmann and Ortega, 2009; Lew, 2011; Mirabet *et al.*, 2011; Braidwood *et al.*, 2014; Guerriero *et al.*, 2014).

However, the striking similarity between the amoeboid growth mechanism described in **Part 1.1.3.1**, and some characteristics of tip-growing plant cells, such as fungal hyphae and land plant pollen tubes and root hairs, has led several authors to consider tip-growth mechanisms in those cell types to be amoeboid-like (Picton and Steer, 1982; Steer and Steer, 1989; Steer, 1990; Harold *et al.*, 1995; Money, 1997; Pickett-Heaps and Klein, 1998; Heath and Steinberg, 1999; Harold, 2002; Steinberg, 2007). Common points include first some obvious similarities about the global cell shape and the growth dynamics in the two systems. In both cases the cell protrusion is more or less a regular, elongated cylinder, terminated by an hemispheric dome in which growth is restricted, and a general flow of cytoplasm seems to accompany the forward progression of the leading front (Steer, 1990; Heath and Steinberg, 1999; Lew, 2005, 2011; Zonia and Munnik, 2009). Many tip-growing plant cells have a cortical cytoplasm profuse in AFs, associated Actin-Binding-Protein (ABPs) like myosins, and also spectrin proteins in some groups, the whole being a possible functional equivalent of the gelated ectoplasm of amoebas (Torralba *et al.*, 1998). However, in contrast to amoeba, AFs generally extend well into the growing tip, as reported in land plants (Pierson, 1988; Vidali *et al.*, 2001; Derksen *et al.*, 2002), green algae (Braun and Wasteneys, 1998), eumycetes (Torralba *et al.*, 1998; Virag and Griffiths, 2004; Riquelme and Sánchez-León, 2014), oomycetes (Jackson and Heath, 1990; Walker *et al.*, 2006), xanthophycean algae (Gavrilova and Rudanova, 2000; Alessa and Oliveira, 2001) and brown macroalgae (Kropf *et al.*, 1989; Karyophyllis *et al.*, 2000*a*; Ouichou and Ducreux, 2000; Varvarigos *et al.*, 2004). AFs in the growing tip are organised into specialised structures, that often take the form of an "apical cap" underlying the inner face of the cell membrane, especially in lineages belonging to the Stramenopiles kingdom (see references above concerning oomycetes, xanthophycean and brown algae), or an apical fringe in land plant pollen tubes and root hairs (Lovy-Wheeler *et al.*, 2005; Chebli *et al.*, 2013).

In fungi, the possible existence of turgor gradient along fungal hyphae (Money, 2008) and the ability of the cytoplasm to retract from the cell membrane in pulsatory waves by actin-dependent mechanisms (Torralba and Heath, 2001; Reynaga-Peña *et al.*, 2005), have been put forward as evidence of a contractile ectoplasm participating in the forward migration of the cytoplasm. Consistent with these amoeboid-like contractile movement, the existence of strong connections between the cortical AFs and the cell wall have also been demonstrated, both in some eumycetes and oomycetes hyphae (Kaminskyj and Heath, 1995; Bachewich and Heath, 1997) and some brown algae rhizoids and apical cells (Wagner *et al.*, 1992; Henry *et al.*, 1996; Ouichou and Ducreux, 2000), which function could reflect that of adherent junctions in locomotive amoebas (see above). Put together, all those characteristics strengthen the view of walled tip-growing cells as "tube-dwelling amoebas" according to the saying of Heath and Steinberg (1999).

A more direct evidence in favour of a conservation of an amoeboid-growth machinery in land plant, algal and fungal lineages is the fact that non-walled cell types in these groups often show an ability to make cell protrusion and to crawl into substrates, with evident animal-cell-like motility. Some examples are wall-less zoospores in eumycetes (Heath and Steinberg, 1999) and in red macroalgae (Pickett-Heaps *et al.*, 2001), in vegetative cells of the oomycete *Achlya bisexualis* or in mutant strains of *Neurospora crassa* (eumycetes) in absence of turgor (Trevithick and Galsworthy, 1977; Money and Harold, 1993; Harold *et al.*, 1995; Money, 1997). In such case, the cytoskeleton is thought to directly propel the cell, as suggested by the profusion of AFs in protrusions or at leading edges, which was shown by fluorescent staining of the cell, for example in eumycetes (Heath and Steinberg, 1999 and reference therein) and red macroalgae cells (Ackland *et al.*, 2007; Li *et al.*, 2008).

1.1.3.2.2. The amoeboid model of plant cell tip-growth

Perhaps the most detailed amoeboid-like tip-growth model in a walled cell context is that established for the Angiosperm pollen tube by Steer and colleagues (Picton and Steer, 1982; Steer and Steer, 1989; Steer, 1990), that is general enough to be applied to other apically-growing cell types in different groups. This model postulates that apical AF meshwork would reinforce the forming cell wall in the apical dome, thus allowing it to be deposited and "matured" without being broken by the high turgor pressure. Because of the high turgor pressure, the prime mechanical role of AF meshwork would be slightly "derived" compared to its role in locomotive amoebas. It would rather reinforce the cell wall enough to prevent bursting, probably with the help of transmembrane focal contacts between AFs and the wall in the sub-apical shank. In parallel, its mechanical state would allow more or less extension of the cell envelope, under the multiple and complex actions of a battery of ABPs and other proteins regulating the rate of AF elongation, bundling, cross-linking, severing and depolymerisation. The mechanical state of AFs would especially be regulated by the internal concentration of Ca^{2+} (Steer and Steer, 1989; Steer, 1990; Torralba and Heath, 2001). Thus, the actin cytoskeleton network would regulate the “yielding” propensity of the cortical layer of the cytoplasm in a controlled manner at spatially defined localised area of the cell, in the present case the apical dome. This "cytoskeletal mechanical patterning" is in fact the equivalent of the "cell wall mechanical patterning" models that will be addressed in **Part 1.1.4**, which links cell morphogenesis to a gradient in cell wall mechanical compliance. It is also important to note that, in the case of walled organisms, the hydrodynamical flow toward the growing tip is replaced by the high turgor pressure, that is no longer generated by the contractile action of the AFs. In parallel, another derived role of AFs and associated motor proteins in walled tip-growth is in the trafficking of wall-building secretory vesicle to the cell membrane (Parton *et al.*, 2001; Virag and Harris, 2006; Zonia and Munnik, 2008*a*; Geitmann and Dumais, 2009; Chebli *et al.*, 2013; Riquelme and Sánchez-León, 2014).

1.1.3.2.3. The especially interesting case of oomycetes tip-growth

In practice, such amoeboid tip-growth model seems especially suited to the case of oomycetes hyphae, in which the actin cytoskeleton is particularly complex and dynamic (Jackson and Heath, 1993*b*; Heath *et al.*, 2000; Torralba and Heath, 2001; Meijer *et al.*, 2014), organized into a strong apical cap made of intermingled AFs, a recurrent structure in tip-growing Stramenopiles as mentioned before (see references above). In several species, hyphal growth rate and cell morphogenesis were shown to be partly independent from turgor. In *Achlya bisexualis*, the maintenance of growth was linked to the cell wall softening at the tip (Money and Harold, 1992), but at least in the pathogenic species *Saprolegnia ferax*, normal hyphae can still normally elongate in the total absence of turgor, indicating that another cellular “motor” must be at play to propel the apical tip forward (Money and Harold, 1993; Harold *et al.*, 1996). In contrast, the thick apical cap was directly shown to mechanically sustain the cell wall at the tip (Jackson and Heath, 1990, 1993) thus potentially down-regulating the extensibility of the cell envelope. Indeed, disruption of AFs by cytochalasin D in actively growing hyphae induced an initial growth rate surge as though the apical cap was actually restricting wall expansion before drug administration (Gupta and Heath, 1997). Walker and colleagues (2006) also showed that, in *A. bisexualis* and *Phytophthora cinnamomi* hyphae growing into solid media, the extreme tip is depleted in AFs, perhaps allowing the turgor pressure to exert more protrusive force on the external medium to force a way in it. Heath *et al.* (2000) further demonstrated that cortical AFs actively regulate the shape of the

growing tip of *S. ferax*. In the same species, when growth occurs in the near-total absence of turgor, this cap was even proposed to generate the force necessary to expand the tip (Money, 1997; Torralba and Heath, 2001; Harold, 2002). This hypothesis was strengthened by the fact that, in weakly-turgid hyphae, disruption of AFs by cytochalasin D blocked growth after the initial growth rate surge (Gupta and Heath, 1997). The mechanisms of force generation is hypothesised to be the same than those encountered in locomotive animal cells: by direct polymerisation of AFs or AFs slippage powered by myosin motors (Condeelis, 1993; Peskin *et al.*, 1993; Mogilner and Oster, 1996). Overall, these data point to the idea of the actin cap being a complex, multi-purpose dynamic cellular device that could switch between a protrusive (motor) and a restricting mechanical role to regulate the apical yielding propensity, according to the cellular (turgor value) and the external (stiffness of the invaded substrate) physical contexts. However, the precise ultrastructure and molecular dynamics of the cortical apical cap and its associated molecular factors has poorly been described in details so far, and these mechanisms and their molecular regulation remain quite speculative (Steer, 1990; Harold *et al.*, 1996; Harold, 1997, 2002; Money, 1997). Indeed, the “apical cap” may actually only result from artefact due to chemical fixative protocols classically used to stain AFs (Heath, 1987; Jackson and Heath, 1990). A study using conventional staining method on *P. infestans* (Ketelaar *et al.*, 2012) did not revealed any thick apical cap, but only thin cortical actin cables evenly distributed along the cortex and actin spots in non-growing areas. *In-vivo* actin dynamic in *P. infestans* observed by LifeAct labelling confirmed those results, revealing only a low density of fine cortical AFs at the tip that cyclically appeared and disappeared by brief flashes (Meijer *et al.*, 2014). An accumulation of AFs in the apical region of hyphae was observed only at the very moment when the hyphae penetrate the plant host cells using the same in-vitro labelling technique (Kots *et al.*, 2017). These last studies showed that the apical cap could be a special device only deployed in certain circumstances, and not a fundamental piece of the mechanical machinery involved in tip-growth of oomycetes hyphae.

1.1.3.2.4. The edifying case of the marine diatom Chaetoceros

An extreme case of tip-growth where the direct mechanical involvement of the cytoskeleton seems obligatory is in the diatom species of the marine *Chaetoceros* genus. These species produce extremely long (sometimes several hundreds of micrometers) and fine (less than 1 µm in diameter) spine-like extension of the stiff, mineral siliceous valves of diatom cells (Pickett-Heaps, 1998). They elongate very fast by tip growth but are devoid of cell wall at the tip, silica being only deposited at the base of the “apical dome”, like bricks on a wall, probably by chemical precipitation (Pickett-Heaps, 1998). It is noteworthy that growth takes place in the absence of turgor, as the cellular body often retracts from the valves during the elongation (Pickett-Heaps and Klein, 1998). A cytoplasmic cortical "sleeve" made of fibrillary electron-dense material is partly underlying the distal extremity of the silica tube, and partly underlying the naked cell membrane in the terminal dome. Despite that its molecular structure and composition have not been investigated, this structure is supposed to be made of AFs and myosin, that would be anchored to the tubular part of the silica wall and would drive the flow of cell wall and membrane material to the tip while pushing the membrane at the tip itself. In parallel, the addition of wall material at the extremity of the tube would prevent any circumferential expansion and would offer new anchorage surface for the sleeve to slide forward in the shaft of the seta, following the rapid progression of the protruding apical membrane (Pickett-Heaps and Klein, 1998). This process has been called “amoeboid” by the authors, but the mechanism should involve direct protruding force exertion on the cell membrane, and may thus be more alike cell migration pathway in metazoans

(Condeelis, 1993; Mitchison and Cramer, 1996). However, the molecular mechanisms by which 1) forces are exerted at the leading tip, 2) building-blocks are transported to the site of secretion and 3) the sleeve itself is built and moves, remain to be elucidated.

1.1.3.2.5. Conclusion

All these pieces of information from different models point toward the idea that tip-growth biomechanics in various eukaryotic walled-cell taxa may have originated in an ancestral amoeboid-like cell protrusion or migratory process, that would have been present since the LECA (Vaškovičová *et al.*, 2013). Numerous data about the molecular regulatory network driving tip growth support this scenario (Heath and Steinberg, 1999; Torralba and Heath, 2001; Steinberg, 2007; Vaškovičová *et al.*, 2013). From an evolutionary point of view, one the most interesting feature of the amoeboid model is the regulation of local "deformability" of the cell envelope, allowing surface expansion under hydrostatic pressure at the growing tip while strengthening the sub-apical part to establish and maintain the tubular shape (see **Fig 1.3**). The complex cortical actomyosin has indeed various mechanical properties and may be "remodelable" by a plethora of enzymatic or non-enzymatic "remodelling" factors, permitting precise spatial and temporal regulation of cell surface local expansion or contraction (Stossel, 1982).

1.1.4. The cell wall as the main mechanical factor of growth patterning

1.1.4.1. The classical theory of cell growth and morphogenesis control by wall mechanics

1.1.4.1.1. The mechanical properties of the wall

The extracellular wall that encasing land plant, fungal (eumycetes and oomycetes) and algal cells is a very complex material, intermediate between a deformable solid and a very viscous liquid. It is endowed with several and interdependent intrinsic mechanical properties, reflecting its deformation capacities (generally called strains) in response to turgor-generated tensile stress. Those properties are briefly defined below, but the reader is directed to several reviews in which those properties are defined and explained in more details (Cleland, 1971; Cosgrove, 1993*c*; Boudaoud, 2010; Mirabet *et al.*, 2011; Guerriero *et al.*, 2014).

The **elasticity** quantifies the immediate and reversible deformation of the cell wall in response to a mechanical force. The reversibility means that the initial form and dimensions of the cell wall are restored when the mechanical force is abolished (Boudaoud, 2010; Mirabet *et al.*, 2011). The elastic deformation is by far the most common mode of wall deformation observed in plants, algal and fungal organisms (Dumais, 2013), and would serve as a way to store huge mechanical energy resulting from the turgor pressure and dampen the difference of turgor resulting from to varying osmotic conditions (the larger the elastic strain, the larger the quantity of energy stored). The **plasticity** represents the immediate but irreversible

deformation of the wall in response to a mechanical load. The irreversibility of plastic deformations implies that the initial form and dimension are not restored upon release of the mechanical flow, but instead the final form is conserved. The wall can also sport a viscous behaviour, i.e. that it can deform in part like a very viscous fluid. This viscous behaviour implies that the wall deformations are not immediate, but instead time-dependent, with the degree of deformation increasing over time during the application of a constant force. These viscous deformations can be reversible (in which case the initial shape and dimensions of the wall will gradually recover its initial stage after the release of the mechanical stress) or irreversible, corresponding to **viscoelasticity** and **viscoplasticity**, respectively (Cleland, 1971; Cosgrove, 1993a,b). Finally, the **Poisson ratio** describes, for any kind of wall deformations cited above the distribution of the deformations (strain) between the three spatial dimensions. Generally, it is used to describe the degree of thinning of the wall in response to a given strain value in the plane of the wall. Its value would depend on several factors of the wall, for example the "compressibility" of the wall, but is rarely measured. In models, values of Poisson ratio are generally posited considering the more probable mechanical nature of the wall (for example in the viscoplastic model of Dumais *et al.*, 2006; see **Part 1.1.4.3**).

However, these different parameters are often confused between each other. Indeed, the immediate elasticity, often measured as a simple linear elastic modulus, is by far the most frequent property measured, or at least approximated, by various techniques like Atomic Force Microscopy (AFM; Geitmann, 2006*a*; Milani *et al.*, 2013; Braybrook, 2015; Weber *et al.*, 2015). Contrary to the assumption of the Lockhart's theory, the wall of plants and fungi has long been considered more viscoelastic in nature, and Ortega extended the equation of Lockhart's to take into account the elastic part of the deformation (Ortega, 1985, 2017; Ortega *et al.*, 1989, 1991, 1995; Geitmann and Ortega, 2009; Pietruszka, 2013). In this new version of the theory, the wall is modelled as a linear viscoelastic Bingham fluid. In the frame of the alternative Loss Of Stability (LOS) theory (Wei and Lintilhac, 2003), the critical value for wall stability is directly correlated to wall elasticity (Lintilhac, 2014).

1.1.4.1.2. Cell growth and variation of the cell wall mechanical properties

Beyond the possibility of regulating the tensile stress itself (for example by gradient of wall thickness, see **Part 1.1.4.6**), the extension of any elemental piece of cell wall also depends on the "local compliance" of the cell wall to the local tensile stress (Harold, 1990, 2002; Schopfer, 2006; Geitmann and Ortega, 2009). Whether or not an elemental piece of cell wall yields in response to the tensile stress, and at which rate, depends on the local mechanical properties and/or "remodability" of the cell wall. These features are all integrated in a single parameter, called the extensibility. This parameter describes the rate of expansion of an elemental piece of cell wall as a function of the tensile stress value (note, however, that the definition of extensibility vary considerably according to the authors; see Cosgrove, 1993a, 2016a). This value can differ between different directions along the cell surface, conferring the wall with anisotropic properties (Baskin, 2005). The control of cell elongation is thus considered to reside into the modulation of the intrinsic wall mechanical properties, usually by its chemical composition and ultrastructure (Chebli and Geitmann, 2017). The mechanical behaviour of the extracellular wall would represent a key control hub which can be finely regulated by structural or metabolic molecular factors, its composition in polymers (polysaccharides or proteins), their cross-linking bonds and the overall network organization (Szymanski and Cosgrove, 2009; Guerriero *et al.*, 2014; Cosgrove, 2016*a*; Chebli and Geitmann, 2017). This allows to link the protein content, structures and activities that result in the synthesis of wall constituents, the cellular dynamic controlling their secretion to the edge

of the cell, and the mechanical processes of localised cell expansion (Mirabet *et al.*, 2011, page 201; Bidhendi and Geitmann, 2016; Chebli and Geitmann, 2017).

Yet, the link between the various wall mechanical parameters listed above and the wall extensibility is still poorly understood, even in land plants which are by far the most studied walled organisms regarding this topic. Indeed, the real mechanical nature of the wall involved in growth is still hotly debated (see **Part 1.4.4.4** and **5** below for a discussion). Two main theories of walled cell growth, the classical theory of Lockhart (1965) and the Loss of Stability theory (LOS; Wei and Lintilhac, 2003, 2007; Lintilhac, 2014), both exposed in **Part 1.1.2,** describes how the cell wall exert a mechanical control over the growth of walled-cells. The first theory by Lockhart (1965) is by far the most accepted of both, and has often led the different authors to consider the wall expansion to result from the plastic or viscoplastic expansion of the wall. In this frame, the expansion of the wall would correspond to the creeping of polymers, passively sliding against one another in response to stress, and therefore on the strength and abundance of non-covalent bonds between polymers and of steric hindrance counteracting the sliding of polymer.

1.1.4.1.3. How to generate localised wall expansion like-tip growth?

If cell growth is regulated by the mechanics of the wall, growing zones should correspond to area of high wall deformability, while non-growing zone correspond to area of higher rigidity (Geitmann and Ortega, 2009). Such spatial variations of wall mechanics would be correlated to local variations of wall chemistry (polymer composition, density, arrangements and cross-links, pH, ions and ROS concentration, water content…) that could impact those mechanical properties.

As tip-growing cells correspond to a single “protrusion” where growth is restricted to the terminal apex, it has been proposed that this extreme form of polarised growth could result from a localised area of great wall deformability at the apex coupled to rapid stiffening of the wall “flows” out of this zone, blocking further expansion and leading to the formation of the definitive tubular shape of the cell. In other words, growth patterning observed in tip-growth cells would result from sharp gradient of wall deformability. This appeared as a sensible mechanical patterning strategy, especially because of the paradox that growth occurs in the apical dome, where the wall tensile stress is logically lower than in the non-growing shanks (see **Part 1.1.2**). This major concept has emerged decades ago in the tip-growth literature (Hejnowicz *et al.*, 1977; Wessels, 1988; Steer and Steer, 1989; Harold, 1990, 2002; Koch, 1994), drawn from a very old hypothesis by Reinhardt (1892), and was first formally conceptualized into theoretical models such as the viscous model of Wessels (1988, 1990, 1993) and the general “soft-spot” model of Koch (1994).

1.1.4.2. Experimental evidence for a cell wall stiffness gradient involved in tip growth

Direct experimental evidence in support to the cell wall mechanical gradient controlling tip-growth are scarce and mainly indirect. Evidences for the molecular bases of such mechanical gradients are even rarer. Yet, during the 2000’s, the development of improved microscopic and (fluorescent) staining techniques to detect wall polymers in situ (Knox, 2008) and of cytomechanical techniques to measure mechanical properties at sub-cellular

resolution (Geitmann, 2006*a*; Routier-Kierzkowska and Smith, 2013) allowed to acquire interesting data on some of the most studied tip-growing systems.

1.1.4.2.1. Pollen tube

Direct wall mechanical gradients measurements in the pollen tube. The pollen tube of angiosperms is, by far, the most studied tip-growing cell type, and most studies dedicated to unravel the mechanics of the cell wall and its link to tip-growth have been conducted on this model system. Taking advantage of micro-indentation techniques, Geitmann and Parre, (2004) and Parre and Geitmann (2005a) showed that the wall is softer and displays viscoplastic behaviour in the apical dome, while distal regions are stiffer and purely elastic, with a progressive gradient from the apical dome to the shank. Those results indicated that the wall has both elastic and plastic properties in the apical dome while the plastic component is rapidly lost (or become undetectable) and the elasticity is reduced twice (i.e. the wall stiffens) at the base of the dome and further along the shank. Such rapid gradient of wall mechanics would allow expansive growth in the former region, then would block wall expansion to establish and maintain the tubular shape (Geitmann and Parre, 2004; Parre and Geitmann, 2005*a*). Moreover, a finite-element model of a pollen tube probed by an indentation stylus demonstrated that the measured wall stiffness was overestimated in the apical dome because of the local cell geometry, suggesting that the apical growing region could be even softer than what was measured (Bolduc et al., 2006). Later, Zerzour and colleagues (2009) used the same microindentation technique to show that, on swollen tips of pollen tube which growth had been temporally arrested, local softening of the wall predicted the site of emergence of a new apical growth site. They also demonstrated that, during normal oscillatory growth of the pollen tube, a phase of increased apical wall softness preceded a phase of high growth rate. All these data supported the idea that increased wall deformability at the apex (elastic, plastic, or both) coupled to rapid stiffening away from the growth zone was at the basis of the biomechanical functioning of pollen tube tip growth (Geitmann, 2006*b*).

The chemistry underlying the wall mechanical gradient. As soon as a mechanical gradient of wall properties was revealed in pollen tube, the same authors looked at the chemical components of the wall that would underpin it. The wall of the pollen tube is mainly made of pectin, and this class of matrix polysaccharides has long been suspected to impact the mechanical properties of wall in the pollen tube (Steer and Steer, 1989). Geitmann and Parre (2004) observed that homogalacturonnan pectins are highly methylesterified in the apical dome, while they become largely demethylesterified in the shanks; this pattern was the best predictor of the longitudinal distribution of wall stiffness. When pectins in growing pollen tube were demethylesterified by treating the pollen tubes with exogenous pectin-methylesterase, the wall stiffened at the apex and growth stopped (Bosch *et al.*, 2005; Parre and Geitmann, 2005*a*), confirming that demethylesterified pectins were responsible for the softer, plastic wall in the dome, allowing its expansion during growth. Methylesterified pectins cannot be cross-linked by calcium (Ca^{2+}) ions and so form only soft, highly deformable gels, while demethylesterification allows cross-linking through calcium chelation, resulting in stiffer elastic gels (Grant *et al.*, 1973; Sato *et al.*, 2008; Mohnen, 2008; Caffall and Mohnen, 2009; Levesque-Tremblay *et al.*, 2015; Bidhendi and Geitmann, 2016). This characteristic distribution of methylesterified and demethylesterified pectins was confirmed in several angiosperm species (Wu *et al.*, 2008; Dardelle *et al.*, 2010; Chebli *et al.*, 2012). Although other wall polysaccharides have been suspected to play a role in the rapid stiffening of the wall along the shank of the pollen tube, including callose (Parre and Geitmann, 2005*b*) and cellulose (Lazzaro *et al.*, 2003; Aouar *et al.*, 2010), pectins soon became the main

component thought to mechanically control cell wall expansion during pollen tube growth (Bidhendi and Geitmann, 2016).

Generating the precise gradient of pectin methylesterification. Additional studies aimed to understand how the cell controls the level of pectin methylesterification along its meridional profile in order to generate the proper mechanical gradient necessary for normal tip-growth. The pectin methylesterases (PMEs), enzymes that remove the methyl function from homogalacturonnan chains, were soon designated as the main molecular player involved in the process (Bosch and Hepler, 2005). However, plenty of other chemicals players are also thought to play a role in the control of wall extensibility, including reactive oxygen species (ROS), calcium ions, pH, and other wall polysaccharides like cellulose and callose (Hepler *et al.*, 2013; Mollet *et al.*, 2013; Julien and Boudaoud, 2018). To what extent each of this parameter control tip-growth, and how they interact with each other to control wall mechanics and expansion will require a model system approach (Hepler *et al.*, 2013).

1.1.4.2.2. Fungal tip-growth (hyphal or yeast)

Positive wall mechanical gradients measurements in fungal hyphae. Compared to the pollen tube detailed above, the search for wall mechanical gradients, and corresponding biochemical gradients that would underpin them, are much less advanced in true fungi (eumycetes). Ma et al. (2005) measured the wall elastic modulus and adhesion at the tip and along the shanks of living hyphae of *Aspergillus nidulans* by AFM in force spectroscopy mode (FS). In parallel, the texture of the cell surface was measured by AFM imaging. Their results showed a small gradient of stiffness from the very tip to the shank (Ma *et al.*, 2005). Their values for old regions (more than 20 µm away from the tip) were in accordance with another AFM study performed in *A. nidulans* growing hyphae (Zhao *et al.*, 2005*b*).

Wall chemistry underlying the positive wall mechanical gradient. The positive stiffness gradient was paralleled by an opposite gradient in adhesion. This opposite gradient indicated that the wall stiffness gradient was correlated to the chemical nature of the wall. AFM imaging of the surface of the hyphae also revealed differences in the topology of the hyphal surface, characterised by small, ellipsoid structures 20-30 nm in diameter. In young hyphal regions, these structures were elongated with a preferential orientation in the circumference of the wall, while in older regions, these structures were shorter and rounder (Ma *et al.*, 2005). The authors tentatively attributed these structures to be triple helices of (1-->3)-β-D-glucans or glycoproteins. However, many more biochemical characterisations of hyphal wall along the longitudinal axis remain to be conducted in order to connect the observed gradient of stiffness to wall chemistry. Indeed, the exact chemical nature of surface structures observed by Ma and collaborators (2005) remains to be characterised in more details; moreover, they only represent the outermost layer of the wall, that could be different from the most load-bearing layer. To our knowledge, a precise gradient in the distribution or the cross-linking level molecular components of along the hyphal longitudinal axis has not been displayed yet (Bowman and Free, 2006; Riquelme *et al.*, 2011).

Nevertheless, a model of wall deposition and progressive cross-linking based on the knowledge of fungal wall formation and composition was proposed a long time ago by Wessels (1990, 1993), which fits quite well with the observed stiffness gradient observed in *A. nidulans.* In this model, progressive cell wall stiffening occurs by progressive formation of chitin chains by membrane-located chitin-synthase, and their subsequent crystallisation into microfibrils (α-chitin). In parallel, newly deposited β-(1→3)-glucan chains get progressively branched in position C6 and are covalently linked to some of the chitin chain before their

crystallisation. This would allow the cross-linking of chitin MFs by interlocking scaffold of glucans (Wessels, 1990) and be the basis for wall maturation and stiffening during hyphal tip growth. Direct evidence for correlation between the degree of chitin cross-linking and wall mechanics has not been given yet.

A negative stiffness gradient in the mating projection of the yeast. The results described above should be nuanced by more recent experimental data acquired on the cell mating protrusion in reproducing baker's yeast (*Saccharomyces cerevisea*) by Goldenbogen et al. (2016). The more or less elongated conical projection resembles a hypha emerging from the spherical main cell. The authors measured the stiffness (elastic modulus) of the wall i) in the main cell body (yeast cell *per se*); ii) in the collar, i.e. at the junction zone between the cell body and the protrusion; iii) in the "shaft" and iv) at the tip of the protrusion, using spectroscopy AFM, in Quantitative Imaging (QI) mode to obtain high-resolution maps of cell surface properties. They used only low indentation depth, much lower than the cell wall thickness, and very thin probe tip to measure only the elastic properties of the wall and exclude the mechanical forces generated by the turgor pressure. Their results showed that the wall was significantly softer in the cone-shaped (shaft) region of the mating projection and in the collar region, than in the rest of the cell surface. Surprisingly, the extreme tip was stiffer, keeping a comparable elastic modulus to that of the spherical cell body (Goldenbogen *et al.*, 2016). Similar values were obtained for in-plane moduli value using cell shrinking – inflation series under short osmotic stress shocks, suggesting a low wall anisotropy between in-plane and normal directions. Thus, growth of the hypha-like mating projection of yeast is associated with an opposite mechanical gradient, compared to the pollen tube and to the hyphae of *A. nidulans*. The authors also demonstrated, using computational modelling, that such spatial distribution of elasticity is important for the whole cell morphology, but cannot be used as a proxy for the real cell wall extensibility (see **Part 1.1.4.3.2**, Goldenbogen *et al*., 2016). However, it should be noted that, in this particular case, the site of wall expansion is not known, even though tip-growth has been demonstrated in similar mycelial protrusion from *Candida albicans* cells (Staebell and Soll, 1985).

1.1.4.2.1. *Vaucheria terrestris*: an interesting case of tip growth

A common problem with the previously cited AFM or micro-indentation studies conducted in land plants and fungi is that these techniques provide the wall stiffness mainly in the normal direction. Yet, the mechanical parameters in that direction are less relevant for growth control than that measured into the plane of the wall (Cosgrove, 2016*a*). Direct measurements of the in-plane wall extensibility in a tip-growing cell are very rare in the literature. Such valuable measurements were made, though, on the apical cell of *Vaucheria terrestris*, a xanthophycean giant celled-algae (Mine and Okuda, 2003; Mine *et al.*, 2008). This group of algae belongs to the Stramenopile kingdom, and is therefore more closely affiliated to brown algae and oomycetes than to land plants and fungi (Baldauf, 2008; Guiry, 2012). Even though the study was conducted on apical cell wall fragments excised from the rest of the filaments and cleared out of cytoplasm (cell wall "ghosts"), it is particularly interesting and deserves some special consideration here. However, it is not known whether those values reflect true viscoplastic or viscoelastic properties of the wall because the wall retraction after wall rupture was not monitored (Mine and Okuda, 2003).

Results showed a global positive gradient toward the tip, with larger extensibility at the extreme tip, and decreasing toward the base of the dome. Low but positive extensibility was also observed on sub-apical areas of the shank, where the wall creep still occurred (Mine and

Okuda, 2003). Interestingly, this extensibility gradient was shown to be generated by wall proteins. Pre-treatment of wall ghost with protease for 24 h before the experiments largely increased the overall extensibility and abolished the gradient in the dome. Moreover, circumferential creep was also observed along the shank upon protease treatment, while it is not observed there in untreated wall ghost. These results show that unknown wall proteins are responsible for the gradient of wall extensibility along the meridional profile of the tip-growing cells, some increasing it at the extreme tip of the cell while other reducing it in subapical areas (Mine and Okuda, 2003). These wall proteins would especially play a role in reducing the wall extensibility in the circumferential direction at the base of the dome and on the shank, against the larger tensile stress in that direction, allowing the maintenance of the tubular shape. These putative structural proteins would replace the mechanical role normally assigned to cellulose MFs, as the latter are orientated in the longitudinal direction in *V. germinata* (Kataoka, 1982). A population of wall proteins seems specifically involved in increasing the extensibility at the extreme tip. However, a specific matrix component embedding the cellulose microfibrils was shown to increase the extensibility at the tip of *V. terrestris* emerging buds, which appeared to be different from proteins (Mine *et al.*, 2007). This indicates that the control of the cell wall extensibility differs between steady-state growing apical cells and emerging buds. A putative negative wall pH gradient (from alkaline to acid) along the meridional profile may also generate the extensibility gradient (Mine and Okuda, 2003), but the actual pH of living cell wall remains to be observed for now. Alternatively, another interesting hypothesis is that the cytoskeleton may exert "additional forces" generated on the external wall, impacting on its local compliance to turgor-generated stresses (see **Part 1.1.3.2**). These forces could be generated by the actomyosin network that could further push on the cell wall in the apical-most area of the dome while reinforcing it in the shanks (Mine and Okuda, 2003). This hypothesis is possible considering the existence of an apical cap of AFs revealed by fluorescent labelling (Alessa and Oliveira, 2001).

1.1.4.2.2. Putative mechanical gradient in oomycetes hyphae.

In hyphal oomycetes, a putative mechanical gradient starting from the extreme tip has not been sought. However, some data pointed toward the possibility of a softer apical wall compared to the “mature” shank. Money and Harold (1992) showed that the tensile strength of the apical wall of *Achlya bisexualis* decreased in proportion to the decrease in turgor pressure in hypertonic conditions, as measured by apex bursting in response to an increased turgor. If the wall has a constant thickness along the cell surface (as in *Saprolegnia ferax*, cf Heath and Kaminskyj, 1989) then cell bursting should occur in the shank and not at the apex, because the tensile stress is higher in the shank. So, this result suggests that the apical wall of *A. bisexualis* has a gradient of strength starting from the very tip of the cell. Considering the wall tensile strength as a proxy to wall extensibility, and knowing that this organism does not regulate its turgor pressure (Money and Harold, 1992, 1993), the authors hypothesised that the cell could actively regulate the wall extensibility (strength) in the growing tip to maintain wall expansion in keeping with varying levels of tensile stress. Money and Hill (1997) showed that the apical wall softening was correlated to higher secretion of endoglucanases in the extracellular medium. As extracellular enzymes are generally excreted at the apex, a gradient of delivery and/or the time-dependent activity of endoglucanases could create a gradient of apical wall softness. However, this hypothesis has not been tested further in oomycetes, and these preliminary results dealt with the apical wall strength, i.e. the maximum tensile stress it can endure before tearing, a parameter not necessarily linked to the wall deformability.

1.1.4.3. Theoretical models supporting the "wall mechanical gradient" concept

Many of the theoretical models have tested the "wall mechanical gradient" concept and have shown how it could efficiently account for tip-focused cellular expansion. However, the mechanical nature of the cell wall (depending on its supramolecular organisation), and consequently the nature of its expansion under the turgor-generated tensile stress differ between the models. Roughly, theoretical models of tip-growth can be classified in two main categories: the "**plastic models**", in which the wall expansion corresponds to an irreversible, somewhat viscous deformation, in accordance with the Lockhart's hypothesis, and the "**elastic models**", in which the expansion simply corresponds to the stretching of an elastic material, like a loaded spring, that is reversible in nature (Goriely and Tabor, 2008). In the second category of model, the molecular mechanisms transforming the elastic stretching into an irreversible wall expansion are generally not clearly defined; such mechanisms should be more complex than that involved in a pure viscous flow.

1.1.4.3.1. The plastic tip growth models

Most mechanical models of plant cell tip growth rely on the mathematical formalism of Lockhart (1965), where the cell wall extension is considered the flow of a very viscous fluid under a tensile force generated by the turgor (Goriely and Tabor, 2008; Kroeger and Geitmann, 2012*b*). The implicit assumption in those models is that the polymers constituting the cell wall network are only connected by non-covalent, low-energy ionic bonds, and consequently slip against each other without being stretched or deformed (Kroeger and Geitmann, 2012*b*). Usually, only the in-plane tensile stress (shear stress) is taken into account, as most of the work of expansion occurs in those directions. In the classical acceptance of the Lockhart's theory, the wall extensibility is considered as an inverse of wall viscosity (Geitmann and Ortega, 2009; see above, **Part 1.1.2**). During tip-growth, gradual reduction of the wall expansion (strain) along the meridional contour of the cell is due to an increase in the wall viscosity (decrease in extensibility) or in the yield-threshold (Goriely and Tabor, 2008).

The soft-spot viscous model for steady-state tip-growth of eumycetes hyphae. One of the oldest formal theory of a "cell wall mechanical gradient" for tip-growth was the soft-spot conceptual model, developed primarily for hyphal fungi (Wessels, 1986, 1988, 1990, 1993; Koch, 1994). It was the first comprehensive, self-consistent steady-state mechanical model of tip-growth. The model is math-less and it does not include the notion of a yield-threshold, below which the cell wall expands only elastically. Though, the authors stated that the cell wall is viscoelastic at the tip, and only elastic in the non-growing tubular shank. The model is built on the contemporary knowledge about wall composition and synthesis in the apical region of fungal hyphae. The hyphal wall was regarded as a "fiberglass" material, with unidirectionnal fibers (chitins microfibrils) evenly distributed into a glass (matrix) that gradually sets by cross-linking between the matrix polymer and with the microfibrils (Wessels, 1990; Koch, 1994). In the growing tip, the wall is plastic enough to yield irreversibly, while rapid crystallisation of chitin fibrils and cross-linking with glucans rapidly increases the viscosity (in the order of some minutes for rapidly growing hyphae), slowing growth until complete arrest at the base of the expanding dome (Wessels, 1990).

The originality of this model is that it proposed a somewhat integrated mechanism between wall deposition and expansion, and finely describes how a gradient of deposition of wall material (i.e. exocytosis of glucans and synthesis of chitins by membrane-bound chitin-

synthases) is coupled to the opposite gradient of wall expansion in the apical dome to maintain a local "soft-spot". The cell wall material is deposited on the inner face of the apical dome, with a decreasing rate from the extreme tip to the base of the dome, where it becomes null. This newly deposited layer of cell wall consists of a mixture of unbound polymers that cannot yet bear tensile stress, but immediately start to set, whether it is stretched or not. At any point of the cell surface, all layers are expanded at the same pace, the strain rate depending on the viscosity of the older, outer, more cross-linked layer. The outer layer thus controls the maximum rate of wall expansion that can happen. The in-plane expansion makes the wall layers thinning down, and simultaneous addition of new wall materials makes them displaced from the inside to the outside face of the wall. This outward migration is complete only for those that are deposited at the extreme tip, partial for those deposited at a point between the extreme tip and the base of the dome, and null for those deposited at the boundary between the apical dome and the shanks. In this region, the outermost layer is stiff (viscous) enough to block wall expansion, establishing the cylindrical shape, and the underlying layers only set without expansion, furthering the maintenance of the shank.

The strength of the model is that it predicts several experimental observations, like the longer apical dome in fast-growing hyphal fungi compared to slow-growing fungi. The model also predicts that, if the growth is blocked, the continuing cell wall stiffening in the dome will ultimately make it too viscous for growth to resume there. Instead, the growth usually resumes by branching at a point slightly distal to the apical dome (Roberson and Rizvi, 1968). However, an important limit of the model is its lack of support by experimental quantitative data pertaining the exact viscous properties of the cell wall, even though a slight stiffening along the hyphae has been measured by AFM (Ma et al., 2005; Zhao et al., 2005; see **Part 1.1.4.2.2**).

The viscoplastic model of Dumais et al. (2004, 2006) for root hairs of terrestrial plants. The first quantitative, mathematical model describing tip-growth with a "viscous" wall expansion is the viscoplastic model of Dumais et al. (2004, 2006) that has been primarily developed for the root hair of land plants (*Medicago truncatula*), but which is suited to other cell types in various taxa (Dumais *et al.*, 2006). The model takes into account the cell geometry (expressed as the local curvatures of the cell surface), cell wall thickness and turgor to calculate the tensile stress of the cell surface, in both the meridional and circumferential directions. In parallel they computed the pattern of cell wall strain along the apical dome from time-lapse of living *M. truncatula* root hair labelled with fluorescent surface markers (Shaw *et al.*, 2000; Dumais *et al.*, 2004), an approach similar to that previously used on tip-growing rhizoids of the green alga *Chara* (Hejnowicz *et al.*, 1977). Any point of the cell surface was assimilated to an infinitesimal piece of wall, on which both the tensile stress and the strain was calculable in the three spatial dimensions. This allowed to quantify the relationship between the two parameters along the cell surface, as a proxy of the local wall extensibility. Dumais and colleagues (2004, 2006) then calculated the constitutive relation between the wall stress, the wall viscoplastic properties and the strain rate. Congruent with Lockhart's law, the wall flows plastically if the local tensile stress is above the local yield threshold σ_y, and the strain is then proportional to the tensile stress above σ_y and to the wall extensibility factor Φ. Their model predicts that, considering the wall thickness constant over time, the cell wall extensibility must vary steeply along the meridional axis to restrict surface expansion to the dome. Therefore, the extensibility must be higher (lower viscosity) in the apical dome and then must decrease rapidly for the cell wall to transit from the ellipsoid to the tubular shape. The same result can be generated by an opposite gradient of yield-threshold (lowest at the extreme tip, then rapidly increasing toward the shank). A wide range of gradient for these parameters can generate similar steady-state tip shapes, indicating the robustness of the

system facing spatial and temporal variability in wall stiffening. However, those gradients are totally *had-hoc* and cannot inform about the mechanisms that generate and sustain them. In parallel, the model also allowed the authors to foresee that the wall must be at least transverse isotropic, with the same viscoplastic properties between the "in-plane" directions (meridional and circumferential) but different from the orthogonal direction (*z* direction). Thus, the simple maintenance of a local “soft-spot” is sufficient for sustained tip-growth and does not require additional anisotropies. This idea is sound as wall polymers are generally thought to be mostly aligned parallel to the cell membrane, especially the cellulose MFs, but with no special orientation between the meridional and circumferential directions. This was confirmed for cellulose MFs in radish root hairs (Newcomb and Bonnet, 1965).

Bernal et al. (2007) developed a similar model in which the cell wall was modelled as an inflated rubber balloon which stiffness increases with its level of stretching (used as a proxy of viscous flow), a process called “strain-hardening” (Dumais *et al.*, 2006). The tubular rubber balloon has both an inflated part and a narrower, uninflated moiety, both regions being separated by the “apical dome”, in which the elastic rubber of the non-inflated region is progressively stretched (enlarged) and incorporated into the inflated region. The process makes the “apical dome” advance, mimicking the elongation of a tip-growing cell, with the inflated part of the balloon representing the shank of the cell. Strain-hardening lowers and finally blocks surface expansion, making the transition from apical dome to tubular shank. The observed pattern of strain rate in the “apical dome” closely matches that observed in living *M. truncatula* root hair, although the rubber balloon is completely isotropic. This results suggest that strain-hardening would be a sufficient mechanism able to generate a sharp gradient of wall deformability leading to tip growth. Moreover, strain hardening would naturally result from the extension and straightening of cross-linked network of polymers (Bernal *et al.*, 2007), and thus would more realistically represent the mechanical behaviour of a plant cell wall than a purely viscous material, which would require a sharp gradient of viscosity to block growth. It could represent a simple, straightforward way to generate gradients of σ_y and Φ, as predicted by the viscoplastic model, without requiring additional molecular regulations of the wall properties along the meridional profile of the cell. Such elegant mechanism still waits for experimental validation.

The generalist viscous model of Campàs & Mahadevan (2009). The model of Campàs and Mahadevan (2009) reproduces the tip shape and growth rate of tip-growing cells simply by considering the delivery of a fluid wall at the tip, which expands while the viscosity (μ) progressively increases toward infinity, so that local wall expansion asymptotically tends to 0, thereby establishing a tubular shape. No anisotropy between the meridional and circumferential directions was necessary. This generalist model, that is applicable to any tip-growing organism, does not even require any yield-threshold as in the Lockhart’s equation. In parallel a negative gradient of wall material delivery rate (γ) was introduced, with a maximum at the tip, defining a finite area of wall delivery. Simulations showed that these two parameters were sufficient to reproduce a steady-state tip growth with constant dome shape and final tube diameter. The profiles of μ and γ will determinate the growth rate, the shape of the apical dome and the final tube diameter, with a large range of possible profiles generating a diversity of tip shapes, some resembling actual tip-shapes observed in different organisms (Campàs and Mahadevan, 2009; Campàs *et al.*, 2012, page 2012).

Generating the gradient of wall viscosity: the role of wall deposition. During steady tip-growth, a major problem is to maintain a constant gradient of wall mechanics despite the fact that wall material will unescapably be chased off the apical region. The above-mentioned models have often pointed toward the wall delivery as the key process for maintaining such “soft-spot”.

Assuming the wall to be a viscous liquid, the newly delivered wall building material could be imagined to mix and diffuse rapidly in the wall layers, like droplets dropped on a liquid layer. However, the wall polymers of plants, fungi and algae are much more complex materials than a simple liquid. The gradual increase in wall "viscosity", or more generally in "plasticity", is dependent on extensive cross-linking of polymers that progressively increase the density of chemical bounds and establishe complex macromolecular networks that mechanically behave more like a solid (Cleland, 1971). Though, the delivery of fresh, unbound material is generally considered to result in an averaging of the mechanical properties between the newly-delivered and the pre-existing, cross-linked materials (Kroeger and Geitmann, 2012a). In other words, the rate of delivery of new uncross-linked wall material on the inner face of the wall would directly affect the local bulk mechanical properties of the wall at the point of delivery. The former being less viscous because of lower cross-linking levels or polymer lengths, this would result into lowering the wall viscosity at the site of wall deposition, locally increasing viscous wall expansion. This concept is inherent of most of the viscous models cited above, including that of Bernal et al. (2007), the generalist model of Campàs and Mahadevan (2009) and others, like the similar, "wall ageing" model by Eggen et al. (2011). However, the relationships between the ratio of cross-linked to non-cross-linked polymers and the bulk wall mechanical properties is probably more complex than a simple "averaging" of these properties, especially because it is not well known how the uncross-linked polymers diffuse in the pre-deposited layers (Hepler *et al.*, 2013). Still, in the more realistic case where the newly deposited material does not mix with the older layers (see above) but forms different layers with different viscosity, the "soft-spot" model showed how a simple gradient of wall delivery, with a maximum at the extreme pole, can generate proper steady tip-growth (Wessels, 1990).

Another difficulty arises from the fact that the molecular mechanisms responsible for wall rigidification (for example any reaction forming new chemical bonds between two polymers) can be independent from the delivery of new polymers, i.e. wall setting would continue whenever wall deposition continues or not. Consequently, to ensure a highly regular tip-growth, the gradient of wall delivery would have to be tightly positioned to the site of the "soft-spot", and delivery rate closely adjusted to the rate of wall stiffening. Thus a control of the delivery rate by the local strain rate, putatively by mechanosensitive proteins in the wall or in the membrane (for example stretch-activated membrane ions channels) has been hypothesised (Wessels, 1990). In the Soft-Spot theory of Koch (1994) the delivery of new material is facilitated in young, low viscous areas, while it is prevented in older, rigidified areas where the matrix is already set. By such mechanism, the formation of a "soft-spot" would trigger the continued fusion of new exocytic vesicles at the same area, keeping the apical wall in a permanent "young" state while being expanding, in a sort of positive feedback loop (Koch, 1994). Nevertheless, it is difficult to imagine how such a simple mechanism would allow the establishment and determination of the size and edges of the growth site. Koch thus proposed that its Soft-Spot concept is coupled to some sort of Vesicle Supply Center mechanism (Bartnicki-Garcia et al., 1989) to bias the wall delivery toward the very tip. However, simulations from the recent modelling studies with varying profiles of wall delivery and wall stiffening rate lead to a diversity of dome shapes that mirrors the diversity of shapes observed in the different phylogenetic groups (Campàs and Mahadevan, 2009; Eggen *et al.*, 2011; Campàs *et al.*, 2012). This suggests that a tight spatio-temporal adjustment of both processes may not be required for the system to function properly, allowing a certain degree of stochasticity. Whatever it be, the diverse "viscous" models all point toward a same, very basic mechanism to control the gradient of wall compliance, suggesting that this would be an efficient mechanism that could have been repeatedly acquired by various tip-growing cell types during evolution.

1.1.4.3.2. The elastic tip-growth models

Alternative tip-growth models consider that the wall expansion is elastic in nature, rather than being the flowing of a viscous material. This would mean that the cell wall polymers (and/or their cross-links) are stretched under the tensile stress, increasing the cell wall surface while storing the mechanical energy and keeping their positions relative to each other. The simplest models use the linear, Hookean elasticity theory, with two major parameters that are the bulk and shear moduli, the first being the Young's modulus (*E*) and the second being the Poisson ratio that represents the ratio of elastic deformation between two different directions (Goriely and Tabor, 2008). However, more adequate models use the exact nonlinear elasticity theory, that can describe large elastic deformations that occur in soft living materials, with apparent stiffness depending on the degree of deformation (Goriely and Tabor, 2003a, 2008). As the wall can be modelled as a shell with a finite thickness that can support bending moments, elastic bending deformations can also be included (Boudaoud, 2003), while plastic models generally only consider the in-plane mechanical compliance of the wall. Alternatively, the elastic deformations may not directly constitute the basis for wall expansion, but could still interfere with the process (Ortega, 1985, 2017; Geitmann and Ortega, 2009). Some models explore these complex relationships and their potential (see the models developed by Goldenbogen et al., 2016).

If the elastic wall deformation stands for wall expansion, thus the mechanical models would integrate growth mechanisms in addition to elastic deformations, allowing the wall extension to become permanent. However, the biochemical reactions or structural remodelling that result in effective cell wall expansion, called "morphoelastic" (Goriely and Tabor, 2008) must be more complicated than that expected for “plastic” model. Indeed, clear hypotheses about such mechanisms are often overlooked in the elastic models of tip growth. This issue point to the hot debate about the real nature of wall expansion. This process may be, actually, subtler than a pure mechanical stretching of the wall, and would rely on complex wall “remodelling” processes that rearrange the spatial organisation of the polymer networks (see **Part 1.1.4.4**).

The non-linear elastic model of tip growth by Goriely and Tabor. The model of Goriely and Tabor (2003a,b) was originally developed to account for tip-growth of Streptomycetes, a group of filamentous bacteria (prokaryote). However, it is generalizable to eukaryotic tip-growing organisms (Goriely and Tabor, 2008). The model draws from the large-deformation elasticity theory to calculate the pattern of wall expansion in the apical growing region as that of a stretchable elastic membrane deformed by the turgor-generated in-plane tensile stress (Goriely and Tabor, 2003a,b). The simulations successfully reproduce the self-similar growth of the Actinomycetes without any need for anisotropic mechanical properties between the three spatial directions. It only relies on the basic assumption of the soft-spot hypothesis of Koch, *i.e.* an extensible apical wall that asymptotically stiffens toward distal regions (Goriely and Tabor, 2008). The "growth" is simulated by a simple re-parameterization of the cell contour after an elastic load under constant turgor pressure, thus taking the stretched cell contour at equilibrium as a new, less-stretched contour out of equilibrium (Goriely and Tabor, 2003*a*). This meridional gradient of cell wall stiffness is calculated as a gradient of “effective pressures” (the pressure that effectively makes the wall stretch), and is described by an equation dependent on two main parameters: i) the gradient of wall material delivery rate, traced on the observed gradient of integration of N-acetyl-glucosamine, one of the building block of the bacterial peptidoglycan wall (Gray et al., 1990); ii) the cell surface geometry (curvature). The wall is very soft at the extreme tip, where the curvature is maximal, and gradually stiffens toward the tubular shanks as the curvature decreases until a tubular shape is obtained, where growth ceases. As a consequence, wall expansion is restricted to the apical

pole, where cell curvature is the highest, and thus the traditional paradox that growth occurs at the apical pole where tensile stress is the lowest, is circumvented in this model. Yet, it is not explained how the curvature would positively impact the elasticity. Goriely and Tabor (2003a,b) hypothesized that the gradient of wall elasticity in the apical region is also generated by the polarized peptidoglycan synthesis in apical wall of Streptomycetes. When adjusted to the profile of peptidoglycan deposition rate experimentally measured on *S. coelicolor* (Gray *et al.*, 1990), the equation describing the wall elastic modulus along the meridional profile accurately reproduced the tip shape of growing filaments. In other words, a high rate of wall synthesis at the tip would give a more elastic wall.

Model of Fayant et al. (2010) (pollen tube). A similar approach to that of Goriely and Tabor was used by Fayant et al. (2010) to model the tip-growth of pollen tube, with the difference that they built a finite-element (FE) model rather than an analytical one. The authors made the assumption that the cell wall expansion at the apex of the pollen tube is elastic in nature, and is subsequently "fixed" in its extended state, resulting in positive growth. The wall elasticity is modelled as a simple Newtonian elastic modulus, that can be different between the meridional and the circumferential axes. The growth is simulated simply by a re-parameterization of the elastically-stretched cell contour, just as in the model of Goriely and Tabor. The simulated strain pattern and dome morphology were compared to the experimental model in order to predict adequate stiffness gradient pattern. Their FE model predicted a slow increase in cell wall stiffness along the major meridional profile in the apical dome, then a steep stiffness increase at the base of the apical dome toward the shank, resulting in the establishment of the tubular shape because of growth arrest. This pattern matches the meridional distribution of methylesterified and de-methylesterified pectins (homogalacturonan), with a sharp transition from methylesterified pectin-rich apical region to a de-methylesterified pectin-rich distal region (Fayant *et al.*, 2010). This pattern also corresponds to the activities of pectin-methylesterase inhibitors (PMEIs) involved in the regulation of pectin de-methylesterification (Fayant *et al.*, 2010).

Dynamic growth model of Goldenbogen et al. (2016) (mating projection of yeast). More recently, Goldenbogen and colleagues (2016) developed dynamic FE models for actively growing finger-like mating projection of *S. cerevisae* (cf **Part 1.1.4.2.2**). The cell surface was represented as a mesh of triangular elements, each potentially having different mechanical properties, curvature and wall thickness. In accordance with the Ortega's development of the Lockhart theory (Ortega, 1985, 2017; Geitmann and Ortega, 2009), the authors made the assumption that the elastic deformation (elastic strain) impacts the plastic deformation and the growth pattern. Some other authors have also explored the complex interplay between the two parts of the wall mechanical behaviour and its significance for the process of walled cell growth, for example Boudaoud (2003). The authors built on the one hand a "steady-state" model, where no growth occurs and in which the wall displays only elastic properties, and on the other hand two "dynamical models", where the mating projection is actively elongating by tip-growth. This corresponds to two different scenarios regarding the interplay of elasticity and plasticity during the growth of the mating projection.

The first version of the dynamic models is a "stress-dependent" model (DM1) where the elastic and "plastic" deformations are independent of each other. The wall expansion is equivalent to a classical plastic yield of the wall directly under the tensile stress, like in the "viscous" models described above. The local expansion rate is given by the classical Lockhart formulae, being proportional to the extensibility and to the tensile stress above a yield-threshold. The growth is predicted to occur at the extreme tip and to need a short-scale gradient of wall extensibility, with the highest expansion rate at the extreme tip, generating a tapered apical dome. In this first version of the model the observed shape of the mating

projection is adequately reproduced. However, it grows longer and larger when the predicted inverted gradient of elastic modulus (based on AFM data and the "static" FE model cited above) is included, compared to a situation where elastic modulus is kept constant over the cell surface. Thus, this model predicts a negative link between the apical wall elasticity and growth at the tip, so that the growth is restricted to the stiffer apical pole. This effect can be increased by the higher tensile stress at the extreme tip that results in locally stiffer wall (Goldenbogen *et al.*, 2016).

The second version of the model is a "strain-dependent", elastoplastic model, where the elastic and "plastic" deformations are correlated. The implicit hypothesis is that the level of elastic stretching experienced by the wall corresponds to a "stored" mechanical energy available for the work of expansion, as in the model of Boudaoud (2003). Therefore, the expansion rate is proportional to the level of elastic stretching, and as a consequence correlated to wall "softness" (the inverse of the elastic modulus). A similar hypothesis has been advanced for the growth of the fission yeast cell (Davì and Minc, 2015). In this second version of the model, the extensibility is thus called the "strain-dependent extensibility" and the local expansion rate is proportional to this extensibility factor and to the elastic volumetric strain above a "strain threshold". Again, the model effectively reproduces the observed cell shape, with a longer mating elongation when the inverted gradient of stiffness is included. The difference with the first version of the model is that the mating projection is slightly larger, and the highest expansion rate is predicted to be positioned in an annulus-shaped region centred on the extreme tip, giving a blunter apical dome shape (Goldenbogen *et al.*, 2016). The higher wall stiffness at the extreme tip would thus relegate the growth on the softer "shoulder" of the growing dome. However, the stiffness gradient along the mating projection could not generate by itself the adequate pattern of wall expansion, and a gradient of plastic extensibility needed to be introduced to correctly simulate the growth of the mating projection. This important result shows that, even if wall elasticity were positively correlated to the wall ability to expand, it cannot be the only determinant of extensibility. This demonstrates that other cellular determinants are involved in polarised growth in *S. cerevisiae* that remain to be characterized.

These models by Goldenbogen and colleagues offer interesting insights into the role of wall elasticity in the process of cell elongation and how sub-cellular variations of this parameters could impact localised cell growth activities. To gain further understanding about the role of elasticity, it would be interesting to discriminate the two opposed scenarios mentioned above by experimental testing, including a precise quantification of the curvature and strain profile of the mating projection during growth, to compare it to the divergent predictions of the models.

1.1.4.4. Limitation of the wall mechanical gradient concept

1.1.4.4.1. Limitation of the "cell wall mechanical gradient" models

Apparent from the experimental and theoretical studies cited in **Part 1.1.4.2** and **3**, it is clear that the mechanical nature of the cell wall deformation during tip growth is far from being solved. This is a major pitfall in the "wall mechanical gradient" concept of tip-growth, because it is not clear how the mechanical properties measured or predicted in those studies impact the process of wall expansion. The overall mechanical nature of plant, algal and fungal

walls in itself has been a matter of debate for decades (Cleland, 1971), and several models, sometimes quite exotic, have been devised for them (for example a model of wall structure as a "liquid crystal", Vian *et al.,* 1993). Below is a brief summary of the debate regarding the limiting role of wall intrinsic mechanical properties in plant cell growth, which is meant to point toward the limitation of the "cell wall mechanical gradient" as a sufficient physical patterning agent for the process of tip-growth.

1.1.4.4.2. The wall expansion cannot be a simple "plastic" or "viscous" flowing of the wall

The initial biophysical theory of plant cell growth of Lockhart (1965) represented the wall as a viscous fluid, passively flowing under the tensile stress. Such idea has been repeatedly opted for by most of authors working on cell- and tissue-growth of plant or fungal organism (Cleland, 1971; Taiz, 1984; Cosgrove, 1986). However, it has long been argued that modelling the wall as a highly viscous liquid is too simplistic, and sometimes not even a realistic approximation of the wall mechanical behaviour (Dumais, 2013). The "viscous" parameter is actually considered only as a "proxy" for wall remodelling, involving in part the *in muro* metabolism and involving different wall proteins (Dumais, 2013; Julien and Boudaoud, 2018, and see below the cell wall loosening theory of D. Cosgrove). Its role would be only partial, minor or even inexistent (Cosgrove, 1993a,b, 1997, 2016a). However, this opinion is still debated. Some authors argued that a purely viscous behaviour can still be a good approximation of an elastic deformation converted into an irreversible strain (Goriely and Tabor, 2008; Dumais, 2013). In the case of the pollen tube, Campàs and Mahadevan (2009) argued that the viscosity represents a realistic properties of the pectic wall specific for the pollen tube, and that viscous flow accounts for its mechanical expansion at the apex. Indeed, the wall is very rich in pectin, a component which can display viscous behaviour *in vitro* when the density of Ca^{2+}-cross-linking is below a threshold value (Campàs and Mahadevan, 2009).

1.1.4.4.3. Wall elasticity may be important for wall expansion, but its role remains unclear

Even more than with the "viscous" character of the wall, the role and importance that wall elasticity may play in the regulation of wall expansion is highly debated. At least, it is now recognized that the mechanical energy stored in the form of elastic stretching of the wall polymers can be used for the process of wall expansion (Cosgrove, 1986; Dumais, 2013) and thus that wall elasticity does play a role of some sort in cell and tissue growth and morphogenesis (Braybrook and Jönsson, 2016). But diametrically diverging opinions have been expressed by various authors as to whether elasticity promotes or inhibits wall expansion. For some, elasticity may negatively regulate the wall expansion. The dimensional analysis of Ortega's extended equations (Ortega, 2017) reveals three dimension-less parameters Π that impact the cell growth rate. One of the dimensionless parameters, Π_{pe}, represents roughly the ratio of relative plastic deformation rate over relative elastic deformation rate (volumetric, relative rate in both case). During stress relaxation (see below), the time constant of the turgor decays over time is equal to $1/-\Pi_{pe}$, so the higher the plastic deformation rate over the elastic deformation rate, the faster the stress relaxation. Elastic deformations store mechanical energy in the wall, while plastic deformation dissipate it into thermal energy by stretching wall polymers and their bonds (Ortega, 2017). Π_{pe} is largely

superior to 1 in the few cell types where it could have been measured, meaning that the plastic deformation rate largely exceeds the elastic deformation rate in those cell types. This would mean that during expansive growth, the wall does not stock large amount of mechanical energy in the form of elastic stretching, but rather would use it for the work of wall expansion (Ortega, 2017). The author concludes that experimental measurement of the elastic deformability of cell surface is not relevant to understand the process of cell morphogenesis. In apically growing cells, especially, the observed elasticity gradient in the pollen tube (Geitmann and Parre, 2004; Parre and Geitmann, 2005*a*) and in *A. nidulans* hyphae (Ma *et al.*, 2005) would not explain the restriction of growth at the apex. However, such hypothesis fits the inverted gradient observed in the mating projection of yeast by Goldenbogen et al. (2016) (see above). Their "stress-dependent" dynamical FE model suggested that the stiffer apical wall compared to the "shaft" allowed locally increased "plastic strain", i.e. higher wall extensibility. The interpretation of Goldenbogen and colleagues is comparable to Ortega's: lower elastic strain (correlated with higher stiffness) at the extreme tip dissipates less mechanical energy and locally increases the tensile stress. This higher tensile stress would represent higher mechanical energy for the work of wall expansion, even though this effect is insufficient in itself to restrict growth at the extreme tip (see above).

On the contrary, other authors consider that elasticity positively impacts the wall expansion. For example, in the frame of the alternative LOS theory, expansive growth would advent only in the area where the critical value above which the wall stability is lost, P_{CR}, is minimal (Wei and Lintilhac, 2003, 2007). This model represents a convenient biophysical mechanism to drive expansion in only a very restricted area of the cell surface, a situation typical of tip growing cells. As explained above, P_{CR} is proportional to the wall elastic modulus, *i.e.* in the case of tip-growing cells, a decreased wall stiffness at the apex, as observed in the pollen tube will reduce P_{CR} there, potentially enough to restrict growth in these area. Outside the frame of the LOS theory, the "elastic wall growth" is implicitly conceptualized as a kind of biphasic, incremental process during which the cell wall is first elastically stretched, then some of the strained bonds and/or polymers would be cut in part and replaced by new, unloaded bonds, making the wall expand and some of the tensile force transferred to the newly formed bonds. Consequently, the larger the elastic strain, the larger the "deformation" that can be fixed in place, and so the expansion rate will be correlated to softer wall that gives higher strain (Boudaoud, 2003; Minc *et al.*, 2009), with an effective expansion only when the wall has reached a certain degree of elastic deformation, a "strain-threshold" (Davì and Minc, 2015; Goldenbogen *et al.*, 2016). If true, so the wall expansion would be a subtler process than a simple mechanical stretching of the wall, and the wall mechanics at sub-cellular spatial resolution would actually not be so strongly tied to the expansion pattern.

1.1.4.5. Beyond the wall mechanics: tip-focused wall expansion driven by wall remodelling

1.1.4.5.1. Intrinsic mechanical properties *vs* remodelling: a long lasting debate

The idea of wall expansion being an elastic stretching coupled to the modifications of cross-linking bonds between polymers is in favour of the alternative theory according to

which the wall expansion is not a purely mechanical process, but would depend, at least to some extent, on processes of "remodelling" of the network of polymers, resulting in a modification of their spatial arrangement. Such concept was advanced a long time ago for tip-growth of hyphal fungi (Bartnicki-Garcia and Lippman, 1972), in which apical wall expansion was proposed to result from the delicate balance between wall lysis and wall synthesis activities. The authors explained the bursting of hyphal fungi in response to certain chemical treatments by the unbalance of the two opposed processes: enhancing the lytic activities or inhibiting the synthetic ones that would lead to wall disintegration. In this model, the intrinsic mechanical properties of the wall at the apex do not have any real significance in the process of growth, as the wall would be a very dynamic structure and not a "passive" fluid or solid. Other authors, including Burström (1971), Money (1997) and Harold (1997, 2002) have expanded this idea, arguing that, although the tensile stress is necessary, wall expansion is a complex biochemical process, which control relies on complex molecular mechanisms acting *in muro* or from the cytoplasm. Such concept is also at the heart of the "cell wall loosening" theory of D. Cosgrove, who claimed for now more than three decades, that the "extensibility is not determined exclusively, or even principally, by the intrinsic mechanical properties of the wall" (Cosgrove, 1993*a*). In that sense, the wall "extensibility", a parameter long looked after by experimentalists, is not an intrinsic mechanical properties of the wall, but reflects the active remodelling of the wall, mediated by metabolic, enzymatic and non-enzymatic chemical reactions and non-chemical rearrangements of the cubic organisation of the polymer network (Cosgrove, 1993a,b,c, 1996, 1997, 2016a,b; see also Szymanski and Cosgrove, 2009). The rheological properties of an actively expanding piece of wall are thus called "chemorheological", to underscore the fact that those apparent properties are the resultant of both its intrinsic mechanics and of ongoing chemical reactions. In the frame of the Lockhart's theory of plant cell growth, this "wall loosening" would simply enhance the rate of stress relaxation, necessary to promote water entry and cell volume. However, as wall expansion always entails the slippage of polymers between each other, it is necessarily impacted, in some way, by the viscoelastic properties of the wall, with some remodelling mechanisms potentially acting by breaking wall matrix polymers or inter-polymer-bonds, thereby reducing the wall viscosity (Cosgrove, 1993*c*; Park and Cosgrove, 2012*a*). A similar idea has been raised in the frame of the surface-stress theory for bacterial cell growth (Koch, 1983), according to which element of wall could endorse viscous properties only at the very moment when they get inserted in the wall, under the action of tension-activated hydrolases (Harold, 1990). It is quite clear that, until now, the question of the interdependence between wall intrinsic mechanics and growth remains a highly complex issue, even in the case of land plants, that are by far the most extensively studied group (Cosgrove, 2016a), and that a variety of strategies have probably emerged in the course of evolution between different phylogenetic groups.

Wall loosening may cover different types of wall modification, possibly mechanical, chemical or structural in nature, and may affect the extensibility by modifying its intrinsic viscoelasticity or only by enhancing stress relaxation. A number of molecular factors, enzymes, non-enzymatic proteins, or ROS, have been identified as potential factors of wall loosening (or "stiffening", preventing growth) in land plants (Cosgrove, 1997, 1999, 2005, 2016a,b; Szymanski and Cosgrove, 2009). A high diversity of remodelling mechanisms probably exists between different cell types and distantly-related taxonomic groups.

1.1.4.5.2. *In muro* remodelling

As remodelling activities could result in "chemorheological" behaviour closely resembling that of a viscous flowing material (Dumais, 2013), many of the "viscoplastic" models of walled-cell tip-growth described in **Part 1.1.4.3.1** equally account for tip-growth driven by gradients of wall remodelling factors or activities. However, to our knowledge, no experimental evidence for this has been reported so far. However, some studies have shown that remodelling factors like expansins and extensins, are necessary for the proper elongation of tip-growing plant cells, including the pollen tube, and the root and cotton hairs (Ruan *et al.*, 2001; Harmer *et al.*, 2002; Cho and Cosgrove, 2002; Sharova, 2007; Gu and Nielsen, 2013; Mollet *et al.*, 2013). However, their exact remodelling activities and degree of importance in the wall expansion is unclear, and no data about the distribution or activities along the longitudinal axis of the cell, as it has been undertaken for pectins in the pollen tube, are currently available. At least, pH and ROS concentration in the apical wall of *A. thaliana* root hair have been shown to control growth rate (Monshausen *et al.*, 2007), suggesting that tip-restricted remodelling activities are likely involved in the sub-cellular modulation of the wall ability to expand in this cell type.

1.1.4.5.3. Cell-wall-deposition-dependent remodelling

In the particular case of tip-growing cells, one of the most interesting remodelling mechanism may be that induced by the deposition of new building materials. Newly-delivered wall material (mainly polysaccharides or structural proteins) that would trigger the displacement of some bonds from the ancient, cross-linked polymers to the new ones, just as expected in the hypothetical "elastic growth" process cited above. This mechanism would be particularly relevant for tip-growth, because it may directly couple the wall expansion at the apex to the polarised deposition of wall building vesicles, without requiring additional *in muro* remodelling factors which activities would have to be tightly regulated along the meridional profile of the cell. The idea of wall expansion being directly driven by the addition of new polymers is actually an old idea dating back to the pioneering work of Reinhardt, (1892) on hyphal fungi (Goriely and Tabor, 2008). Since then, many authors have acknowledged that polymer delivery to the apical wall, by exocytosis or membrane-bound synthesizing proteins, could directly increase the local cell wall extensibility and thus promote growth (Koch, 1994; Boyer, 2009; Rojas *et al.*, 2011; Hepler *et al.*, 2013). However, the putative molecular mechanisms by which such effect would be mediated are still poorly known, especially in eukaryotic cells (Dumais, 2013), and several theoretical mechanisms have been proposed for the specific case of tip-growing cells.

The general phenomenon by which the delivery of wall material at the tip directs local wall expansion is named intussusception, defined as "a process of wall expansion whereby new wall material gets inserted within the pre-existing wall fabric, thus expanding its surface area" (Dumais, 2013). Such principle was at the basis of one of the first computational tip-growth model, designed for fungal tip-growth, in which the wall-building vesicles are delivered to the cell membrane by ballistic or passive diffusion from a point-like body in the apical cytoplasm, called the Vesicle Supply Centre (VSC) (Bartnicki-Garcia *et al.*, 1989; Bartnicki-García, 1990; Gierz and Bartnicki-Garcia, 2001), commonly assimilated to the Spitzenkörper observed in many hyphal eumycetes (Steinberg, 2007; Riquelme and Sánchez-León, 2014). Each wall-building vesicle that successfully hits the cell membrane automatically fuses with it, delivers its content of polymers into the wall, and consequently increases the wall surface by a determined amount of surface. From this basic assumption the

authors successfully reproduced the apical dome shape of several species of hyphal fungi (Bartnicki-Garcia *et al.*, 1989; Gierz and Bartnicki-Garcia, 2001). Other, more recent computational models of tip-growth have also applied this concept of stress-dependent wall expansion controlled by the rate of localised deposition to the fission yeast (*S. pombe*) in which no mechanical gradient along the meridional profile of the fission yeast has been observed (Drake and Vavylonis, 2013; Abenza *et al.*, 2015). Again, thought, these models are limited by the fact that no mechanism is proposed to explain how the exocytosis of material at the apical dome would remodel the wall, and the interaction of such process with wall mechanical properties. The former VSC model is only a geometrical model, attempting to infer the geometry and growth pattern of the cell simply from geometrical and ballistic laws. It is not a real mechanochemical model, in that it does not consider the molecular processes that translate the addition of “fresh” wall material into the expansion of the current wall fabrics, and is now deemed unrealistic from a biophysical point-of-view by several authors (Koch, 1994; Money, 1997, 2008; Julien and Boudaoud, 2018). In the fission yeast, while such mechanism is highly suspected, its molecular and supramolecular bases remain to be discovered (Abenza *et al.*, 2015; Davì and Minc, 2015).

Indeed, the intussusception would be a rather complex process, encompassing a complete series of steps that would be induced by the simple addition of new wall material into the wall, each potentially impacted by all sorts of chemical or physical parameters. The input of new material would have first to tear apart some bonds between the in place wall matrix polymers, expanding the wall volume and generating new spaces into its cubic network, where the new polymers could insert themselves. Finally, these new polymers must have to cross-link with the former polymers of the network, re-establishing the initial wall structure and strength. Alternatively, the newly-delivered wall polymers would have to first diffuse through the pores of the wall fabrics to be in close contact with the in-place, cross-linked polymers and as such favour exchange of chemical bounds across the whole thickness of the wall. This process would be thus under the influence of a plethora of parameters. Among those parameters are, for example, the size and conformation of the delivered polymers, the size of the wall pores, both impacting the rate and completeness of the diffusion of new polymers into the thickness of the wall.

Morever, the process would not be thermodynamically spontaneous, but would rather require energy input, that is provided by the turgor-generated tensile stress. Indeed, if the wall of a cell is not mechanically stressed (for example in hypertonic conditions in which turgor is abolished), no expansion occurs and the continually delivered wall materials accumulate in a thick layer between the existing wall and the cell membrane (Park and Robinson, 1966; Cosgrove, 1993*c*; Harold, 1997; Boyer, 2009). In compliance with the “wall loosening” theory of Cosgrove, the intussusception is thus proposed as a real “remodelling” mechanism, rearranging the polymeric network to allows its stretching under tensile force (Kroeger and Geitmann, 2012*a*). The wall tensile stress weakens the existing cross-links and by so favours their breakage. The addition of new, unbound polymers in the load-bearing matrix would create a chemical disequilibrium that favour an exergonic reaction in which the breaking of pre-existing bonds and new "unstressed bounds" are formed, thereby relaxing the stress and thus promoting cell wall expansion (Ray, 1992; Dumais, 2013, page 201; Hepler *et al.*, 2013). An integrated, multi-level tip-growth model of walled-cell tip-growth by intussusception would have to encompass all those factors (chemical, structural, geometrical, mechanical) and their complex interactions. If such endeavour is far from being achievable for now, some mechanochemical models of intussusception have been proposed, that have great potential for tip-growth understanding.

A mechanochemical model of wall intussusception in growing pectic wall of green algae and land plants. In charophyte green algae, a detailed and very interesting chemical, non-enzymatic model for wall loosening by intussusception of pectate material has been proposed for cell elongation. Called the “pectate distortion model”, it is drawn from considerable experimental evidences acquired on the giant internodal cell of *Chara* (Proseus et al., 2000; Proseus and Boyer, 2005, 2006a,b,c, 2007; Boyer, 2009, 2016). While it has been developed for diffusely growing cells of characean algae, this model may be directly applicable to a tip-growing cell. In these models, the wall expansion is driven by the delivery of pectin chains on the inner face of the wall. The turgor pressure applies on the inner face of the wall, pushes on the exocytosed pectate chains, and makes them diffuse into the liquid phase filling the pores of the jellified pectin matrix (Proseus and Boyer, 2005). In the latter, the tensile stress distorts some of the "egg-box" structures in which the calcium ions are chelated between at least two anti-parallel demethylesterified pectin chains. This distortion lowers the affinity for calcium. As the calcium has higher affinity for unstressed pectin chains, the newly delivered, unbound pectate polymers chelate some of the calcium ions that were packaged into load-bearing cross-links. As a consequence, some of these junctions are broken, reducing the density of stress-bearing bonds, relaxing the tensile stress and making the wall expands. In parallel, galacturonic acid residues that have been freed by breaking former junctions chelate new calcium ions taken from the external medium or from the liquid phase of the wall, forming new cross-links. The uncross-linked, free-floating pectate chains bound to calcium also form *de novo* junctions, thereby becoming incorporated in the matrix gel, restoring the initial density of cross-links, increasing again the wall stiffness and thickness and lowering the expansion rate. Interestingly, the processes of wall delivery and of expansion can be separated in time, as observed several times *in vivo* and consequently is called the "stored growth phenomenon" (Boyer, 2009; Kroeger and Geitmann, 2012*a*).

A similar pectate-distortion mechanism is supposed to drive the wall loosening and expansion in land plants (Boyer, 2009, 2016, page 201). *De facto*, a mathematical model of the tensile force-driven polymerisation and expansion of the pectate wall matrix was recently built by Ali and Traas (2016). The authors suppose that the primary cell wall of land plants is organised into a biphasic structure: i) a porous-solid phase containing the cellulose microfibrils embedded into the cross-linked matrix polymers, including pectins, and ii) a liquid phase containing unbound, soluble polymers and proteins, and ions. According to the model, the cross-linking and integration of free-floating pectate polymers from the liquid phase into the porous solid phase (cross-linked matrix) will happen if the chemical reaction is exergonic, so if the energy of the unbound state (E_u) is higher than the energy of the bound state (E_b), i.e. if $\Delta E = E_b - E_u < 0$. This condition is met if the concentration of free pectate polymers is above a critical concentration (c_0^*). Therefore, exocytosis of new wall material at localised area of the cell surface can locally trigger or promote local expansion rate by increasing the concentration of free unbound polymers into the liquid phase of the wall. This process is enhanced by the tensile stress borne by the pectate gel, because the force decreases c_0^*, probably by a distortion of the calcium-junctions between pectate polymers as in the model of Proseus and Boyer (Proseus and Boyer, 2007; Boyer, 2009). The critical concentration c_0^* is indeed inversely correlated to the tensile force and to the level of elastic stretching of the matrix. Overall, the expansion rate rises with the elastic energy stored into the wall, the concentration of unbound polymers in excess of the critical concentration, to the tensile force and to the elastic strain, but decreases with the energy stored of the jellified matrix (E_b) (Ali and Traas, 2016).

The pollen tube case. The mechanochemical model of “pectate-distortion” described above is well suited for the case of the pollen tube growth, the extracellular wall of which is

mainly made of a pectic matrix, especially at the expanding tip (Steer and Steer, 1989; Parre and Geitmann, 2005*a*; Chebli *et al.*, 2012; Hepler *et al.*, 2013; Mollet *et al.*, 2013). McKenna et al. (2009) showed that during the oscillatory growth of the pollen tube, the amount of delivered material during a peak of exocytosis is a major determinant of the rate of wall expansion during the subsequent peak of growth rate, thus indicating that the cell wall extensibility depends mainly on the available quantity of freshly-delivered unbound polymers. Indeed, a model of pollen tube tip-growth with a wall remodelling mechanism closely resembling the pectate-distortion has been developed by Rojas and colleagues (2011). According to the model, the pectin matrix would behave like a network of connected elastic springs with random orientation (isotropic material), loaded by the wall tensile stress. The demethylesterified galacturonic acid residues on the newly-delivered pectate polymers have greater affinity for calcium than the "loaded" residues on the pectate matrix and consequently enhance their dissociation. The breakage of the tensile-stress-loaded bonds is enhanced by the concentration of unbound (free) demethylesterified sites on pectin chain (r_d). The strain rate of the wall is dependent on r_d, on the rate constant of cross-link dissociation (k_d), and of the average strain generated by the liberation of one load bearing bonds (ε_i). The newly delivered demethylesterified residues instantaneously reform new bonds, in part with free-floating pectate chains, thereby incorporating them into the matrix. As a consequence, the density of cross-links along the meridional contour of the cells is kept constant over time despite the surface increase. In other terms, each volume of delivered material that will contribute to a certain quantity of *de-novo* formed cross-links will ultimately result in a determined surface increment, just like expected for an intussusception mechanism.

The model allows one to make several interesting predictions in accordance with experimental data. A gradient of wall stiffness starting from the apical dome, as observed in the pollen tube of *Papaver rhoeas* (Geitmann and Parre, 2004) would serve to enhance wall loosening specifically in the apex. The elastic strain anisotropy is predicted to linearly scale with the rheological ("plastic") strain rate anisotropy, that is observed experimentally on living growing cells labelled with fluorescent markers (Rojas *et al.*, 2011). Moreover, the model accurately predicts that phases of apical wall thickening precede phases of maximum growth rate during oscillatory growth as observed experimentally (McKenna *et al.*, 2009).

A limitation of the model is the fact that the pectin polymers are delivered into a highly methylesterified form in the apical wall, and are then progressively demethylesterified by the action of PMEs (Bosch and Hepler, 2005). Pectate methylesterification reduces the r_d parameter, so it would damper the "loosening activity" of unbound pectate chains. This seemingly contradicts the proposed model as described above. At least, the pectate-distortion mechanism in the pollen tube gets slightly more complex considering this second layer of chemical remodelling, not integrated in the current version of the model of Rojas and collaborators, although the authors recognise that PMEs and PMEIs must have a role in pollen tube elongation. The simplest explanation would be that pectin methylesterification would prevent the formation of excess cross-links in the pectinaceous matrix, that would automatically block growth (Boyer, 2009). An alternative hypothesis advanced by Rojas and colleagues (2011) and Hepler et al. (2013) is that methylesterification would give less cross-linked pectin gel with higher porosity. As the diffusion of the matrix polymer into the matrix would increase with the pore size in the network, methylesterified pectin would favour wall relaxation in the apical region by enhancing insertion and diffusion of new pectic material at the apex.

1.1.4.6. Beyond the cell wall mechanics: control of the tensile stress by a cell wall thickness gradient

In this last subchapter, we will address an alternative, by which the cell wall could exert a direct mechanical control on the strain rate pattern during tip-growth, but without requiring the direct regulation of its mechanics at a sub-cellular scale. The wall thickness directly impacts the local tensile stress (Castle, 1937; Green, 1965; Von Dassow *et al.*, 2001) and its subcellular regulation has long been suggested to control plant cell morphogenesis (Green, 1965; Hejnowicz *et al.*, 1977).

1.1.4.6.1. The regenerating tip of *Acetabularia acetabulum*.

The green algae in the Dasycladalean order are made of a single, giant cell with strikingly complex morphologies reminiscent of that of land plants (Dumais and Harrison, 2000; Mine *et al.*, 2008). *Acetabularia acetabulum* is the most thoroughly studied species in the group and its stalk consists in an alternation of whorls of fine hairs and of tubular-like interwhorls. The stalk elongation takes place in the terminal region, called the “apex”, which corresponds to the whole region distal to the last whorl of hairs. The apex is composed of an ellipsoid-shaped dome sat at the top of a cone-shaped shank (Serikawa and Mandoli, 1998; Von Dassow *et al.*, 2001). Site of growth was determined by time-lapse observations of the growing apex marked with carbon particles regenerated after transversal sections of the stalk (the cutting was necessary to obtain apex not masked by hair whorls). The results revealed a steep gradient of wall strain rate from the extreme tip toward the base of the apex both in meridional and circumferential directions, indicating that the apex elongates mostly by tip-growth (Von Dassow *et al.*, 2001). A sharp peak of strain rate was observed at the extreme tip of the apex, and the major part of wall strain was restricted to the first 50 µm from the tip (less than the dome meridional length), while some residual expansion took place further away in the shank beyond 100 µm.

The same authors asked whether this pattern of wall strain could be directly caused by a corresponding gradient of wall stress. Taking into account the cell wall curvature and thickness, they computed the wall mechanical stress along the apex between the most apical region of the dome (0-30 µm away from the tip), and far in the "shank" (70-100 µm from the tip) (Von Dassow *et al.*, 2001). The shape of the apex was approximated a demi toping of a cylindrical shell. In parallel, the wall thickness was measured on wall ghosts and showed a gradient from the extreme tip toward the base of the cell, with a minimum between 0.5 and 5 µm at the extreme tip of the cell. However, the magnitude of the gradient was greatly variable between the individual cells, and in most measured cells, it seemed quite shallow, with only a doubling / trebling of the value between the extreme tip and distal regions.

The results showed that the meridional tensile stress is on average twice as large in the dome than in the shank (ratio of about 0.5), while the circumferential seems only slightly increased (ratio slightly above 1) in the dome. In other words, the thinner wall in the dome increases the meridional stress in this region, while variations in circumferential stress is "buffered" along the meridional apex, resulting in roughly constant values. However, the calculations remained very approximate, because of the oversimplification of the apex as a perfect cylinder topped by a hemisphere. Moreover, because the shank continues to widen toward the base of the apex, the actual tensile stresses in both directions would be higher than those calculated, which would damper the difference in tensile stresses between the apex and the shanks. Notwithstanding that difficulty, the authors emphasised that the wall thickness

gradient would effectively lower the stress in the shank relatively to the apical dome with an amplitude enough for the growth to be restricted to the terminal dome (Von Dassow *et al.*, 2001). The only condition necessary to make this mechanism plausible is that the yield-threshold of the wall is equal or close to the value of circumferential stress in the shank. Progressive thickening of the wall shell would decrease the tensile stress back to the yield-threshold, making the strain rate dwindle and generate the nearly-tubular shank. Observed residual circumferential strain in the shanks could result from circumferential stress faintly exceeding the yield threshold in this region. Dramatic increase in the wall tensile stress in the apical dome would cause the sharp peak of growth rate calculated in the terminal dome.

The work of Von Dassow and colleagues (2001) was the first to point out a gradient of wall thickness as a plausible mechanical patterning in a tip-growing system. A major limitation of their work is that all their observations were made on regenerating apices, that reformed from cut stalk. Thus, the observed dynamic of the apex may not correspond to a steady tip-growth but rather to a healing process. The observed gradient of wall thickness may result from the sharp gradient of wall strain centred on the middle of the “healing membrane”, rather than being the cause of that gradient. In such situation the wall thickness gradient would vary in the course of time. The large difference in thickness gradient between the cells may be congruent with such effect, but this calls for experimental confirmation.

1.1.4.6.2. The branch of Arabidopsis leaf trichome

Leaf trichome of *A. thaliana* develops three spine-shaped branches, which elongation is intermediate between tip- and diffuse growth, a particular case called a polarised diffuse growth. Although it does not correspond to a strict tip-growth event, it is easily available for live cell imaging, and ideal to enquire about the molecular, cellular and biophysical mechanisms involved in complex plant cell morphogenesis (Mathur *et al.*, 1999; Mathur, 2006, page 200). As the trichome branch elongates, its base keeps a constant radius, while the extreme tip gets tapper (gradual increase in curvature). Analysing the kinetics of surface expansion using fluorescent microbeads stuck on the surface of the cell revealed a gradient of wall strain, which is maximum near the extreme tip and which gradually decreases toward the base of the branch. In addition, the strain is clearly anisotropic, with a strong bias toward the meridional direction, explaining the large increase in branch length correlated to very low increase in width (Yanagisawa *et al.*, 2015). The same authors showed, using a FE material modelling approach comparable to that of Fayant et al. (2010), that a positive gradient of wall thickness or a gradient of wall elastic modulus along the meridional profile of the branch was an essential feature required to account for such pattern of wall strain. TEM imaging and propidium iodide labelling (revealing pectin) confirmed the existence of such thickness gradient, with an approximate 2.5 times increase between the tip and the base of the branch. When integrated into the model, this gradient was sufficient to reproduce the wall strain and branch morphology without any need for a gradient of stiffness. This study thus demonstrated the involvement of a wall thickness gradient in mechanically generating a strain pattern at the sub-cellular level in land plant cell morphogenesis by generating a gradient of tensile stress.

Curiously, the predicted wall deposition rate along the branch meridional must follow an opposite gradient. Indeed, to maintain the cell wall thickness constant over time, the maximum wall deposition rate would be at the base of the branch, indicating that this case of tip-growth-like morphogenesis actually is not generated by any kind of wall secretion focused toward the tip of the cell, but quite the opposite. Whatever it be, how the gradient of wall deposition is generated remains unclear, although the actin cytoskeleton appears necessary

(Yanagisawa *et al.*, 2015). Another, much more critical issue is that if wall thickness truly governs the morphogenesis of the trichome branch, the mechanism by which it is initiated must involve a different mechanism. In addition, Bidhendi and Geitmann stressed, in their critical review, that the causal link between the gradient of wall strain and wall thickness remained unclear in the study of Yanagisawa and collaborators (Bidhendi and Geitmann, 2018). As in the study of *A. acetabulum* apex described above, the problem is that the elongation of *Arabidopsis* leaf trichome branch is not a real steady tip-growth, and it is not clear whether the wall thickness gradient is stable or increases during time. In order to demonstrate a direct stress and strain patterning role for a wall thickness gradient, study of a steadier tip-growth process, in normal conditions (i.e., not in response to injury) is required.

1.1.4.6.3. The apical cell of the vegetative filaments of the brown alga *Ectocarpus* sp.

Despite the occurrence of tip-growth in brown algae (Katsaros, 1995; Charrier *et al.*, 2012), tip-growth mechanisms are largely understudied in this clade, although their unique evolutionary history and their particular physical environment make them worth of interest for the study of fundamental cellular morphogenetic mechanisms. Very recently, the mechanical functioning of tip-growth of the apical cell of the vegetative filaments of *Ectocarpus sp.*, a model species for brown algae (Peters et al., 2004; Charrier et al., 2008; Cock et al., 2010, 2012), was investigated (Rabillé et al., in revision). Quantitative biological data on the main structural and mechanical parameters of the cell, *i.e.* the turgor value, the thickness of the cell wall, and the shape (curvature) of the cell, were acquired experimentally and used to feed a viscoplastic model of tip growth that is mainly drawn from the viscoplastic model of Dumais et al. (2004, 2006; see **Part 1.1.4.3.1**). A sharp thickness gradient along the axis of the apical cell was observed, with a very thin wall in the dome (~40nm thick) and a continuous wall thickening on the shank toward the base of the cell, plateauing at a mean value of ~500 nm far beyond the apical dome. Calculating the tensile stress with the constitutive equations of Dumais revealed a negative tensile stress gradient, with the highest value at the extreme tip of the cell, that then dramatically dwindles toward the base of the cell. Knowing the mean axial elongation rate of the apical cell and considering that the surface growth is orthogonal, the wall strain pattern was computed, and strain rates were plotted as a function of the corresponding stress values. The relationship between stress and strain strictly followed the Lockhart's mathematical formulae (Lockhart, 1965; Geitmann and Ortega, 2009), indicating that the wall expansive growth in *Ectocarpus* apical cells can be described with a unique value of yield-threshold (σ_y) and extensibility (Φ), at least in the expanding apical dome. These results strongly suggest that the wall mechanics do not vary at a subcellular scale in the apical cell of *Ectocarpus*, and hence that the detailed strain pattern necessary to insure the transition toward the tubular shape is entirely and directly generated by the thickness gradient (Rabillé et al., in revision). Dynamical simulations of apical cell growth demonstrated that the measured thickness gradient was enough to generate proper tip-growth, and the shape thickness profile determined the steady shape of the apical dome and the tube diameter.

This model makes the assumption that the cell wall thickness is kept tightly constant over time, at a given point of the cell surface. The same hypothesis is often adopted by most of the tip growth models. It implies that the cell establishes a precise pattern of wall deposition rate (by exocytosis and / or by cellulose microfibrils synthesis) so that the wall thinning due to the strain is perfectly compensated for. Using their model, Rabillé and collaborators predicted the adequate pattern of wall deposition rate along the meridional profile of the cell, knowing the wall strain pattern and the corresponding rate of wall thinning at any point of the cell. It

showed a slight gradient with a maximum at about 5 µm from the extreme tip, very gradually decreasing toward 0 in the distal direction, and a lower rate at the extreme tip. When the comparing with the Tobacco pollen tube, the amplitude of deposition was lower by several orders of magnitude in the apical cell of *Ectocarpus*. This reflects the huge amount of wall that must be delivered to the Tobacco tip, because of the thicker apical wall and the higher wall strain rate (considering the fast elongation rate of the pollen tube). *In vivo*, the wall deposition rate may slightly fluctuate in space and at short time scale, which may account for the variability in wall thickness, dome curvature and apical cell diameter that is observed in the living *Ectocarpus* sporophyte filaments.

1.1.5. Turgor and associated hydrodynamic flows as the main mechanical factor of the growth patterning

1.1.5.1. Can turgor vary into a single cytoplasm?

Although the turgor is generally considered as a scalar force, with exactly the same value throughout the cell, some authors have challenged this view and advanced that transient variations in turgor pressure and/or directional cytoplasmic flow could play a central mechanical role during tip-growth in walled plant cells. Such hypothesis has been drawn from results obtained in animal cells, in which pressure surge leading to local blebbing can be inhibited in some part of the cell (for example by a local hypertonic stress) (Charras *et al.*, 2005, 2009). Those results were advanced to support an alternative model of eukaryotic cytoplasm structure where, rather than being considered as a homogeneous, viscous aqueous solution, is regarded as a poroelastic three-dimensional network of contractile cytoskeletal elements filled by interstitial fluid containing ions and soluble proteins, comparable to a “fluid-filled sponge” (Charras *et al.*, 2005, 2009; Rosenbluth *et al.*, 2008). In such model, the local hydrostatic pressure would depend on the degree of contraction of the cytoskeletal phase, while limited diffusion of the interstitial fluid phase would maintain transient pressure gradient between different regions of the cytoplasm, for a short time scale (about tens of seconds). Such transient turgor gradients would generate temporal hydrodynamic flows that could insure the long-range transport of cellular organelles and the bulk cytoplasm flows from regions of higher pressure toward regions of lower pressure. Turgor gradients have indeed been proposed to drive the forward flux of cytoplasm in *Neurospora crassa* hyphae (Lew, 2005). In addition, intracellular current could also generate directional pushing forces on the cell envelope toward which the water is flowing, driving local protrusion (Chengappa *et al.*, 2018). From this alternative view, a research group has proposed an original, yet highly disputed hydrodynamic model for the pollen tube (Zonia *et al.*, 2006; Zonia and Munnik, 2009, 2011) in which turgor variations, and more specifically the resulting water movements along the longitudinal axis of the cell, plays a significant mechanical patterning role. This particular model is discussed in the following section.

1.1.5.2. The hydrodynamic model of tip growth of the pollen tube

1.1.5.2.1. Overview of the model

The hydrodynamic model of Zonia and Munnick has been developed after a series of observations on the pollen tube growth dynamics (especially the regular oscillation in axial growth rate) and its relation to 1) lipid signalling pathways (Zonia *et al.*, 2002; Zonia and Munnik, 2004), 2) variations of the apical region volume and sensibility to osmotic stresses (Zonia and Munnik, 2004, 2007; Zonia *et al.*, 2006) and 3) pattern of endo- and exocytosis (Zonia and Munnik, 2008*a*,*b*). The authors integrated this large set of observations into a model that incorporates both cytomechanical and molecular mechanisms, both levels interacting and regulating each other by putative osmo- and mechanosensing signalling pathways. The first component of the model (ACE) describes the pattern of exo- and endocytosis in and close to the growing region and its spatial and temporal regulation, and the second (H) presents the biophysical mechanisms involved in the regulation of the pollen tube oscillatory behaviour and, most importantly here, in its directional elongation (Zonia and Munnik, 2009). This model is summarised below.

The ACE component of model states that the exocytosis of cell wall vesicles and consecutive wall expansion are restricted to the sub-apical part of the pollen tube, rather than in the apical dome (even though some growth could also occur in the most basal part of the dome, see **Part 1.1.2**). Massive endocytosis of small, recycling vesicles occurs in the apical dome, forming the inverted cone of vesicles. Exocytosis of clathrin-coated-vesicles would also occur all along the shank of the pollen tube, but with a much lower rate than in the apical dome (Zonia and Munnik, 2008*a*,*b*). Coupling exocytosis into the sub-apical growth area and endocytosis in the apical dome generates a massive flow of cell membrane material toward the tip (anterograde movement), while an opposite flow toward the shank (retrograde movement) would also occur because of endocytosis activity in distal regions (Zonia and Munnik, 2009). Strangely, according to the authors, such bidirectional flow of membrane material would be correlated to a comparable “bidirectional cell wall expansion” in the growth area. However, the mechanical *raison d’être* and principle of such bidirectional flow coupling between wall expansion and membrane lipids flows are not explained.

1.1.5.2.2. Tip-oriented hydrodynamic flows as the motor of pollen tube elongation

The actin cytoskeletal array is weaker at the tip of the pollen tube than in the sub-apical and more distal regions. Ions exchanges between the cytosol and the extracellular medium are also differentiated between the apex and the shanks, the apical dome being a site of oscillation in the concentration of free calcium ions (Ca^{2+}; (Zonia, 2010; Hepler *et al.*, 2012, 2013). In addition to the fact that pollen tube plasmolysis always tends to take place at the apex during hyperosmosis (Zonia *et al.*, 2006; Zonia and Munnik, 2007), these data were regarded as a proof that the osmotic pressure is weaker in the apical region than in the shanks. The pressure differential between the two cytoplasmic regions would be generated by electrochemical, osmotic and molecular crowding between the two regions (Zonia and Munnik, 2011). This difference in hydrostatic pressures would cause an anterograde hydrodynamic flow of water along the pollen tube axis, from the distal to the apical regions. This flow is thought to be fundamental for both the polarised elongation of the pollen tube and the molecular regulation of the whole process. The actin fringe in the sub-apical cytoplasm would play a direct role in

driving the exocytosis in this area. Thus, this model does not require a mechanism for driving secretory vesicles up to the apical cell membrane, as demanded in the classical model of pollen tube tip growth.

The hydrodynamical (H) component of the model describes the mechanical process of pollen tube elongation as a biphasic process. During a phase of high growth speed, the apical cell volume is small, and specific osmo-sensing pathways would stimulate water entry in the sub-apical region of the shanks. This would generate a transient turgor increase in this region and would result into 1) a forward flow of water toward the apex and 2) a reduction of growth rate (entry into a phase of low growth rate). These two combined physiological responses would result in a water “replenishment” of the apical region, thus extending the local volume by elastic stretching of the cell wall and membrane. Mechanosensing pathways, potentially involving stretch-activated ion channels (Zonia and Munnik, 2007, 2009) would then activate exocytosis while inhibiting endocytosis, fuelling the wall with “fresh” material for the future phase of high growth rate. When the cell wall stability threshold is reached, the authors posit that the cell wall in the sub-apical growth area would be destabilized by a LOS mechanism. The critical tensile stress would be attained more rapidly here, earlier than in the apical dome as the turgor-generated tensile stress is higher in the former than in the second (see **Part 1.1.2**). In parallel, putative osmosensing pathways in the apex would activate the "regulatory cell volume decrease pathway", that would latter promote water efflux off the apical zone through the membrane of the apex while inhibiting water entry in sub-apical parts. Overall these responses would segue into a significant oriented vectorial hydrodynamic force pushing on the quiescent apical dome (Zonia *et al.*, 2006). The latter would thus “pull” on the rest of the pollen tube cell wall, leading to longitudinal extension in the sub-apical growth region that has been previously destabilised and supplied with unbound, young wall material. The resulting growth rate increase corresponds to a new phase of high growth rate.

From a biomechanical point of view, this model has the advantage to offer a very simple, elegant way to establish the cylindrical shape. As in the axon in metazoans, the leading tip pulls on the sub-apical region of the cell as it moves forward, automatically resulting in an extremely anisotropic growth pattern where the tubular shanks are elongated in their longitudinal axis without any circumference increase. However, the initial establishment of the tube diameter would depend on a different, unknown mechanism occurring during the germination of the pollen grain or soon after, maybe imposed by the diameter of the aperture on the pollen grain, from which the pollen tube emerges. In high growth rate phase, strong water efflux at the apical tip could drive the forward flow of the whole cytoplasm in concert with the protruding tip. In this way, the model of Zonia and Munnick intends to explain, in a single unified frame, all the morphogenetic processes occurring during the life of the pollen tube, from the germination (that could be initiated by the rehydration and swelling of the pollen grain on the stigmata), to the apex inflation and bursting that allow the discharge of sperm cells into the ovule (Zonia and Munnik, 2007; 2011).

1.1.5.2.3. Shortcoming of the model

However, despite the appealing elegance of this model, it suffers from inconsistencies that contradict the physics of pressure and hydrodynamics and other erroneous premises about the pollen tube growth pattern and physiology. First, as noted in **Part 1.1.2**, the growth is not sub-apical but occurs in the apical dome, as demonstrated by direct measurements of wall strains (Fayant *et al.*, 2010; Rojas *et al.*, 2011). All the wall material deposited in the apex thus contributes to the building of the shanks, and thus there is no support for a massive

recycling of wall by endocytosis in the apical dome, even though endocytosis occurs in the region (Geitmann and Dumais, 2009; Chebli *et al.*, 2013). Furthermore, it is hard to imagine how a flow of cell membrane could drive a parallel "flow" of cell wall, as both compartments are not chemically bound (or only by weak bonds), and because the cell wall is far less fluid than the cell membrane. Such mechanism would also not be consistent with the idea of the apical dome being a stiff and quiescent "wedge" to force a way through the female tissues. For all these reasons, the "bi-directional" nature of wall expansion in the supposed sub-apical growing region as imagined by the authors is not valid.

The role of turgor in cell growth proposed in this model largely contradicts the classical theory of plant cell growth and the whole model is deemed impossible on physical grounds (see Winship *et al.*, 2010, 2011, for a detailed critic). The possibility of large turgor pressure gradients into the pollen tube cytoplasm, especially, is considered physically impossible by most plant physiologists. Winship *et al.* (2010, 2011), stressed that the measured variations of turgor in blebbing animal cells measured by Charras and colleagues (2005) is only of the order of hundreds of Pascal. However, to drive the polarised growth of the pollen tube, turgor gradient must be at least 100 times larger in amplitude, thus requiring a cytoplasm at least 100 times more heterogeneous or dense than in blebbing animal cells. It must also be added that the vectorial force generated by the putative hydrodynamic flow pushing on the cytoplasmic face of the leading tip is probably far too weak to generate a significant pulling force in the sub-apical growth area, all the more so as the water passes through the apical cell membrane and wall, making the "effective" pushing force weaker than expected. However, in support of the hydrodynamic model, even a very weak additional tensile stress might be efficient enough if the stress in this area is very close to the critical value of stability (according to the LOS theory, see **Part 1.1.2**). In this case only a slight extra "pulling" force in the longitudinal axis of the cell could promote elongation in this particular direction. However, this would require the turgor to be very constant in time, in order to keep the wall tensile stress very close the limit stability threshold, and this is not consistent with the cyclic variations of turgor postulated by the authors. A more likely hypothesis would be that the cell wall is strongly anisotropic, yielding much more easily in the meridional (longitudinal) than in the circumferential direction. The discussion by the authors of the model (Zonia *et al.*, 2006) is also sometimes inconsistent about the direction of the transient increases in hydrostatic pressure, and whether they are the cause or the consequence of hydrodynamic flows and cell volume variations. Water flow from the shank toward the apical cytoplasm is sometimes said to locally result in a "local pressure surge", while this hydrodynamic flow should result from a pressure being minimal at the tip. This is confirmed in Zonia (2010), where the author wrote "spatial non-equilibrium osmotic pressure is predicted to be highest near the apex and diminish toward the distal tube". This suggests that, in the author's mind, the turgor pressure is higher in the apical region, thus favouring growth in this area. However, water flow toward the tip could not occur in such situation. Quite the reverse, an opposite water flow would ensue (Winship et al., 2010, 2011). Worst, the supposed forward flow of water toward the apical dome is not coherent with the massive, rapid retrograde transport of vesicles in the central region of the cytoplasm observed by time-lapse microscopy (Zonia and Munnik, 2008a,b). For a more comprehensive criticism of the model, see Winship et al. (2011).

1.1.6. Conclusion and perspectives

Current understanding of the diversity and evolution of the biomechanical patterning mechanisms involved in tip-growth. The experimental and modelling studies of tip-growth biomechanics reviewed here tend to suggest that there could be a high diversity of biomechanical mechanisms driving tip growth (**Fig 1.3**). It is not sure, however, whether this diversity underlies a true diversity of biophysical strategies. Such apparent diversity may be due to a lack of experimental data, and simply results from the unrestrained imagination of theoreticians. As long as the models are realistic from a physical point-of-view, though, they deserve consideration until they are proven wrong on experimental ground, and for now the available evidence are not enough to dismiss most of the models. The problem is particularly significant concerning the "cell wall mechanical gradient" models for walled cell tip-growths, because of the current lack of understanding of the mechanism of wall expansion (**Part 1.1.4.4**). The phenomenon of wall expansion appears to be a complex interplay of chemical, thermodynamic and mechanical processes, and thus its connection to the mechanical properties of the wall is muddled. This situation has segued into the emergence of numerous, sometimes irreconcilable models, depending on the school of thought the authors belong to.

Even if proven, it is not clear to what extent such diversity of biomechanical strategies is linked to i) the physical conditions of the external medium the cell is invading, and ii) the phylogenetic position of the organism. At least, given the extremely ancient divergence between bacteria and eukaryotes (at least 2 Bya) and the radically different physical structure of their cells, the biomechanical mechanisms of tip growth between both lineages are probably not homologous, and likely emerged independently in the course of evolution.

In the eukaryote realm, interestingly, there are several hints toward the idea that tip-growth in walled cells derived from an ancestral, amoeboid-like locomotion form based on the dynamic of the actin cytoskeleton and associated myosin motors (see **Part 1.3**), that may have been more or less been conserved in today's amoebas. The cortical actomyosin network is strikingly reminiscent of the complex polysaccharide cell wall that can display similar mechanical properties (elasticity, plasticity, viscosity, viscoelasticity, poroelasticity…) or be "remodelled" to effectively promote local expansion in surface (Stossel, 1982; Fukui, 1993). Hence, the amoeboid-locomotion would rely on the higher "remodabillity" of the cortical network of actin filaments at the leading tip than on the "lateral" flanks, allowing local protrusion under internal hydrostatic pressure forces. Biomechanical strategies of tip-growth or other general cell morphogenesis relying on one system or the other, or on a combination of both, could then be imagined (Mathur, 2005). This hypothesis supposes a close, physical interaction between the cortical actin cytoskeleton and the cell wall, the both components forming a general "cell envelope" that could mechanically control the local expansion of the cell boundaries (Mathur, 2005, 2006). Indeed, in the course of evolution, the initial actomyosin-based biomechanical system might have derived to adapt to new cytomechanical contexts, especially the progressive acquisition and complexification of a stiff extracellular matrix. This new cell compartment would have progressively acquired the prime role of mechanical control of cell morphogenesis that the cytoskeleton was ancestrally endowed with (Mathur, 2005, 2006; Fig 1.3, bottom line). In parallel, transmembrane connections between the actomyosin cortex and the substrata would have been replaced by connections with the wall, when this structure had become stiff enough to serve as a mechanical support. The ancestral, cytoskeleton-based system may have been more or less conserved in certain walled-cell groups (Steer and Steer, 1989; Steer, 1990; Pickett-Heaps and Klein, 1998; Heath and Steinberg, 1999) and largely derived in others, especially in terrestrial plants, where the wall would have taken almost entirely the primary role of the mechanical patterning agent. In such

cases, the function of the cytoskeleton would have almost completely relegated to the regulation of cell polarity and vesicle trafficking in the most "derived" systems, like terrestrial tip-growing plants (Gibbon *et al.*, 1999; Ketelaar, 2002; Gossot and Geitmann, 2007; Bou Daher and Geitmann, 2011; Chebli *et al.*, 2013). These evolutionary innovations could be adaptations to various cellular cytomechanical contexts and external physical environments. For example, the necessity to invade and colonise complex and sometimes very hard media may have resulted in the convergent recruitment of stiff cell walls and high turgor in hyphal fungi and oomycetes (Money *et al.*, 2004; Money, 2008). Taken together, the data cited above allow to converge toward a preliminary, rough scenario for eukaryotic tip-growth, already foreseen more than three decades ago by several research teams (Picton and Steer, 1982; Steer and Steer, 1989; Steer, 1990; Pickett-Heaps and Klein, 1998). It would derive from an amoeboid-like locomotion form that existed in the Last Eukaryotic Common Ancestor (LECA; Vaškovičová *et al.*, 2013). This scenario, suggesting repeated transitions from the cytoskeleton-based toward the cell wall-based strategies, could serve as a working model for future broad-scale evo-devo studies of tip-growth processes.

Potential impact of the molecular toolkit on the evolution and diversity of tip-growth mechanisms. Numerous reviews exist regarding the molecular regulatory pathways involved in the control of the various physiological, cellular and biomechanical processes occurring during tip-growth in land plants and fungi (Palanivelu and Preuss, 2000; Gu *et al.*, 2003; Harris and Momany, 2004; Harris *et al.*, 2005; Cole and Fowler, 2006; Šamaj *et al.*, 2006; Cheung and Wu, 2008; Kost, 2008; Lee and Yang, 2008; Sudbery, 2008; Zonia, 2010; Guan *et al.*, 2013; Vaškovičová *et al.*, 2013; Chen *et al.*, 2015). The rare evo-devo surveys of these molecular mechanisms spanning different taxonomic taxa suggested that these growth modes may be controlled by a conserved molecular toolkit that emerged only once, before the LECA, and then was repetitively recruited in the various form of invasive growth that occurred across the Eukaryotes (Vaškovičová *et al.*, 2013; Rensing, 2016; see the Introduction). This strengthens the idea that tip growth in different eukaryotic groups is derived from a single, ancestral, amoeboid-like organism. Alternatively, if tip-growth emerged independently several times in various branches, these different apically-growing cell types may have repeatedly recruited the same conserved molecular toolbox. However, the current knowledge is too scarce and limited to favour one particular scenarios, and the degree of conservation of such core molecular machineries must be characterised more precisely. Putting together the current understanding of the biophysical and molecular functioning of tip-growth suggests that the "versatility" of the dynamic cellular biomechanical processes drives the change of cell shape (reversible or not) to insure different forms and functions and to comply to various abiotic external conditions. In contrast, the evolution of mechanical strategies of cellular morphogenesis would be less dependent on the nature of the underlying molecular pathways, the latter being curiously more "rigid" and less prone to evolutionary innovation.

Current obstacle impeding the evo-devo study of tip-growth. As tip-growth research has been, until now, largely focused on some overrepresented taxa, our current knowledge of both tip-growth biomechanics, physiology and molecular regulation is too fragmentary to draw any clear picture of the evolution of tip-growth across the whole tree of life. The theoretical models often lack experimental validation, impinging our knowledge of the real diversity of tip-growth biomechanical strategies. Worse, the connections between biophysics and molecular regulation of the cell have barely been explored until now. Most biomechanical tip-growth models barely include any molecular factors. In the future, more integrative, multi-level models, incorporating cell biomechanics, physiology, molecular effectors and regulators all together will be required for a deeper understanding of such complex biological systems.

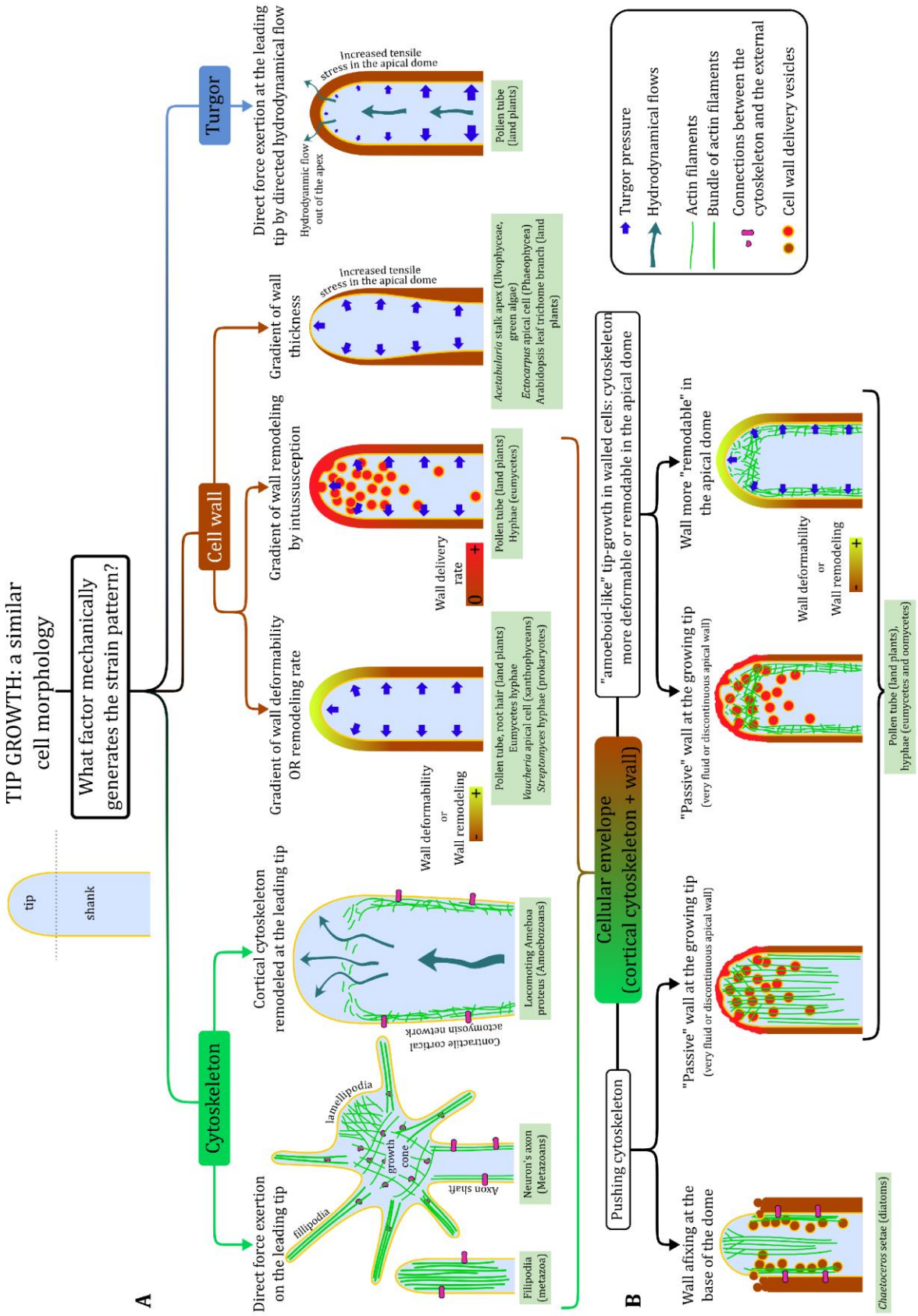

Figure 1.3 - Classification of the different mechanical "strategies" observed or envisioned for tip-growing cells *(caption in the next page)*

(Figure 1.3, *continued*) In this figure, the diversity of biomechanical strategies that have been unravelled or theorised are schematized and classified according to the main mechanical patterning factor. (**A**) Models in which only one factor is at play are listed, following the plan of the review. In the cytoskeleton part (left), the finger-like protrusion of naked cell, called filiopdias, is also represented next to the growth cone of the axon, as the mode of elongation of filipodia protrusion is reminiscent of a tip-growth. (**B**) Models in which both the cytoskeleton and the wall are involved are presented. Those models correspond to tip-growths of walled-cell organisms in which the actin cytoskeleton is still considered to play a direct mechanical control on the wall strain pattern. They represent putative "evolutionary steps" by which an ancestral, "ameboid-like" tip-growth mechanism may have diverged into "modern" tip-growth mechanisms in which the cell wall, by its mechanical properties or by its active remodelling, entirely control the pattern of wall expansion. At left, correspond to model where the cytoskeleton "pushes" the cell envelope, and the wall only ensure the mechanical stability of the shanks, whether because it is only deposited in the region (as in the *Chaetoceros* setae), or whether because new wall deposited at the tip is so fluid that it does not oppose a significant mechanical resistance to the protruding force exerted by the cytoskeleton. At right, "amoeboid tip-growth" models imagined by some authors for pollen tube or hyphal fungi *lato sensu*, in which the cortical cytoskeleton mechanically reinforces the cell envelope (the ensemble made of the cell wall, the cell membrane and the cortical cytoskeleton). Growth is restricted to the apical dome by higher cortical deformability or "remodelability" of the cortical cytoskeleton in this region compared to the shanks. In such situation, two different scenarios can be distinguished. In the first (left), the cell wall is, again, deposited at the apex in an extremely fluid form, giving the cytoskeleton full mechanical control over surface expansion. In the second (right), both the cell wall and the cortical cytoskeleton mechanically control the extensibility of the envelope, both being. This last situation can be seen as a transitional form toward biomechanical strategies in which only the wall mechanically control the surface growth pattern (see **A**).

In the case of the "cytoskeleton" and "cell wall mechanical gradient" models, the models should propose and test hypotheses about the connexion between i) the global mechanical properties of the cell wall, of the cortical cytoskeleton or of cellular envelope made of an assemblage of the two, and ii) the biochemical composition of these cellular components, their detailed structure, and the diverse "remodelling" molecular factors that drive their deformation in response to exterior forces. The models will also have to integrate the external forces exerted by the external medium (often hard, complex and heterogeneous semi-solid media) on the invading cell (compressive and frictional forces), that are generally ignored by the current models (an exception is the recent model by Goriely *et al.*, 2010). However, these forces likely significantly impact the morphogenesis of the cell, at least by interfering with the mechanical deformations (strain profile) of the cell surface (Goriely and Tabor, 2008; Sanati-Nezhad and Geitmann, 2013), and also on the underpinning cellular and molecular mechanisms controlling tip growth, by putative mechanosensing pathways (Wessels, 1990; Davì *et al.*, 2018).

Finally, an important step further toward an evo-devo investigation of tip-growth is to extend both theoretical and modelling studies to underexplored taxa. Interesting groups worth of investigation includes the fungi-like oomycetes, all the three major groups of (macro)algae (red / green / brown algae), and several other groups of algae, like the diatoms and the xanthophycean algae. Oomycetes, brown algae, diatoms and xanthophycean are especially appealing, because they all belong to the Stramenopiles "kingdom", and thus evolutionary very distant from both the Archaeplastida (comprising land plants) and the Opisthokonts (comprising eumycetes and metazoans). Consequently, they are the most likely taxa to have developed alternative cell developmental pathways (see Charrier et al., 2012 for the case of brown algae).

Coupled with phylogenetic and evolutionary studies of tip-growth and related cellular cell migration processes, such studies would give us the first understanding of how the evolution of a simple, yet fundamental cellular morphogenetic process has been impacted by constraints imposed by the physical world and the organisms' cellular and molecular toolboxes reflecting their evolutionary heritage.

1.2. Brown algae: an ideal and stimulating groups for discovering alternative morphogenetic mechanisms

1.2.1. General overview of brown algae

Now that the mechanical models of tip-growth have been reviewed in details in the preceeding section, in this part the brown macroalgae, a particular group of walled multicellular organisms, will be presented. The goal is to demonstrate the immense potential of this as yet almost untamed class of organisms for the discovery of alternative molecular, cellular and biomechanical mechanisms controlling cell, tissue and organism morphogenesis.

1.2.1.1. Life style and environment

Brown algae, or Phaeophyceae, are almost purely marine macroalgae (only 10 known species are found in freshwater environment up to now). They are in large majority sessile macroalgae that develop in coastal ecosystems, from the upper intertidal to the subtidal zone. They colonise the coasts at temperate and cold latitudes, where they can account for most of the biomass. Some species are genuine habitat-structuring organisms, forming dense underwater canopy offering shelter and foods for numerous animals, fishes and many other marine organisms (De Reviers, 2003). This particular environment exposes brown algae, as well as the other groups of macroalgae, to various physical constraints, like reduced perception of gravity, limited light and oxygen availability, oxidative, desiccation and osmotic stresses linked to incoming tides and ebb, and huge compressive and drag forces generated by currents and waves (Koehl, 1984; Charrier *et al.*, 2012; see **Part 1.2.3**). All these constraints make the coastal environment radically different from the terrestrial one, to which most of the intensely studied model species for development (in metazoans and land plants) belongs. Such radically different conditions have probably impacted to large extent the developmental mechanisms of macroalgae.

Phaeophyceae, that currently comprises between 17 and 20 orders (Silberfeld *et al.*, 2010, 2014; Guiry and Guiry, 2018), display a very large range of morphological complexity (see below for more details), ranging from simple, near-microscopic filamentous forms like *Ectocarpus* and other genera of the Ectocarpacean family, to large, complex parenchymatous forms which thalli are differentiated into anchoring holdfast, stipes and light-collecting blades or lamina, like the giant kelp *Macrocystis pyrifera* (Fritsch and Salisbury, 1920; Chapman, 1962). Actually, brown algae display the largest morphological complexity of all macroalgae (Chapman, 1962). A small subset of the diversity of brown macroalgae morphologies is presented in **Fig 1.5A**.

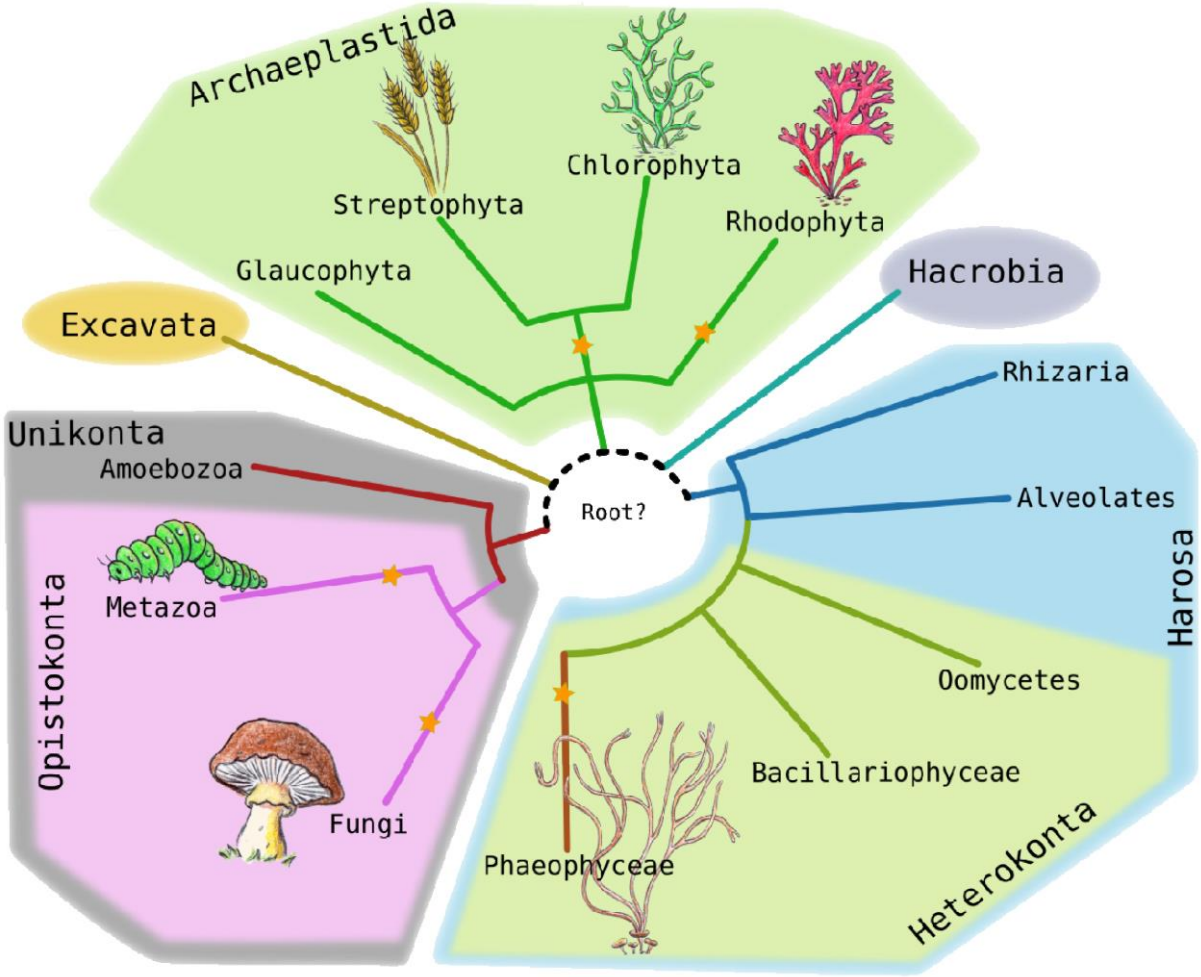

Figure 1.4 - Phylogenetic positions of brown algae (Phaeophyceae)

This highly simplified version of the Eukaroyotic tree highlight the main multicellular eukaryotes (whose branch are labelled with a star), all displaying various tip-growing cell types. The huge evolutionary gap between the brown algae and the other multicellular taxa is obvious. The brown algae are the only complex multicellular taxa in the Harosa, one of the major division of the eukaryotic tree. Yet, tip-growth is also found in several other groups in Heterokonta like the Bacillariophyceae (diatoms) and the oomycetes (fungi-like organism forming hyphae), that are two diverse, emblematic groups belonging to this kingdom. The mechanism of tip-growth in brown algae may be more similar to that in these groups than they are in true fungi (Opistokonta) and land plants (Streptophyta).

The figure is exerpted from the thesis report of Z. Nehr (Nehr, 2013), that herself adapted it from Baldauf (2003).

1.2.1.2. Phylogenic position and evolutionary history

The class of Phaeophyceae belongs to the Stramenopiles (formerly Heterokontes). Stramenopiles is a vast kingdom comprising numerous algal classes like Bacillariophyta (Diatoms), and non-photosynthetic classes like the Oomycetes (hyphal pseudo-fungi) (Baldauf, 2003, 2008; **Fig. 1.4**). Stramenopiles belong to the Super-kingdom Harosa or SAR, for "Stramenopiles-Alveolates-Rhizaria" (Burki *et al.*, 2007; Baldauf, 2008), one of the main branch of the Eukaryotic tree, which date of divergence from the rest of eukaryotes date back to at least 1.6-1.8 billion years (Parfrey *et al.*, 2011; **Fig 1.4**). Brown algae are among the few eukaryotic groups to have acquired a complex multicellularity, and the only group of the SAR super-kingdom. Thus, they have acquired this trait completely independently of the other eukaryotic multicellular taxa, that include the Streptophytes (Charophyte algae and land plants), the Chlorophytes (other green macroalgae), the Rhodophytes (red macroalgae), the Eumycetes and Metazoans (Niklas, 2014).

However, brown algae gained their multicellularity very recently in the course of evolution; the common ancestor of all extant orders lived only approximately -180 million years ago (first half of the Jurassic period; Silberfeld *et al.*, 2010). The radiation of the current order occurred gradually over time, mostly during the Cretaceous period (Silberfeld *et al.*, 2010). Thence, the developmental mechanisms acquired in this lineage, besides having emerged in a radically different evolutionary context, may also have remained simpler compared to the mechanisms in the most studied multicellular taxa, namely the animals and the terrestrial plants, with emerged much earlier during evolution and had more time to develop complex morphologies. The brown algae represent a unique opportunity for evo-devo studies of the mechanisms that led to the emergence of multicellularity and the acquisition of morphologies of increasing complexity. Yet they are, for now, largely understudied in this respect (Charrier *et al.*, 2012).

1.2.2. Morphological diversity and morphogenetic pathways in brown algae

As mentioned above, the brown algae encompass a very large range of complexity in thallus morphology and underlying architecture (Bogaert *et al.*, 2013). The simplest forms, like that found in genera in Ectocarpacea, are made of uniseriate filaments of cells (De Reviers, 2003). More complex forms are made of uniseriate filaments stacked together to form pseudoparenchymatous tissues, that can be bidimentional, like in Dictyocales (Katsaros and Galatis, 1985; Katsaros, 1995), or tridimentional, like the hollow "bladder" build by *Adenocystis utricularis* (Ectocarpales; Clayton, 1985). This pseudoparenchymatous building principle seems common in many orders of brown algae (Chapman, 1962; Bogaert *et al.*, 2013). The most complex thalli are, however, made of true parenchymatous tissues, as in Laminariales and Fucales, which differentiate into distinctive organs (holdfasts, stipes and blades) each comprising several specialized tissues: the epidermis, the cortex and the central medulla. The latter is generally made of elongated non-photosynthetic cells separated by large spaces filled with abundant mucus-like extracellular material. Especially in Laminariales, these particular cells are sometimes differentiated into trumpet-shaped sieve elements involved in long range transport and, maybe, systemic communication between distant part of the thallus (Charrier *et al.*, 2012).

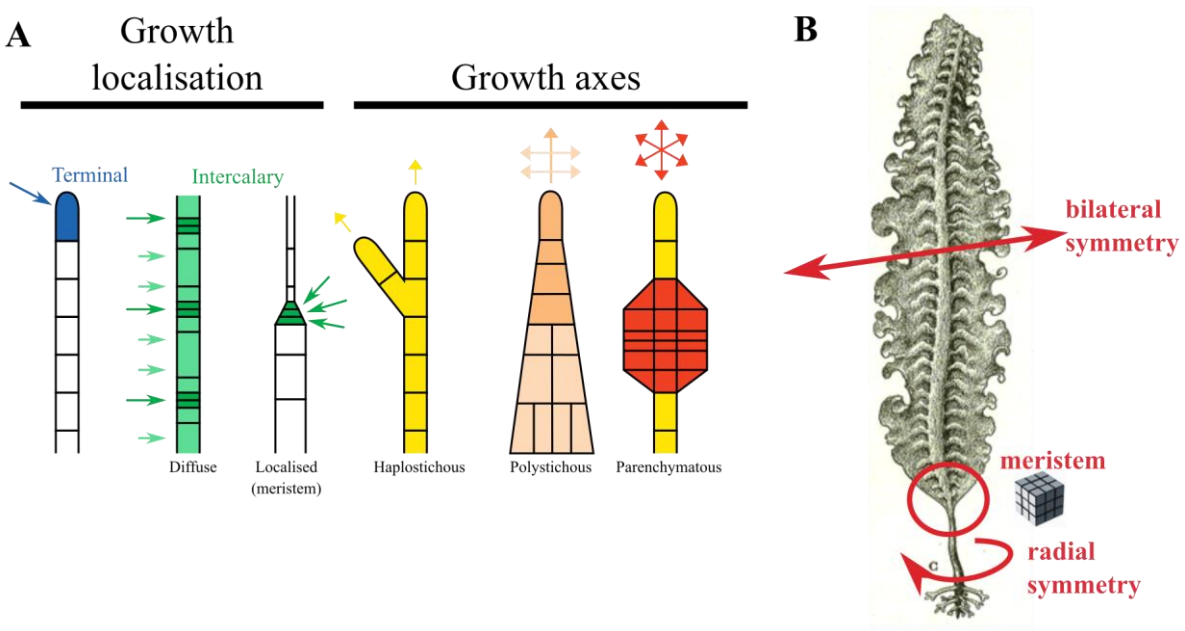

Figure 1.5 - Overview of the diversity of thallus construction modes in brown algae

(**A**) Mode of thallus construction. Growth can be restricted either to the extremity (apical growth, blue box) or to a particular intermediate site of filaments or thallus (intermediate localised growth, green box). Alternatively, growth can occur in multiple areas along or even on the whole filament or thallus (diffuse growth, green box). When cell growth and division always occur in the same direction, uniseriate filaments are built (yellow box). Pseudoparenchymatous thallus can be built by several uniseriate filaments stacked together (not shown). Real, simple parenchymatous thalli can be constructed from single filaments when several rounds of cell division and/or expansion occur in different directions at different times, giving polystichous thallus (orange box). Finally, complex parenchymatous thalli are built by meristems in which cell division and expansion occur in several directions at the same time (red boxes). This figure is reproduced from Charrier *et al.* (2012). (**B**) In the most morphologically complex Laminariales, a real intermediate meristem generates both an axially symmetric stipe and a bilateral blade, supposing complex developmental mechanisms at play.

Like land plants, however, morphogenesis in brown algae is constrained by the presence of a complex cell wall that encases and glues together the cells, prohibiting any form of cell migration or complex tissues folding of the kind occurring during the development of metazoans (Lecuit *et al.*, 2011). Rather, growth and morphogenesis in this group can only be achieved by the pattern of cell division and expansion. As such, the diversity of thallus morphologies is achieved by a rather restricted set of growth patterns, defined by the position growth along the thallus and the preferential direction of cell division and/or elongation (Charrier *et al.*, 2012; **Fig. 1.5A**). Growth can be restricted to a small part of the thallus, whether in the distal end or margin of the thallus body ("apical" or terminal growth) or in an intermediate zone in the thallus (localized intercalary growth, **Fig. 1.5A**). In these cases, the growth area is generally designated as a meristem or a "pseudo-meristem". Alternatively, growth can occur along most of the thallus, and in this case is called diffuse intercalary growth. Any of these growth distribution patterns can, theoretically, occur on any of the body plans described above (from uniseriate filaments to true parenchymatous tissues). The major growth axis is dependent on the main direction of cell division and subsequent cell expansion (although this last parameter was often overlooked in kinetic analysis of brown algae development). When divisions happen in a single direction, they lead unescapably to the formation of uniseriate cell filaments (haplostichous growth, **Fig. 1.5A**), stacked or not into pseudo parenchymatous tissues, like in the blade of *Zonaria* (Dictyotales, Katsaros, 1995) or the "bladder" of *Adenocystis utricularis* (Clayton, 1985). A particular case and relatively common form of haplostichous intercalary growth is the trichothallic growth, in which an intercalary meristem generates by transversal divisions a basipetal row of large, photosynthetic cells (building the main thallus body), and a acropetal row of thinner, non-photosynthetic cells that constitute a hyaline hair. True parenchymatous tissues can be obtained by several patterns of growth division, with a graded series of transitional mode growth patterns between pseudoparenchymatous tissues direct generation of 3D tissues. Parenchymatous tissues can be generated by several rounds of cell divisions occurring in different directions, generally more or less orthogonal between subsequent rounds. This is the morphogenetic mode of, for example, the polystichous thalli of Sphacelariales (leptocaulus construction, Katsaros, 1980, 1995; Katsaros and Galatis, 1990), or of the blade of some Dictyotales, like *Dictyopteris membranacea* (Katsaros, 1980, 1995; Katsaros and Galatis, 1988). In these cases, the general shape of the thallus is sometimes dictated in large part by the expansion and shape of the often voluminous initial cells only, and the subsequent divisions then compartmentalize the thallus into many smaller, specialised cells, without much more volume expansion (Katsaros, 1980; Katsaros and Galatis, 1985, 1988, 1990). The complex parenchymatous thallus of Laminariales algae are built by genuine intercalary meristems that generates the stipe in the basipetal direction and the blade in the acropetal direction (Charrier *et al.*, 2012; **Fig. 1.5A** and **B**). On the contrary, the branched fronds of Fucales are generally build by apical meristem containing, in their center, a large, quiescent, pyramidal apical cell that divide regularly on each side to generate smaller meristematic cells (Chapman, 1962; Katsaros, 1995; Linardić and Braybrook, 2017). This latter form closely resembles shoot apical meristems of bryophytes or ferns, and is a remarkable example of convergent evolution.

1.2.3. Physical constraints on the development and morphogenesis of brown algae

The development of the brown algae, and more broadly of all marine macroalgae, is also constrained by the physical properties of the coastal ecosystems in which they thrive. In particular, the large mechanical stresses imposed by the water currents and waves imposes specific shapes and mechanical properties of macroalgal thallus (Gerard, 1987; Denny and Gaylord, 2002). Water flows generate huge drag forces resulting in large extensional, bending and torsional strains, which put the organism at risk of being torn apart or dislodged from its anchoring point (Koehl, 1984; Denny and Gaylord, 2002). To withstand or avoid such mechanical constraint, the thalli shapes have adapted to reduce the drag forces (Koehl, 1984; Denny and Cowen, 1997; Gaylord and Denny, 1997; Koehl *et al.*, 2008). In parallel, the thalli evolved to be both highly flexible (supposing a high level of elasticity) and tough, both at the level of the organ and of the whole organism. High deformability allow to reconfigure the shape of the thallus, giving the thallus a more streamlined profile or reducing its frontal area, allowing to attenuate the drag force (Koehl and Wainwright, 1977; Koehl, 1984; Hale, 2001; Denny and Gaylord, 2002; Boller and Carrington, 2006, 2007; Harder *et al.*, 2006; Martone *et al.*, 2012). The mechanical resilience ("toughness") allow the organs or the whole thalli to resist to fracture propagation and breakage despite the multiple and repeated extension, bending and torsion deformations they endure (Koehl and Wainwright, 1977; Hale, 2001; Lubsch and Timmermans, 2017). Such requirement for high flexibility and mechanical resilience, and for other physical properties, for example buoyancy, had probably imposed huge constraints on the composition, structure and mechanical properties of the cell wall (Tesson and Charrier, 2014*a*) and the anatomy of tissues and organs. The mechanisms of wall expansion and mode of thallus edification have probably been strong impacted by these constraints.

The precise level of mechanical stress the algae are subjected to greatly depends on the local environment (for example between well-protected and wave-exposed habitats). As such, macroalgae are endowed with great developmental plasticity, allowing them to acclimate their shape to local conditions and optimize their resistance to stress while maximizing their exposure to light (Gerard, 1987; Johnson and Koehl, 1994; Carrington *et al.*, 2001; Kitzes and Denny, 2005; Koehl *et al.*, 2008; Charrier *et al.*, 2012; Tesson and Charrier, 2014*a*). The underlying cellular and molecular mechanisms regulating growth and morphogenesis have thus probably been adapted also to allow great responsiveness to environmental cues and large and rapid shift in rate and pattern of organ growth expansion. This constraint may, for example, require the retention of low thalli complexities, as morphologically or anatomically complex thallus may be more difficult to reconfigure (Charrier *et al.*, 2012; Tesson and Charrier, 2014*a*). Whatever it be, all these particularities make the developmental studies of brown algae (and macroalgae in general) all the more so worthy.

1.2.4. Cellular peculiarities

Brown algae are also interesting because of their particular cell organization, that distinguish them from that of land plants. Beyond numerous common features, the most fundamental of which are the presence of a polysaccharidic cell wall and of a large internal hydrostatic pressure, many particularities exist in the structure of the cytoplasm (Katsaros, 1980; Charrier *et al.*, 2008) and in the structure of the cell wall (Michel *et al.*, 2010*b*; Popper *et al.*, 2011*b*; Ficko-Blean *et al.*, 2015). Their chloroplast, for example, is derived from a secondary endosymbiosis with a red microalgae, an event that probably occurred very early during the evolution of the SAR supergroup (Baldauf, 2008; Cock *et al.*, 2012; Burki, 2014). This particularity had important consequences on the architecture of the endomembrane trafficking system, on the cellular metabolism and on the genomic baggage of the cell (Charrier *et al.*, 2008), that remain, for now, poorly understood (Cock *et al.*, 2012). The sequencing of the genome of *Ectocarpus* (Ec32 strain; Cock *et al.*, 2010) revealed that this alga possesses a unique mixture of gene homologous to genes in land plants, metazoans and fungi, and some gene with no apparent homologues in any of these lineages (Cock *et al.*, 2012). In the context of the study of cell morphogenesis and developmental, the structure of the cytoskeleton (Menzel, 1996; Fowler and Quatrano, 1997; Ketelaar, 2002; Katsaros *et al.*, 2006) and the structure, composition and mechanical properties of the wall (Geitmann and Ortega, 2009; Braybrook and Jönsson, 2016) may be of special relevance.

1.2.4.1. The cytoskeleton

The cytoskeleton of brown algal cells, represented by the microtubules (MTs) and the actin filaments (AFs), have already been extensively investigated (Katsaros *et al.*, 2006), with a special focus on the fucoid embryos, that was the main model for the study of embryogenesis of plant organisms for decades (Harold, 1990; Fowler and Quatrano, 1997). Their spatial organization in vegetative brown algal cells shows major differences with that observed in land plants (Katsaros *et al.*, 2006).

1.2.4.1.1. Microtubules

In brown algal cell, all MTs radiate from one or two centriol-containing centrosome located close to the nucleus, a situation that resembles what is observed in animal cells, although in the latter the centrosome is not duplicated for most of the cell cycle (Katsaros *et al.*, 2006). Those centrosomes are surrounded by pericentriolar proteins and constitute true MTs Organizing Centers (MTOCs) from which most of MTs radiate out into the whole volume of the cytoplasm, while other stay close and surround the nucleus. The (+)-end of radiating MTs generally reach the cortical cytoplasm; yet, true cortical MTs seems generally to be absent of brown algal cells (Katsaros *et al.*, 1991, 2006; Katsaros, 1992; Katsaros and Galatis, 1992). Consequently, contrary to land plants cells (Tsekos, 1999; Baskin, 2005), MTs cannot be involved in the regulation of the deposition of cellulose microfibrils (Katsaros *et al.*, 2006). Some exceptions seem to exist, though, for example in the *Fucus* embryos, in which a direct mechanical role of this component of the cytoskeleton in shaping the rhizoid as even been hypothezised (Corellou *et al.*, 2005). The role of MTs in mitosis, cell division and polarity axis fixation in fucoid embryo is well established (Katsaros and Galatis, 1992; Katsaros *et al.*, 2006; Bisgrove, 2007; Katsaros, 1992). A network of cortical MTs seems to

accumulate, after the establishment of the polarity axis and concurrently with accumulation of endomembranous material, at the site of emergence of the future rhizoid of fucoid embryo (Corellou *et al.*, 2005; Bogaert *et al.*, 2013). This positioning is independent of the alignment of the two centrosomes close to the nucleus and seems to act as a MTs polymerization center to build the rhizoid-pole-focused MTs array present during tip-growth (Corellou *et al.*, 2005). A similar phenomenon is observed in some other polarly growing or branching brown algal cells (Katsaros, 1992; Karyophyllis *et al.*, 1997; Katsaros *et al.*, 2006), pointing toward a conserved pathways that would properly organize of the cytoskeleton in polarly growing cells. This particular array of MTs is more or less longitudinal to the growth axis of the incipient rhizoid of *Fucus* embryo. The same organisation is observed in germinating mitospore of *Ectocarpus* (Green *et al.*, 2013) and in steady tip-growing apical cell of *Sphacelaria* (Karyophyllis *et al.*, 1997). The importance in cell growth is revealed by the effect of MT depolymerization, that block growth and lead to misshapen cells (Katsaros *et al.*, 2006). The mechanistic role of MTs and especially in tip-growth is, however, not clear. In relation to their role in cell polarity, they seem, at least, involved in the transport and asymmetric distribution of organelles along polarity axis (Katsaros *et al.*, 2006; Peters and Kropf, 2010; Bogaert *et al.*, 2013).

1.2.4.1.2. Actin filaments

The actin cytoskeleton of brown algal cells is highly developed and complex (Katsaros *et al.*, 2006). Extensive networks of AFs extend in the perinucleolar, central and cortical region of the cytoplasm, with cortical network apparently being the most developed (Karyophyllis *et al.*, 2000*a,b*; Katsaros *et al.*, 2002, 2003, 2006). This component of the cytoskeleton seems involved in virtually all the basic cellular processes directly linked to development and morphogenesis, including cell polarization, cytokinesis, cell wall deposition and formation, and cell growth *per se* (Katsaros *et al.*, 2006). A certain level of redundancy seems to exist between the functions of MTs and AFs, suggesting important interactions between these two components of the cytoskeleton (Katsaros *et al.*, 2006), and promising numerous research avenues for the future.

AFs are absolutely required for cell morphogenesis in brown algae. During zygote polarization, a network of cortical AFs is accumulated at the presumptive site of emergence of the future rhizoid (Kropf *et al.*, 1989; Alessa and Kropf, 1999). It is primordial for all the cellular processes that accompany the stabilisation of the polarity axis and the emergence of the rhizoid, like the accumulation of endomembranes, the generation of local pH and Ca^{2+} gradients, and wall formation and expansion at the tip (Hable and Kropf, 1998; Kropf *et al.*, 1998; Pu *et al.*, 2000; Bisgrove and Kropf, 2001; Bisgrove, 2007).

At further stages, a dense actin cap was maintained during the steady tip-growth of the rhizoid (Kropf *et al.*, 1989), supporting the hypothesis that actin mechanically strengthens or protrudes the apical wall (Steer, 1990). However, during the protrusion of the rhizoid tip, the cortical patches appeared to rearrange into a sub-apical collar at the base of the apical dome (Alessa and Kropf, 1999; Pu *et al.*, 2000). Similar phenomenon was observed during the germination of gametophytic cells in *Macrocystis pyrifera*, in which the collar generate many radials AFs that extend into the cytoplasm of the main cell body (radial-circular configuration; Varvarigos *et al.*, 2004). These radial filaments seem to be involved in the organisation of ER strands extending radially from the apical pole (Varvarigos *et al.*, 2007). Later on, however, an apical cap reformed at the apex of the branch, suggesting the importance of this structure for steady wall expansion at the tip.

The role of AFs in controlling cell polarization and morphogenesis is also thought to rely on strong connections between cortical AFs and the external cell wall, via transmembrane protein complexes at the rhizoidal pole (Kropf *et al.*, 1988, 1998; Henry *et al.*, 1996; Menzel, 1996; Fowler and Quatrano, 1997; Quatrano and Shaw, 1997; Ouichou and Ducreux, 2000), suggesting that AFs may have direct physical influence on the mechanical properties of the wall (Steer, 1990; Fowler and Quatrano, 1997; Kropf *et al.*, 1998). On the cell membrane and cytoplasmic sides, such connections would be made of protein homologous to animal proteins involved in focal contacts, like integrins and alpha-actinins (Kropf, 1992; Ouichou and Ducreux, 2000; Quatrano *et al.*, 1991; Menzel, 1996). On the wall side, specific wall components, possibly a sulphated or non-sulfated fucan (Quatrano and Crayton, 1973; Bisgrove and Kropf, 2001; Torode *et al.*, 2015) or a vitronectin-like protein (Quatrano *et al.*, 1991; Wagner *et al.*, 1992), would be essential to anchor those connections to the apical wall.

The only study exploring the role of the cytoskeleton in the mechanics of steady tip-growth in brown algae was performed in the apical cell of *Sphacelaria rigidula* (Karyophyllis *et al.*, 2000*a*,*b*). They observed a complex network of cortical AFs, which organisation varied along the polarity axis of the cell. In the apical dome, short and randomly oriented AFs were observed. At the junction zone between the apical dome and the shanks, a dense collar of long, transversally oriented AFs were present, and in the shanks, AFs were axially or helicoidally oriented. At those three locations, the general orientation of AFs was parallel to that of cellulose microfibrils in the innermost layer of the cell wall (Karyophyllis *et al.*, 2000*b*). When AFs were depolymerized by cytochalasin B, the orientation of newly deposited fibrils became random. This demonstrated that the orientation of cortical AFs controls the orientation of cellulose MFs, thus replacing the role normally invested by MTs in plant cells. The same direct relationship between cortical AFs and cellulose fibrils was since demonstrated in several other brown algal species (Katsaros *et al.*, 2002, 2003, 2006). As the preferential orientation of cellulose microfibrils are thought to control plant cell morphogenesis (Green, 1962, 1965, 1969; Tsekos, 1999; Baskin, 2005; Cosgrove, 2005), this strongly suggests that actin cytoskeleton directly controls cellular morphogenesis in brown algae (Katsaros *et al.*, 2002, 2003, 2006). However, no conspicuous accumulation of cortical AFs in the apical dome of *S. rigidula* was noted, questioning its role in tip growth.

1.2.4.2. The cell wall

1.2.4.2.1. Cell wall chemical composition

Brown algae are also especially interesting because of their particular cell wall, that again set them apart to land plants and fungi. The cell wall elasticity in this groups is on average 1000 time higher than that in land plants (Tesson and Charrier, 2014*a*), and this high deformability is probably linked to its particular composition. Cell wall in brown algae is rich in two families of anionic polysaccharides, the sulphated fucose-containing-sulfated-polysaccharides (FCSPs) and the alginates, that both represents a major fraction of the wall (Frei and Preston, 1962; Mabeau and Kloareg, 1987; Deniaud-Bouët *et al.*, 2014*a*, 2017). In also contains celluloses microfibrils, but this in contrast to FCSPs and alginates, this latter component is present only in low abundance (1 to 8 % of cell wall dry weight). Remarkably, the cellulose microfibrils have a ribbon-like shape, about 2.6 nm in thickness but with variable width (Katsaros *et al.*, 1996; Tamura *et al.*, 1996; Tsekos, 1999; Terauchi *et al.*,

2016). The FCSP is a very large and diverse category of polysaccharides that comprises "true" sulphated fucans (L-fucose backbone) and many other polymers made of various sugar and including various proportions of L-Fucose, designated as "heterofucans" or "fucoidans" (Ficko-Blean *et al.*, 2015; Deniaud-Bouët *et al.*, 2017). The alginates are linear chain of β-1,4—D-mannuronates (M units) and α-1,4-L-guluronates, organized in blocks of homopolymers (MM and GG) and of heteropolymers with regularly interspersed M and G units (MG-blocks) (Haug *et al.*, 1966). Alginates are deposited in the cell wall as pure MM-homopolymer (Michel *et al.*, 2010*a*). The G unit are formed *in muro* by irreversible epimerization of M units on the C5 carbon (Haug and Larsen, 1969*a*) by mannuronate-C5-epimerase (MC5E), of which numerous copies exist in brown algal genomes (Tonon *et al.*, 2008; Fischl *et al.*, 2016). It has been shown *in-vitro* that alginate can form gel which viscosity dependents on the M/G ratio, more specifically on the proportion of G-blocks, as only the latter can chelate the calcium in egg-boxes structure, resulting in strong gelation (Smidsrød *et al.*, 1972; Grant *et al.*, 1973; Draget *et al.*, 1994; Ertesvåg, 2015; Draget and Taylor, 2011).

A series of recent studies have expanded the range of proteins and polysaccharides known to be present in brown algal walls. Hervé *et al.* (2016) detected arabinogalactan proteins in *Fucus serratus*, where they have been shown to regulates the development of the embryo. AGP where also detected, along with Rhamnogalacturonan I (RGI)-like polymers (probably galactan) and β-(1→3)-glucans (callose) on *Fucus serratus* and *Laminaria digitata* (Raimundo *et al.*, 2016, 2017). Finally, various brown algal species were shown to contains mixed-linked-glucans ((1→3),(1→4)- β-D-glucans; Salmeán *et al.*, 2017). Aside these major polymers, the cell wall of brown algae also contains various proteins (Terauchi *et al.*, 2017), phlorotannins (halogenated or sulfated phenolic compounds) and various ions, including significant proportion of halogenated compounds like iodine (Michel *et al.*, 2010*a*; Deniaud-Bouët *et al.*, 2017). A short overview of wall composition in brown algae is shown in **Fig 1.7** in the next sub-section (**Part 1.3**).

The brown algal cell wall is thus likely to be a highly complex, highly variable compartment of the cell, with numerous functions in physiology, response to stress, development and morphogenesis (Deniaud-Bouët *et al.*, 2017). Its very unique composition would be the product of the particular evolutionary history of brown algae. For example, while FCSPs would be an ancient component of eukaryotic cellular matrix and thus would have very ancient evolutionary roots, alginates would be a much more recent acquisition, resulting from horizontal transfer of alginate-metabolism genes from actinobacteria (Michel *et al.*, 2010*a*; Popper *et al.*, 2011*b*; Deniaud-Bouët *et al.*, 2014*a*).

1.2.4.2.2. Cell wall structure and mechanical properties, and their link to wall composition

Although the wall composition of brown algae is becoming increasingly well known, the in-muro interactions between all those components and the resulting 3D organization and mechanics of brown algal walls remain poorly understood. Though, some theoretical models of wall structure have been proposed, since the 1960s. In the classical view, the cellulose and alginates form the "skeletal" (i.e. fibrillar) part of the wall, along some FCSPs molecules, while most of the fucans may rather be component of the intercellular amorphous material (Mabeau and Kloareg, 1987; Michel *et al.*, 2010*a*). The fibrillar nature of the alginates *in muro* was recently evidenced in the wall of *Ectocarpus*, where they form a net-like network of electron-dense, ~4nm-wide fibrils interspersed by an amorphous material (Terauchi *et al.*,

2016). In a more recent model of the 3D structure of the cell wall has recently been proposed by Deniaud-Bouët *et al.* (2014, 2017), in which the wall of Fucales species is made of two independent skeletal networks: one based on cellulose fibrils interlocked by FCSPs and potentially other "hemicellulose" polymers, and a second based on alginates fibrils cross-linked with polyphenols, with potentially important role in determining wall mechanics.

The key molecular component traditionally though to control wall "deformability" (even though this parameter is not strictly defined by authors that dealt with this question) of brown algal cell walls are the alginates (Michel *et al.*, 2010*a*; Popper *et al.*, 2011*a*; Tesson and Charrier, 2014*a*; Deniaud-Bouët *et al.*, 2014*a*; Linardić and Braybrook, 2017). Because of the different gelling properties of MM-, MG- and GG-blocks, the regulation of the M/G ratio is believed to be a key mechanism the gelling level of brown algal wall, and then possibly the cell and tissue growth (Mabeau and Kloareg, 1987; Ponce *et al.*, 2007; Michel *et al.*, 2010*b*; Tesson and Charrier, 2014*a*; Deniaud-Bouët *et al.*, 2014*a*, 2017; Salmeán *et al.*, 2017). However, the links between alginates content and rheological properties have essentially been investigated *in vitro* on purified alginate gels, essentially because of the extreme importance of this class of polymers in agri-food, pharmaceutical, agricultural and other chemical industries (Draget *et al.*, 1994; Draget and Taylor, 2011; Borhan *et al.*, 2016). *In vivo,* hints about the relationships between alginate composition and wall mechanics have essentially been obtained at the level of the organism or of the organ. This is not ideal to unravel relation between a particular wall component and wall mechanics, because at such scale, the apparent deformability dependent on numerous parameters beyond the wall itself (Cosgrove, 1993*a*; Mirabet *et al.*, 2011). Still, some studies showed that GG-alginates abundance was higher in stipes or holdfasts, organs that are generally stiff, concordantly with their role in anchorage (Craigie *et al.*, 1984; Cheshire and Hallam, 1985; Kloareg and Quatrano, 1988). However, over studies did no observed such relationships (Jothisaraswathi *et al.*, 2006; McKee *et al.*, 1992), or even observed the opposite (i.e., stiff organ or tissues associated with lower GG content; Miller, 1996). At the single-cell level, available data are even more scarce. At least, Terauchi *et al.* (2016) showed that alginate cross-linking by calcium was fundamental to guarantee wall integrity and strength. Yet, on the developing *F. serratus* embryo, Torode *et al.*, (2016), (Linardić and Braybrook (2017) and Linardić (2018) performed immunostaining of alginate using monoclonal antibodies, but they did not find any clear-cut correlation between the distribution of MM, MG and GG epitopes and wall ability to deform (measured by AFM by Linardić, 2018). Clearly, the relative importance of each of the numerous constituents of brown algal wall in controlling wall mechanics, and how those properties are impacted by the structures of the different wall networks remain an open question.

1.3. About the transposition of canonical mechanical models of cell wall expansion to brown algae

Gazing at cell wall expansion under a golden light

Accepted in *Trends In Plant Science* (October 2018)

Bénédicte Charrier[1,*], Hervé Rabillé[1], Bernard Billoud[1]

[1]UMR8227, CNRS-Sorbonne Université. Station Biologique, Place Georges Teissier, 29680 Roscoff, France.

*Correspondence: benedicte.charrier@sb-roscoff.fr (B. Charrier)

http://www.sb-roscoff.fr/en/team-morphogenesis-macroalgae-mma

Keywords: Brown algae, Cell wall, Mechanics, Evolution, Polysaccharides, Remodelling

1.3.1. Abstract

In plants, cell growth is constrained by a stiff cell wall – at least this is the way textbooks usually present it. Accordingly, many studies have focused on the elasticity and plasticity of the cell wall as prerequisites for expansion during growth. With their specific evolutionary history, cell wall composition and environment, brown algae present a unique configuration offering a new perspective on the involvement of the cell wall – viewed as an inert material with yet intrinsic mechanical properties – in growth. In light of recent findings, we explore here how much of the functional relationship between cell wall chemistry and intrinsic mechanics on the one hand, and growth on the other hand, has been uncovered in brown algae.

1.3.2. Cell wall expansion: does the known matter really matter?

The most common paradigm of plant cell growth involves the generation of tensile stress, mainly due to cell turgor, causing the cell wall to yield. In response to this tensile stress, cell volume increases due to the influx of water and cell wall biosynthesis is activated, maintaining cell wall thickness and preventing disruption (Davì *et al.*, 2018). This increase in volume tends to attenuate turgor, but the ongoing re-establishment of the intracellular osmotic potential maintains the tensile stress. These dynamic processes lead to continuous growth – but only if the cell wall is able to yield. Many studies in land plants, fungi, green and yellow-green algae have attempted to link the intrinsic chemical and mechanical (elasticity (see glossary), plasticity, as assessed by short-term experiments) features of the cell wall to its potential for growth (a potentially long-term process). Seemingly intuitive, this relationship

can be tested using current technologies that allow the acquisition of quantitative mechanical data. However, it remains plausible that cell wall growth does not necessarily involve cell wall resistance countering strong tensile stress, like two players pulling a rope in opposite directions, but instead may build on collaborative factors where tensile stress and remodelling factors work in concert to promote growth. In some cases, the regulation of the intrinsic mechanical properties of the cell wall may only be a potential third player, whose role depends on its relative influence in the physical scrimmage. Determining the extent to which cell wall growth directly depends on the intrinsic features of the cell wall – viewed as an inert material that nevertheless has dynamic intrinsic properties – will benefit from widening the range of walled-organisms studied.

1.3.3. Uncoupling cell wall growth from the intrinsic properties of the wall

Growth implies an irreversible deformation of the cell wall, and thus implicitly involves the plasticity of the material that makes up the cell wall. By definition, irreversibility is detected after the growth event has taken place. Hence, growth can be a two-step process in which the cell wall yields according to the elastic nature of the material and this deformation is simultaneously made irreversible through consolidation of cell wall material (Fayant *et al.*, 2010). Or, growth can be a one-step process based on the plastic nature of the cell wall material, for which deformation itself is irreversible and deformation takes place only when the applied stress exceeds a given threshold (the 'yield threshold'). These two cases rely on the intrinsic mechanical properties of the cell wall taken as a physical material (**Fig 1.6A**) in which growth is made possible only when the mechanical properties of the cell wall are modified. A third mechanism is characterised by cell wall remodelling without modifying the intrinsic mechanical properties of the cell wall (**Fig 1.6B**). In this process, yielding is made possible – or is enhanced – due to modification in the organisation of the cell wall material, and not necessarily in its actual chemical composition. These two mechanical properties, i.e. (1) intrinsic mechanical properties (namely elasticity and/or plasticity) and (2) remodelling can theoretically be involved in cell wall growth in all organisms.

Experimentally, assessing the intrinsic mechanical properties of the cell wall is easier than deciphering the process by which the cell wall remodels. In particular, many available techniques can quantify cell wall elasticity, such as indentation using atomic force microscopy (AFM), or stretching (Cosgrove, 1993; Ahmad and Ahmad, 2014; **Tab 1.1**). As a result, reports abound on the close relationship between growth and the intrinsic elasticity of the cell wall (e.g., recently in fungi (Haneef *et al.*, 2017). Emergence and growth of buds in the *Arabidopsis* apical meristem have been correlated with an increase in elasticity (Peaucelle *et al.*, 2011), in a process similar to that occurring in the tip-growing pollen tube, in which elasticity continuously decreases from the tip to 20 µm behind it (Geitmann and Parre, 2004). Similar observations have been reported in fungal hyphae (Ma *et al.*, 2005), but far away from the growth zone. However, the technical flaws pertaining to AFM techniques (**Tab 1.1**) recently highlighted by D. Cosgrove (Cosgrove, 2016*b*) raises *de facto* some issues about the thus far demonstrated role of intrinsic elasticity in growth. At the cellular level, physical measurements of the cell wall ability to yield, which requires quite large cell wall surfaces (e.g., *Chara* and *Vaucheria*, Mine and Okuda, 2003), are rarely performed to confirm AFM data, especially in living cells. Nonetheless, in some cases, cellular expansion in response to

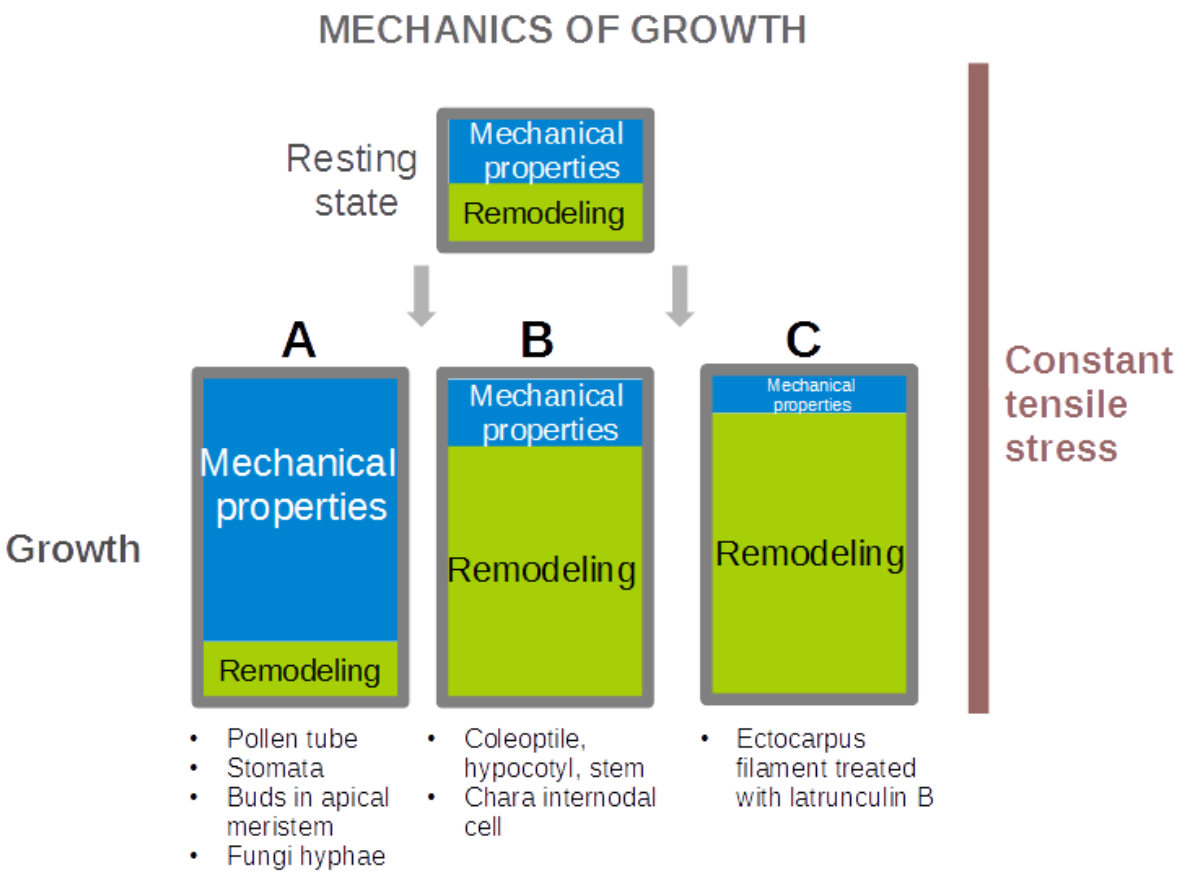

Figure 1.6 - Cell wall mechanical properties involved in cell wall expansion

Cell wall mechanical properties involved in cell wall expansion. Growth involves cell wall yielding, either in response to increased tensile stress (not considered here) and/or in response to an increase in the cell wall amenability to expand (shown here). The thick grey border represents the cell contour following cell wall growth. Colour boxes represent the relative part played by either the intrinsic mechanical properties (blue) or remodelling (green) in cell wall growth. The resting state is represented, by default, with boxes of equal areas. (**A**) Intrinsic mechanical properties are modified to allow cell growth. Among them, elasticity can promote growth due to the activity of enzymes (e.g., pectin-methylesterase inhibitor in the pollen tube in Angiosperms, which maintains inactive PME and methyl-esterified pectins in the growing tip). Using nano- and micro-indentation techniques (**Tab 1.1**), elasticity has been shown to be involved in the growth of many plant, algal and fungal cells (see text for references). However, the reliability of nano- and micro-indentation is questioned. The involvement of 'true' cell wall intrinsic plasticity has been debated (Nolte *et al.*, 1997), because it is often confused with visco-elasticity. Analyses of indentation curves require more complicated models to infer quantitative data on the propensity of the cell wall to plasticity (hysteresis; Fernandes *et al.*, 2012). (**B**) Cell wall remodelling factors (e.g., expansin, xyloglucan endo-transglycosylase) displace the load-bearing bonds between components without modifying the overall chemical composition of the cell wall (e.g., expansins modify the bonds between cellulose and hemicellulose), thereby promoting growth. For example, in the green alga *Chara*, diffuse growth of the internodes relies on the cycling of distorted to non-distorted calcium-pectate complexes in new cell walls and calcium delivery to the cell membrane (Boyer *et al.*, 2016). Dynamics in this cycle results in windows of increased cell wall elasticity and growth. (**C**) In the brown alga *Ectocarpus*, a treatment with 1 µM latrunculin B resulted in an increase in growth whereby the cell increased its width significantly. Simultaneously, the cell lost its capacity to swell in response to a hypo-osmotic shock, meaning that its intrinsic elasticity (and potentially plasticity) was reduced (unpublished data from the authors).

hypo-osmotic treatments has confirmed the overlapping patterns of cell wall elasticity and cell growth (Kierzkowski *et al.*, 2012). When neither of the two intrinsic mechanical properties discussed above seem to be involved, and when growth is shown to require heat and/or living cells, then cell wall remodelling factors releasing the load-bearing bonds are introduced as necessary factors for the cell wall to yield (**Fig 1.6B**). The extent to which remodelling is separate from the intrinsic mechanical properties has been debated and most likely depends on the cell, species and growth mode (diffuse or localised, e.g., at the tip of an apical cell). Since the 1892 demonstration that ascomycete *Peziza* hyphae bursts at the base of the apex where growth is slower and not at the tip where growth is higher (Wessels, 1988), it has been clear that the most deformable positions do not necessarily correlate with actively growing zones. Similarly, stiffness does not correlate with slow-growing cells either. The inner layer of the cell wall of Aspergillus spores is extremely stiff (elastic modulus E up to 30 GPa; Zhao *et al.*, 2005); nevertheless, this is where bud emergence takes place to initiate hyphal growth. Bamboo culms grow very fast via cell elongation at the base of internodes (cumulative growth rate of ~ 30 mm h^{-1}), where secondary cell wall biosynthesis and lignification, initiated before the cessation of cell elongation, lead to very stiff cell walls (*E* ~ 20 GPa; Boyer, 2016). This cell wall is 10,000 times stiffer than the cell wall of the pollen tube which has an elongation rate 100 times slower (~ 300 µm h^{-1}). Beyond these simple observations, experimental data have since demonstrated further this lack of correlation between the intrinsic mechanical properties and growth in land plant cell walls (Park and Cosgrove, 2012, reviewed by Cosgrove, 2018).

Brown algae are macroscopic, multicellular organisms displaying many differences with their land counterparts. Their ancestor likely diverged > 1.6 Mya (Baldauf, 2008), a period during which three endosymbiotic events took place (Stiller *et al.*, 2014), leading to organisms with specific cellular and genomic features (Charrier *et al.*, 2008; Cock *et al.*, 2010). More importantly here, their environment features mechanical properties completely different to those experienced on land. When immersed, most of their growing cells are permanently exposed to seawater moving at a density more than 1000 times greater than the air, generating forces similar to hurricane-forces every few seconds (Denny and Gaylord, 2002). Wave-swept animals develop very stiff bodies to resist these forces, but seaweeds opted for a different strategy: their stiffness is ~100-1000 times lower than land plants, and they have high extensibility. In addition, due to periodic tides in their natural environment, brown algae are usually exposed to a large range of osmotic variations due to dehydration at one extreme of the range and to flooding with rainwater at the other. When immersed in pure water or 2 M NaCl (corresponding to four times the seawater concentration), cells of the brown alga *Ectocarpus* respectively expand by up to 70% (in pure water) and shrink down to 35% of their volume (corresponding to 40% of their surface area; unpublished personal data). In comparison, cells of the tomato shoot apical meristem expand and shrink by about 9% in surface area (Kierzkowski *et al.*, 2012).

Nevertheless, there is a disconnection between these intrinsic mechanical properties of the cell wall and growth potential (**Fig 1.6C**). For example, in the apical cell of the filamentous brown alga *Ectocarpus*, treatment with the actin-depolymerising drug latrunculin B promotes doubled growth in width, but fully blocks cell swelling in the same axis after immersion in half-concentrated seawater (unpublished personal data). This strongly suggests that in these conditions, the underlying mechanics required for growth is distinct from the elasticity/plasticity involved in rapid volume changes, regardless of the exact role of actin in this process. Similar cell wall stiffening has been observed in the pollen tube in response to cytochalasin D, another actin-destabilising drug (Zerzour *et al.*, 2009), but the morphological effects are less pronounced and this result was attributed to micro-indentation artefacts due to

the dome shape. This explanation is excluded when elasticity is measured from changes in cell volume and when deformability can be directly measured in the plane of the cell wall, as performed in the case of *Ectocarpus*.

1.3.1. Cell wall growth: demystifying polysaccharide chemistry

Cell walls are a mixture of compounds whose relative organisation is still obscure, especially in brown algae. At the chemical level, > 80% of brown algal cell wall is chemically different from land plant cell walls (**Tab 1.2**). As in land plants, polysaccharides are the main components, but they are represented by large and rare cellulose microfibrils immersed in abundant alginates (~40%) and sulphated fucans (~40%; Deniaud-Bouët *et al.*, 2014; **Fig 1.7**). That results in cell walls with a much lower degree of crystallinity compared to land plants, and altogether these major differences hinder any reliable transposition between the two groups of organisms.

In the context of growth, a link between cell wall chemical composition and its propensity to expand is intuitively natural. Fungal cell wall biosynthesis mutants are impaired in cell growth (Uchiyama *et al.*, 2018) and the level of pectin methylesterification in angiosperm pollen tubes is directly proportional to growth rate (Parre and Geitmann, 2005*b*). However, the role of alginates in growth, and especially of mannuronans which are described as 'soft' components in in vitro studies (Braccini *et al.*, 1999), has no support thus far. In the brown alga *Sargassum*, the position of new buds is not correlated with a specific spatial pattern of alginates (Linardić and Braybrook, 2017), and no correlation has been found between the active growth site in the rhizoid of the embryo of the brown alga *Fucus* and the presence of soft or stiff alginates (Torode *et al.*, 2016).

In brown algae, can the polysaccharide composition control the intrinsic mechanical properties of the cell well, if not its expansion? 'Soft' mannuronan alginates have been shown to be preferentially extracted from organs with flexible properties, whereas stiff guluronan alginates (Braccini *et al.*, 1999), which form *in vitro* complexes with calcium as pectins do (**Fig. 1.7**), have been extracted from load-bearing organs exposed to drag forces (e.g., kelp stipes in environments exposed to waves (Jothisaraswathi *et al.*, 2006), and references therein). However, completely contrasting observations have also been reported. Miller (1996) found that the highest levels of the stiff guluronans were measured in the most mucilaginous and flexible seaweeds of their study, regardless of their age. This echoes similar observations made in the *Arabidopsis* shoot apical meristem, where an increase in pectin demethylesterification co-locates with an increase in elasticity (Peaucelle *et al.*, 2011), but stiffens the cell wall in the shanks of the pollen tube (Parre and Geitmann, 2005). Therefore, these examples illustrate that, in brown algae as in land plants, the complexity of the mechanics of the cell wall, and moreover of growth cannot be reduced to the presence or absence of a single, or even a handful of polysaccharides. Knowledge of the complete interacting molecular network is the first step before translating chemical composition into mechanics (Shtein *et al.*, 2018). Even in land plants where most of the cell wall chemical components have been identified and where there is a comprehensive set of positional patterns of cell wall components (e.g., along the tip-growing pollen tube; Chebli *et al.*, 2012), the interactive network remains vague and incomplete (Mollet *et al.*, 2013), preventing any simple, straightforward conclusion as to the role of these compounds in growth. Other factors such as the degree of hydration, the ion concentration or the rate of degradation of

Table 1.1 - Techniques employed for the study of cell wall mechanics during expansion[a]

Underlying Mechanical basis	Scale	Technique[b]	Parameters[c]	On Living material (non-destructive)	Benefit	Disadvantage	Refs.[d]
Growth	Organ / tissue	Size measurement	Geometry	yes	Non-intrusive; Cheap	Average of several tissues / cells	[9]
	Cell	Size measurement	Geometry	yes	Automation possible	Tissue accessibility	[9]
	Cell Wall	Marker displacement	Local strain	yes	Resolution < µm	Cells adhesion required	[6]
Intrinsic mechanical properties (including elasticity and plasticity)	Tissue level	Extensometer	Wall loosening	yes	Long-lasting experiments Wide parameter range	Indirect Requires precise cutting Low spatial resolution Averaged data	[9]
		Osmotic pressure shift	Elongation kinetics	yes	Mimics natural conditions	Low resolution	[3]
		Resonance frequency (vibration)	Stiffness Damping coefficient	yes	High-throughput Non-destructive	Large scale, indirect	[12]
		Pressure-block	Stress relaxation	yes	Precise control	Indirect	[2,8]
	Cellular level	Extensometer (instron)	Compressive modulus of elasticity	yes	Overall figure at the cell level	Requires precise cutting Low spatial resolution	[5]
			Plastic compliance Creep	no	Wide range, in the plane of growth, both elasticity and plasticity	-	[2]
		Micro-extensometer (ACME)	Elasticity Plasticity	yes	Microscale, 3D, automated, In the plane of growth Both elasticity and plasticity	Sophisticated equipment, Very recent	[7]
		Creep measurement	Plastic yield stress	no		Stress-strain Not only CW properties	[2]
		Micro-manipulation	Elasticity	yes		Artificial samples	[2]
		Ball tonometry		yes	Overall figure at the tissue level	Low spatial resolution	[4]
		Relaxation spectra	Stress relaxation	yes	Wide parameter range	Requires data smoothing	[2]
		Mercury inflatation	Multiaxial plastic extensibility Creep recovery	no		Intrusive; hazardous	[9]
		Microfluidics (“lab-on-a-chip”)	Compression potential	yes	Continuous measurement with varying growth conditions Automation possible	Low spatial resolution Artificial environment	[1,10]
		Inflation/deflation (osmotic changes)	Elastic modulus (linearity)	yes	Easy to design	Approximate Mainly 2D	[2]
	Cell wall level	Extensometer	Elastic compliance	no	Wide range Both elasticity and plasticity	Require precise cutting Low spatial resolution	[2,8]
		Cellular force microscopy: indentation	Cell wall stiffness	yes	High resolution Relatively high forces (µN)	Complex equipment	[5]

Table 1.1 *(continued)*[a]

Underlying Mechanical basis	Scale	Technique[b]	Parameters[c]	On Living material (non-destructive)	Benefit	Disadvantage	Refs.[d]
Intrinsic mechanical properties (including elasticity and plasticity) *(continued)*	Cell wall level *(continued)*	Atomic force microscopy: microindentation	Stiffness, Elasticity, Plasticity, Adhesion	yes	High spatial resolution (µm scale) Surface mapping Outer and inner wall layers Possible in aqueous media	Complex equipment In z axis (not the growth plane) Sensitive to indentation angle Require adherent sample	[9]
		Atomic force microscopy: nanoindentation		yes	High spatial resolution (nm scale) Surface mapping Low force (nM) possible in aqueous media	Complex equipment In z-axis Only outer cell wall layer Sensitive to indentation angle Requires adherent samples	[1,11]
		Dynamic nanoindentation (nanoDMA)	Viscoelasticity Storage/loss stiffness	yes	High resolution (nanoscale) Can be coupled to TEM and SEM	Require sophisticated equipment	[2]
		Uniaxial stress	Mechanical anisotropy	no		Intrusive	[9]

[a]The list of techniques is not exhaustive.

[b]The acquisition of accurate data of cell wall mechanics during growth should be performed using a technique that can take measurements (i) on living organisms, (ii) over a period of time in accordance with the dynamics of growth, (iii) at the precise position of the cell surface where growth takes place, whatever the scale, (iv) in the direction of expansion (mainly tangential position along the cell surface; z-axis is less relevant); and that is (v) adequate for 3D objects (e.g., AFM is sensitive to the orientation of the contact plan, as in the dome of the pollen tube), (vi) compatible with the mechanical properties of the biological sample (e.g. biological materials, and especially the cell wall, do not behave as linear elastic materials) and (vii) able to measure the overall cell wall mechanical features, and not only the superficial, outermost layer (e.g. nano-indentation). Literature cited: [1] Ahmad & Ahmad (2014); [2] Cosgrove (2016b); [3] Cosgrove (2018); [4] Geitmann (2006); [5] Al-Zube *et al.* (2017); [6] Rabillé *et al.* (2018a); [7] Robinson *et al.* (2017); [8] Schopfer (2006); [9] Taiz (1984); [10] Vogler (2015); [11] Zhang *et al.* (2016); [12] Nakata *et al*. (2018).

[c]Parameters listed are based on the author's terminology, but the exact definition of parameters may be subject to subtle variations between authors.

[d]Mainly reviews are cited.

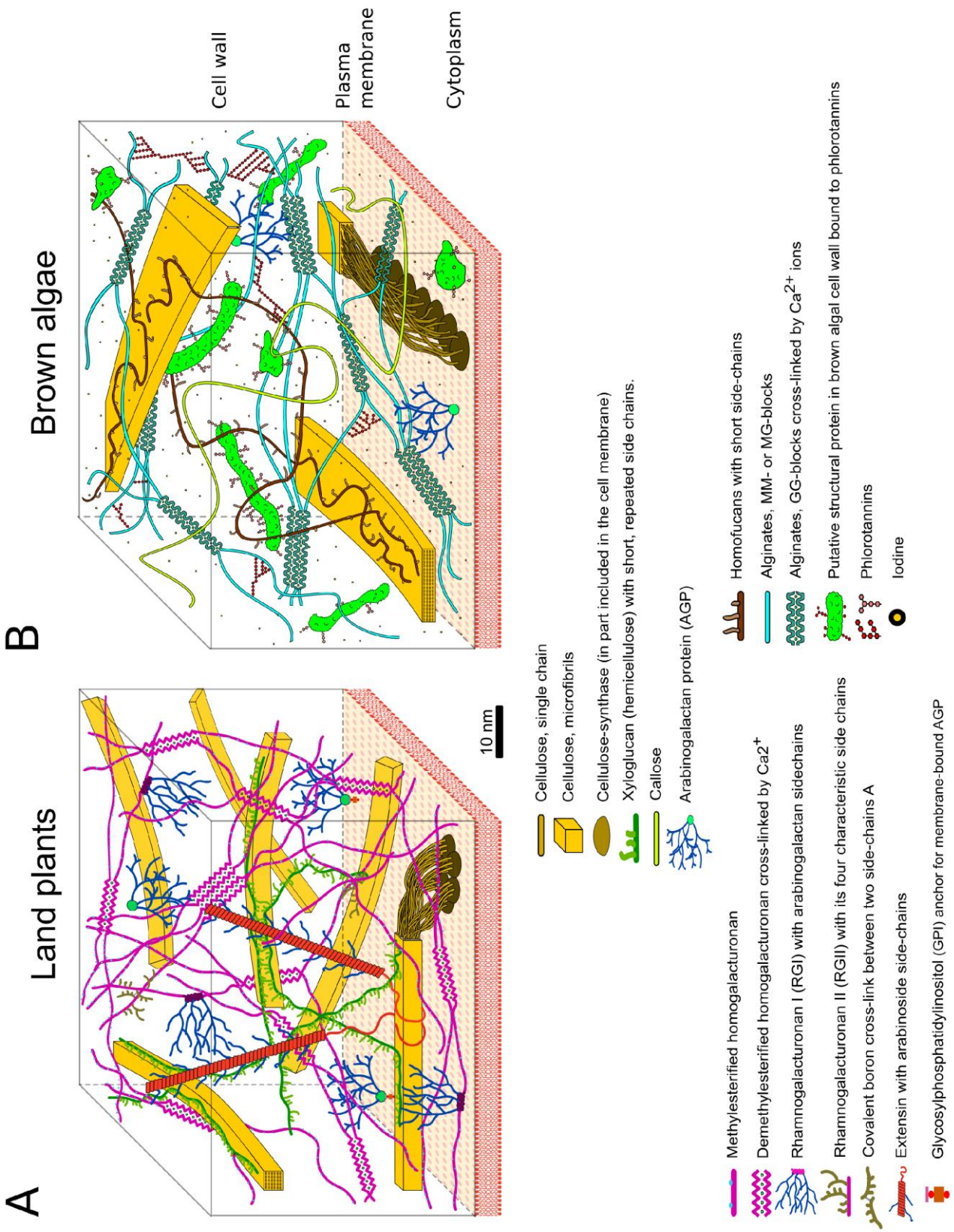

Figure 1.7 - Comparison of the cell wall chemical composition and structure in land plants and brown algae
(caption on the next page)

(Figure 1.7, *continued*) Only the primary cell wall is considered. (**A**) In land plants (angiosperms), the cell wall is mainly composed of two networks: (i) cellulose microfibrils (MFs, both crystalline and non-crystalline; Aouar *et al.*, 2010) which are cross-linked by hemicelluloses chains (for simplicity only xyloglucans, XG, are represented in the drawing) via hydrogen bonds, and (ii) pectin gel network. Pectins are composed of several sub-structures: homogalacturonan (HG) and rhamnogalacturonan I and II (RGI and II). Demethylesterified HGs are crosslinked by calcium ions and RGII are cross-linked by borate. Extensins, which are structural proteins potentially cross-linking cellulose and pectins, and arabinogalactan proteins (AGP) are also shown, although their detailed structure and interaction are not certain (Carpita and Gibeau, 1993; Carpita and MacCann, 2000). For a detailed review on the composition of the cell wall of the pollen tube, see Mollet *et al.* (2013). (**B**) In brown algae, much less is known about the detailed composition and structure of the cell wall compared with land plants. The model presented here is mainly based on Terauchi *et al.* (2016). The cell wall is likely composed of at least two independent networks: (i) cellulose MFs cross-linked with fucose-containing sulphated polysaccharides (FCSPs) and proteins, and (ii) alginate gel networks cross-linked by phlorotannins. Cellulose MFs are ribbon-shaped and much less abundant than in land plant cell walls (0-8% dry weight, Table 2). For simplicity, only homofucans FCSPs are represented in the drawing. The identity and structure of putative cross-linking proteins (in blue, including recently identified AGPs) and phlorotannins are speculative. β-(1→3)-glucans (callose) and β-(1→3)-(1→4)-glucans (mixed-linkage glucans, MLG, not shown in the drawing) have also been identified in brown algal cell wall (Table 2), but their interactions with other components are unknown (Raimundo *et al.*, 2017; Salmeán *et al.*, 2017). The cell wall of brown algae is also rich in halogenated compounds (up to 19% dw), especially iodine species in the form of free ions (up to 1.0% dw, i.e. 30,000-fold the concentration of the seawater) or included in halogenated molecules (especially phlorotannins, La Barre *et al.*, 2010). All components are drawn to scale.

Table 1.2 - Cell wall components of land plants and brown algal cell walls[a](caption in the next page)

Class	Sub-class	Abundance	
		Land plants	Brown algae
Cellulose	No sub-class	15-33 %	1-8 %
Hemicelluloses	Homoxylans (X)	~ 8 %	n.d.
	Arabinoxylans (AX)		n.d.
	Glucuronoxylans (GX)		n.d.
	Glucuronoarabinoxylans (GAX)		n.d.
	Xyloglucans (XyG)	~ 20 %	n.d.
	Xyloglucuronans		Present
	Mannans (M)	Scarce	n.d.
	Glucomannans	Scarce	n.d.
	Galactomannans	Scarce	n.d.
	Galactoglucomannans	Scarce	n.d.
	Glucuronomannans	Scarce	n.d.
	Mixed-linkage-glucans (MLG)	Scarce*	Present
	Callose (β-1,3-glucans)	Potentially abundant	Present
Pectins	Homogalacturonnans (HG)	6-15 %	
	Rhamnogalacturonans I (RGI)	5-10 %	Present
	Rhamnogalacturonans II (RGII)	1-4 %	
	Apiogalacturonans	Scarce	
	Xylogalacturonans	Scarce	
Alginates	No sub-class	n.d.	~ 40 %
Fucose-Containing Sulphated Polysaccharides (FCSP)	Fucans	n.d.	~ 40 %
	Fucoglucuronans	n.d.	
	Fucogalactans	n.d.	
	Xylofucoglucuro-mannans	n.d.	
	Uncharacterised FCSPs	n.d.	
Non-catalytic remodeling proteins	Expansins	Present	n.d.
	YoaJ-like proteins	n.d.	Present
	CBM32-containing proteins	n.d.	Present
Catalytic remodeling proteins	Glucosidases	Present	n.d.
	Glucanases	Present	n.d.
	B-galactosidases	Present	n.d.
	Polygalacturonases (PGs)	Present	n.d.
	Pectate-lyases (PLs) and Pectase-lyase-like (PLLs)	Present	n.d.
	Xyloglucan EndoTransglycosidases (XETs)	Present	n.d.
	Xyloglucan endo-hydrolases (XEH)	Present	n.d.
	Xylosidases	Present	n.d.
	Pectin-Methyl-Esterases (PMEs) And PME-Inhibitors (PMEIs)	Present	n.d.
	Pectin acetylesterases	Present	n.d.
	Xyloglucan acetylesterases	Present	n.d.
	Mannuronate-C5-Epimerases	n.d.	Present
	Vanadate-dependant Halogenoperoxidases (vHPO)	n.d.	Present
	GH88-familiy proteins	n.d.	Present
	Alginate-lyases	n.d.	Present
	Pectin-lyase-fold Virulence factor domain proteins	n.d.	Present
	Metalloproteinases and inhibitors (TIMP)-like proteins	n.d.	Present
	Subtilisin-like serine proteases	n.d.	Present
	CBM1-containing proteins	n.d.	Present
Structural proteins	Arabinogalactan Proteins (AGPs)	Present	Present
	Prolin-Rich Proteins (PRPs)	Present	n.d.
	Hydroxyprolin-rich proteins (HPRPs) including Extensins	Present	n.d.

Table 1.2 (continued)[a]

Class	Sub-class	Abundance	
		Land plants	**Brown algae**
Structural proteins (continued)	Glycin-rich proteins (GRPs)	Present	Present
	Many uncharacterised CW proteins	Present	5-9 %
Phenolic compounds	Para-coumaryl acid	>2 %	n.d.
	Phlorotannins	n.d.	Present

[a]The table shows the nature and approximate abundance (% dry weight) of the different components of the cell wall in land plants (only primary cell wall; both dicotyledonous and monocotyledonous (Carpita and Gibeaut, 1993; Carpita and MCann, 2000; Aouar *et al.*, 2010; Mollet *et al.*, 2013) and in brown algae (La Barre *et al.*, 2010; Raimundo *et al.*, 2017; Salmeán *et al.*, 2017; Deniaud-Bouët *et al.*, 2017).

* Much higher abundance in Poales (monocotyledonous). Abbreviations: n.d., no data available.

polysaccharides are alternative driving forces in cell growth (as discussed in Peaucelle et al. 2008; Bidendhi and Geitmann, 2016).

As a result, attempts to piece together partial knowledge lead to complex scenarios, such as those featured for pollen tube growth, where differential and often counter-intuitive gradients of factors including calcium concentration and pectin-methylesterase enzyme (PME) activities, are squeezed into a possible mechanism of tip growth (Bosch and Hepler, 2005; Wallace and Williams, 2017). However, the different biological contexts call for putting all the cards back on the table. In brown algae, alginate stiffness is described as depending directly on the calcium concentration, but this relationship degenerates when calcium concentration is 10 times that of the seawater (Cuadros *et al.*, 2012), a situation that can be reached locally *in muro* in emerged thalli, especially in poro-elastic cell walls (Chebli *et al.*, 2012). As for PME, recent studies suggest that the control of methylesterification (including both PME activity and a PME inhibitor, PMEI) is especially important for the fast growth of angiosperm pollen tubes, and less determinate in gymnosperms in which the gradients of esterified pectins are less pronounced and PMEI is absent (Wallace and Williams, 2017). Furthermore, studies of growth mechanisms in more basal green cells, such as in the charophyte alga *Chara*, argue that the role of PME as described in the pollen tube may be limited to the more recently evolved green plants (Boyer, 2016). This is just a sign of the diversity of mechanisms that may be encountered in organisms whose phylogenetic position is distant to the most studied plant models, and an indication that our understanding of their role in plant cell growth *lato sensu* should mature with future evo-devo studies.

Interpretation of results becomes even more complex when cell wall polysaccharides of different natures compensate each other. In brown algae, degradation of alginates leads to a stiffer cell wall unable to expand in response to hypo-osmotic shock, suggesting that alginates are necessary to ensure intrinsic cell wall elasticity (unpublished personal data). However, a closer look shows that this decrease in elasticity is due to an over-accumulation of cellulose at the sub-cellular location where growth takes place. The high stiffness of cellulose [E of up to 175 GPa (Geitmann, 2006), compared with alginate with value of $E \sim$ a few kPa (Larsen *et al.*, 2015), and pectin E of up to 1 MPa (Niu *et al.*, 2017)] easily accounts for the observed decrease in cell wall extensibility. Similar cellulose accumulation occurred during the over-growth of the apical cell in response to LatB treatment, showing that despite its high stiffness, cellulose does not hinder growth. On the contrary, in plants, cellulose has also the potential to promote growth (Hu *et al.*, 2018). This uncoupling between the role of cellulose in both the intrinsic mechanical properties and cell wall expansion echoes the recent finding that growth and cellulose biosynthesis are regulated by distinct pathways in the *Arabidopsis* hypocotyl (Ivakov *et al.*, 2017). Uncoupling metabolic activity from light-dependent circadian rhythms demonstrated that cell wall biosynthesis is controlled by the former and growth by the latter. Furthermore, cellulose synthases (GT2 family of glucosyl-transferases), as defined from sequence similarity, may not synthesise only cellulose but instead produce mixed-linkage polysaccharides (MLGs) or even new polysaccharides, such as arabinoglucan recently shown in the moss *Physcomitrella* (Roberts *et al.*, 2018). These results show that the links between cell growth and cellulose and/or cellulose synthase genes – as a proxy for cellulose accumulation – are not direct. Clearly, there is a need to revisit the assumption that the presence of stiff components in the cell wall prevents or mitigates its expansion.

So, are polysaccharides more than just inert structural components subjected to the activities of remodelling proteins during growth? Several distinct remodelling mechanisms have been described in land plants, green algae and fungi. In *Chara*, the ongoing delivery of new cell wall components modifies the dynamics of pectate-Ca^{2+} complexes formed *in muro* (the so-called ‘pectate distortion’ mechanism; Boyer, 2016), thereby remodelling the cell

wall. However, proteins are central factors in most of the remodelling processes described so far. In land plants, the xyloglucan-endo-transglycosylases-hydrolases (XTH) participate in cell wall expansion through hemicellulose cutting and joining (Eklöf and Brumer, 2010) and expansins modify hemicellulose-mediated bonds between stiff cellulose fibres (Cosgrove, 1993, and subsequent papers). Any resulting gaps are filled with freshly made or delivered material, allowing the overall expansion of the local cell wall. In fungi, radical coupling catalysed by an oxidase occurs between the cell wall polymers glucosaminoglycan and beta-glucan (Wessels, 1988).

Brown algal cell walls have been shown to contain proteins in significant amounts (>5% of the cell wall biomass; Deniaud-Bouët *et al.*, 2014, 2017) and with a high diversity (> 900 different proteins secreted in brown algae; Terauchi *et al.*, 2017). Interestingly, in brown algae, none of these proteins share similarity with expansin, PME or even cellulase (**Tab. 1.2**; from genomic analysis; Michel *et al.*, 2010). Domains of cell wall remodelling proteins have been identified among secreted proteins (e.g. carbohydrate binding module CBM32 interacting with alginates; Terauchi *et al.*, 2017) making them prime candidates for remodelling factors (Nardi *et al.*, 2015). In addition, families of secreted brown algal proteins are specific (e.g., alginate C5-epimerases) or expanded (vanadium haloperoxidase, metalloproteinases) relative to those of land plants (Ye *et al.*, 2015; Terauchi *et al.*, 2017). Finally, signalling proteins such as the Notch-Domain proteins, previously thought to be specific to animal cells, are over-represented in brown algal cell walls (Terauchi *et al.*, 2017). Therefore, in light of recent data, our current understanding, which still requires more knowledge on cell wall molecular composition and organisation in dynamic conditions, is that brown algae developed a specific secretome for cell wall remodelling.

1.3.2. Concluding remarks and future prospects

Work on non-conventional models phylogenetically distant from land plants gives the opportunity to unveil the existence of alternative mechanisms of growth. In these organisms (and previously noted in land plants and green algae; Proseus and Boyer, 2007), the causal relationship between cell wall growth and intrinsic cell wall mechanical properties, or cell wall growth and cell wall chemical composition, are not obvious. Furthermore, the difference in growth strategies may also be related to the type of organ (e.g., shoot apical meristem or pollen tube in land plants, internodes in green alga *Chara*), its growth mode (respectively tip-growing or diffuse) or its growth dynamics.

The first results obtained in brown algae show that the distribution of cell wall polysaccharide determinants is not easily linked to the cell growth pattern, and that the intrinsic mechanical properties may not systematically correlate with growth potential. This leaves plenty of room for alternative processes, including cell wall remodelling with no alteration of the intrinsic mechanical properties. However, due to the very different composition and organisation of the cell walls in green plants and brown algae, the molecular toolkits of the remodelling machinery are likely fundamentally different. Beyond the potential conservation of molecular factors, cellular and biomechanical studies carried out in brown algae will most likely lead to breakthroughs in alternative mechanisms of cell wall remodelling (see also outstanding questions).

1.3.3. Glossary

All related to the cell wall:

Elasticity: refers to the ability of a material to recover its initial dimensions after deformation (once the stress is released). Reversible deformability.

Extensibility (as defined by D. Cosgrove): The capacity of the cell wall to grow through cell wall loosening (remodelling) in response to a stress.

Growth (or **chemo-rheological expansion**, as defined by Nolte and Schopfer, 1997): The increase in surface area, resulting from either enhanced stress or a modification of the cell wall propensity for deformation due either to an increase in elasticity or plasticity, or to cell wall remodelling.

Intrinsic mechanical properties: elasticity, visco-elasticity or plasticity of a material. Measurements of the intrinsic mechanical properties are performed either directly by intrusive equipment in contact with the biological material (e.g. nano-/micro-indentation), or indirectly by measuring strain on material undergoing external physical forces (creeping, stretching, osmotic pressure).

Plasticity: refers to the irreversible deformation of the cell wall. This process has a temporal dimension and, therefore, plasticity may be taken for visco-elasticity when the dynamics of viscosity are very slow (i.e. much longer than observation time). Also confusingly named "irreversible elasticity" by some authors (e.g., Boyer, 2016).

Remodelling: Defined here as the process by which the arrangement of the various cell wall components interacting with each other is modified. Remodelling does not change the net chemical composition of the cell wall and does not necessarily modify its intrinsic mechanical properties, e.g., modification of the position of hydrogen bonds without modifying their number, resulting in unchanged elasticity. It is promoted by molecular remodelling factors: expansin, xyloglucan endotransglucosylase/hydrolase, redox reactions (e.g., cross-linking bonds in fungal cell wall polysaccharides; Riquelme *et al.*, 2011) or finely tuned chemical cycles involving the interaction of calcium with polysaccharides (e.g., pectate distortion in green algae; Boyer, 2016). The term 'cell wall loosening' is used for remodelling processes resulting in growth.

Stiffness: The opposite of deformability (both elastic and plastic). Assessed using Instron strain measurement techniques, indentation (atomic force microscopy), cell compression, stretching devices, etc. (Cosgrove, 1993*a*; Geitmann, 2006*a*; Ahmad and Ahmad, 2014).

(Taiz, 1984; Carpita and MCann, 2000; Schopfer, 2006; Aouar *et al.*, 2010; La Barre *et al.*, 2010; Fernandes *et al.*, 2012; Vogler *et al.*, 2015; Zhang *et al.*, 2016; Raimundo *et al.*, 2017; Salmeán *et al.*, 2017; Al-Zube *et al.*, 2017; Robinson *et al.*, 2017; Nakata *et al.*, 2018; Rabillé *et al.*, 2018*a*)

****

Acknowledgment: We thank Cécile Hervé for fruitful discussion about the cell wall composition.

1.4. *Ectocarpus* as a model system to study cellular morphogenesis in brown algae

1.4.1. A model species for the brown algae

The filamentous brown alga *Ectocarpus* of the subgroup *siliculosi*[1] (Montecinos *et al.*, 2017) has been elected fourteen years ago as a model species for the study of fundamental biology of brown algae (Peters *et al.*, 2004; Charrier *et al.*, 2008). It belongs to the Ectocarpales order and to the Ectocarpaceae family. Because of their extremely simple morphology (often reduced to branched uniseriate filaments), Ectocarpales have long been considered a "primitive" order, one of the very first to have diverged during the radiation of brown algae (Fritsch and Salisbury, 1920; Chapman, 1962). However, recent phylogenetic analyses demonstrated that they have, instead, emerged only recently (approximately around the end of the Cretaceous period) and are, surprisingly, a sister group of Laminariales, that comprises the morphologically most complex brown algal genera (Silberfeld *et al.*, 2010; Coelho *et al.*, 2012*a*; see **Part 1.2**).

The numerous species belonging to the *Ectocarpus* genus are mostly found in temperate marine coastal environment, where they generally develop as epiphytes on other seaweeds (Charrier *et al.*, 2008; Coelho *et al.*, 2012a; Montecinos *et al.*, 2017). In addition to the large literature that already exist pertaining to various aspects of its biology (Charrier *et al.*, 2008), this model offer numerous other advantages for experimental studies. It can be very easily maintained and cultivated in laboratory all the year round. Its rapid life cycle, that has been well characterized, can be completed in less than 3 months, making it very prone for genetic crossing (Le Bail and Charrier, 2013). During sexual reproduction, the diploid sporophytes generate haploid spores by meiosis in unilocular gametangia (UL), that settle on the substrate and germinate into dioecious (i.e. female or male) gametophytes. These gametophytes produce gametes by mitosis into plurilocular sporangia (PL). Gametes fuse to form a zygote that, when settled to its substrate, develop into a new sporophyte. Sporophytes can also propagate parthenogenetically from diploid mitospores produced in plurilocular sporangia (PL). Unfertilised gametes can also grow into haploid parthenosporophytes (PS) that are morphologically indistinguishable from true sporophytes but haploid, and can also reproduce vegetatively by release of haploid mitospores. This particular situation is ideal for genetic studies, as is allows one to observe the direct impact of a particular mutation on the development of both generations.

Ectocarpus genome is ~214 Mbp and has been sequenced (Cock *et al.*, 2010). Because of this, numerous genetic, genomic, transcriptomic, and proteomic tools have been developed for this model, including several culture collections of WT and mutant strains (Coelho *et al.*, 2012*a*), genetic maps (Heesch *et al.*, 2010) and a complete, annotated genome available online (Cormier *et al.*, 2017). Yet, a current shortcoming of this model is that, despite several

[1] The genus *Ectocarpus*, because the species delineation in this genus is still problematic and under revision (see (Coelho *et al.*, 2012*a*; Leliaert and Clerck, 2017; Montecinos *et al.*, 2017). For this reason, we do not refer, in this thesis report, to a species name, but only to the genus. All the works presented in here were conducted on parthenosporophytes of the Ec32 strain (see main text) belonging to the *siliculosi* species complex of *Ectocarpus* (Montecinos *et al.*, 2017), that was formerly attributed to the species *siliculosus* at the time when it was chosen as a model species for brown algae (Peters *et al.*, 2004; Charrier *et al.*, 2008).

years of efforts, a protocol for genetic transformation is still lacking, impeding the study of gene functions.

1.4.2. Ectocarpus (partheno)sporophytes are ideal for the study of cell morphogenesis

Ectocarpus is particularly suitable for the study of morphogenesis at the cell and tissue levels, because of the extreme simplicity of its thallus. The vegetative body of the sporophyte generation, especially, is made of prostrate filaments (PF) that develop primarily at the surface of the substrate (**Fig 1.8A** to **D**). As these filaments can be grown on glass surfaces, filaments can be observed by optical microscopy, making *Ectocarpus* very suitable for the techniques of cell biology, with numerous protocols already available (Coelho *et al.*, 2012*a,b,c,d,e*; Le Bail and Charrier, 2013). As *Ectocarpus* can be cultivated in controlled conditions under a microscope, the growth and development of living filaments can be followed by time-lapse videomicroscopy. Individual cells, that are all in direct contact with the external environment, can easily be tracked over time. This allowed to define four main cell types: i) tubular apical cells (type A), about 7 µm in diameter (Le Bail *et al.*, 2008), found at the distal ends of each filaments; ii) tubular elongated cells (type E); iii) intermediate cells (type I) that are losing their tubular shape progressively; and iv) central, photosynthetic round cells (type R). A fifth type corresponds to branching R cells (named type B) (**Fig 1.8)**.

As in other macroalgae, the development of WT PS filaments presents a high level of plasticity, both in term of cell differentiation and kinetics of branching. Yet, cell differentiation and branching (see below, **Part 1.4.2**) were not random along the filaments but spatially and temporally regulated (Billoud *et al.*, 2008; Le Bail *et al.*, 2008). This early development has been modelled using a stochastic cellular automaton called “Ectomat”, that successfully reproduced the pattern of cell division and differentiation experimentally observed along growing filaments (Billoud *et al.*, 2008). These developmental rules are only based on direct communication between adjacent cells in the filament, and does not require regulation at a systemic level, suggesting that the early development of the sporophyte is not regulated at the whole organism level (Billoud *et al.*, 2008). Yet, at latter stages auxin-mediated apical dominance, would take control of the pattern of development of the whole filaments (Le Bail, 2010; Le Bail *et al.*, 2010).

1.4.3. Cellular morphogenesis and tip-growth in prostrate filaments

The growth of prostrate filaments is based first on the elongation, then on the division of A type cells (Le Bail *et al.*, 2008). This is in contrast with the growth of the erect filaments, which develop at later stages by intercalary growth and bear the sporangia and gametangia. Each sub-apical E cell, daughter of the A cell mitosis, progressively differentiates into I and then R cell type, at a rate that globally conserve the ratio of E over R cells at the scale of one filament (Billoud et al., 2008; Le Bail et al., 2008). Consequently, the E cells are confined to the distal ends of the filaments, while R cells are packed in the central region. Lateral branches emerge preferentially on R cells. This combined effect results in the progressive

acquisition of an approximate radial symmetry in the tuft of prostrate filaments (Le Bail et al., 2008; Le Bail, 2010).

The development of prostrate filaments is thus the combination of three major morphogenetic processes that occur at the cell level:

i) **Tip-growth** in the apical cells, coupled to their transversal division that gives rise to cylindrical E cells (**Fig 1.8D**, **E** and **F**).

ii) **Cell rounding**, during which the E cells progressively lose their cylindrical shape (transitorily becoming I cell type), and inflate until they acquire a balloon-like shape, i.e. R type cells (**Fig 1.8B**, **C**). Cells often divide transversally during this process into two rounds cells

iii) **Budding of new apical cells** from lateral wall of cells of the primary filaments (generally R cells), initiating the elongation of new filaments. The microtubule cytoskeleton, at least, is involved in the process (Katsaros, 1992). Both the cell rounding and branching have been recently modelled by a poroelastic model (Jia et al., 2017).

Apical cells have the typical shape of tip-growing cells, i.e. elongated tubular zone topped with a hemi-ellipsoid apical dome (**Fig 1.8D**). Wall expansion is entirely restricted to the apical dome, as revealed by labelling living filaments with Calcofluor White Brightener, a fluorochrome that stains the glucanes of the wall (Le Bail et al., 2008; **Fig 1.8E** and **F**), thus demonstrating that the elongation of apical cells is due to a real tip-growth mechanism. Recently, the rhizoid of *Fucus serratus* was also demonstrated to elongate by true tip growth using the same technique (Linardić, 2018). As far as we know, this is, for now, the only two averred occurrence of tip-growth in brown algal, but it is probably much more widspread, as thallus construction by growth of terminal cells is commonplace in brown algae (Katsaros, 1995; Charrier *et al.*, 2012). In the Order Sphacelariales, apical cells are also considered to elongate by true tip-growth, which is supported by a polarized gradient of distribution of ER, dictyosomes and wall-delivery vesicles toward the apical dome (Katsaros, 1980, 1995; Katsaros *et al.*, 1983, 2006; Katsaros and Galatis, 1990). However, the location of wall expansion *per se* has never been measured, so it remains possible that, despite a positive gradient of wall expansion toward the apical dome, wall expansion still occurs on the shanks of the cell, giving what Katsaros (1995) describes a “tip-like growth” process.

Tip-growth of *Ectocarpus* apical cells is remarkably slow compared to the very high elongation rate of plant and fungal tip-growing cells, which can be several hundreds of µm per hours (see for example, for the pollen tube, Benkert *et al.*, 1997; McKenna *et al.*, 2009). In contrast, *Ectocarpus* apical cells elongate only at a rate of about 2.5 µm h^{-1}, which is similar to the growth speed of the rhizoid of *F. serratus* (Linardić, 2018). The cytoplasm appears polarized, with the chloroplast in general stacked toward the apical pole, while the base of the cell looks mainly occupied by the vacuoles. When observed in longitudinal sections by TEM, organelles, especially ER, Golgi, and putative wall delivery vesicles, appear associated with the chloroplast (a distinctive feature of brown algal cells; see Charrier et al., 2008), but their distribution is only vaguely polarized toward the apical dome (unpublished results).

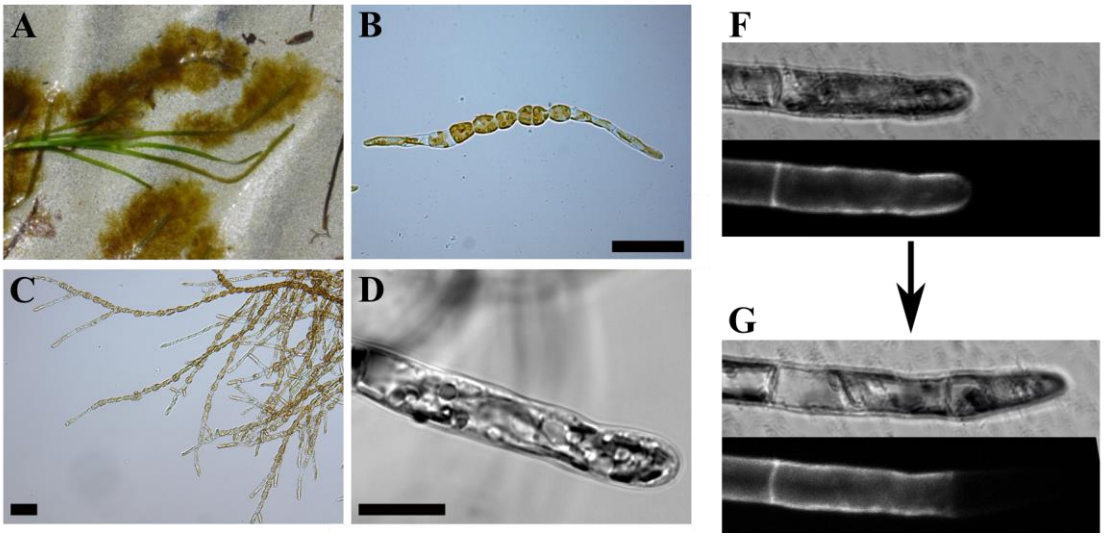

Figure 1.8 - *Ectocarpus* (Ec32 strain) general morphology and early pattern of growth

(**A** to **D**): General and apical cell morphology of vegetative filaments of *Ectocarpus sp*. (**A**) Tuft of *Ectocarpus siliculosus* growing epiphytically on *Zostera*). (**B**): Ten days old sporophyte in culture (scale bar = 10 µm). (**C**): Branched young sporophyte (scale bar = 250 µm). Picture from L. Dartevelle, FR2424, Station Biolgique de Roscoff. **(D)**: High magnification of an apical cell (scale bars = 10 µm). (E and **F**) Evidence that prostrate filaments elongate by real tip-growth, by Calcofluor White staining. (**E**): Bright field (bf) and fluorescent picture of an apical cell of Ec32 just after staining by Calcofluor, under confocal microscopy. (**F**): bf and fluorescent pictures of the same apical cell than in E, after 16h of growth, showing that growth (unstained region of the cell) is restricted to the very tip of the cell. Scale bar = 10 µm.

1.4.4. étoile: a tip-growth mutant of Ectocarpus

Étoile (*elt*) is a recessive single-locus mutant that has been generated by random UV mutagenesis on gametes of Ec32 (according to a protocol described in Le Bail and Charrier, 2013), and is the first morphological mutant of *Ectocarpus* that have been studied in the host team (Le Bail, 2010; Le Bail *et al.*, 2011; Nehr, 2013). This mutant has initially been retained for its hyperbranching phenotype. Indeed, detailed kinetic analysis of branching in the young PS of this mutant showed that, in comparison to the WT (Ec32) that the timing of branching is decoupled from the growth of the primary filaments (Nehr *et al.*, 2011). Simulation using the "Ectomat" model (Billoud *et al.*, 2008) suggested that this developmental defect may be linked to altered cellular communication between adjacent cells (Le Bail *et al.*, 2011). Congruently, four transmembrane Lin-Notch-containing proteins are down-regulated in *etl*, pointing toward potential molecular players involved in the intercellular communication (Le Bail, 2010; Nehr *et al.*, 2011). However, *etl* is also clearly associated with a defect in the tip-growth process of apical cell, leading to misshapen apical cells. Like E cells, A cells show an abnormal tendency to get around prematurely, i.e. the differentiation into R cell is enhanced (Le Bail *et al.*, 2011, and unpublished results). In this mutant, then, the tip-growth defect may be associated to an instability of the tubular shanks. Alteration of cell morphogenesis in *etl* was also linked to altered Golgi structure, altered wall structure and increased wall thickness (Le Bail *et al.*, 2011).

The identity of the mutated gene has been deciphered during the thesis of Z. Nehr (2010-2013). Although her work had remained unachieved, the results pointed toward the gene Esi0533_0012 as the more likely candidate (Nehr, 2013). Interestingly, this gene code for a Rho-GTPase-Activating-Protein (Rho-GAP) with a BAR (Bin-Amphiphysin-Rvs) domain. During tip-growth of pollen tubes and root hairs of Angiosperms, Rho-GAP proteins have been involved in the regulation of the actin cytoskeleton, by modulating the activity of Rho-GTPases (Kost *et al.*, 1999; Kost, 2008, 2010). In fucoid embryos, the Rho-family *Rac1* gene was shown to regulate the polymerization of AFs at the rhizoidal pole and then to control tip-growth initiation (Muzzy and Hable, 2013; Hable, 2014). These date suggest that *ETOILE (ETL)*, by regulating the activity of the Rac1 homologue in *Ectocarpus*, directly control tip-growth of prostrate filament apical cells, potentially *via* the actin cytoskeleton. The BAR domain, which homologues have been shown to bind to curved cell membrane in animal and plant cells (see the relevant literature in Nehr, 2013) could then play a role in localizing activity of ETL to the specific location, at the cell membrane or in specific endomembrane compartments (Nehr *et al.*, 2011). All these preliminary data pointed as a plausible molecular regulator of the mechanism of tip-growth in a brown alga. Its role, however, await experimental validations, the first of which being the confirmation of the identity of the *ETL* gene.

1.5. Thesis objectives

The aim of my thesis is to characterize the mechanisms of tip-growth in the apical cell of the prostrate filament of *Ectocarpus*, and then to provide the first conceptual model of steady-state tip-growth in a brown alga. In the frame of the general research topics of the host team, we used tip-growth as an ideal case study to explore the degree of originality of the fundamental cellular developmental processes acquired by brown algae during their evolution, and to understand to which extent these processes have been influenced by the particular evolutionary history of brown algae and their abiotic environment.

As cellular morphogenesis is, first and foremost, a biophysical process (Boudaoud, 2010; Mirabet *et al.*, 2011), **the first objective** of the thesis was to characterise the biomechanical functioning of tip-growth using a combination of experimental measurements of relevant cellular parameters, namely the turgor, the cell wall strain pattern, the cell wall thickness, and the surface curvature, and of a modelling approach. The acquired data were used to feed the model with proper biological values. The model and numerical simulations were used to identify the key cellular parameters that control the wall strain pattern in the apical cell, and thus tip-growth (link "wall stress/strain"). This model is a first appraisal of the originality of tip-growth mechanism in brown algae. These data led to a **first paper**, in revision in the journal *PLoS Biology* (**Part 2.1**).

The second objective was to approach the extent to which components of the cell wall are involved in cell wall expansion (link "wall chemistry/strain"). The role of alginates in the control of the wall mechanical properties has been studied with a combination of immunolocalisation and biophysical approaches on *Ectocarpus* protraste filaments. This led to a **second paper**, still in preparation (**Part 2.2**).

The third objective was to investigate the role of actin in *Ectocarpus* tip-growth, and its potential regulation by the *ETL* gene (link "cortical factors/strain"). A combination of pharmacological approaches using AF-depolymerizing drug, time-lapse videomicroscopy, fluorescent staining of actin filaments, and biomechanical measurement of the wall mechanics have been used. The results provided essentially some insights about the role of actin filaments (AFs) in controlling the mechanical properties of the cell wall. Those results are presented in **Part 3**. During this thesis, the positional cloning of *etl* causal mutation has also been completed (results not shown in this report).

In the future, the results obtained in the course of this thesis and thereafter will also broaden the spectrum of tip-growth mechanisms identified across the tree of life. They will contribute to lay the foundations for future evo-devo comparisons of tip-growth mechanisms spanning large portions of the phylogenic tree. Such evo-devo approaches will be required in order to answers critical questions like: 1) has tip-growth and similar kinds of cell growth a unique evolutionary origin, or rather did it emerge independently several times during evolution? 2) to which extent are the mechanisms conserved / derived between distant lineages? 3) are biophysical mechanisms of tip-growth more influenced by the molecular toolkit of the organism, by the physical environmental conditions, or by some inescapable constraints imposed by the physical laws?

2. Biomechanics of the apical cells and biomechanical strategy of the apical cell tip-growth

2.1. A mechanical model of *Ectocarpus* tip-growth

The brown algal mode of tip-growth: keeping stress under control

Article 2 *in revision for publication in PLoS Biology*

Authors: Hervé Rabillé[1†], Bernard Billoud[1†], Benoit Tesson[2], Sophie Le Panse[3], Élodie Rolland[1], Bénédicte Charrier[1]*

[†]: these authors contributed equally to this work.

*: corresponding author

[1]: CNRS, Sorbonne Université, Morphogenesis of Macro Algae, UMR8227, Station Biologique, F-29680 Roscoff, France

[2]: SCRIPPS Institution of Oceanography, University of California, San Diego, CA 92093-0202, USA.

[3]: MerImage platform, FR2424, CNRS, Sorbonne Université, Station Biologique, F-29680 Roscoff, France

Author for material and correspondence: Bénédicte Charrier, benedicte.charrier@sb-roscoff.fr

2.1.1. Abstract

Tip growth has been studied in pollen tubes, root hairs, fungal and oomycete hyphae, and is the most widely distributed unidirectional growth process on the planet. It ensures spatial colonization, nutrient predation, fertilization and symbiosis with growth speeds of up to 800 $\mu m \cdot h^{-1}$. Although turgor-driven growth is intuitively conceivable, a closer examination of the physical processes at work in tip growth raises a paradox: growth takes place where biophysical forces are low, due to the increase in curvature in the dome. All tip-growing cells studied so far rely on the modulation of cell-wall extensibility via polarized excretion of cell-wall-loosening compounds at the tip. Here, we used a series of quantitative measurements of cellular parameters and a biophysical simulation approach to show that the brown alga *Ectocarpus* has evolved an original tip-growth mechanism based on the control of the wall stress through the establishment of a steep gradient of cell-wall thickness that can compensate for the variation in cell curvature. Bootstrap analyses showed the robustness of the process and FRAP experiments confirmed the active vesicle trafficking in the shanks of the apical cell which is inferred from the model. In response to auxin, biophysical parameters were modified

in agreement with the model. Altogether, these results converge to an alternative strategy of tip growth developed by brown algae, which is based on the control of the cell wall thickness along the cell with no requirement for cell wall mechanical property fluctuation.

2.1.2. Author summary

Tip growth is known in organisms made of filaments, like fungi, plants and algae. The driving force for growth in these organisms is the difference in osmotic pressure (turgor) between the cell interior and the external medium, a force contained by the cell wall. Physical laws imply that the higher the curvature of the cell, the lower the pressure (stress) perceived by the cell wall. Yet, growth takes place at the cell apex which displays a dome shape, and therefore a high curvature. Tip-growing cells studied so far (mainly plants) compensate the low wall stress in the apex by chemically loosening their cell wall. We studied the brown alga *Ectocarpus*, which is among the most divergent eukaryotes compared to land plants, fungi and green algae. Our approach involved a series of quantitative measurements of cellular parameters and the use of a biophysical model. We found that the cell wall is thinner at the tip (36 nm) than on the shanks (170 to 500 nm). Moreover, the cell wall thickness gradient and the dome curvature match together, so that the stress displays the profile required for growth, without changes in biophysical properties of the cell wall.

2.1.3. Introduction

In multicellular organisms, morphogenesis — from the cell to the organ level — relies on mechanical processes (Mirabet *et al.*, 2011; Davidson, 2017). Cell expansion results from the balance between forces promoting extension (turgor, cytoskeleton) and structural resistance to deformation (cytoskeleton, cell wall, plasma membrane and cytoplasm). Tip growth is one of the simplest cases of cell morphogenesis, characterized by pronounced cell polarization ensuring unidirectional exploration and colonization of the surrounding space through the expansion of the most distal region of the cell: the tip. It is encountered in many Eukaryotes throughout the tree of life (Heath, 1990), with a diversity of cell shapes (Campàs *et al.*, 2012) and growth rates (from 2.5 to 800 $\mu m \cdot h^{-1}$) (Harold *et al.*, 1996; Benkert *et al.*, 1997; Menand *et al.*, 2007) (**Fig 2.1**). Physical laws imply that wall stress (σ, force per unit of area) due to internal pressure is lower in the tip compared with the shanks of the cell, because the cell-wall curvature increases in the dome (Castle, 1937). Beyond the apparently simple process of shifting material to the cell front, a wealth of mechanical, cellular and chemical mechanisms are required to ensure growth where wall stress is low, and to prevent it where wall stress is high.

In plants and fungi, the cell wall is the most resistant compartment of the cell. Fungal hyphae and tip cells of land plants (*e.g.*, pollen tubes and root hairs) secrete cell-wall-loosening factors together with cell-wall-building components, making cell walls susceptible to stretch despite the low wall stress at the tip, whereas the more proximal cell wall in the shanks becomes stiffer, resisting the higher wall stress (Geitmann and Ortega, 2009; Riquelme, 2013).

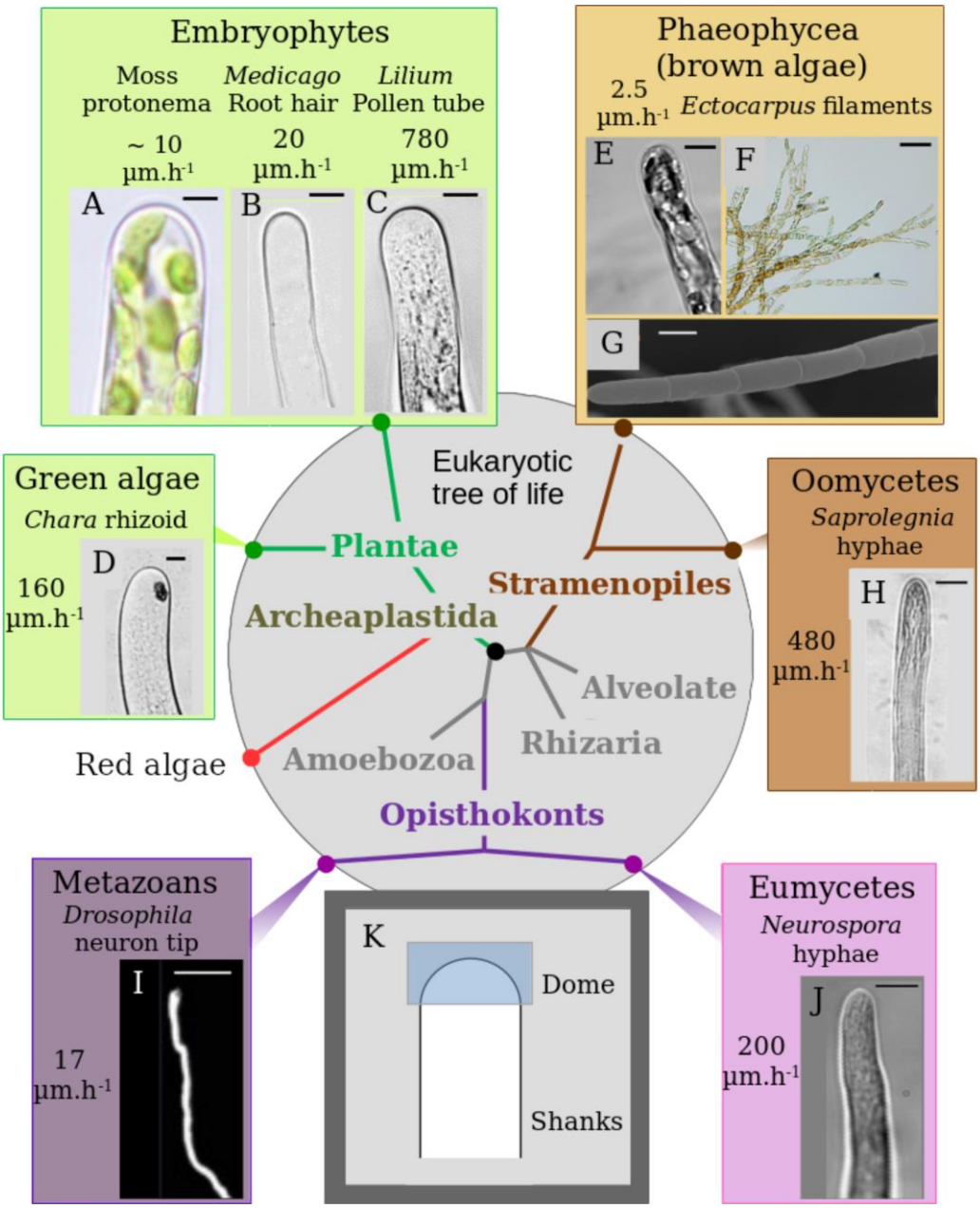

Figure 2.1 - Diversity of tip-growth in the Eukaryotic tree

Phylogenetic position of eukaryotic taxa with tip-growing organisms. Cell shapes and growth rates are shown. (**A, B, C, D**) Archaeplastida group. (**A**) Moss protonema; (**B**) Root hair; (**C**) Pollen tube; (**D**) Green algal filament. (**E, F, G, H**) Stramenopiles, which include the coenocytic oomycetes and the multicellular brown algae, among which the filamentous alga *Ectocarpus*. (**E**) *Ectocarpus* apical cell of a prostrate sporophyte filament; (**F**) *Ectocarpus* tuft with several branches; (**G**) *Ectocarpus* filament viewed with scanning electronic microscopy (SEM); (**H**) Oomycete hyphae. (**I, J**) Tip growth in the Opisthokont group. (**I**) Neurons of metazoans; (**J**) Fungal hyphae. (**K**) Two main cellular territories defining tip growing cells. Top frames are the two taxa compared in this study (pollen tube and brown algal filament). Bar = 5 µm (**A, B, C, E, H, I, J**), 10 µm (**G**), 20 µm (**D, F**). Photos credits: (**C**) B. Kost, Erlangen Univ, Germany; (**D**) B. Brown, Erlangen University; (**G**) A. Le Bail Station Biologique Roscoff CNRS-UPMC France, (**H**) from Yuan *et al.* (1995); (I) from Liu *et al.* (2018); (**J**) from Silverman-Gavrila and Lew (2002).

To explore potential mechanistic conservation or alternative strategies, we studied tip growth in the model brown alga *Ectocarpus* (Charrier *et al.*, 2008) belonging to the Stramenopiles, a distinct branch of the eukaryotic tree of life (Baldauf, 2008) (**Fig 2.1**). Brown algae can be microscopic or as large as land plants (up to 40 m) and are harvested for human subsistence and activities (McHugh, 2003). Their relatively recent emergence (~ 200 My; (Silberfeld *et al.*, 2010) compared with land plants (450 My; (Kenrick and Crane, 1997), green algae (750 My; (Leliaert *et al.*, 2012), red algae (~ 1.2 By; (Butterfield, 2000) and metazoans (~ 600 My; (Dunn *et al.*, 2014), occurred independently of the other multicellular organisms (Baldauf, 2008). In addition, their growth in marine environments (high salt concentration, high external pressure and reduced perception of the gravitational force compared with land conditions) raises further questions on the physical forces these organisms rely on to promote their growth. Previous studies have illustrated the uniqueness of these organisms regarding their energetic and primary metabolisms (Michel *et al.*, 2010*b*), their cell structural components (Katsaros *et al.*, 2006; Deniaud-Bouët *et al.*, 2014*b*) and their genetic features (Cock *et al.*, 2010). *Ectocarpus* has emerged as a model for brown algae in the past 15 years (Charrier *et al.*, 2008; Cock *et al.*, 2010). As a tiny uniseriate filamentous brown alga (**Fig 2.1E, F, G**), *Ectocarpus* displays a low body complexity and each cell making its filament are easy to observe and to handle (*e.g.*, laser capture microdissection (Saint-Marcoux *et al.*, 2015) or atomic force microscopy (AFM; (Tesson and Charrier, 2014*b*), making it particularly amenable to sophisticated fundamental studies in cellular and developmental biology. Zygote germination, filament growth and subsequent branching occurs via tip growth (Le Bail *et al.*, 2008) and resulting apical cells exert both growing and branching negative controls on sub-apical tissues (Le Bail *et al.*, 2010), making apical cells key organizing centers for further development.

In this article, we characterized a biophysical mechanism able to account for tip growth in *Ectocarpus* apical cells, while embracing the different cellular and molecular factors involved in it. We compared it with the pollen tube, used here as a representative of the other Eukaryote tip-growing cells.

2.1.4. Results

2.1.4.1. Growth is taking place in the apical dome and is orthogonal to the cell surface

The prostrate filaments of the alga *Ectocarpus* develop by tip growth (Le Bail *et al.*, 2008). Pulse chase experiments using the cell wall dye Calcofluor allowed to localize the growth in the first 3 µm from the tip of the cell, corresponding to ~ half of the dome (**Fig 2.2A**). Growth direction was estimated at the local level by using a method initiated in other plant cell types

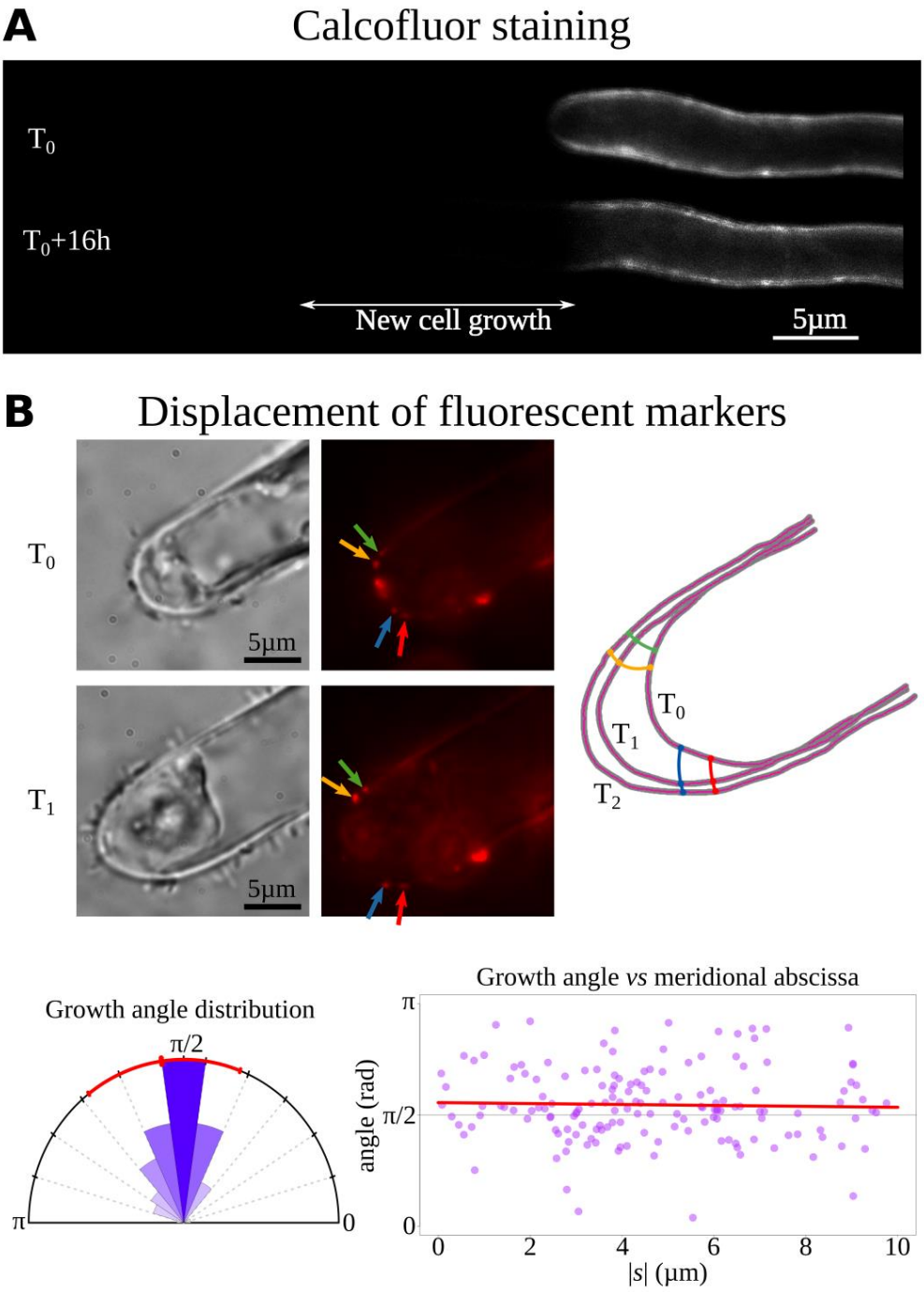

Figure 2.2 - Position and direction of cell wall expansion during growth

(**A**) Pulse-chase experiment using Calcofluor dye during growth. Filaments were washed to remove Calcofluor immediately after staining and observed again after 16 h. The dark zone corresponds to the material recently grown. (**B**) Orthogonal growth in the apical cell. (Top) Cell-wall deformation at the apex of an apical cell during growth, monitored by following the displacement of fluorescent micro-spheres stuck at the cell surface after 24h. (Left) Bright-field pictures; (Right) Corresponding confocal pictures showing the micro-spheres as red fluorescent dots. Note the progressive displacement of 4 micro-spheres from the dome towards the shank of the cell as the cell grows. Bar = 5 µm. (Bottom) Distribution of angles between the cell surface and the growth direction (sectors); (Left) Red line and tick marks denote the mean and standard deviation. (Right) Angle values plotted as a function of meridional abscissa |s|, showing that angle is stable along the position in the dome (red line: linear regression).

(Shaw *et al.*, 2000), and recently developed in *Ectocarpus* (Rabillé *et al.*, 2018*a*): the displacement of 0.2 µm FluoSpheres was monitored at the surface of apical cells during growth. Statistical analyses of the angular distribution showed a moderate deviation (relative mean difference < 10%) between the fluorescent marker trajectory and an orthogonal displacement. Moreover, linear regression exhibited no systematic dependence of the angle *vs* meridional abscissa (Pearson correlation coefficient r = -0.03), indicating that growth can be considered orthogonal to the cell surface in the dome, independently of the position along the meridional abscissa (**Fig 2.2B**; *see also Suppl. Fig 1*).

2.1.4.2. The dome of the Ectocarpus apical cell is subject to a high wall stress

In plant organisms, growth cannot take place without turgor which contributes to the force making cell wall yield (**Fig 2.3A**). Despite that the turgor exerts the same pressure from point to point of the cell wall, the wall stress σ_e perceived locally by the cell wall varies because it depends on both the curvature of the cell κ and the cell wall thickness δ at each position of the cell wall surface. For calculation, the stress is partitioned into three directions: meridional (s), circumferential (θ) and normal (n) (*see Supplementary information equation S2*). As the cell wall is thin compared to the cell dimensions, the normal component of the stress is considered negligible beside the two others (Meyers and Chawla, 2008).

In order to calculate the wall stress in each position of *Ectocarpus* apical cell, we measured the turgor, the curvature and the cell wall thickness in this cell. The turgor in the apical cells was measured using the non-intrusive technique of incipient plasmolysis (Wright and Reed, 1988*b*) on > 100 cells for each of the 10 solutions of different osmolarities used in the experiment (**Fig 2.4A**). The value was subsequently corrected to take into account cell shrinking according to the protocol described in (Wright and Reed, 1988*b*); *Suppl. Table 1*). The calculated apical cell turgor was 0.495 MPa, which is ~ 5 times the atmospheric pressure and is in the same order of magnitude as the other tip-growing organisms, including the pollen tube ([0.1-0.4] MPa, average at 0.2 MPa; (Benkert *et al.*, 1997).

To obtain curvature measurements, the contour of *Ectocarpus* apical cells was drawn manually, from which a smoothed cubic spline was computed, as illustrated for one cell in **Fig 2.4B** (left). From 17 individual cell contours (*Suppl. Fig 2*), both the meridional and the circumferential curvatures as well as an average cell contour were calculated (**Fig 2.4B**, right). The same procedure was used for the tobacco pollen tube contour (n = 6, not shown). Compared to the pollen tube, *Ectocarpus* apical cell displays a sharper tip and a higher circumferential curvature on the flanks, which denotes its smaller radius.

Finally, the cell wall thickness was measured. Staining with the dye Calcofluor, which labels mainly cellulose (1–4) and callose (1–3)-beta-D-glucans (Ponce *et al.*, 2007) displayed a very clear gradient of thickness from the tip to the shanks of the apical cell (**Fig 2.5A**, also visible in 3D reconstruction from confocal microscopy, not shown). However, cellulose microfibrils are only a minor component of the brown algal cell wall (8 % max dry weight) as they are immersed in a more abundant matrix of polysaccharides (45 % DW) made of alginates (linear polymers of β-(1→ 4)-D-mannuronate and α-(1→ 4)-L-guluronate) and fucans (α-L-fucosyl residues) (Popper *et al.*, 2011*a*; Deniaud-Bouët *et al.*, 2014*b*). Therefore, we prepared longitudinal sections of apical cells for transmission electron microscopy (TEM). First, serial sections (300 nm thick) stained with toluidine blue showed that the most meridional sections displayed a gradient of thickness with the lowest value at the tip (**Fig**

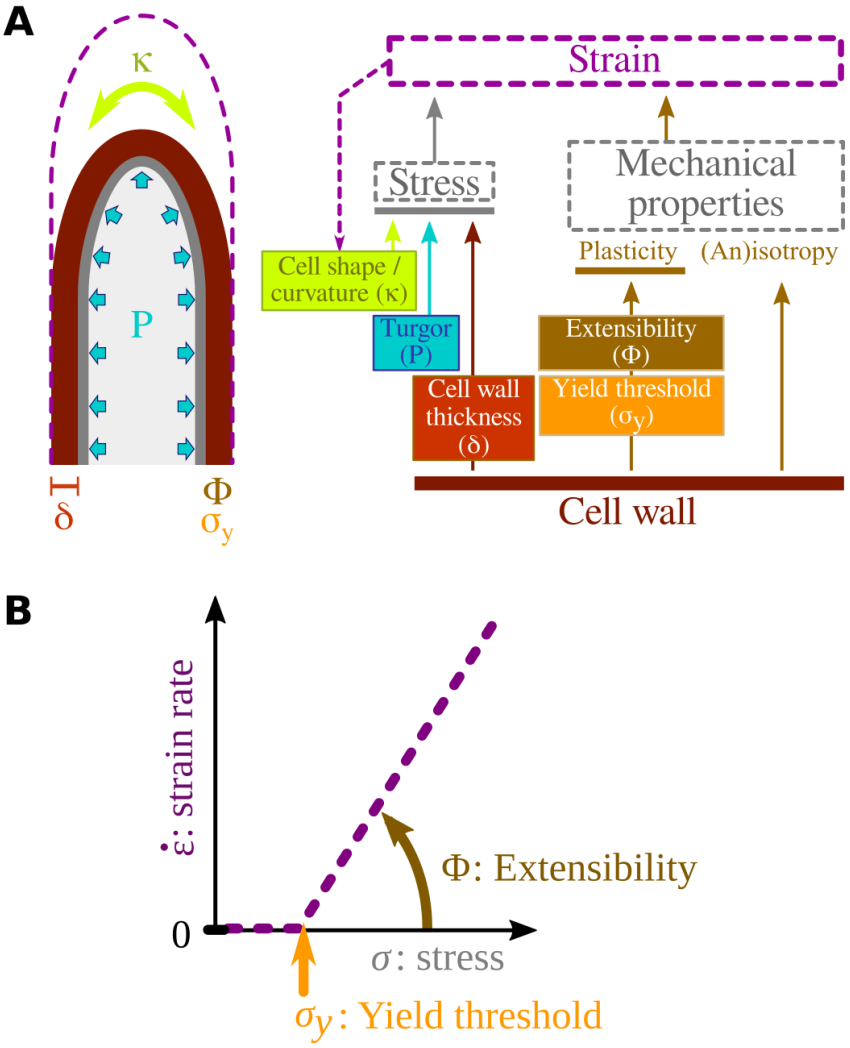

Figure 2.3 - Viscoplastic model of tip growth

(**A**) Schema showing the relationship between the different factors involved in cell wall growth. The wall stress depends on the cell turgor (P), the cell curvature (κ) and the cell wall thickness (δ). In the viscoplastic model (Dumais *et al.*, 2006), the strain rate (dashed purple lines) in each point of the cell surface is a function of both the wall stress and the mechanical properties of the cell wall (i.e. isotropy and propensity to yield represented by the extensibility Φ and the yield threshold σ_y). Strain results in a new cell shape (downwards dashed arrow). (**B**) Strain rate as a function of the stress, according to the Lockhart law for growth of viscoplastic cell walls.

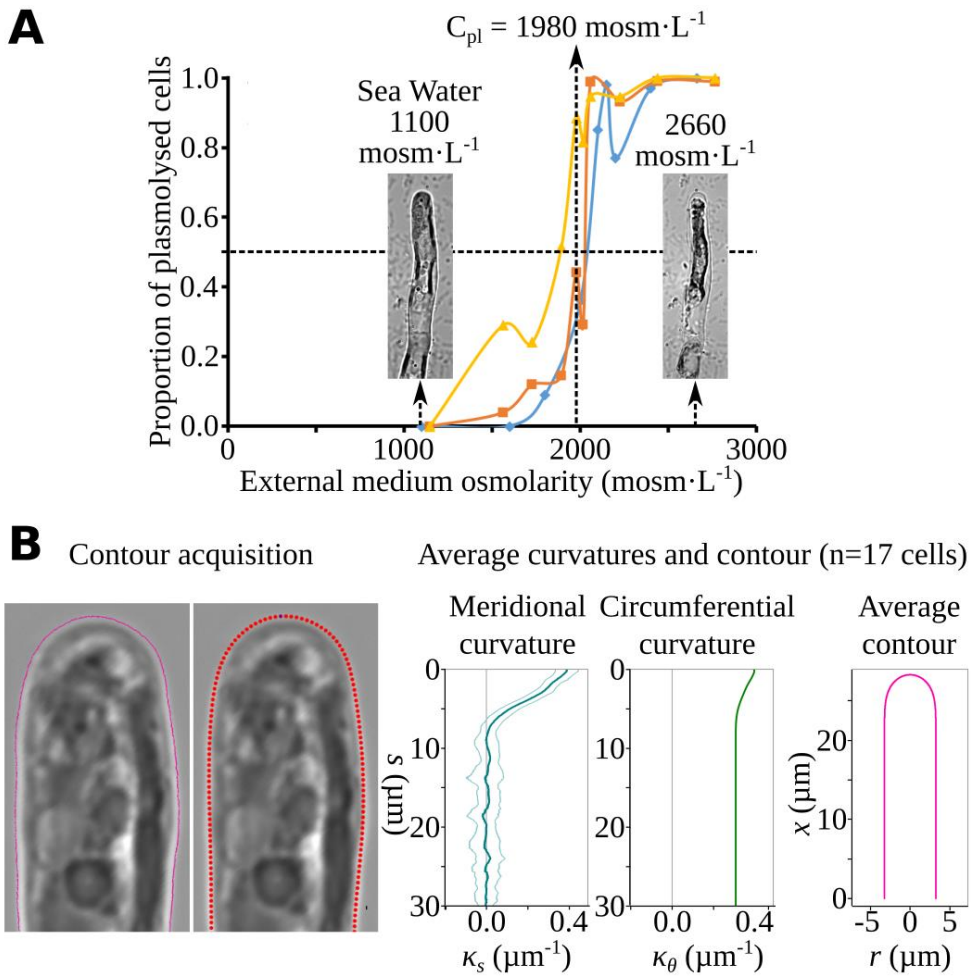

Figure 2.4 - Turgor and curvature of the apical cells

(**A**) Turgor value in apical cells measured using the limit plasmolysis method (Wright and Reed, 1988). Different osmolarities (C_e) were applied to *Ectocarpus* filaments and plasmolysis was monitored in apical cells (n>100 for each osmolarity). Limit plasmolysis concentration (C_{pl}), which is the solute concentration for which 50% of apical cells were plasmolysed, was 1980 mOsm.L^{-1} (colored lines denote the three independent experiments). Corrections as explained in Methods allowed to reach a final turgor value of 0.495 MPa. (**B**) Apical cell curvature. (Left) *Ectocarpus* apical cell contour was drawn manually on microscope images. From the contour of each cell, a smoothed cubic spline was computed. (Right) The meridional curvature of each cell was calculated from the discretized contour. All such curvature series (for n=17 *Ectocarpus* apical cells) were averaged (blue curve, SD shown as light blue curves) and the mean curvature was used to create a mean contour. Circumferential curvature (green curve) was then inferred from the mean contour. Grey lines are for curvature = 0. The same procedure was used for 6 tobacco pollen tube cells (not shown).

2.5B, middle section), while the most tangential sections displayed even thickness along the cell (**Fig 2.5B**, top and bottom sections). Detailed observations were performed on sections 70 nm thick on which measurements of the cell wall thickness were carried out every 386 nm in average along the cells from the tip ($s = 0$) to $s = \pm 70$ µm on both sides (**Fig 2.5C**). In order to limit measurement artifacts due to askew sections, longitudinal sections with the thinnest walls were considered in priority (*all images are shown in Suppl. Fig 3*). In addition, a correction based on the expected cell diameter (6.54 µm) was applied to correct the potential remaining artifacts (*Suppl. Table 2*). As askew sectioning results in cell walls look thicker, the only expected bias is towards an over-estimate of the thickness at the tip. The corrected 2500 measurements were plotted as a function of *s*. The distribution depicted a gradient which could be modeled as a Pearson-like function characterized by the lowest value $\delta_{min} = 36.2$ nm at the tip ($s = 0$), the asymptotic maximum value $\delta_{max} = 591$ nm and reaching its mid-point at $s_{1/2} = 16.8$ µm (**Fig 2.5C**). Cell wall thickness at the exit of the dome ($s = 8$µm) was 169 nm, *i.e.* 4.7 times the thickness at the tip (**Fig 2.5C** close-up).

The establishment of a cell wall thickness gradient contrasts with most tip-growing cells from the other eukaryotic groups (McKenna *et al.*, 2009; Riquelme, 2013), in which cell-wall thickness is either constant (*e.g.*, 250 nm in pollen tube; (Lancelle and Hepler, 1992) or higher at the tip (*e.g.*, oscillating growth in the pollen tube; (Cai *et al.*, 2011; Zonia and Munnik, 2011).

Using this set of biological data, wall stress was calculated in both the meridional (σ_s) and the circumferential (σ_θ) directions, which allowed to calculate the overall wall stress σ_e (Fig 3A; equation S3). While in the pollen tube σ_e fluctuates between 2.5 and 3.5 MPa (with the lowest value in the dome), it reaches a maximum of 38 MPa in *Ectocarpus* tip area, and decreases to reach values similar to that in the pollen tube 70 µm away from the tip. This stress value in the dome of *Ectocarpus* apical cells is remarkably high compared to the other tip-growing cells (note the different scales between *Ectocarpus* and tobacco pollen tube) in which, moreover, the stress gradient from tip to flanks is opposite.

Fig 2.6A, **B**, **C** and **D** show a schematized comparison of these biophysical features between *Ectocarpus* and pollen tube apices.

2.1.4.3. Spatial variation in wall stress, not in cell wall mechanical properties, accounts for the viscoplastic strain pattern in Ectocarpus

2.1.4.3.1. Implementation of a viscoplastic model

We investigated how the wall stress gradient observed in *Ectocarpus* apical cell impacts the growth rate and geometry. Despite that plant cell wall growth used to be attributed to plastic deformation only (Cosgrove, 2005), some biophysical models consider the intrinsic elasticity of the cell wall as a significant factor in cells subject to transpiration or shortage of water (Ortega, 2017). Because *Ectocarpus* growth is extremely slow (~ 300 times slower than pollen tubes) and takes place always in immersed conditions (in-lab controlled conditions), we considered that the elastic component due to rapid and reversible fluctuations of osmotic pressure is negligible and that the growth process relies only on the viscoplastic component of the cell wall.

The physical laws governing plastic growth of a cell subject to turgor pressure were initially established by Lockhart (Lockhart, 1965). They showed that the growth rate G = dL/dt of a cylindrical cell depends on the one hand on the turgor and on the other hand on the capacity of the cell wall to yield in response to this turgor, both at the qualitative (orientation of the deformation) and at the quantitative levels. However, in a context of cell morphogenesis, both local deformation orientation and local rate can vary along the cell surface (due *e.g.*, to the activities of enzymes), especially in the tip of an apical cell with a dome-shape geometry. In simulation approaches these parameters are discretized along the cell surface to account for a sub-cellular scale approximating infinitesimal portions of cell wall. Due to rotational symmetry of the (modeled) cell, all values can be expressed as functions of the meridional abscissa *s*. The deformation rate (also called strain rate $\dot{\varepsilon}(s)$) at each point of the cell surface results from the local wall stress $\sigma_e(s)$ and of i) the local cell wall intrinsic anisotropy, ii) the local plastic yield threshold $\sigma_y(s)$ and iii) the local plastic extensibility $\Phi(s)$ (**Fig 2.3A**) (Dumais *et al.*, 2006) (*equation S5 and details in Supplementary information*). Growth of each cell wall portion occurs only if $\sigma_e(s) > \sigma_y(s)$. Below $\sigma_y(s)$, the portion area remains unchanged and does not contribute to the overall cell growth (**Fig 2.3B**) (Hill, 1998).

In order to apply these physical concepts to *Ectocarpus* tip growth pertinently, the model was supplied with additional biological data obtained from *Ectocarpus* apical cells. We already showed that growth was approximately orthogonal to the cell surface in the dome of the apical cell (above and **Fig 2.2B**). Secondly, we examined the cell wall organization to assess its structural isotropy. Cell wall was denatured and the remaining cellulose fibers were observed using atomic force microscopy (AFM). Apparent diameter of cellulose microfibrils is in agreement with previously published results (12.6 ± 4.9 nm) (Terauchi *et al.*, 2016). Images showed that in the dome cellulose microfibrils were intermingled along the cell surface, indicating that the main, stiffer components of the cell wall have no specific direction in this dimension (*Suppl. Fig 4A, left, middle*). Similar organization was observed in partially denatured cell wall, showing that the treatment does not displace the cellulose microfibrils (*Suppl. Fig 4A, right*). This finding supports that the cell wall of the tip is transversely isotropic, a feature shared by other *Ectocarpus* cell types (Terauchi *et al.*, 2016).

As a second step, we aimed to calculate the rate of growth of each portion of cell wall, which depends on its capacity to yield, and hence on the two parameters defining its growth plasticity: $\sigma_y(s)$ and $\Phi(s)$. However, it is currently impossible to gain experimental access to the values of $\sigma_y(s)$ and $\Phi(s)$ in every portion of the cell wall during growth. While AFM nanoindentation allows inferring cell wall intrinsic mechanical properties like elasticity (Elastic modulus), adhesion and potentially plasticity in the z-axis, it does not account for forces in the x and y-axes at play during growth (Cosgrove, 1993*a*). Nevertheless, transverse isotropy of the cell wall and orthogonal growth together make equations of the viscoplastic model tractable. This allowed to express the expected strain rate $\dot{\varepsilon}^*(s)$ as a function of local geometrical values and without any prior knowledge of $\Phi(s)$ and $\sigma_y(s)$, by assuming self-similar growth (Goriely and Tabor, 2008) (*i.e.* growth without distortion, globally similar to axial translation, see details in Supplementary information). As expected, its pattern is similar to the strain rate pattern of the pollen tube (**Fig 2.6E**), with yet a much lower rate due to a slower growth rate (2.5 µm·h^{-1} compared to 540 µm·h^{-1} for the tobacco pollen tube). Remarkably, when plotted as a function of the wall stress along the cell, the calculated expected strain rate value $\dot{\varepsilon}^*(s)=f(\sigma_e(s))$ displays the characteristic curve that would result from the Lockhart equation (Fig 3B) for the viscoplastic strain rate $\dot{\varepsilon}_e(s)=\Phi(s)(\sigma_e(s)-\sigma_y(s))$ in the particular case where Φ and σ_y are constant along the cell wall (**Fig 2.7A**, left). According

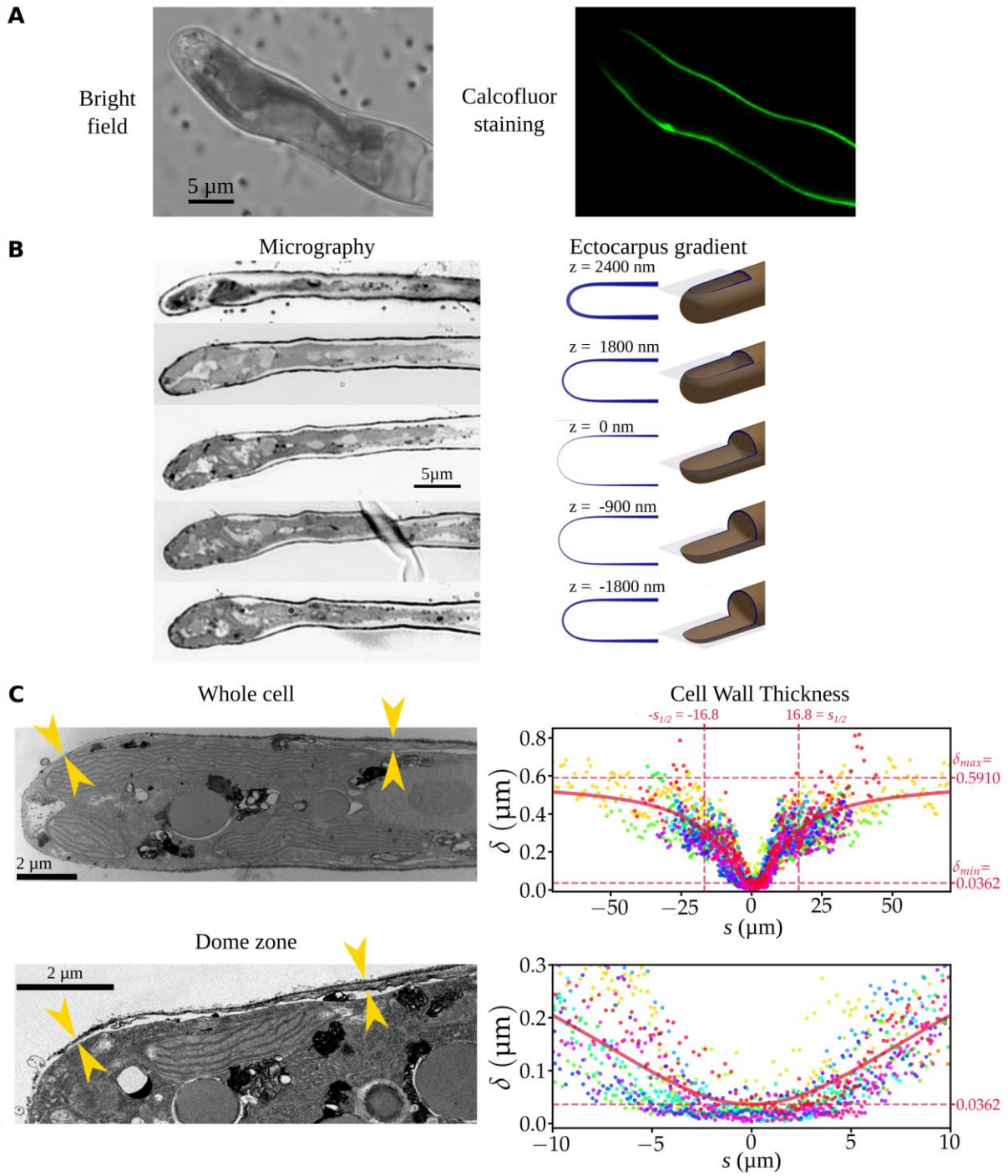

Figure 2.5 – Cell wall thickness in apical cells

(**A**) Confocal images of *Ectocarpus* apical cells stained with Calcofluor white. The most apical part of the cell is barely visible because the cell wall is thin. (**B**) Serial sections (300 nm thick) of an apical cell compared to theoretical sections with the cell wall gradient observed in (C). Theoretical sections were rendered using the Persistence Of Vision ray-tracing software (Buck *et al.*, 2013). In the meridional position, the cell wall is barely visible at the tip while it is in the shanks. In non-meridional sections, cell wall is visible both at the tip and in the shanks. (**C**) Left: Ultrathin (70 nm) longitudinal sections of apical cells observed by TEM, showing the cell-wall thickness gradient from the tip to the base of the cell, from a large field view (top) and from a close-up focused on the dome region (bottom). (Right) Plotted distribution of the corrected measured cell-wall thickness values (each dot color corresponds to one value measured on one given cell; one color per cell) as a function of the meridional distance (*s*) (n = 15 cells). The curve shows the theoretical gradient adjusted to the data, according to a law adapted from Pearson's function. Adjusted cell-wall width at s = 0 is δ = 36.2 nm and the plateau on the flanks is at δ = 591 nm. The distribution focused in the dome area is shown (bottom).

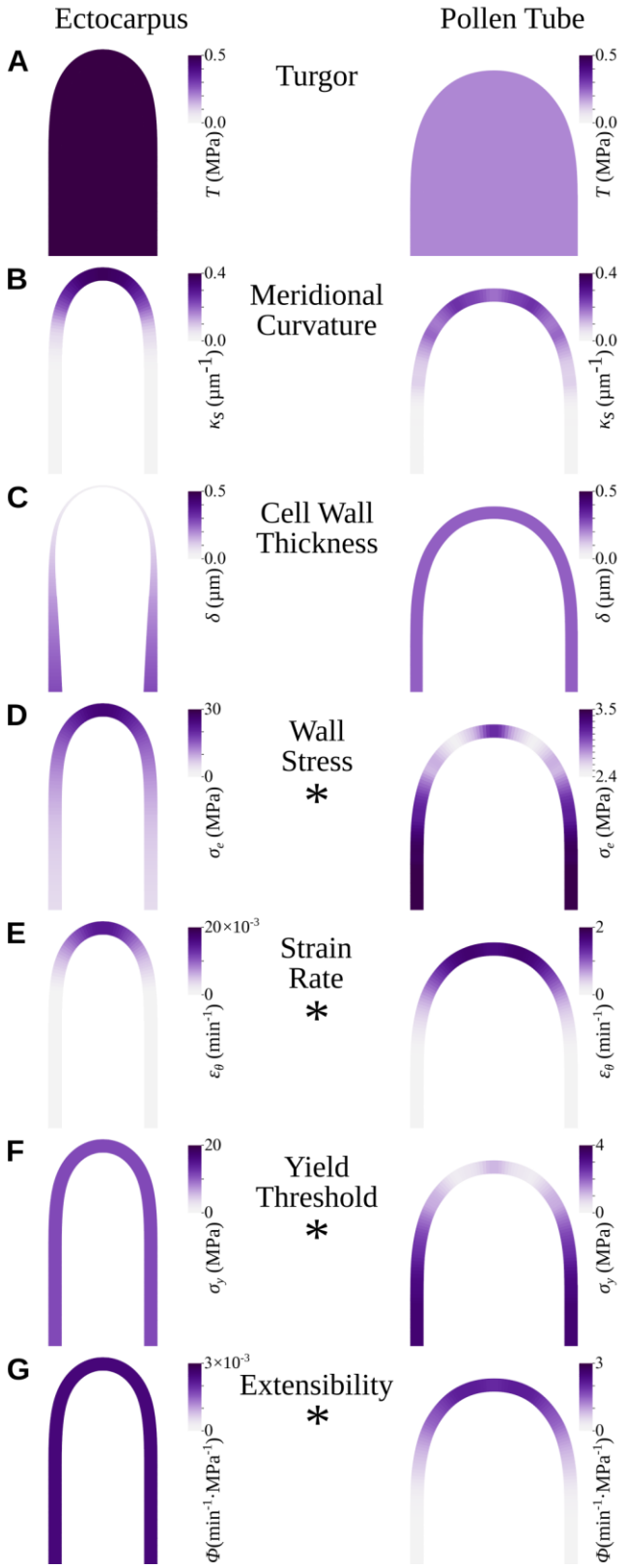

Figure 2.6 - Schemes summarizing the biophysical properties of two tip growing cells: Ectocarpus filament apical cell and tobacco pollen tube

2-D profiles are shown. (**A**) Turgor; (**B**) Meridional curvature; (**C**) Cell wall thickness; (**D**) Wall stress; (**E**) Strain rate pattern; (**F**) Cell wall plastic yield threshold; (**G**) Cell wall plastic extensibility. Note that the color scale differs between *Ectocarpus* and pollen tube in (**D**), (**E**), (**F**) and (**G**), denoted by *.

to this graph, if σ_y and/or Φ were to change along the cell, an increase of one would have to be compensated by a simultaneous increase of the other. For instance, lowering σ_y would soften the wall while simultaneously lowering Φ would harden it. Beyond being non parsimonious and counter-intuitive, such combination of variations is incompatible with experimental data obtained from plant cell walls where simultaneous variations of Φ and σ_y are always opposite, so that they modify the cell wall stiffness in the same direction (Nakahori *et al.*, 1991), in agreement with physico-chemical cell wall models (see for example (Passioura *et al.*, 1992).

In order to test the robustness of the previous result, we conducted a bootstrap assay using 3000 resampling sets among the cells used to compute the average contour, and those used to infer the cell wall thickness gradient parameters. As the test assesses the similarity of the curve $\dot{\epsilon}^*=f(\sigma_e)$ with the Lockhart function, we considered the linearity of the increasing part of the curve (i.e. for points having $\sigma_e > \sigma_y$). The mean linear regression r^2 value was 0.974, and for 95% of the samples r^2 was higher or equal to 0.907 (**Fig 2.7B**). Thus, despite variations in cell shape and cell wall thickness between samples, the fit with the Lockhart curve remained very robust (*see also Suppl. Fig 5*).

Spatial steadiness of plastic features of the cell wall is unusual: in tobacco pollen tubes, Φ and/or σ_y must vary along the cell to allow growth in the dome, which is supported by experimental evidence (Geitmann and Steer, 2006). As a result, the function $\dot{\epsilon}^*(s)=f(\sigma_e(s))$ cannot depict a typical Lockhart equation in these organisms, as variable values of Φ and/or σ_y with s prevent occurrence of the typical affine behavior in the domain where $\sigma_e > \sigma_y$, as illustrated for the pollen tube in **Fig 2.7A** (right). Plotting σ_y and Φ together with the cell wall thickness δ clearly illustrates the different strategies developed by *Ectocarpus* and the pollen tube (**Fig 2.7C**): in *Ectocarpus*, δ is the only varying parameters while in the pollen tube, both σ_y and Φ vary and δ remains constant.

2.1.4.3.1. Inferred viscoplastic features of *Ectocarpus* apical cell wall and effect of auxin

Estimates for Φ and σ_y values were inferred from long-term simulations by testing different couples of values. Simulations were run for 600 steps of ~ 40 nm of linear progression each, over a distance of 25 µm corresponding to ~ 5 times the dome length. They showed that the constant values σ_y = 11.18 MPa and $\Phi = 2.51\times10^{-3}$ MPa$^{-1}\cdot$min^{-1} allowed to maintain the algal apical cell shape during growth (**Fig 2.8A**, middle; *Movie 1 in SI*). Simulations with different pairs of cell wall Φ and σ_y values did not result in the expected self-similar growth and, instead, produced either misshapen cells when varying σ_y (**Fig 2.8A**, bottom; *Movie 2 in SI*) or inappropriate growth rates when varying Φ (**Fig 2.8A**, top; *Movie 3 in SI*).

In order to test the model experimentally, we treated the apical cells with three concentrations of auxin indole-3-acetic acid (IAA). This phytohormone, previously shown to be present in *Ectocarpus* filaments (Le Bail *et al.*, 2010) sped up linear tip growth (**Fig 2.8B**, top) and reduced turgor in the apical cell (0.186 MPa instead of 0.495 MPa in the control, *Suppl. Table 3*), while no modification of the original cell shape could be noticed. Using these biophysical parameters, and assuming that the thickness gradient was not modified during this experimental time lapse, we managed to simulate tip growth again with constant values of plastic extensibility and yield threshold along the cell, similarly as in the control conditions. In addition, while constant along the cell, Φ and σ_y values were different from those in the control: in response to 1 µM IAA, Φ increased to 13.35×10^{-3} min$^{-1}\cdot$MPa^{-1} (*i.e.* 5.3 times

higher than in the control) and σ_y decreased to 4.20 MPa (2.7 times lower) (**Fig 2.8B** bottom). Interestingly, a similar response was reported in land plants: tip growth increased in IAA-treated pollen tubes. Biophysical measurements showed that IAA-treated hypocotyls of *Vigna* displayed a higher strain rate correlated with an increased Φ and a decreased σ_y (Nakahori *et al.*, 1991). Therefore, notwithstanding the phylogenetic distance between the two eukaryotic phyla, auxin might have the same effect on cell wall mechanical properties: facilitation of the plastic deformation to increase growth rate. Beside this hypothesis, these data support the model in which Φ and σ_y remain constant along the cell.

2.1.4.1. Cell wall thickness gradient: impact on cell shape and growth rate

Using the model, we tested the impact of the cell wall thickness gradient on both tip shapes and growth rates. Steeper or wider cell wall thickness gradients were sufficient to substantially alter the proper *Ectocarpus* cell shape and growth rate, suggesting that the cell-wall thickness gradient must be tightly regulated *in vivo* (*Suppl. Fig 6, central column; Movie 4*). However, cells display some significant variations in the cell wall thickness, which most likely are real (**Fig 2.5C**). Actually *in vivo* observation of *Ectocarpus* tip growth also showed variability in the growth rate and in the cell shape (*e.g. displayed in Suppl. Fig 2*), which might be due to cell wall thickness transitory variations. The extremely low growth rate of this species can easily allow the activation of regulatory mechanisms adjusting the cell wall thickness gradient by modifying cell wall biosynthesis.

Simulation of tip growth from three different initial cell shapes (flat, *Ectocarpus*-like and sharp) using the *Ectocarpus* cell-wall thickness gradient "Normal" resulted in convergence of the resulting shapes to the *Ectocarpus* shape (*Suppl. Fig 6, middle row; Movie 5*). This suggests that the cell-wall thickness gradient might also govern the tip resilience to deformation so that initial cell shape can be recovered after transient deformation (*e.g.*, due to an accident during growth). Finally, simulations using modified cell wall thickness gradients ("Steep" or "Gentle") on these three different cell shapes further showed that all cells grew and converged to the same final shape specific to a given gradient (*Suppl. Fig 6, top and bottom rows; Movie 6*). These simulations supplement those by Dumais et al. (2006) who explored various gradients in Φ and σ_y. in a context where the cell wall thickness was constant.

2.1.4.1. Maintenance of the cell wall thickness gradient

The preponderant role of the cell-wall thickness gradient in the control of tip growth raises the question of how this gradient is established and maintained. Calculations considering the cell-wall extension rate and the maintenance of the cell-wall thickness gradient during growth allowed to infer the level of cell-wall material delivery or/and biosynthesis along the cell. According to this calculation, the overall rate of cell-wall material delivery and/or synthesis in the pollen tube is much higher than in *Ectocarpus* (note the different scales of the x-axis in **Fig 2.9A**, left, top *vs* bottom). Its maximum culminates 3.0 µm away from the most distal position and drops to null in the tube shanks (**Fig 2.9A**, top left). This calculation is in agreement with former *in situ* observations using FM4-64, which labels both endocytic and exocytic vesicles (Parton *et al.*, 2001; Bolte *et al.*, 2004; Toyooka *et*

al., 2009); **Fig 2.9A**, top middle) and TEM (Derksen *et al.*, 1995); **Fig 2.9A**, top right) in pollen tubes, and also in other tip-growing walled cells, for example in root hairs and green algae (Domozych *et al.*, 2013) and in ascomycetes hyphae (Riquelme, 2013), where vesicle trafficking is concentrated in the most distal part of the tip. This mechanism contrasts with *Ectocarpus* where the cell wall flux is predicted to be significant in the shanks of the cell, despite that the maximum in the dome is at a similar relative position (meridional abscissa 3.8 µm; **Fig 2.9A**, bottom left) as in the pollen tube. How cell wall is made in brown algae is still unknown for a large part. Cellulose would be synthesized from cytosolic UDP-glucose by linear complexes of cellulose synthases localized in the plasma membrane, where they elongate cellulose microfibrils into the cell wall (Tsekos, 1999). How the other cell wall main components alginates and fucans reach the cell wall at the tip of the *Ectocarpus* apical cell is unknown, but TEM observations on dividing cells of *Silvetia* – a brown alga from another order than *Ectocarpus* – showed that alginates and fucans are delivered to the new forming cell wall by Golgi-derived vesicles (Nagasato *et al.*, 2010). Based on this finding, we used FM4-64 to investigate the pattern of vesicle trafficking in *Ectocarpus*. FM4-64 displayed a homogeneous spatial pattern all along the cell, with no specific vesicle localization (**Fig 2.9A**, bottom middle). This was supported by TEM where no concentration of vesicles was observed in a meridional section of the dome of an apical cell (bottom right). Instead, chloroplasts and chloroplastic endoplasmic reticulum (CER), known to be in close vicinity to the Golgi apparatus and to be involved in the production and trafficking of photosynthates (Charrier *et al.*, 2008), could be observed in both the dome and the shanks of the cell (**Fig 2.9A**, bottom right). Therefore, the biological observations are compatible with the establishment and maintenance of a cell wall thickness gradient at an extremely slow rate, where CER and potentially Golgi vesicles would deliver the main components of the cell wall all along the cell with yet a highest rate in the dome. To confirm this initial observation, we performed Fluorescence Recovery After Photobleaching (FRAP) assays on *Ectocarpus* apical cells. We compared the fluorescence signal recovery dynamics in 5 different zones along the dome and shanks of the cell (**Fig 2.9B**, left). Considering the increase in the fluorescence signal as a function of time, we used the normalized slope at $t = 0$ as a proxy for the intensity of membrane replacement by exocytosis, potentially reflecting cell wall building activity (*Suppl. Fig 7*). The results showed that the highest exocytosis activity coincided with the highest cell wall flux predicted by the model, *i.e.* at the base of the dome (s = 5-7 µm) (**Fig 2.9B**). In addition, a significant traffic was observed in the shanks (zone E ~ 10 µm from the dome end), which is compatible with *de novo* cell wall material delivery at these positions and resulting cell wall thickening. Altogether, FRAP and TEM observations are compatible with the calculation of the cell wall flux inferred from the model.

2.1.1. Discussion

Using a combination of serial longitudinal sections observed by TEM and optical microscopy, we showed first that *Ectocarpus* displays a gradient of cell wall thickness in the apical cell of the prostrate filaments of its sporophyte. The gradient ranges from 36 nm at the very tip to 169 nm at the exit of the dome, where cell wall stops participating in cell growth. However, cell wall keeps thickening in the cylindrical part of the cell, progressively reaching ~ 500 nm 70 µm away from the tip. Attempts to display cell wall thickness variations were reported in other organisms. However, in most cases, the technologies used did not allow accurate measurements. Cell wall from either living cells or ghost cells were stained with

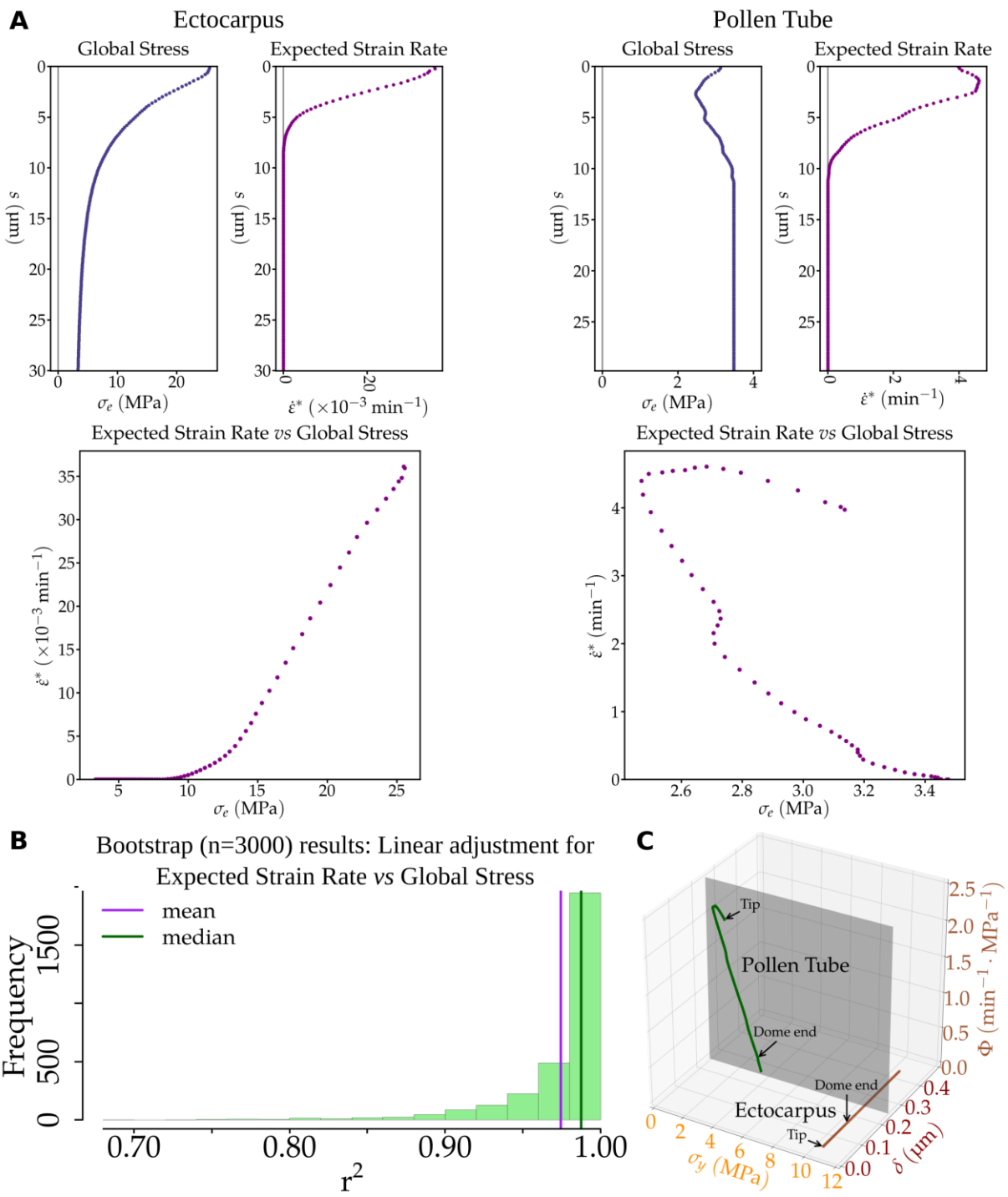

Figure 2.7 - Contribution of the cell wall biophysical parameters in *Ectocarpus* and pollen tube tip growth

(**A**) Relationship between stress and expected strain rate in *Ectocarpus* apical cells (left) and in the tobacco pollen tube (right). For each cell type, the global stress σ_e was computed using measured values of turgor, curvature and cell wall thickness (equation S2 in Supplementary information). Knowing normal velocity V_n at each point, the expected strain rate is computed according to equation S10 (see Supplementary information on the online version of the paper). Then instead of plotting each parameter against the abscissa s, these values are plotted against each other to show how the stress results in strain. In *Ectocarpus*, but not in pollen tube, behaves according to the Lockhart equation with constant values for Φ and σ_y (compare with Fig 2.3B). (**B**) Robustness of this result was tested by bootstrap analysis with 3000 replicates. For each sample, the linearity of the increasing part of the curve (where $\sigma_e > \sigma_y$) was estimated by linear regression. The distribution of the values of r^2 shows that linearity is well supported. (**C**) Relationship between the three biophysical features of the cell wall: plastic yield threshold (…)

(Figure 2.7, *continued*) (σ_y, x-axis), thickness (δ, y-axis) and plastic extensibility (Φ, z-axis). In *Ectocarpus*, only variation of δ accounts for tip growth (brown line), while in pollen tubes, both σ_y and Φ vary while the wall thickness remains constant (green line).

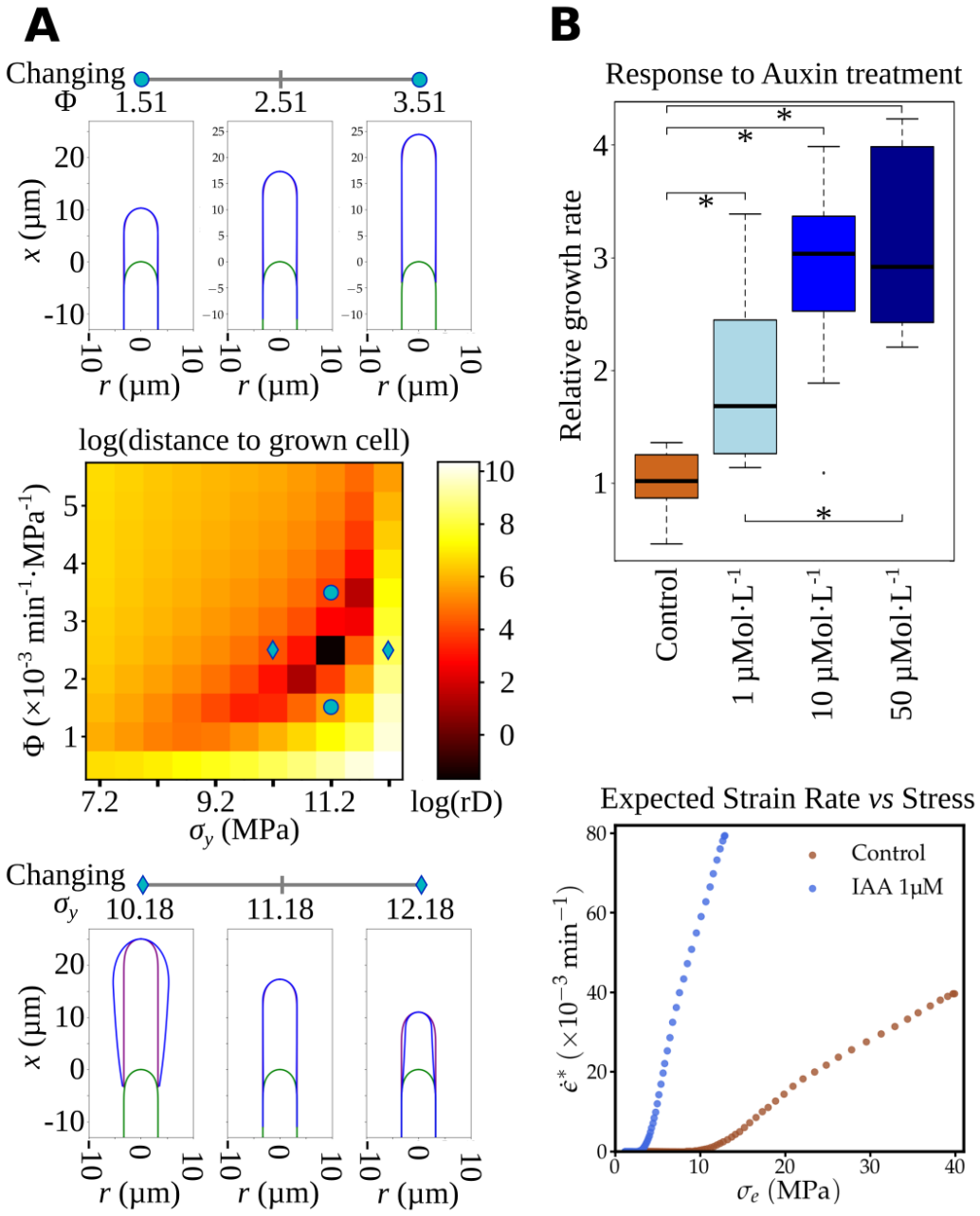

Figure 2.8 – Impact of yield threshold (σ_y) and extensibility (Φ) variations on *Ectocarpus* tip growth

(**A**) Simulation of tip growth in Ectocarpus with varying extensibility (Φ) and yield threshold (σ_y). (Middle) Heat-map representing the logarithm of mean weighted distance residuals (rD) for a range of σ_y (horizontal axis) and Φ (vertical axis) (one complete simulation for each pair of σ_y and Φ values). The darker the color, the lower the rD and the better the simulation. rD is calculated as the linear distance of points sharing the same meridional (s) distance between the simulated final cell contour and the initial one translated forwardly of 25 µm. Optimized values were 2.51 MPa^{-1} for the cell-wall extensibility (Φ) and 11.18 MPa for the yield threshold (σ_y). (Bottom) Impact of variation of cell wall yield threshold σ_y on tip growth simulation. The diagram shows the 2-D profile of apical cells before the simulation (initial stage, green contour) and at the end of the simulation (blue contour). The purple contour represents the translated initial shape to help comparison with the initial contour. σ_y values were 10.18, 11.18 and 12.18 MPa (diamonds on the heat-map). Simulations were run for 5 h 27 min, corresponding to a growth of 25 µm forward for the fastest simulation. (Top) Impact of the cell wall extensibility Φ on tip growth simulation. Same color code as in the bottom figure. Φ values were 1.51, 2.51 and 3.51×10-3 min-1·MPa^{-1} (circles on the heat-map). Simulations ran until the first simulation reached 25 µm in distance. (**B**) Response to auxin treatment. (Top) The linear growth rate (ΔL/Δt) was measured 24 h after adding 1, 10 or 50 µM of indole-3-acetic acid (IAA). Relative growth rate was calculated as the ratio to the mean growth rate in the control condition

(Figure 2.8, *continued*) (2 µM NaOH, see Materials and Methods for details). * denotes pairs of conditions for which a pairwise Mann-Whitney tests showed significant differences (p-value < 0.05 after Holm correction for multiple tests). (Bottom) Expected strain rate *vs* stress for control conditions and in the presence of 1µ Mol·L^{-1} IAA. The curve shows that both σ_y and Φ are affected by the presence of IAA: σ^y decreases while Φ increases, both modifications corresponding to a cell-wall loosening effect.

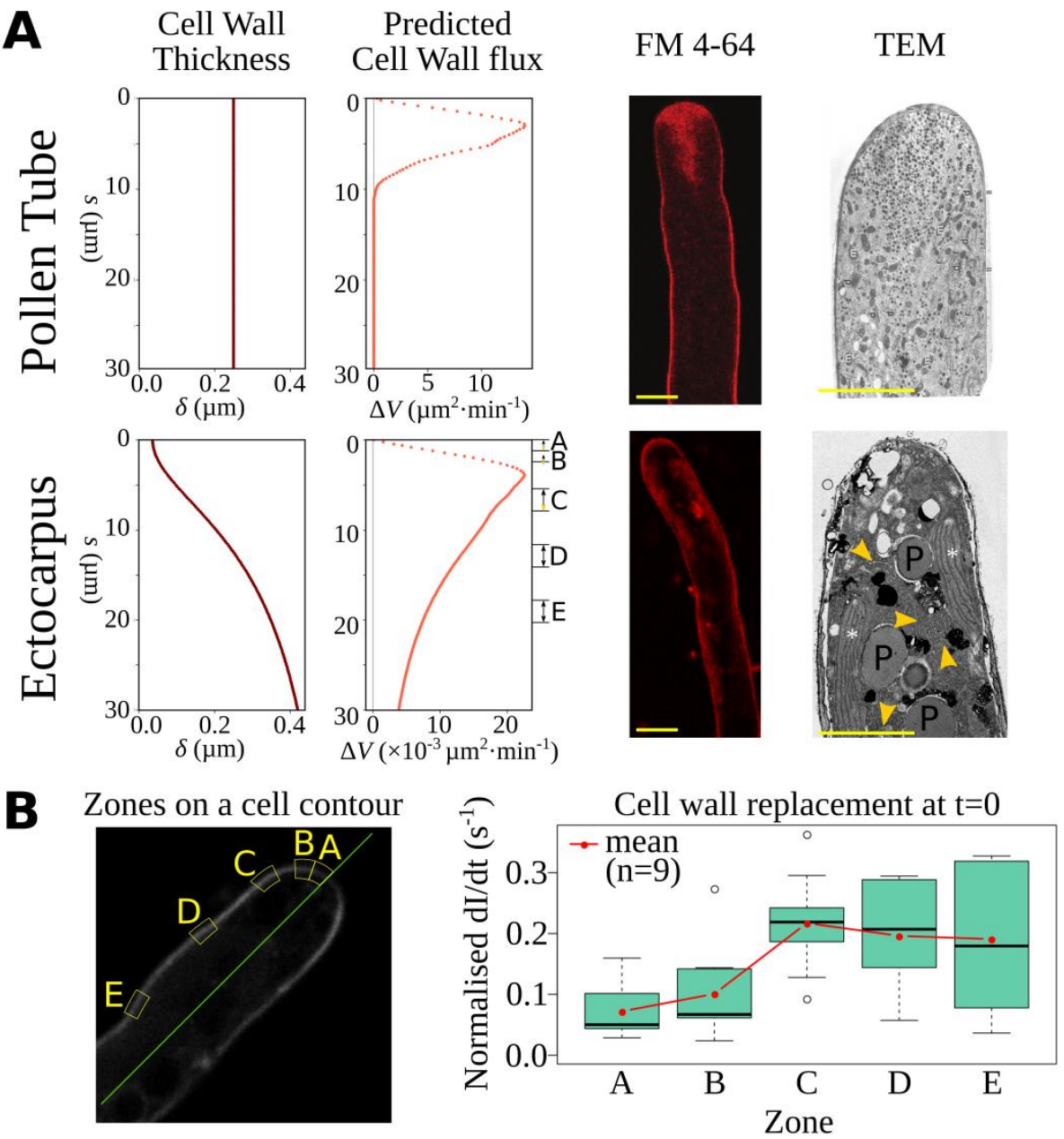

Figure 2.9 – Impact of the cell wall thickness gradient and pattern of cell wall biosynthesis

(**A**) Dynamics of cell wall synthesis in the pollen tube (top) and *Ectocarpus* apical cell (bottom). From left to right: Cell wall thickness δ from which the computed cell-wall flux was inferred using the model. Note the different x-scales between *Ectocarpus* and the pollen tube. Vesicle pattern displayed by FM4-64 labeling. Confocal image ~ 30 min after addition of FM4-64 at RT in living *Ectocarpus* and in the pollen tube (Courtesy of G. Grebnev & B. Kost, Erlangen Univ, Germany). Bar = 5 µm. Longitudinal sections observed using transmission electron microscopy (TEM). In contrast to the pollen tube (top) where a dense distribution of vesicles was observed in the dome (Derksen et al., 1995); Reprinted by permission from Springer, Protoplasma), no specific network of vesicles was observed in the dome of the *Ectocarpus* apical cell (bottom). Instead, chloroplasts and associated reticulum (see (Charrier et al., 2008), for the description of the overall intracellular organization) are present all along the cell axis. White stars: chloroplasts; Orange arrow heads: chloroplastic endoplasmic reticulum. P: pyrenoids. Bar = 5 µm. (**B**) FRAP experiment. (Left) Definition of the zones A-E from which fluorescence recovery was measured (also shown in panel A). (Right) Quantification of cell wall replacement expressed as the increase in normalized fluorescence intensity at t = 0 (time of photobleaching).

fluorescent dyes observed in optical microscopy (propidium iodide fluorescence intensity on plant trichome (Yanagisawa *et al.*, 2015); bright field microscopy of entire ghost cell walls of healing tip of the green alga *Acetabularia*; (Von Dassow *et al.*, 2001). Recently, Davì *et al.* (2018) developed a technology on fission yeast enabling a resolution of 30 nm in living cells. However, this resolution is in the limit range of *Ectocarpus* cell wall thickness, and hence, TEM appeared to be the most reliable technique. Variability was observed between cells and even between cell sides. It was most likely due to i) inter-individual and local disparity and ii) different section plans as *Ectocarpus* filaments do not grow strictly parallel to solid surfaces. However, the 2500 measurements every ~ 400 nm along both sides of 15 cells, which were corrected to account for sections deviating from the meridional plans, allowed to propose a mathematical function for the distribution of the values. Cell wall thickening followed a steep gradient: 467 % increase in s = 8µm, *i.e.* an average slope of 16 nm per longitudinal µm or 1.6 %. No such gradient was reported in the growing zone of the other organisms. In the apical cell of *Neurospora* cell wall thickness gradually increases along the shanks while thickness is constant in the dome (Trinci and Collinge, 1975); in the fission yeast, the two growing ends display cell walls with a constant thickness lower than in the center of the cell (Davì *et al.*, 2018); in the diffusely growing trichome of *Arabidopsis* cell wall thickness increases along the cell with a slope of 0.3 % (Yanagisawa *et al.*, 2015).

At the biophysical level, this gradient of cell wall thickness resulted *de facto* in a decrease of the stress from the shanks to the tip. The biological parameters specific of *Ectocarpus* apical cell (turgor, dome geometry and cell wall thickness) were integrated into the viscoplastic model initially proposed by Lockhart and further developed for tip growth by Dumais et al. (2006). The observed cell wall thickness gradient was shown to quantitatively compensate for the reduction of stress due to the increase in curvature from the shanks to the tip. After adjusting the plasticity parameters, the model was able to achieve self-similar growth at the speed observed *in vivo*. Regarding the cell wall mechanical properties, the model inferred two main differences with the pollen tube. First, the extensibility Φ and the yield threshold σ_y remained constant along the cell of *Ectocarpus*, in contrast to the pollen tube models where the constant thickness of the cell wall necessarily requires modification of the cell wall mechanical properties to allow growth (Fayant *et al.*, 2010). Using a Lab-on-a-Chip platform, (Shamsudhin *et al.*, 2016) confirmed that the pollen tube displays an apparent increasing elastic modulus from the tip to the shanks, which is correlated with the presence of methyl-esterified pectins (Parre and Geitmann, 2005*a*). However, the preponderant role of these cell wall component gradients could be restricted to the pollen tube as opposite observations were reported in other plant tissues (reviewed in Cosgrove, 2016, 2018).

Secondly, compared to the pollen tube, the overall value of strain rate is ~ 100 times lower, while stress is ~ 10 times higher in *Ectocarpus* (**Fig 2.6**), suggesting that *Ectocarpus* cell wall is altogether more resilient to yielding during growth. Obviously, experimental work is still needed to refine the values of the yield threshold and extensibility, but our calculation of the wall stress which was based on experimental data provided a solid basis to infer their order of magnitude. Interestingly, nano-indentation of *Ectocarpus* cell wall produced values of Elastic modulus much lower (~ 1-4 MPa; Tesson and Charrier, 2014) than those reported in the pollen tube (~ 20-400 MPa; Shamsudhin *et al.*, 2016), However, the different nano-indentation experimental procedures used in these studies (depth of indentation, shape of the indenter, osmotic conditions, physical model) make comparisons not very reliable (Cosgrove, 2016*a*). Nevertheless, if taken together with the cell wall mechanical properties inferred from the growth model, this would suggest that *Ectocarpus* cell wall is more elastic but less prone to deformation during growth than the pollen tube cell wall. Distinction between cell wall elasticity and growth was already noticed in the green alga *Chara* (Proseus *et al.*, 1999) and

since was reported in other plant cells (reviewed in Cosgrove, 2016). The inverse relationship noticed in *Ectocarpus* is fairly compatible with the dual role of the cell wall in brown algae: 1) cope with frequent environmental changes in osmotic pressure (tides), requiring a high level of cell wall elasticity, and 2) resist to yielding because of the high wall stress due to both the high turgor and the thin cell wall. Examples of a lack of functional relationship between intrinsic elasticity and cell wall extensibility have already been reported in land plants (Cosgrove, 2016*a*). How the very low growth rate specific of *Ectocarpus* is related to these cell wall mechanical properties is a puzzling question. Part of the answer might reside in the composition and structure of brown algal cell walls. At least two independent networks, one made of cellulose microfibrils cross-linked with proteins and fucose-containing sulfated polysaccharides and the second composed of alginate fibrils cross-linked with phlorotannins could ensure cell wall stiffness and/or propensity to yield during growth (Deniaud-Bouët *et al.*, 2017). However, no correlation between these components and cell wall extensibility was displayed so far. At the tissue level, seaweeds with the most flexible thalli were reported to contain high levels of stiff guluronan alginates (Miller, 1996). As far as cell growth is concerned, the location of soft alginates (mannuronan) did not coincide with the position of emerging buds in the shoot apex of the brown alga *Sargassum* (Linardić and Braybrook, 2017) and similar lack of functional relationship was observed in the growing area of the rhizoid of *Fucus* (Torode *et al.*, 2016). Therefore, in brown algae as in land plants (e.g., Peaucelle *et al.*, 2011; Park and Cosgrove, 2012, and reviewed extensively in Cosgrove, 2016), the presence of stiff or soft polysaccharides – as assessed *in vitro* – does not correlate with the expansion of the cell wall during growth.

Another puzzling question is how *Ectocarpus* controls the cell wall thickness gradient necessary to ensure the maintenance of cell shape. Whether the cell wall thickness fluctuates during growth, as recently reported in the fission yeast (Davì *et al.*, 2018) is unknown but this could account for cell shape and growth rate variations observed in time-lapse movies (not shown). In all cases, the gradient requires regulation of cell wall biosynthesis, which in brown algae like in land plants involves both *in muro* cellulose synthesis and the delivery of other components (fucans and alginates in brown algae) through vesicle trafficking (Golgi and flat cisternae respectively in Fucales; Nagasato *et al.*, 2010). FRAP data showed that the highest exocytosis activity was localized in the basal region of the dome, just before the cell adopts its cylindrical shape. This coincides with the highest cell wall flux computed from the model and with the pattern described in the pollen tube (Bove *et al.*, 2008; Chebli *et al.*, 2013). How exocytosis vesicles are targeted to these positions is unknown. In Yeast and land plants, mechanosensors localized *in muro* control cell wall biosynthesis enzymes in order to modulate cell wall thickness and respond to cell wall damage (Hamant and Haswell, 2017; Davì *et al.*, 2018). *Ectocarpus* codes for several mechanosensor proteins (Integrins, WSC-containing trans-membrane proteins; Cock *et al.*, 2010; Michel *et al.*, 2010), and these proteins could as well be key regulatory factors in this process.

The palette of tip growing strategies among species is not restricted to the control of cell wall thickness and of cell wall mechanical properties through pectin methyl-esterification. Other molecular mechanisms, including pectate distortion cycle in *Chara* (Proseus and Boyer, 2007), secretion of glucanases and chitinases in Fungi (Riquelme, 2013) and intussusception in prokaryotes (Cava *et al.*, 2013) were proposed to account for the differential cell wall mechanics along the cell. Therefore, distinct key cell wall biophysical factors, and potentially a combination of them (Davì *et al.*, 2018), seem to have been selected during the evolution to achieve cell wall growth. Among these organisms, *Ectocarpus* has favoured a singular approach based on the cell wall thickness and hence on the control of the wall stress. Whether its slow growth makes this control more efficient than the control of the cell wall mechanical

properties is an exciting question which remains difficult to investigate in a close future because of technique limitation in this alga (e.g. lack of transgenesis). Meanwhile, future studies will focus on the molecular factors involved in the establishment and the maintenance of the cell wall thickness gradient.

2.1.2. Materials and Methods

Culture of Ectocarpus parthenosporophytes. Parthenosporophyte filaments of *Ectocarpus* sp. (CCAP accession 1310⁄4) were routinely cultivated in natural sea water (NSW) as described in Le Bail and Charrier (2013). For microscopic observations and time-lapse experiments, early parthenosporophytes were obtained from gamete germination on sterile coverslips or glass-bottomed Petri dishes.

Auxin treatments. *Ectocarpus* prostrate filaments were treated with 1, 10 and 50 µM Indole-3-Acetic Acid (IAA; Sigma-Aldrich **I3750)** prepared in 2, 20 and 100 µM NaOH respectively (final concentration). Growth rates were measured for each concentration 24 h post treatment (n = 10), using natural sea water supplemented with 2 µM NaOH as a control. Turgor was measured in 1 µM IAA using 2 µM NaOH as the control (see Measurement of turgor in the apical cell and correction for details).

Measurement of turgor in the apical cell and correction. *Ectocarpus* filaments were immersed for 1 min in a range of sucrose concentrations (diluted in NSW) and the proportion of plasmolysed apical cells was measured by counting apical cells (n > 100) with an optical microscope. The rate of plasmolysis was plotted against external osmolarity (c_e). The limit plasmolysis (c_{pl}) corresponds to the value of c_e at which 50 % of apical cells were plasmolysed. The mean c_{pl} value was calculated from three independent experiments. Solution osmolarities were measured with an osmometer (Osmometer Automatic, Löser, Germany). Because the cell wall of Ectocarpus is partly elastic, plasmolysed cells have a reduced volume that must be taken into account to calculate the real internal osmolarity (c_i) and thus the real internal turgor (P). To do so, the coefficient of apical cell volume shrinking (x, equal to the ratio of the cell volume upon plasmolysis to the cell volume in normal growth conditions) was measured on apical cells (n = 9) and the corrected internal osmolarity was calculated as $c_i = x . c_{pl}$. The difference between internal and external osmolarities is $\Delta c = c_i - 1100$ with the sea water osmolarity = 1100 mOsm·L^{-1}, and the turgor is $P = \frac{c_i - c_e}{410}$, in MPa.

Apical cell curvature. Apical cell contours were drawn manually from confocal images of meridional plans of apical cells immersed in NSW. Similar procedure was followed for tobacco pollen tubes from photos given by Greb Grebnev (B. Kost's lab, Erlangen Univ, Germany). We devised a python3script to compute the average contour for a series of images, and used it on Ectocarpus (n = 17; *Suppl. Fig 2*) and tobacco pollen tubes (n = 6; not shown). The program starts with a hand-drawn contour for each cell, from which it computes a smoothed cubic spline curve. A set of equidistant points (we used a point-to-point distance of 50 nm) are extracted from the spline and the meridional curvature κ_s is computed at each point (*Suppl. Fig 2*). To obtain average symmetrical curvatures, a pair of windows starting from the tip point and sliding in both directions was used (window width = 200 nm, sliding step = 50 nm). The discrete values of the $\kappa_s = f(s)$ function were used to iteratively compute the position of cell-wall point coordinates as values of x (the axial abscissa) and r (the

distance to the axis), together with the meridional abscissa s, the curvatures κ_s and κ_θ, and φ the angle between the axis and the normal to the cell wall. In particular, the circular symmetry of the dome imposes at the tip (where s = 0), that $\kappa_\theta = \kappa_s$ thus $\sigma_\theta = \sigma_s$, whereas in the cylindrical part of the cell $\kappa_s = 0$ thus $\sigma_\theta = 2\sigma_s$.

Serial longitudinal sections of *Ectocarpus* apical cells. *Ectocarpus* filaments were prepared for transmission electronic microscopy (TEM). Filaments grown on sterile glass slides were fixed with 4% glutaraldehyde and 0.25 M sucrose at room temperature and washed with 0.2 M sodium cacodylate buffer containing graded concentrations of sucrose. The samples were post-fixed in 1.5 % osmium tetroxide, dehydrated with a gradient of ethanol concentrations, and embedded in Epon-filled BEEM capsules placed on the top of the algal culture. Polymerization was performed first overnight at 37°C and then left for 2 days at 60°C. Ultrathin serial sections were cut tangentially to the surface of the capsule with a diamond knife (ultramicrotome) and were mounted on copper grids or glass slides. Two types of sections were produced. 300 nm-thick serial sections were stained with toluidine blue to show the main cellular structures, including the cell wall, and mounted on glass slides. 70 nm thick sections were stained with 2 % uranyl acetate for 10 min and 2 % lead citrate for 3 min, mounted on copper grids (Formvar 400 mesh; Electron Microscopy Science) and examined with a Jeol 1400 transmission electron microscope. A compilation of the sections for the 15 cells is shown in *Suppl. Fig 3*. Original photos are available at **http://abiboom.snv.jussieu.fr/TipGrowth/TEM_CWT.tgz**.

Measurement of the cell wall thickness and correction. From TEM pictures obtained on fixed *Ectocarpus* apical cells, only longitudinal sections with the thinnest walls were considered to avoid bias due to askew sections. Measurements were carried every 400 nm along 15 different cells, at meridional abscissa from tip (s = 0) up to s = ±70µm using Fiji image analysis software. Altogether 2500 measured values of apparent thickness w were corrected making the assumption that actual cell radius was R = 3.27 µm, but was seen as apparent radius a, and applying the following formula: $\delta = R - \sqrt{a^2 + R^2 - (a+w)^2}$ (*Suppl. Table 2*).

Function of the topological distribution of the cell wall thickness. Cell wall thickness corrected values δ were plotted as a function of the position s along the cell. As the relation δ = f(s) displayed the aspect of an inverted bell, we designed three functions with this shape, derived from classical functions, to match them with the experimental values:

(1) "Gauss": $\delta = \delta_{max} - (\delta_{max} - \delta_{min}) \exp(-(s/s_{1/2})^2 \log(2))$;

(2) "Lorentz": $\delta = \delta_{max} - (\delta_{max} - \delta_{min})(1 + (s/s_{1/2})^2)^{-1}$;

(3) "Pearson": $\delta = \delta_{max} - (\delta_{max} - \delta_{min})(1 + 3(s/s_{1/2})^2)^{-1/2}$.

The parameters δ_{min}, δ_{max} and $s_{1/2}$ were adjusted for each of these functions, with a respective residual standard error of 0.08, 0.05 and 0.04. Therefore, we used the "Pearson" model with its optimized parameters δ_{min} = 36.2 nm, δ_{max} = 591 nm, $s_{1/2}$ = 16.81 µm for further modeling (Fig 5C).

Atomic force microscopy. *Ectocarpus* cells were boiled twice in 1 % SDS, 0.1 M EDTA and then treated with a solution of 0.5 M KOH at 100°C. Pellet was rinsed extensively with MilliQ water and dried on a glass slide. Imaging was performed on dried samples. A Veeco Bioscope catalyst atomic force microscope coupled with a Zeiss inverted fluorescent microscope was used for imaging. RTESP probes (Bruker) were used in Scanasyst mode.

Orthogonality of tip growth. Protocol was adapted from Shaw *et al.* (2000) and is described in details in Rabillé *et al.* (2018). Young sporophyte filaments grown in glass-

bottom Petri dishes were covered with sonicated 0.1 % (w:v NSW) of FluoSpheres™ amine, 0.2 µm, red (F8763, Molecular Probes), washed with NSW and mounted under a TCS SP5 AOBS inverted confocal microscope (Leica) controlled by the LASAF v2.2.1 software (Leica). The growth of 25 apical cells growing parallel to the glass surface was monitored, and bright-field and fluorescent pictures of median planes for each apical cell were acquired at several time points. Cell-wall contours were hand-drawn on time-lapse images using GIMP, together with their respective indicator points. The position of the extreme tip (s = 0) was fixed for each meridional contour and the drawing of cell contours and micro-sphere positions were aligned during the time course using steady micro-spheres attached on fixed positions. A spline was adjusted on each contour, and on each series of indicator points. The angle at each possible intersection between these trajectories and the cell contour splines were computed, making use of their first derivatives. Further analysis performed using R (R Core Team, 2017) consisted in (1) determining the distribution of angles, their mean and standard deviation, and (2) testing the hypothesis of dependence between the angle and the meridional abscissa. From the 156 measured angles between the tangent to cell wall and the trajectory, we computed the mean value $m = 1.71 = \pi/1.83$ radian (or $\pi/2$-9.16 %) and the standard deviation $s = 0.52 = \pi/6.09$ radian. To test independence between the angle and the position in the dome, we computed the Pearson correlation coefficient between the angle and the absolute value of meridional abscissa. It was $r = -0.031$.

Calcofluor labelling. Staining of *Ectocarpus* filaments with Calcofluor white was carried out as described in (Le Bail *et al.*, 2008).

FM4-64 vesicle labeling and FRAP. FM4-64FX (F34653, Invitrogen) stock solution was diluted to 385 µM in DMSO, and then diluted to 7.7 µM in NSW. Coverslips with Ectocarpus filaments were immersed in 50 µL of 7.7 µM cold FM4-64FX on ice and immediately mounted on a confocal microscope. Endocytosis and further trafficking of the fluorochrome was followed for 1 h at room temperature. The fluorochrome was excited with a 561 nm neon laser, and emission observed with a 580-630 nm PMT.

For the FRAP assay, filaments were stained with 100 µM FM4-64FX for 10 min at 4°C and rinsed 4 times with cold fresh sea water. Photobleaching was performed on ~ 25 µm (s) along the cell from the tip, and recovery was monitored using an inverted Nikon Ti Eclipse Eclipse-E microscope coupled with a Spinning Disk (Yokogawa, CSU-X1-A1) and a FRAP module (Roper Scientifics, ILAS). Images were captured with a 100x APO TIRF objective (Nikon, NA 1.49) and a sCMOS camera (Photometrics, Prime 95B). For the defection of the FM4-64 stained samples we used a 488 nm laser (Vortran, 150 mW) for the excitation and the bleaching steps and collected the fluorescence through a 607/36 bandpass filter (Semrock). Image acquisition using the MetaMorph software 7.7 (Molecular Devices) was as follows: 1 image/s, displaying 6 images before bleach, 1 image at the precise time of bleaching, 50 images during the recovery phase, for a total of 57 images by cell.

Images for one given cell were processed as a stack using ImageJ2 (Schindelin *et al.*, 2012) and R (R Core Team, 2017). For each time point t (taking $t = 0$ at the time of bleaching), the background signal Z(t) was averaged from 4 separate square regions of ~ 1µm² ; the spontaneous fluorescence decrease was estimated by monitoring the signal U(t) in an unbleached region ; the local signal was recorded in regions A-E as defined in Fig 9B. Note that all zones including E are sufficiently far from the frontier of the photobleached zone to be devoid of homogenization by membrane lateral flux in the considered time scale. Following (Phair *et al.*, 2003), the corrected signal for region A (and similarly for regions B-E) was computed as :

$$A_c(t)=(A(t)-Z(t)-(A(0)-Z(0)))\frac{U(0)-Z(0)}{U(t)-Z(t)}$$

The recovery activity was estimated by matching the measured $A_c(t)$ values to the function $Y(t) = Y(0)+\alpha(1-\exp(-t/\tau))$ where $Y(0)$, α and τ are free parameters. We computed the normalized slope at t=0 as $(1/\alpha)(dA_c/dt)(0) = 1/\tau$, for 9 observations in each of the 5 (A-E) zones retained (see *Suppl. Fig 7*).

Tobacco pollen tubes. The meridional contours of six tobacco pollen tube apices were traced from photos given by Greb Grebnev (B. Kost's group, Erlangen University, Germany), and the curvature was computed as described for *Ectocarpus* cells. Turgor and cell-wall thickness were obtained from the literature (McKenna *et al.*, 2009). In the absence of precise determination of their respective values, we derived a working hypothesis from previous literature reports showing that variations of Φ and σ_y occur simultaneously in opposite directions (Nakahori *et al.*, 1991; Passioura *et al.*, 1992; Geitmann and Steer, 2006). This intuitive relationship is consistent with molecular models of the cell wall (Passioura *et al.*, 1992). Given that our model can derive the value of the expected strain rate $\dot{\varepsilon}^*$ from other parameters (*Suppl. Information*), we propose to partition this product equally between its two members. Thus, we computed $\Phi=\sqrt{\dot{\varepsilon}^*}$ and $(\sigma_e-\sigma_y)=\sqrt{\dot{\varepsilon}^*}$, leading $\sigma_y=\sigma_e-\sqrt{\dot{\varepsilon}^*}$. These arbitrary values were useful for giving an example of what could be a possible state (**Fig 2.6F** and **G**; **Fig 2.7A** right) and performing simulations.

Code availability. Programs developed as part of this work were written in Python 3.6 [83], making use of numpy [84] and matplotlib [85] libraries, in a GNOME-Ubuntu environment (laptop and workstation). The source code is available at http://abiboom.snv.jussieu.fr/TipGrowth/TipGrowthSoftware.tgz.

Modeling and simulations. Modeling is described in the Supplementary information. The simulation program performed a simple simulation with graphic output, or an array of simulations within a range of Φ and σ_y values. The input was a list of cell wall point coordinates and parameters from, for instance, computations of average contours (ad hoc generated data were also used for simulations starting with geometrically designed profiles). For each point, the stress was computed from turgor, curvature and cell-wall thickness values. Then, using Φ and σ_y, the strain rate and the normal velocity were computed. The velocity and displacement direction (normal to the cell wall) gave the new position of the point, calibrated for a tip growth of 1 nm at each step. After computing new positions for all points, the program designed a cubic spline (without smoothing) from which a new sample of points was extracted, thus keeping a constant distance between points throughout the simulation. Accuracy of the simulation was evaluated by averaging point-to-point distances between the simulated profile and the initial profile translated at the expected speed. Values of Φ and σ_y were progressively optimized using a steepest descent approach. As starting values, we used the coefficients of the linear model derived from the points $(\sigma_e,\Phi(\sigma_e-\sigma_y))$ for which $\Phi(\sigma_e-\sigma_y)) > 1$: $\Phi = 2.5\times10^{-3}$ $min^{-1}\cdot MPa^{-1}$ and $\sigma_y = 11$ MPa. These values were used to simulate growth up to 25 µm, and divergence with the expected behavior was evaluated by comparing them to the initial points translated by 25 µm in the axial direction. As a numerical value, we took the logarithm of rD (residual distance) which was the weighted average point-to-point distance, where the weight was $\exp(s^2\log(2))$ to maintain the dome shape. Optimized values $\Phi = 2.51\times10^{-3}$ $min^{-1}\cdot MPa^{-1}$ and $\sigma_y = 11.18$ MPa gave a simulation with a log(rD) of -3.0. As a comparison, the mean log(rD) between the initial contour and the 17 experimental contours used to build it was -4.41, with a standard deviation of 0.35.

Robustness. In order to assess the robustness of the results, we performed a bootstrap analysis. 3000 samples were constructed by drawing with replacement 17 cell contours and 15

cell wall TEM images out of their respective datasets. For each sample, the average contour and the cell wall gradient were computed as explained above. The stress σ_e and expected strain rate $\dot{\varepsilon}^*$ were computed as functions of the meridional abscissa *s*. To test consistency with the model, the (σ_e ; $\dot{\varepsilon}^*$) points were fitted a Lockhart equation by adjusting parameters Φ and σ_y, and computing the Pearson correlation coefficient (r^2) for the increasing part of the function, i.e. $\sigma_e > \sigma_y$; $\dot{\varepsilon}^* > 0$.

****

Acknowledgments. We thank Benedikt Kost (Erlangen Univ, Germany) for the photo of the tobacco pollen tubes in bright field, Greb Grebnev (Erlangen Univ, Germany) for the tobacco pollen tube stained with FM4-64, Aude Le Bail (Erlangen Univ, Germany) for photos of *Physcomitrella* filaments and Burka Brown (Erlangen Univ, Germany) for the photo of the *Chara* rhizoid. We are greatly indebted to Mark Hildebrand (Scripps, CA, USA) for access to the atomic force microscope at the SCRIPPS Institution of Oceanography.

The present work has benefited from the cytometry/electronic microscopy/light microscopy facility of Imagerie-Gif, (http://www.i2bc.paris-saclay.fr), member of IBiSA (http://www.ibisa.net), supported by “France-BioImaging” (ANR-10-INBS-04-01), and the Labex “Saclay Plant Science” (ANR-11-IDEX-0003-02).

H.R. PhD is funded by Sorbonne Université and Région Bretagne.

Author contributions. H.R, B.B and B.C designed the experiments and wrote the manuscript. E.R. prepared the algal material, B.T. obtained the AFM data and S.L.P the TEM pictures. H.R. and B.C. obtained and analyzed the other biological data. B.B. performed the computational work.

Competing financial interests. The authors declare no competing and financial interests linked to this work.

2.2. The mechanical role of alginates in *Ectocarpus* cell walls

Microscale mapping of alginates along the uniseritate filament of *Ectocarpus*
Alginates help brown algal cells cope with stress

Article 2 *in preparation, to be submitted to the journal New Phytologist*

Authors:

Hervé Rabillé[1], Thomas Torode[2], Benoit Tesson[3], Aude Le Bail[1*], Bernard Billoud[1], Elodie Rolland[1], Sophie Le Panse[4], Bénédicte Charrier[1]

Affiliations:

[1]: Morphogenesis of Macroalgae, UMR8227, CNRS-UPMC, Station Biologique, Place George Teissier, Roscoff 29680, France

[2]: The Sainsbury Laboratory, University of Cambridge, Bateman Street, Cambridge CB2 1LR, United Kingdom

[3]: Marine Biology Research Division, Scripps Institution of Oceanography, University of California San Diego, La Jolla, CA, USA

[4]: Platform Merimage, FR 2424, Centre National de la Recherche Scientifique, Station Biologique, Place Georges Teissier, 29682 Roscoff Cedex, France

[*] Department of Biology, Erlangen University

Corresponding author: Bénédicte Charrier. email: benedicte.charrier@sb-roscoff.fr

Keywords: alginate, immunolocalisation, cell wall, brown alga, Ectocarpus, stress, biophysics

Abbreviations: ASW: Artificial Sea Water; G: L-guluronate residues; M: D-mannuronate; NSW: Natural Sea Water; NSWp: NSW completed with Provasoli Enrichment Medium;

2.2.1. Introduction

The brown algae (Phaeophyceae) belong to the Stramenopiles, which have been phylogenetically separated from other plant and algal lineages for ~1.5 billion years (Baldauf, 2008). They are thought to have arose ~200 mya (Silberfeld *et al.*, 2010) making it a relatively recent event in comparison to the colonisation of land and diversification of land plants ~510-630 mya (Raven and Edwards, 2001; Clarke *et al.*, 2011). In this time the brown algae have independently evolved complex multicellularity and have diversified into the largest and most morphologically intricate of the macroalgae. The unique evolutionary history of brown algae and their lifestyle in a marine ecosystem (characterized by strong abiotic

stresses) make them likely to have acquired original cellular and biophysical mechanisms during development (Charrier *et al.*, 2012). Cell walls are of vital importance for the structure and shape of plants and algae, and provide the first line of defence against abiotic stress. The cell walls of brown algae are different in both composition and abundance of cell wall components from that of land plants and other macroalgae (Popper *et al.*, 2011*a*). Cellulose microfibrils are less abundant in brown algal cell walls, accounting for only 1-8% of the cell wall dry weight (Deniaud-Bouët *et al.*, 2014*b*). Consequently, the cell walls of brown algae are more elastic than that of land plants (Tesson and Charrier, 2014*b*), having not evolved to resist compressive forces required for terrestrial growth. The major components of brown algal cell walls are sulphated fucans (~40%) and alginates (~40%) which are anionic polysaccharides. The walls also contain proteins, arabinogalactan proteins, phlorotannins (halogenated or sulphated phenolic compounds) and iodine (Michel *et al.*, 2010*b*; Hervé *et al.*, 2016*b*). In land plants, mechanical properties of cell walls are largely modulated by the pectic hydrogel matrix which is composed of multiple sub-families of polysaccharides of diverse sugar composition and structure (Mohnen, 2008; Bou Daher and Braybrook, 2015; Torode *et al.*, 2018). In brown algae, the hydrogel matrix is composed of alginate which is a linear polysaccharide composed of β-1,4-D-mannuronate (M) and α-1,4-L-guluronate (G). Alginate is produced as pure mannuronate, and is converted into guluronate via mannuronan-C5-epimerases (ManC5-Es). The activity of the ManC5-Es family of enzymes leads to the generation of three distinct regions within the alginate structure, homopolymer blocks of mannuronan (M-blocks) or guluronan (G-blocks), and heteropolymer regions of interspersed M and G (MG-blocks).

The G-block regions are able to form “egg-box” cross-links via calcium, and alginate gels made in vitro show that their viscosity depends on the M/G ratio and more specifically on the presence of G-blocks (Smidsrød *et al.*, 1972; Draget *et al.*, 1994; Ertesvåg, 2015). This is analogous to de-methylated stretches of homogalacturonan which allow calcium cross-linking in land plants. However, whereas de-methylation allows access of calcium ions to the homogalacturonan backbone, the conversion of mannuronate to guluronate in alginate causes a conformational change in the sugar residue resulting in an altered secondary structure in the alginate backbone. This causes a unique combination of sugar linkages whereby M-blocks are connected by diequatorial linkages, whilst G-blocks are connected diaxially and forming strong intra-molecular hydrogen bonds. MG-blocks contain both diequatorial and diaxially linked residues. The modified secondary structure alters the flexibility of the different blocks of the alginate polysaccharide, with MG being the most flexible (MG > MM > GG; Smidsrød, 1973). Interestingly, the secondary structure of MG-blocks allows formation of calcium cross-linking, but has a lower affinity for calcium compared to the G-blocks (Donati *et al.*, 2005; Mørch *et al.*, 2008), allowing for a two-tier hierarchical structure of calcium cross-linking within a single polysaccharide structure.

Furthermore, alginate has recently been reported to form tertiary microfibrils structures of ~4 nm diameter within the cell walls of brown algae (Terauchi *et al.*, 2016). In the brown alga Ectocarpus the cell walls of the (horizontally) growing prostrate sporophyte filaments lack any apparent specific organisation (Rabillé *et al.*, in revision; Le Bail *et al.*, 2011). However, tomography performed on (vertically) growing filaments showed that cellulose microfibrils adopt an isotropic organisation, whereas alginate microfibrils assemble into a cross-linked network mainly in the z-axis (Terauchi *et al.*, 2016). This suggests that the alginate microfibrils function to constrain extension of the cell wall in the z-axis, thereby maintaining the cell wall isotrope transversally. Additionally, the alginate matrix may be fortified via the addition of phlorotannins (Salgado *et al.*, 2009). The formation of a covalently bound alginate-phlorotannin network stabilises the alginate matrix and provides an alternative to

ionically cross-linking via calcium. Incorporation of phlorotannins into the wall can occur naturally over development (Schoenwaelder and Clayton, 1998), and also during wounding responses (Arnold and Targett, 2003; Lüder and Clayton, 2004).

Whilst the mechanical roles of alginate gels have been widely studied *in vitro*, this is not directly informative about the role of alginates within cell walls. Indeed, previous research into the composition of alginate within tissues has demonstrated an opposite relationship between the ratio of G-rich alginates and the stiffness (e.g. Miller, 1996). Recently, monoclonal antibodies have been raised against different blocks of alginates (Torode *et al.*, 2016), allowing for spatial analysis of alginate distribution *in situ*.

Using these antibodies in the large alga *Sargassum*, M-rich alginates were immunolabelled in mature tissues while enrichment in G-units was observed in the quite quiescent, central cell of the apical meristematic region (Linardić and Braybrook, 2017). In the brown alga *Fucus*, M-rich, MG-rich and G-rich alginates were all labelled in the zygote with a similar, ubiquitous pattern, and became undetectable in the growing rhizoid (Torode *et al.*, 2016).

Ectocarpus is a filamentous alga that is easily cultivable and amenable to experimental manipulation. Initial vegetative growth consists of filaments that can attach and grow on a variety of laboratory equipment (e.g. cover slips, slides; (Charrier *et al.*, 2008; Le Bail and Charrier, 2013). In addition, because its filaments are uniseriate, modification of the growth conditions impact all cells, allowing an easier interpretation of cell responses to external cues. Finally, prostrate filaments differentiate into unique cell types with different cell shapes and developmental fates (Charrier *et al.*, 2008). This makes *Ectocarpus* an interesting model organism where cell chemistry, mechanics and shape can be studied in the frame of a whole organism.

In this study, we assessed the importance of alginates in regulating mechanical properties along the developing prostrate filament of *Ectocarpus* sporophytes via immunolocalization of the different alginate blocks and looking for concomitant alterations to cell wall mechanical properties.

2.2.2. Results

2.2.2.1. Cell-specific pattern of alginate occurrence along the filament of Ectocarpus

In the early developmental stages (prostrate), *Ectocarpus* filaments grow as a string of cells. Sub-apical cylindrical cells (E cells), generated from elongation and division of the highly polarised apical cell (A cell), progressively differentiate into spherical cells (R cells). As a result, the centre of the filament is mainly composed of spherical cells, which are the favoured location for branching (Le Bail *et al.*, 2008; **Fig 2.10 A** and **B**). Branches re-iterate the same series of cell events, leading rise to a tuft of filaments after ~4 weeks (**Fig 2.10 C**). Close-up views obtained by scanning electronic microscopy (SEM) display a homogeneous and fairly smooth surface along A and E cell types (**Fig 2.10 D** and **F**), and a more granular surface in I, R and B cell types (**Fig 2.10 E**, **G**, **H**, **I**). The presence of a ring structure of

unknown nature was noticed at the junctions between I and R cells (**Fig 2.10 G**, **H**, **J**, **K**), as well as at the branching site (**Fig 2.10 M**). In some I and R cell types, photos allow to distinguish a double ring within this structure (**Fig 2.10 H**). No other specific structure could be observed by SEM.

In order to map the presence of alginates along these filaments, we immunolocalised whole filaments using independently three different monoclonal antibodies. Each antibody is specific for different conformation of alginates (Torode *et al.*, 2016). BAM6 antibody recognises blocks of mannuronans (M blocks, ranging from 2 to at least 7 consecutive M monomers; Torode *et al.*, 2016). It labelled mainly the dome of apical cells and the R cells. In A cells, mainly the most distal half (**Fig 2.11 A**) or the whole dome (**Fig 2.11 B**) were labelled but in some cases, a larger part of A cells, including both the dome and the shanks, was labelled (**Fig 2.11 C**). In rare cases, shanks of E cells were weakly labelled (**Fig 2.11 D**). On R cells labelling was concentrated especially in the most curved surfaces (**Fig 2.11 E**). A similar pattern was observed on some I cells (**Fig 2.11 E**).

Enrichment of the cell wall with guluronates was assessed using the monoclonal antibody BAM7, which labels mixed blocks of M & G units. Mainly the dome of the apical cell was labelled, in areas ranging from the tip (**Fig 2.12 A,B,C**) to an extended area including the whole dome and the adjacent shanks (**Fig 2.12 D,E**). Interestingly, when the signal intensity was high, two labelled layers were observed (**Fig 2.12 C,E**). E cells initiating transition towards I-type (i.e. rounding on the shanks) also displayed slight labelling in the centre of their longitudinal surface, corresponding to the most curved regions (**Fig 2.12 F**). In the central part of the filaments, both I and R cells were labelled (**Fig 2.12 G,H**), with R cells displaying the strongest signal (**Fig 2.12 I**). On these cell types, labelling of both the external and the internal surfaces of the cell wall was clearly observed (**Fig 2.12 J**), with sometimes a third, internal layer also labelled (**Fig 2.12 H**). Another interesting observation is the presence of two labelled rings framing the transverse separation between two adjacent cells (**Fig 2.12 G,H**). These rings might correspond to the inner surface of the transverse cell wall, but the distance between the two labelled layers seems higher than the transverse cell wall thickness as observed in TEM (see below).

BAM10 binds G-rich regions in mixed MG alginates (e.g. GMGGGM; Torode *et al.*, 2016). It was recently used to recognise alginates enriched in G-units in the brown alga *Sargassum* (Linardić and Braybrook, 2017). In contrast to BAM6 and BAM7, most of BAM10 labelling in Ectocarpus filaments was concentrated in A cells. In this cell type, different patterns were observed, ranging from a labelled tip in the dome (**Fig 2.13 A**), to an extended region encompassing the whole dome (**Fig 2.13 B,C**) and even larger areas overlapping the adjacent shanks (**Fig 2.13 D,E,F**). This pattern is similar to that observed with BAM6 and BAM7. In rare I and R cells, labelling could be observed on the curved shanks (**Fig 2.13 G** and **H** respectively), but more often, it was observed at the transverse sections (**Fig 2.13 I**, **J** for I-type cells; **Fig 2.13 K,L** for R-type cells), a location not labelled with BAM6 and BAM7. Indeed, in contrast to BAM7, BAM10 labelled only one ring, right at the position of the transverse cell wall (**Fig 2.13 I,J**). The different pattern of BAM10 compared to BAM7 in this position confirms that their respective epitopes are different.

Altogether, the three monoclonal antibodies labelled mainly the same areas along the filament: principally the apex of the apical cell (**Fig 2.14**). Some differences were observed in more mature cells: the shanks of rounding (I cells) or round cells would be richer in mannuronans, while the transversal junctions between adjacent cells would be richer in guluronans.

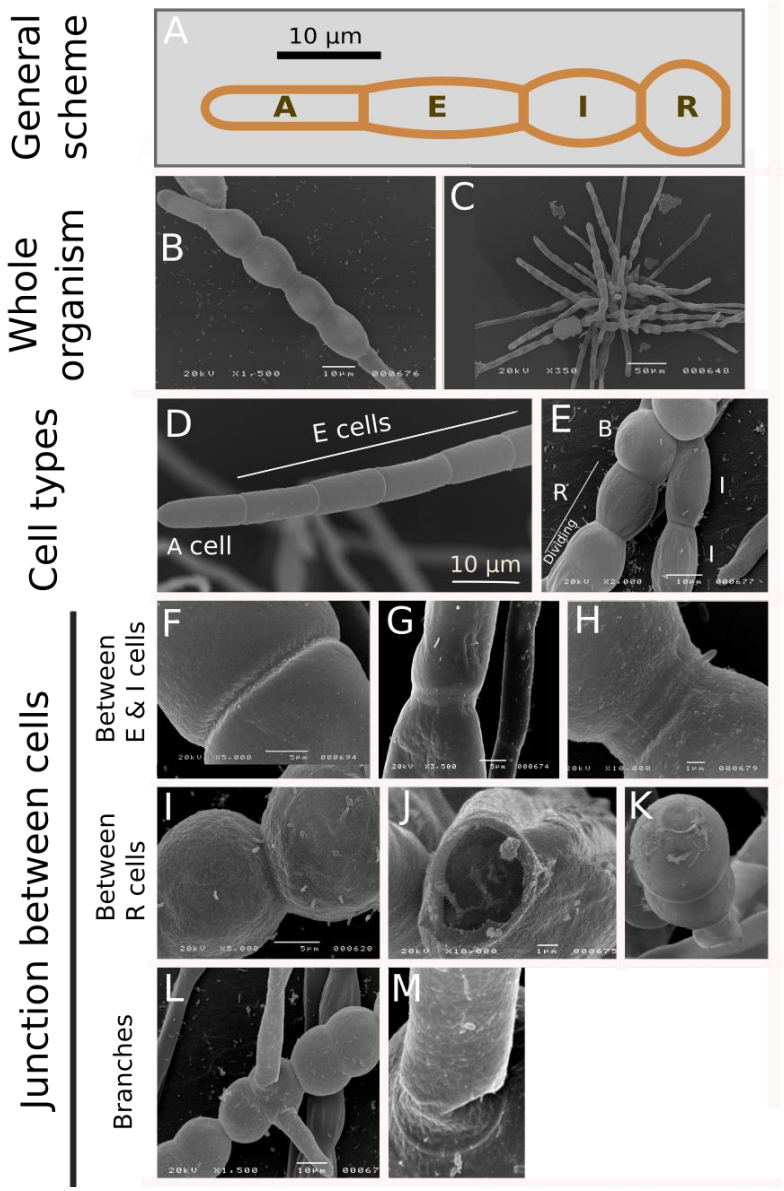

Figure 2.10 – Filament organisation and cell morphologies observed by scanning electronic microscopy

A: Overview of *Ectocarpus* sporophyte filament (prostrate) growing from spore germination. Five cell types are defined, according to their position and shape. A type: Apical cell; E type: Elongated, cylindrical cell; I type: Intermediate cell; R type: Round, spherical cells positioned at the center of the filaments; B type: branched cells, usually R type in the most central part of the filaments. The number of E, I, R and B cells increases with the filament maturation stage. Cells of the same cell types are contiguous. **B,C**: Whole organism observed by scanning electronic microscopy (SEM); at the early stage (**A**; 1 week post germination) and later stage (**B**; 2-3 weeks post germination). **D,E**: Close up on cell types. D: A and E cells at one filament extremity. E: I and R cell types in the center of the filament. **F,G,H**: Close-up on junctions (arrows) between E cells (**F**) and I cells (**G, H**) along the filament, showing either 1 single wall (**F**) or 2 annulus framing the wall (asterisks in **G** and **H**). **I,J,K**: Close-up on junctions (arrows) between R cells. **L,M**: Close-up on branches, showing a ring at the junction site (asterisk).

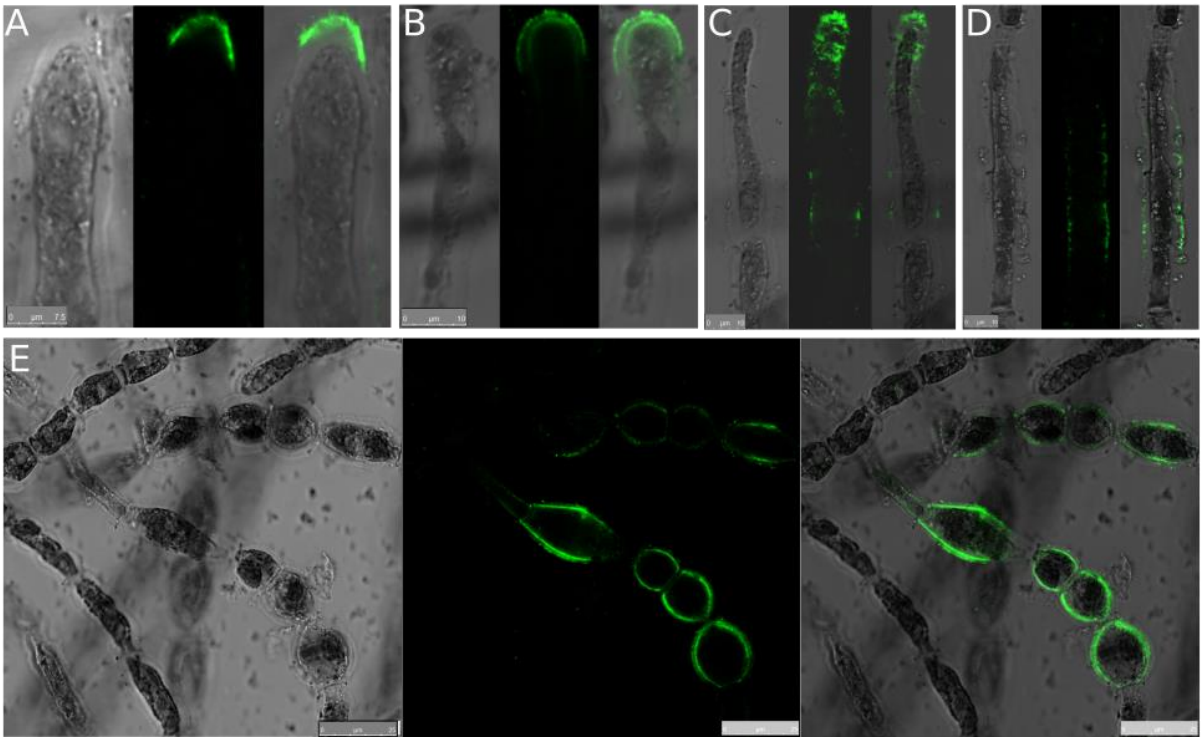

Figure 2.11 – Mannuronate-rich alginate blocks labelled with BAM6 antibody

A,B,C: A-cell types. **D**: E-cell type. **E**: Central part of filaments, showing labelling (FITC fluorescence; green) of I and R-cell types. Bright field, confocal and merge images are shown for each cell. Bars are indicated on each photo. Acquisition time and laser intensity were the same for all photos.

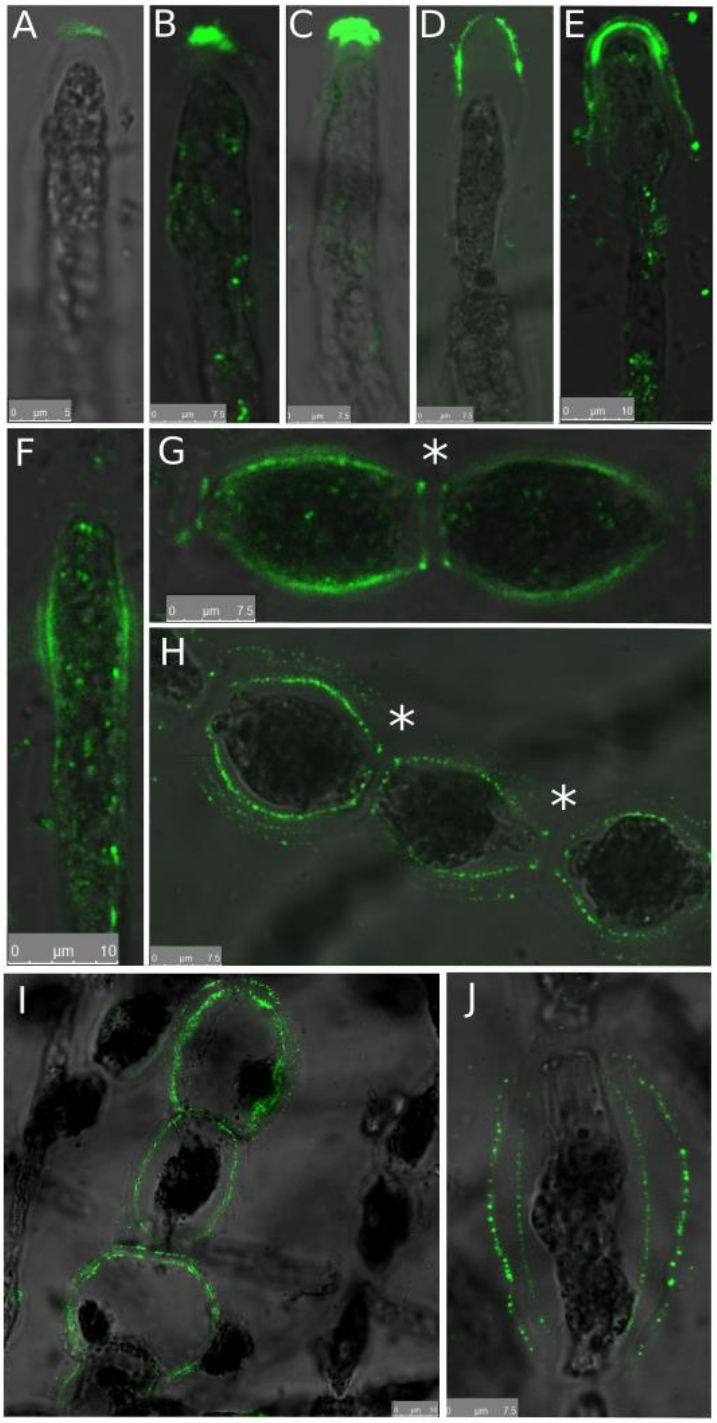

Figure 2.12 – Mannuronan-Guluronan alginate blocks labelled with BAM7 antibody

A,B,C,D,E: A cells. **F**: E-cell. **G,H,I,J**: I and R cells. Merge of bright field and fluorescent signal are shown. Fluorescent signal was acquired with different acquisition times depending on the photo. Asterisk indicates the double rings. Bars are indicated on each photo.

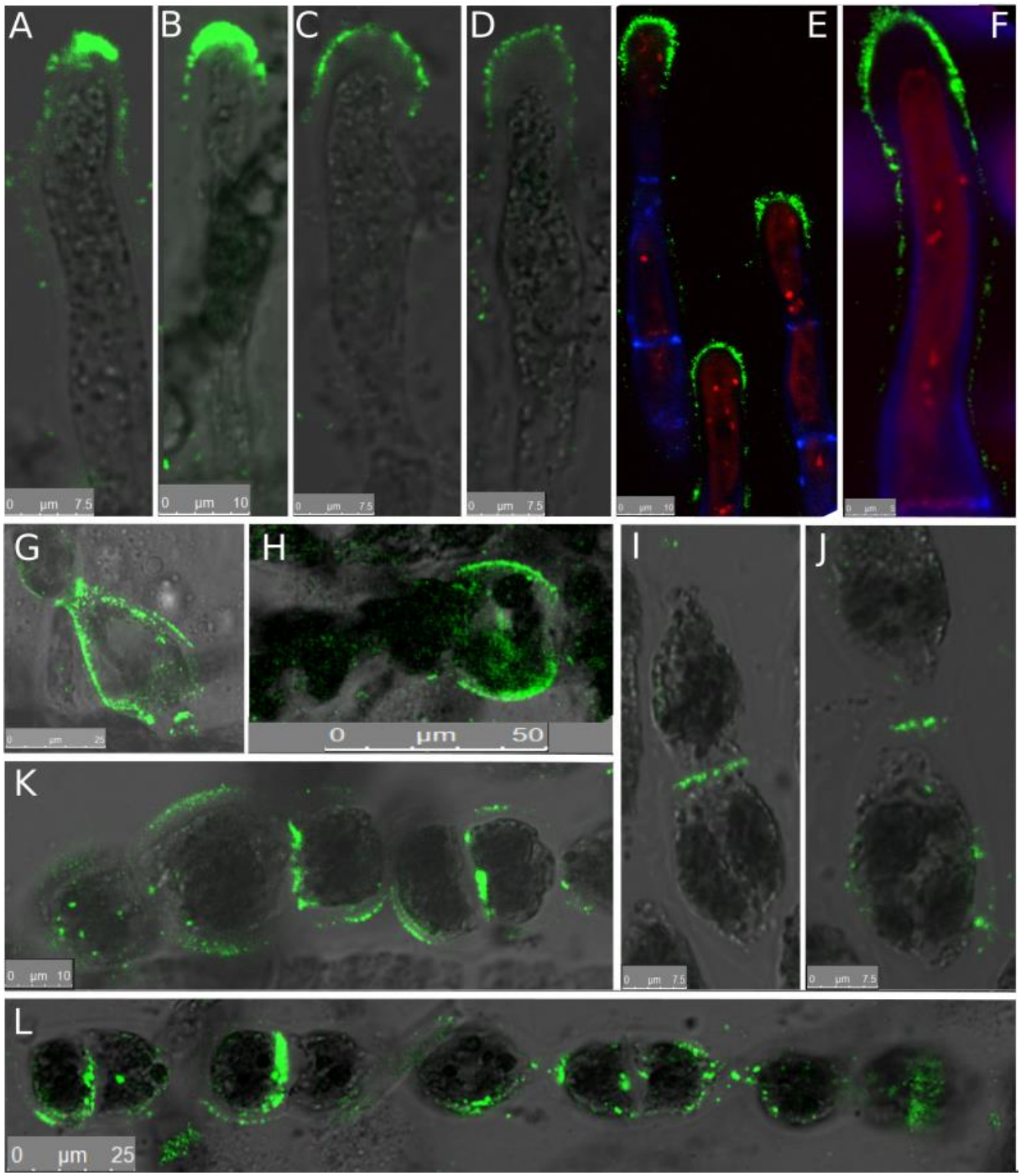

Figure 2.13 – Guluronan-rich alginate blocks labelled with BAM10 antibody

A,B,C,D,E,F: A cells. **H,I,J**: I cells. **G,K,L**: R cells. Merge of bright field and fluorescent signal are shown, except in **E** & **F** where FITC, calcofluor (UV light, blue) and endofluorescence of chloroplast (red) were merged. Fluorescent signal was acquired with different acquisition times depending on the photo. Bars are indicated on each photo.

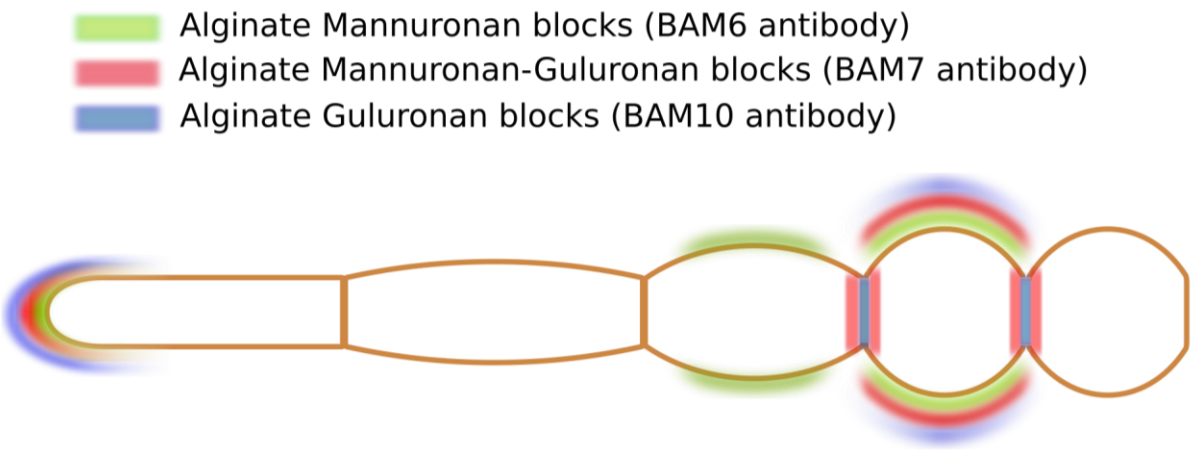

Figure 2.14 – Summary of alginate mapping along the filament of *Ectocarpus*

Stereotype of a sporophyte filament is shown with the four main cell types A, E I and R. Cell types are defined according to their position (for A cells) and their ratio of their length (L) to their width (w) (E, I and R cells). E cell: L/w > 2; I cell: L/w in [1.2; 2[; R cell: T/w < 1.2. Colours indicate where the epitopes of BAM6, BAM7 and BAM10 were immunodetected.

2.2.2.2. Alginates co-localise with areas subject to the highest physical stresses

In order to shed some light on the role of alginates in these cellular territories, we searched for correlation between these immunostaining patterns and *Ectocarpus* cell physiology. No correlation was observed between the alginate pattern and the dynamics of cell maturation. On the one hand, both very young 'A' cells and mature 'R' cells were labelled with the BAM antibodies, and on the other hand the E and I cells were rarely labelled, whereas these cells correspond to the transition states from A to R. A potential cause would be a different cell wall composition or thickness in E and I cells, thereby preventing labelling. In order to check for any structural cell wall differences between E/I and A/R cells, longitudinal sections of filaments were observed by TEM. As previously reported, Ectocarpus sp. cell wall displays usually a bipartite organisation, with a thick inner layer, and a thinner outer part (Oliveira and Bisalputra, 1973) TEM observations of *E. siliculosus* sporophyte cells confirmed this organisation. The inner cell wall layer seemed to be composed of a compact material. The outer layer was darker and looked even more compact than the inner layer (**Fig 2.15 A,B,C**). Three layers could be distinguished at the transverse junctions (**Fig 2.15 D**), where a ring of dark material also observed in most cells (**Fig 2.15 C,D**), which could be related with the alginate ring displayed by immunostaining. When compared between the different cell types along the filament, cell wall displayed similar organisation all along the filament, both in the number of layers, their structure, and their thickness (**Fig 2.15 A,B**). Measurements confirmed that a constant cell wall thickness of ~500nm in average was present in E, I and R cells (**Fig 2.15 E**). Besides, a recent study showed that 'A' cells displayed a thinner cell wall at the tip, and that a thickness gradient ranging from ~40nm thick at the tip to ~400nm in the shanks was established along the cell (Rabillé *et al.*, in revision) (**Fig 2.15 F**). Therefore, while the cell wall is thinner in the dome of the A cells than in R cells, alginates were similarly labelled in these areas with the BAM6 antibody. This observation does not support a possible interference of the cell wall thickness in the detection of the BAM antibody epitopes. In addition, the organisation of the cell wall into two main layers was similarly observed in E, I and R cell types, while R cells were mainly labelled, again precluding any link between the apparent cell wall organisation and the alginate immunostaining pattern. Therefore, labelling of the dome of A cells and of the shanks of R cells seems to be truly due to a modification of the cell wall composition.

In contrast to the curved surfaces, labelling of the junctions between adjacent cells was echoed by a peculiar structure observed in SEM (**Fig 2.10 F-H**) and TEM (**Fig 2.15 C,D**). Up to three additional dark layers were observed specifically at the junction. This layer is believed to make a ring around the junction, as a dark line can be observed in tangent section (**Fig 6 A**). The nature of this ring is unknown, but the fact that it is electron-dense suggests that it is alginate-rich (Terauchi *et al.*, 2016).

Interestingly, when looking at the morphological level of the whole filament (schematized in Fig 6C), the dome of the apical cells and the shanks of the R cells coincide with the most curved surfaces, which are also surfaces in expansion. Indeed, growth of these prostrate filaments takes place in the dome of the apical cell (Le Bail *et al.*, 2008), and R cells are formed from progressive rounding of E cells (Billoud *et al.*, 2008), requiring additional cell wall synthesis in the lateral sides of the cells. Cell expansion is due to the combination of a wall stress and of the cell wall propensity to grow. In order to discriminate between these two main factors with regard to the abundance of alginates, we first calculated the wall stress along the filament. Stress results from several biophysical components. While turgor increases stress, curvature and cell wall thickness decrease it (Castle, 1937; Green, 1965; Hejnowicz *et al.*, 1977). We measured turgor in E and R cells using the technique of limit plasmolysis and

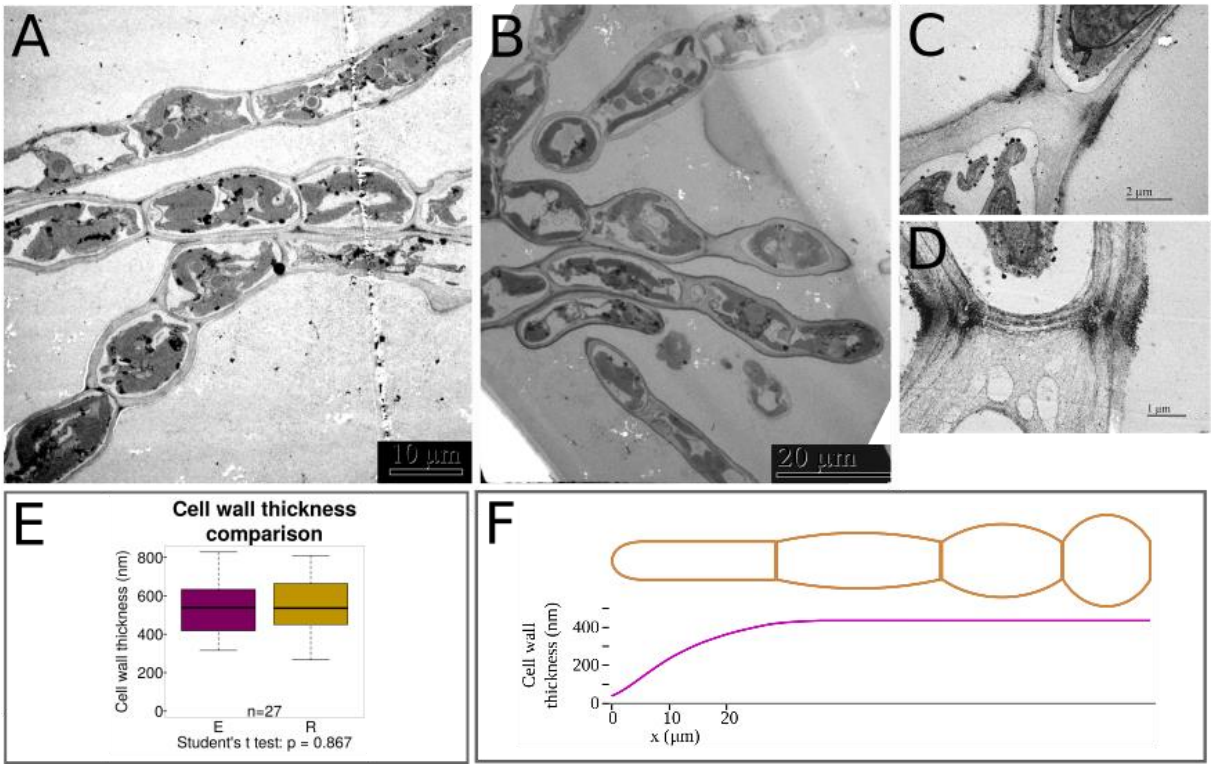

Figure 2.15 – Cell wall thickness and structure along the filament

A,B) TEM longitudinal section along the filament. A, E, I and R cell types can be seen with similar cell wall organisation and thickness. Comparisons between cell types should be made where cell wall is the thinnest, as askew section plans lead to thicker cell walls. Last panel shows close-up of transversal sections, displaying the presence of a specific layer surrounding it (asterisk). Scale is indicated in each photo. **C,D**) Transverse junctions, showing the cell wall layers as well as some dark material surrounding the junction, which nature is unknown.

E: Measurement of cell wall thickness in E and R cell types. Measurements were performed on TEM images on longitudinal sections. Sample size and Student t-test p-value are indicated.

F: Scheme summarizing the cell wall thickness along the filament.

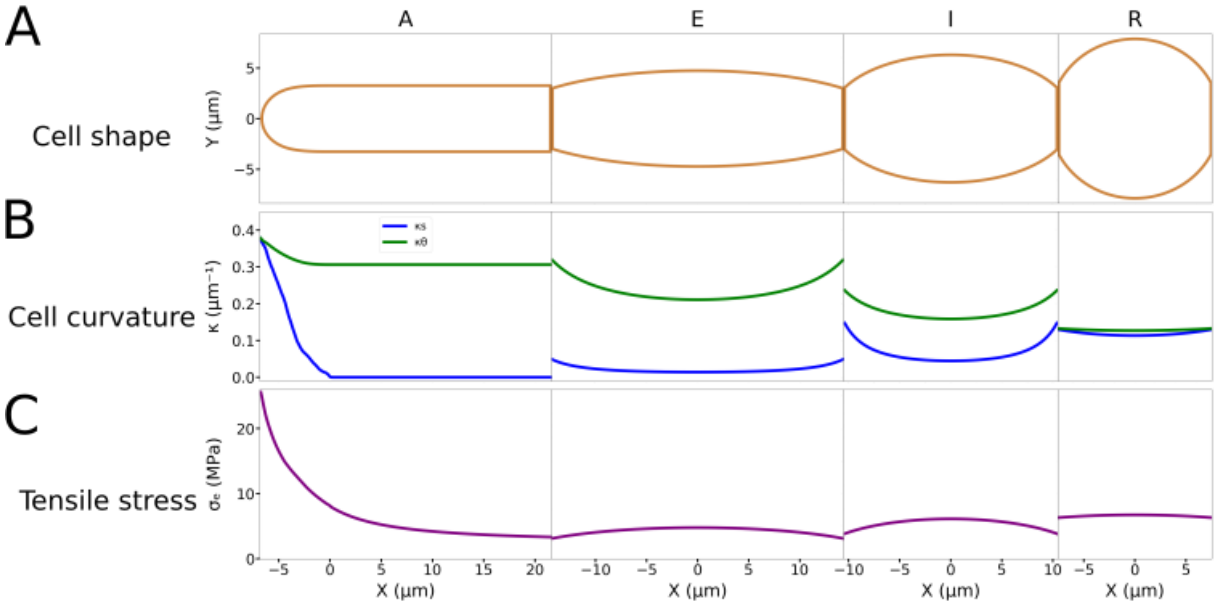

Figure 2.16 – Wall stress along the filament

A) Cell shape; **B**) Curvature profile along the filament. Curvature was calculated for two perpendicular directions: the meridional direction (blue) and the circumferential direction (green). **C**) Wall stress profile along the filament. Stress was calculated with the turgor measured by limit plasmolyse, and the cell wall thickness.

showed that turgor was similar in all cell types (data not shown, t-test, p-value = 0.407, see Material and Methods for details). We used these parameters, together with the curvature calculated for each cell type based on its average geometry (as shown in **Fig 2.14**) to calculate the wall stress (see explanation in Material & Methods). **Figure 2.16** shows that the highest wall stress is in the extreme tip of the A cell, where the cell wall is thin. Wall stress decreases in the shanks of the A cell and reaches a basal level also found close to the boundary of all the other cell types. However, as circumferential curvature decreases in the centre of the E and I cells because ellipsoid-like shape results in radius being slightly longer in the center of the cell (**Fig 2.16 B**, κ_θ, green line), stress slightly increases (σ_e, **Fig 2.16 C**). In R cells, the increase is emphasized. This pattern of stress reflects the pattern of alginate immunodetection: M-, M/G and G-rich blocks were present in the dome of apical cells, where the stress is very high, and MM and MG (and more rarely GG) were found in the shanks of R and to a lesser extent of I cells. Shanks of A cells and E cells were almost never labelled. Therefore, alginates could be involved in the response to wall stresses above a given threshold, here estimated to be ~ 5 MPa (**Fig 2.16 C**). In order to test this hypothesis, we cultivated the filaments in culture media with different osmolarities. First, a hypotonic solution corresponding to half-strength sea water (diluted twice with H_20, corresponding osmolarity of 550 mOsmol.L^{-1}) was used, into which Ectocarpus filaments were immersed for 24h before immunodetection with the three BAM antibodies. Results showed that labelling was altogether more intense than in the control experiment with normal sea water. With BAM6 (MM blocks), while a few cells retained labelling in the whole dome of A cells (**Fig 2.17 A**), most labelling was observed in the sub-apical cells, especially when the A cell burst in response to the hypo-osmotic shock (**Fig 2.17 B,C,D**). Labelling was then mainly at the external contour of the cells (**Fig 2.17 B,C**) but could also be observed at the junction between the A and the sub-apical cell (**Fig 2.17 D**) or even in more proximal junctions (**Fig 2.17 C**). Note that this sub-apical cell is rounder than the expected E cell, showing its swelling in response to the hypotonic shock. Therefore, once the A cells burst (usually immediately after immersion in this hypotonic solution), MM alginates started to over-accumulate in the cells the most exposed to an increased pressure, which is the sub-apical cell. Beside this main pattern, we could also observe a peculiar labelling in the shanks of I cells, like an elongated crown spanning a single, lateral side (**Fig 2.17 E**). This might also display areas physically weakened because of the osmotic shock. Some significant labelling was also observed in I and R cells (**Fig 2.17 F,G**) but not in E cells (**Fig 2.17 F**). Interestingly, in contrast to normal sea water, hypotonic conditions led to labelling of transversal junctions (**Fig 2.17 G**) and of several cell wall layers in R cells (**Fig 2.17 H**), as observed with BAM7 in normal sea water. In hypotonic conditions, BAM7 labelling also gave a different pattern than in sea water. It was overall weaker and concentrated on the apex, where, while only rare A cells retained labelling in the dome only (**Fig 2.17I**), the labelled area was usually extended to or exclusively in the shanks of A cells (**Fig 2.17J,K**) and of the sub-apical cells (**Fig 2.17 L,M**). In some cases, a labelled ring could be observed in more proximal positions, with no relation with the transverse cell wall (**Fig 2.17 M,N**). Labelling was weak and rare in the other cell types, with mainly some shanks of R cells (**Fig 2.17 O)** and some sleeve-patterns in the vicinity of transverse sections (**Fig 2.17 P**) but labelling of transverse sections per se displayed in NSW, could not be observed in these conditions. With BAM10, while labelling was again observed in the dome of some cells (**Fig 2.17 Q**), it was in most cases extended to a larger area, making a very marked sleeve in the sub-apical regions (**Fig 2.17 R,S**). Similarly, a ring was observed in the central part of the filaments, either at the position of transverse junctions (**Fig 2.17 T**) or not (**Fig 2.17 U**). In contrast to the NSW conditions, in hypotonic conditions the shanks of some I and R cells were also labelled (**Fig 2.17 V** and **W**

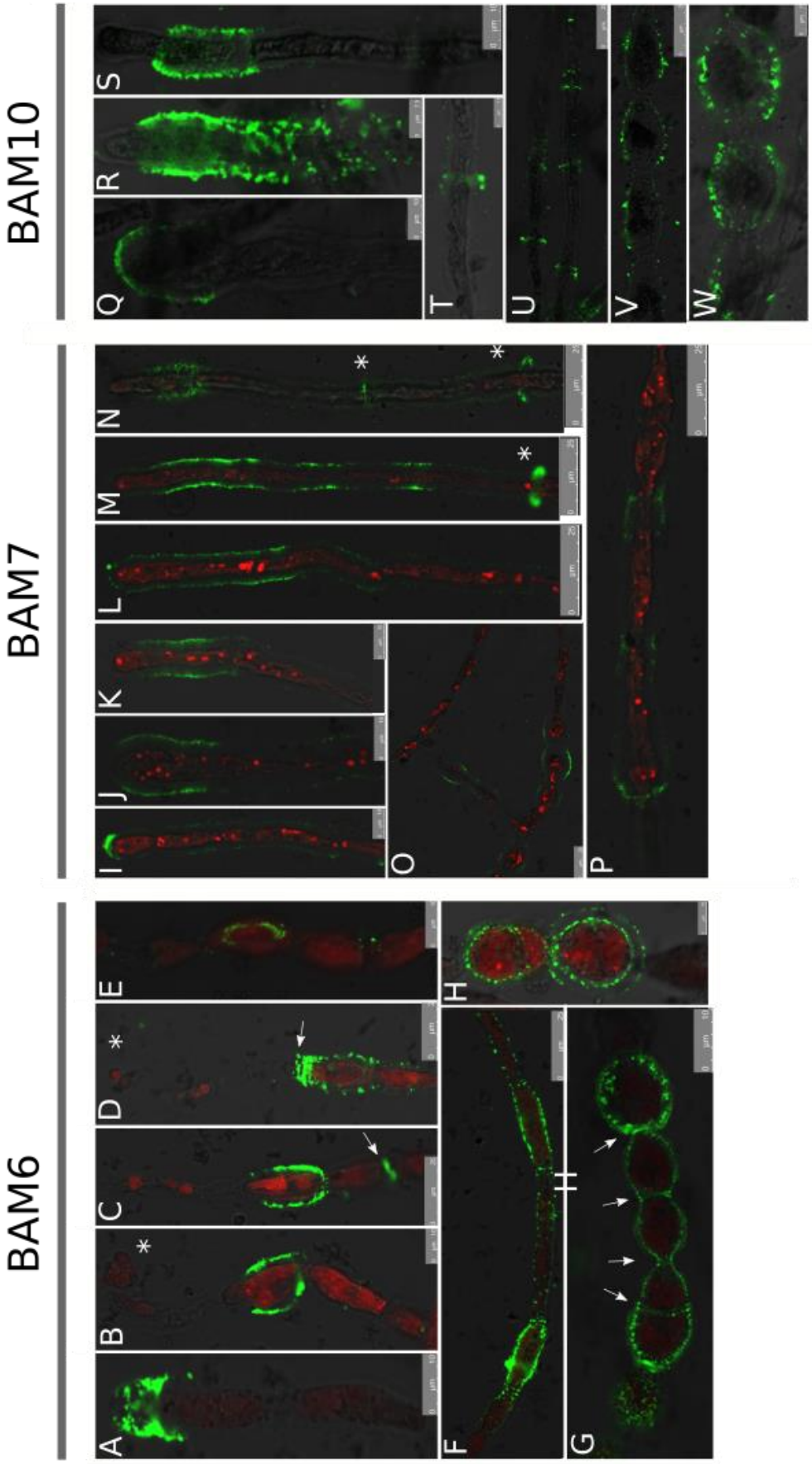

Figure 2.17 – Alginate location in response to a hypotonic shock *(caption on the next page)*

(Figure 2.17, *continued*) Filaments were immersed in a solution of sea water at 550 mOsmol.L^{-1}, corresponding to a 2 times dilution with fresh water. **A-H**: **BAM6 labelling**. **A,B,C,D**) Apex of filaments, showing either intact (**A**) or burst (**B,C,D**) A cells (asterisk: extruded chloroplast in burst A cells). **E**) Crown along I cells, also seen in E and R cells (not shown). **F**) Portion of filament, showing that wider, I cells are more labelled than E cells. **G**) Portion of filament showing R cells uniformly labelled, even at the transversal junctions (arrow). H) Close-up view showing different labelled cell wall layers. **I-P**: **BAM7 labelling**. **I,J,K**) Labelled apical cells. **L,M,N**) Filament extremities showing labelled apical and sub-apical cells as well as very discrete rings in E cells (asteriks). **O,P**) Centred part of filaments showing rare labelled locations either in the shanks of R cells (**O**) or in the vicinity of transverse junctions (**P**). **Q-W**: **BAM10 labelling**. **Q,R,S**: Apical cells. **T,U**: Portion of filament displaying E and I cells. **V,W**: Central portion of filament with R cells. White arrows show transversal junction/wall. Scales are indicated in each photo. Photos are merged confocal pictures taken with three channels: green; FITC; red: autofluorescence from the chloroplast; grey: several lasers to reflect bright-field photos.

respectively). However, no transverse boundaries between these cells were displayed, in contrast to the pattern observed in NSW.

In summary, all antibodies displayed a new labelling site in the shanks of A cells, or in sub-apical cells, especially when the A cell has burst, suggesting that alginates were overproduced at these locations to reinforce the overstressed cell wall due to the hypotonic treatment. Distinction between M-rich or G-rich alginates in these apical parts and in this condition could not be displayed. However, some differences were observed, especially at the transverse junctions, which BAM6 labelled while BAM7 and BAM10 did not, in contrast to the pattern that these two latter antibodies produced in NSW. Instead, some sleeve-pattern were newly observed, whose function is unknown but could as well be to locally reinforce the cell wall, as the crown pattern observed along E and I cells with BAM7 would do.

In order to confirm this pattern, we performed the opposite experiment. We immersed the filaments in a hypertonic solution (2000 mOsmol.L^{-1}) with an osmolarity about twice as low as that of NSW, and immunodetected the BAM epitopes after 24h. Labelling was weak with the three antibodies. With BAM6, apical labelling was almost completely abolished (a few cells were labelled, **Fig 2.18 A**). Weak labelling was also observed in transverse cell walls bordering mainly I and R cells (**Fig 2.18 B**) and on R cells, with more or less intense signals all around the cells (**Fig 2.18 C,D**). BAM7 labelled very weakly the apical cell, either at the tip (**Fig 2.18 E**) or over a larger region along the apical cell (**Fig 2.18 F,G**). Some transverse junctions were also labelled, with the double-ring characteristic of BAM7 observed in NSW (**Fig 2.18 H**). R cells were labelled mainly at these transverse junctions (**Fig 2.18 I**). The G-rich epitopes detected by BAM10 were visible only in very few A cells (**Fig 2.18 J**), and most often in transverse junctions, of both E and I cells (**Fig 2.18 K**) and R cells (**Fig 2.18 L**). Altogether, the three antibodies failed to produce much signal in the apical cells, the transverse junctions remaining the main site of recognition in hypertonic culture conditions.

When gathered, these data show an overall trend: the more stressed the region of the filament, the highest the content in alginates. Moreover, while some differences between BAM antibodies can be observed, the overall spatial pattern is very similar.

2.2.2.3. Alginates co-localise with stiff areas

The role of alginates in locations experiencing the highest stresses can be explained in two ways: the alginates are accumulated either to resist specifically to high wall stresses, or to soften the cell wall where cell growth occurs. In order to discriminate between these two hypotheses, we assessed the stiffness of the cell wall along the filament. Two techniques were employed. First, we assessed the propensity to cell wall expansion of E and R cells by measuring in living filaments the cell wall elasticity in the plane of the cell surface. In order to avoid a limitation of cell expansion due to the adhesion of the filament to the substratum, we used freely floating filaments for this experiment. The cell diameter in the centre of each cell (i.e. ~every 10-15 µm) was measured before (sea water = 1100 mOsm L^{-1}) and 1 min after immersion in fresh water (0 mOsm L^{-1}) resulting in cell swelling. The propensity to expand was then calculated as the percentage of the cell volume increase in response to the transition from sea water to fresh water. R cells increased their initial volume by 30% while E cells swelled by 42% (P value = 0.0106), meaning that in the in-plane axis, R cells are significantly stiffer than E cells (**Fig 2.19 A**).

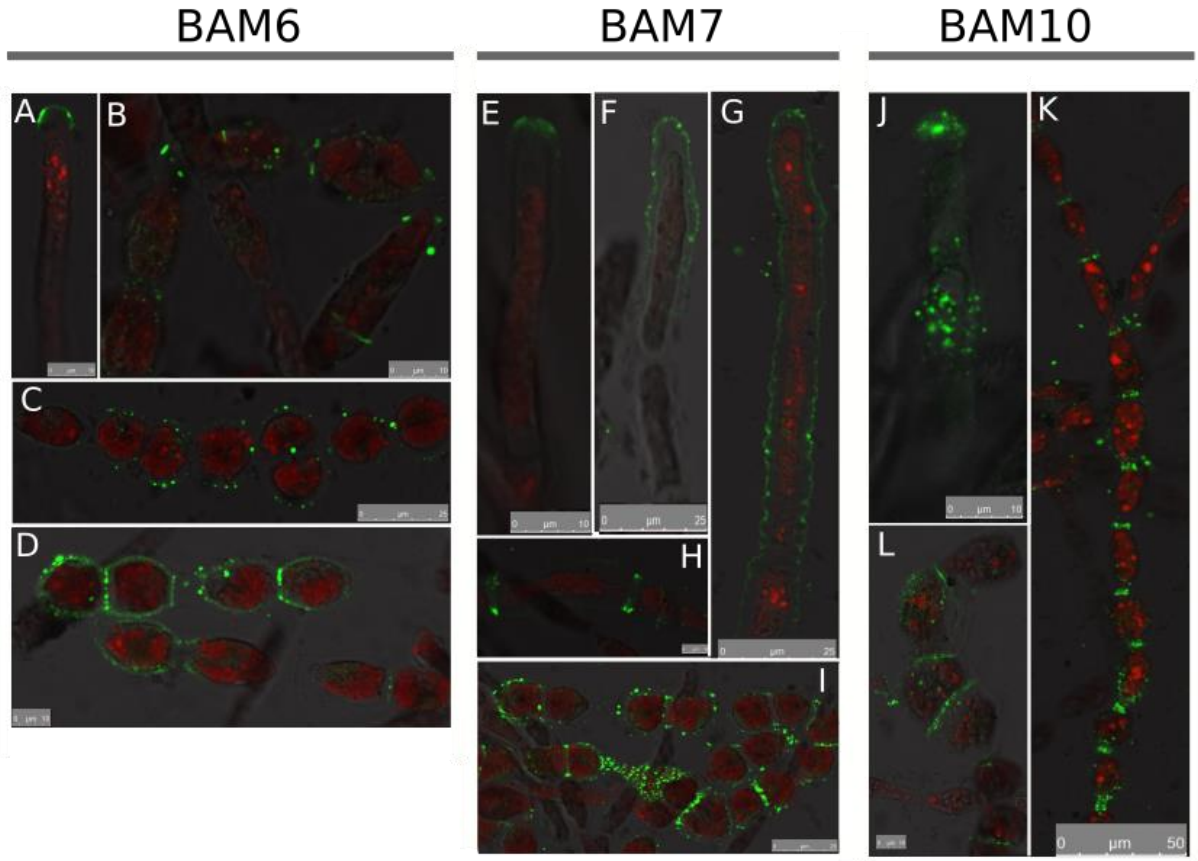

Figure 2.18 – Alginate location in response to a hypertonic shock

Filaments were immersed in a solution of sea water at 2000 mOsmol.L-1, which suppresses the cell turgor. **A-D**: Immunodetection with BAM6. **A**) Apical cell. **B**) I cells. **C,D**) R cells. E-I: Immunodetection with BAM7. **E,F,G**) Apical and sub-apical cells. H) One I cells bordered by its transverse junctions with adjacent **I** cells.) Group of R cells. **J-L**: Immunodetection with BAM10. **J**) Apical cell. **K**) Portion of filament showing a group of E and I cells. **L**) Group of R cells in the centre of a filament. The cell is the centre recently divided. Same confocal detection channels as in **Fig 2.17**. Scales are indicated on each photo.

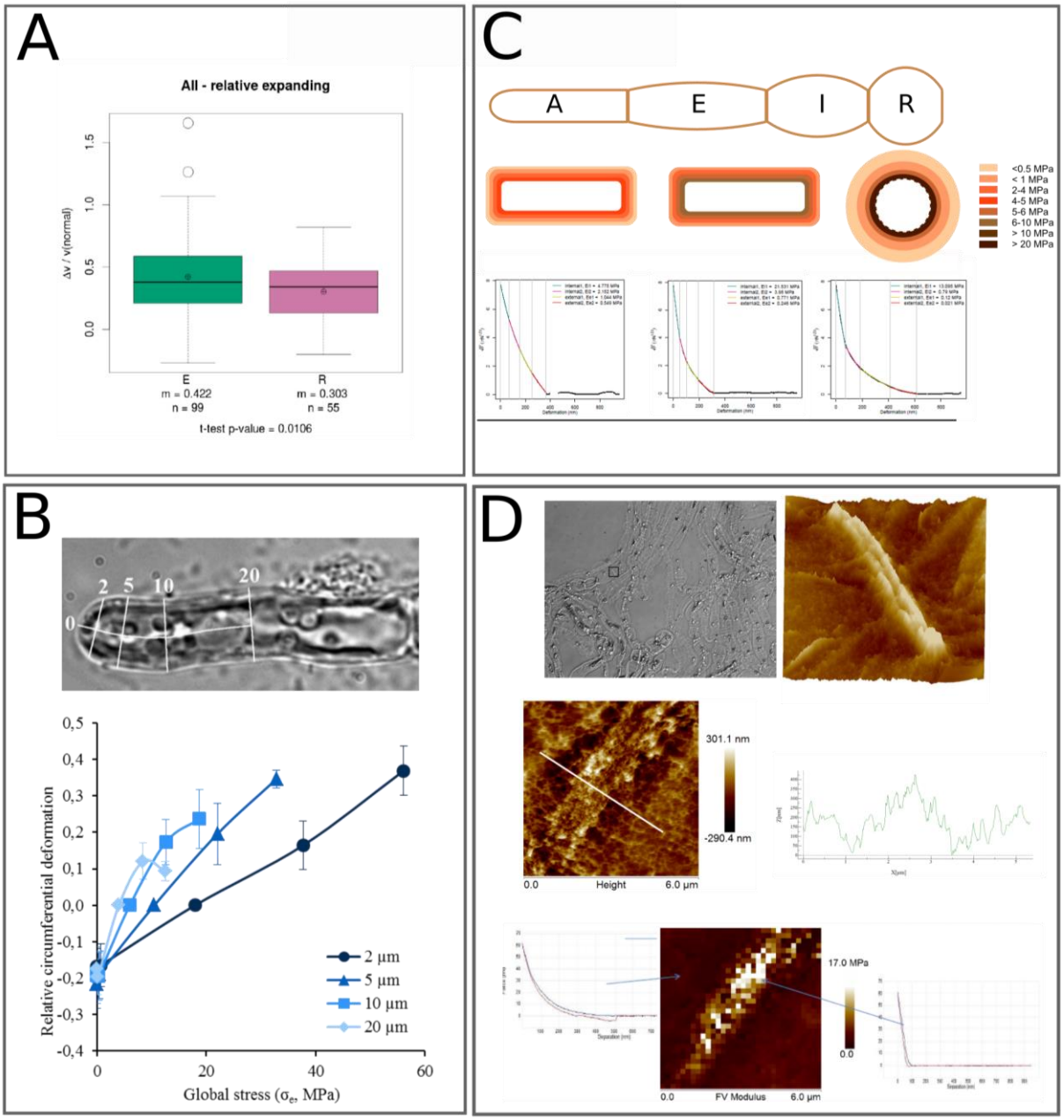

Figure 2.19 – Stiffness along the filament

A: Stiffness between E and R cells by dilatation/retraction
Plot represents the ratio of the difference of volume of E and R cells, observed in response to immersion into fresh water to the initial cell volume. Volumes were calculated from the cell dimensions, namely their length and width assuming that they are symmetrical. Measurements were carried out by ImageJ on bright field photos. Sample size (number of cells measured) is indicated below the box for each cell type.

B: Stiffness in the dome by dilatation/retractation
The circumferential deformation of *Ectocarpus* apical cells is plotted as a function of the distance from the tip. Cells were subjected to inflation or retraction by transfer into hypo- or hypertonic sea waters respectively. **Top**: Relative circumferential deformation was measured at 2, 5, 10 and 20 µm from the tip. **Bottom**: The deformation was plotted as a function of the local cell wall stress (σ_e) calculated at each position after the deformation was stabilized. The number of apical cells measured is indicated on the 2µm curve (mean +/- SD) and are the same for the other curves. Normal condition (sea water ~ 1000 mOsmol.L-1) is set to 0 (no deformation) for the 4 curves.

Figure 2.19 (continued)

C: Stiffness along the filament (between E and R cells) by nano-indentation using Atomic Force Microscopy
Top: Filament stereotype. Middle: Schemes representing the section of cell types with four virtual layers which thicknesses were inferred from the slope of the force curve. Colour stands for the Elastic Modulus calculated from the force curves, based on the Sneddon model. Bottom: Example of force curves for the different cell types. X-axis: distance of indentation (nm); Y-axis: force (nN).

D: Stiffness at transversal junctions by AFM
Top: (Left) DIC image of extracted cell walls from filaments (see mat meth). Transverse junction is framed. Topography image of the transverse junction between two R cells, showing the relief of the central structure (right). Middle: Topography image of a live cell surface at the junction. Height profile across the junction. Bottom. Corresponding elasticity map of 6 x 6 um area extracted from an array of 32x32 force curves. Force curves measured at the junction (right) and surrounding surface (left).

The mechanical properties of the dome of A cells were similarly measured. However, in order to obtain more detailed data for this particular area of the cell, the relative radial deformation was calculated at 2, 5, 10 and 20 µm from the tip, and two hypotonic (275 or 550 mOsm L^{-1}) and two hypertonic solutions (1900 or 2660 mOsm L^{-1}) were used. In parallel, the global in-plane wall stress (σ_e) of the cell wall before and after deformation was calculated according to (Dumais *et al.*, 2006). Strain curves plotted as a function of stress along the cell showed that the cell wall elasticity at 2 µm away from the tip was the lowest, while it increased gradually more distantly from the tip (10 and 20 µm positions; **Fig 2.19 B**). Therefore, these data display a negative gradient of circumferential deformability from the tip to the flanks of the A cell.

In a second step, atomic force microscopy (AFM) was used to assess the stiffness of the cell wall in a direction perpendicular (z-axis) to the axis of cell wall expansion during growth (x-y axes). Force curves were obtained in the centre of each cell type, from which the Elastic Modulus was calculated using a Sneddon model. Results showed differences between A and R cells. In A cells, the outer layer is stiffer than in R cells, but the inner is softer (**Fig 2.19 C**). This makes the stiffness of cell wall of A cells more homogeneous, with an average Elastic Modulus ~3 MPa (**Tab 1.1**). R cells displayed a heterogeneous cell wall stiffness, with a gradient ranging from < 1 MPa for the outer cell wall to ~20 MPa for the inner one. Measurements were performed in turgid cells, but as the turgor is similar in E cells and R cells, it cannot account for the difference in Elastic Modulus. Therefore, an increase in stiffness of the most recent, inner cell wall layer is observed from the apex to more central positions in the filament. Altogether, the cell wall seems to stiffen both in the in-plane axis and in the z-axis as cells maturate from A to R cells.

AFM was also used to focus on the boundaries between adjacent cells. In some places, scanning and measurement of the mechanical properties showed a peculiar stiff structure, potentially doubled, protruding from the cell surface (**Fig 2.19D**). This structure is reminiscent of the double-ring observed with BAM7 immunodetection (**Fig 2.12**).

Altogether, both cell wall extension and AFM showed that the cell regions immunolabelled by the BAM 6/7/10 antibodies are among the stiffest regions of the filament.

2.2.3. Discussion

2.2.3.1. Role of alginates in managing wall stress

In *Ectocarpus*, we showed that alginates co-localise with the stiffest sites at the surface of the filament, including the extreme tip of the apex, and most likely contribute to this stiffness: alginate digestion by alginate lyases promotes cell disruption. A role of alginate in brown algal tissue stiffness was suspected long time ago, because different compositions of alginates were extracted from tissue displaying different stiffness, like the stipe compared to the blade, or wave-exposed blades compared to sheltered ones (Haug *et al.*, 1974; Craigie *et al.*, 1984; Cheshire and Hallam, 1985; Kloareg and Quatrano, 1988; McKee *et al.*, 1992). The data were obtained from whole or portion of tissues, encompassing hundreds of cells. Here, we provide topological information at the cell level within a whole, yet architecturally simple, organism.

Both R cells and the dome of the A cells display the highest stiffness. While R cells are at least 4 days old in mature filament (1 cell division ~every 12 hours, several E and I cells are present ahead of the group of R cells), A cells are continuously growing and are very young cells. *Ectocarpus* sporophytes develop on solid substrates (rocks or epiphytically on other algal thalli). Rhizoids of *Fucus* (Order Fucales) and holdfast of kelp (Order Laminariales) have been shown to grow inside rocky microstructures in which they fill all the free space, providing solid attachment (Tovey and Moss, 1978; Forbes and Hallam, 1979). A stiffer cell wall at the apex of tip-growing rhizoids might thus be an advantage to withstand strong mechanical stresses due to compression and friction with such hard medium (Sanati Nezhad and Geitmann, 2013). Furthermore, brown macroalgae are subject to high variations of salinity during tides, impacting the turgor pressure, and extending the risk of tip bursting. An increased stiffness of the cell wall in the apex would prevent too large deformations and rupture in this position. In parallel, gradual softening of the cell wall on the shanks would allow it to remain deformable, maintaining the ability for the apical cell to balance turgor by volume change, as observed in the cell wall of sieve elements in kelp which can deflate in response to accidental drop on turgor (Knoblauch *et al.*, 2016).

An interesting structural feature of *Ectocarpus* filament was revealed during this study. SEM displayed some protruding surface at the junctions between cells. This structure was more frequently seen between two R cells. G-rich alginates specifically were abundant in the same location, making their involvement in its formation very likely. Longitudinal TEM sections supported this hypothesis, as electron-dense material observed in osmium-treated Ectocarpus sections was shown to be alginate (Terauchi *et al.*, 2016); TEM protocols were different though). AFM further displayed some very stiff junctions. Altogether, these data strongly suggest that alginates control the cell wall stiffness. However, a more robust correlation between the cell wall stiffness pattern and the alginate mapping must be established at lower scales in the future, using fine-mapping technique of cell wall deformation observed in living organism, as recently developed in *Ectocarpus* (Rabillé *et al.*, 2018*a*).

2.2.3.1. Do Mannuronates and Guluronate-rich alginates have different mechanical role in muro?

Alginates are an abundant class of components in the wall of brown algae (Kloareg and Quatrano, 1988; Deniaud-Bouët *et al.*, 2017). They have been shown to insure the structural integrity of the wall in *Ectocarpus* sporophytic cells (Terauchi *et al.*, 2016). This effect is supposed to be mediated by the cross-linking of GG-blocks by calcium ions (Ca^{2+}) forming the so-called “egg-boxes” junctions (Grant *et al.*, 1973; Ertesvåg, 2015). Indeed, it is a long-held opinion that GG-blocks of alginates provide most of the mechanical strength and rigidity of brown algal wall. At the thallus or organ level, some studies have observed a correlation between the apparent rigidity of the organ and the relative abundance of GG-blocks, generally quantified as the M/G ratio (Craigie *et al.*, 1984; Cheshire and Hallam, 1985). However, other studies observed no correlation between GG abundance and apparent organ rigidity (McKee *et al.*, 1992; Miller, 1996; Jothisaraswathi *et al.*, 2006). At the single cell level, a lower abundance of GG-alginate was detected in the terminal cells of *Adenocystis utricularis* (Ectocarpales), where most of growth occurs, and was supposed to give more “expandable” wall in these cells (Ponce *et al.*, 2007). In our own results, MM-digestion led to a lower rate of apex bursting compared to GG-digestion, but the effect was still significant. As the MM-,

Table 2.1 - Elastic Modulus E of the four virtual cell wall layers L_{1-4} inferred from the force curves obtained by atomic force microscopy.

Cell type	**A**				**E**				**I**				**R**			
Sample size	n=6 cells				n=7 cells				n=2 cells				n=4 cells			
E (MPa)	**L4**	**L3**	**L2**	**L1**	**L4**	**L3**	**L2**	**L1**	**L4**	**L3**	**L2**	**L1**	**L4**	**L3**	**L2**	**L1**
Mean	3,84	2,48	1,43	0,46	7,72	4,23	1,99	0,24	18,91	7,29	3,11	0,54	16,88	2,77	0,60	0,21
SD	0,54	0,24	0,36	0,35	2,33	1,19	0,75	0,17	4,12	1,47	2,05	0,10	4,81	1,54	0,34	0,13
Thickness (nm)	0-83	83-176	176-264	264-345	0-69	69-147	147-217	217-286	0-41	41-92	92-155	155-219	0-55	55-129	129-261	261-404

For each cell, the force curve was optimally cut into 4 linear parts. For each of the 4 cell wall layers, the mean (MPa) and SD are indicated, as well as the position (z-axis, or thickness) of the layer boundaries. L_1 is the most external layer (i.e. the oldest), L_4 the most internal one (i.e. the most recent).

MG- and GG-blocks are generally some tens of units long (Haug *et al.*, 1966), alginate chains are more probably made of a mixture of the three kinds of blocks, and thus they are very likely present in all alginate polymers of the cell wall. Interestingly, co-digestion of MM-block alginates and cellulose greatly enhanced apex bursting rate (to more than 50%), while co-digestion of GG-blocks alginates and cellulose did not increase bursting rate compared to single digestion of cellulose or GG-alginates alone (data not shown). This may be the sign of differential role for the two kinds of alginate homomeric blocks.

Immunofluorescence staining detected MM, MG and G enriched alginates in the apex of apical cells, suggesting that the growing wall is not associated with higher MG ratio. (Nagasato *et al.*, 2010) showed that alginates were delivered by flat cisternae, a vesicular body not well characterised so far, and shown to fuse with the plasma membrane. Alginates are thought to be deposited in the cell wall as pure MM-homopolymer (Madgwick *et al.*, 1973; Nyvall *et al.*, 2003) and further converted to some extent into G unit *in muro* by irreversible epimerisation of M units on the C5 carbon (Haug and Larsen, 1969*b*) by mannuronate-C5-epimerases (MC5E; (Nyvall *et al.*, 2003; Tonon *et al.*, 2008).

These enzymes would be delivered to the cell wall through similar or parallel routes as alginates, but their presence in brown algal cell wall has not been displayed yet. Although the MC5-epimerase activity has been detected in brown algal thalli (Madgwick *et al.*, 1973; Ishikawa and Nisizawa, 1981), it was not shown in which cell compartments this activity occurred. However, protoplasts of the brown alga *Laminaria digitata* were shown to excrete MC5E into the extracellular medium during the phase of wall-rebuilding, indicating that these enzymes probably act in the tissue apoplasts (Nyvall *et al.*, 2003). This hypothesis is supported by the recent genome-wide characterisation of the secretome of many brown algae, which identified MC5E as one of the major proteins secreted from *Ectocarpus* filaments, and even more significantly from *Saccharina* thalli (Terauchi *et al.*, 2017). Therefore, our results put in light of the previous studies support the idea that the formation of G units occurs concomitantly to the delivery of M units to the apex, most likely *in muro* within the new cell wall.

2.2.3.2. A role of alginate in the control of growth?

Alginates were immunodetected in positions where growth occurs, namely in the apex of apical cells and in the shanks of I cells, making cells become rounder (R cells). We also showed that the same positions were subject to the highest wall stress, and are therefore potentially involved in growth. However, growth can also be due to the softening of the cell wall, without any requirement for an increase in wall stress (see below).

In the expanding shanks of *Ectocarpus* “I” cells, discriminating between a role in growth and a role in the resistance to stress only is difficult until more morphometric and biophysical data are obtained. However, in the dome of the apical cells we recently showed that tip-growth relies on a gradient of wall stress along the cell, mediated by a gradient of cell wall thickness (Rabillé *et al.*, in revision). In this case, a role of alginates in the softening of the cell wall and thereby in the control of tip growth is not supported. First, on the one hand, the thinness of the cell wall at the tip of the dome (~ 40nm thick) makes the cell extremely prone to rupture. With such a thin cell wall, reinforcement of the cell wall by an increase of its stiffness would be expected in order to prevent tip bursting and to ensure maintenance of the cell integrity. We showed, using cell inflation/shrinking experiments, that this cell presents indeed a gradient of CW stiffness towards the tip. Strikingly, this pattern is the opposite of

what has been observed in other tip growing cells. In land plants (Geitmann and Parre, 2004; Parre and Geitmann, 2005*a*; Zerzour *et al.*, 2009) and in fungi (Ma *et al.*, 2005), the cell wall was shown to be softer in the dome than on the shanks, making cell wall growth possible where the wall stress is low. In the pollen tube, a stiffness gradient between the growing apical dome and the distal region of tubular shanks in the angiosperm pollen tube has been displayed using nano-indentation (Geitmann and Parre, 2004; Zerzour *et al.*, 2009; Chebli *et al.*, 2012). It was shown to be mainly controlled by a gradient of de-methylesterification of homogalacturonan (HG) from the apical dome and the shanks (Geitmann and Parre, 2004; Parre and Geitmann, 2005*a*). This chemical gradient is itself controlled by pollen-specific pectin-methylesterase (PMEs), which activity is tightly regulated par PME inhibitors (e.g. PMEI) and other chemicals factors (Bosch and Hepler, 2005; Bosch *et al.*, 2005; Parre and Geitmann, 2005*a*). Altogether, these factors maintain an extensible cell wall at the dome while rapidly strengthening the shanks to ensure transition to and maintenance of the tubular shape. In Va*ucheria terrestris, an* extensibility gradient was also found in the apical tip-growing part (Mine and Okuda, 2003). This gradient relies partly on the presence of uncharacterised structural proteins, which main role seems to strengthen and reduce the extensibility of the cell wall on the shank, preserving the tubular shape and restricting growth to the apex.

On the other hand, modeling of Ectocarpus tip growth based on the visco-plastic model developed by (Dumais *et al.*, 2006) supplied with biological parameters specific for the Ectocarpus apical cell (namely turgor, cell wall thickness and local curvature) did not support any requirement for a modification of the cell wall mechanical properties during growth (Rabillé *et al.*, in revision). In summary, if growth relied on the elasticity of the cell wall, a stiff cell wall would be an impediment for cell wall expansion. Therefore, dissociating the composition of alginates from the control on growth remains the soundest situation. Other cell wall components, like the fucans, could participate more significantly to this control, but the stiff, growing apex of Ectocarpus firmly rejects a role of this intrinsic mechanical properties in growth. Instead, cell wall remodelling, which factors are fully unknown in brown algae, sounds like a better suited mechanism for cell wall extension in this case.

Altogether, these results have important implications because the congruence between the chemical composition and the intrinsic mechanical properties was shown at the microscale level on an entire organism, which the filamentous, uniseriate body of Ectocarpus allows.

2.2.4. Materials and Methods

***Ectocarpus* culture.** *Ectocarpus sp.* Ec32 (CCAP accession 1310/4; origin San Juan de Marcona, Peru) was cultured *in vitro* as described in (Le Bail and Charrier, 2013). In brief, immature haploid parthenosporophytes containing no up-right filaments, were grown in half-strength, Provasoli-enriched autoclaved sea water (NSWp, pH8.7) in a controlled environment cabinet at 13°C with a 14h:10h light-dark cycle (light intensity 29 µmol photon.m^{-2}.s^{-1}). Culture medium was renewed every 10 days. For culture propagation, small tufts of filaments were transplanted and placed individually in new dishes. For immunolabeling experiments, deformability measurements and TEM observations, parthenosporophytes germinated on sterile glass coverslips or glass slides loaded in the bottom of Petri dishes. For the SEM experiments, sporophytes grew on a polycarbonate filtration membrane (nuclepore, diameter 13 mm, Cat N° 110406N, Whatman).

Immunolocalisation of alginates. Procedure for antibody production by rat immunization is described in (Torode *et al.*, 2016). Immunolabelling of *Ectocarpus* filaments was conducted according to a protocol first developed for *Fucus* embryos (Torode *et al.*, 2016). For each culture condition (Natural sea water, hypotonic and hypertonic media), experiment was performed on three cover slips covered by 2-week-old *Ectocarpus* prostrate filaments growing in separate Petri dishes. Cover slip with algal filaments adhering to it was quickly washed in NSW, and fixed as described in (Siméon *et al.*, 2018). Briefly, filaments were fixed in 8 % paraformaldehyde and 10 % glycerol in PBS:NSW 1:1 for 30 min at room temperature (RT). Filaments were then washed twice with NSW and twice with PBS (50 mM NaCl, 2.7 mM KCl, 10 mM Na_2HPO_4 and 1.8 mM KH_2PO_4) and then incubated overnight in 5 % milk protein in PBS (MP-PBS). They were then incubated with hybridoma supernatants containing the primary anti-alginate antibody diluted 10-fold in MP-PBS, for 1h at RT. Samples were then incubated 1h with the secondary antibody, an anti-rat IgG coupled to fluorescein isothiocyanate (FITC), diluted 100-fold in MP-PBS. Samples were mounted in PBS and a small drop of Citifluor (Agar Scientific). Observations of the FITC fluorescence were carried out using an TCS SP5 AOBS inverted confocal microscope (Leica). Monoclonal antibodies BAM6, BAM7 and BAM10 were used.

Measurement of cell wall circumferential deformability. Using ImageJ software, the longitudinal (axial) and circumferential deformations were measured from relative variation before and after the immersion of filaments in hypotonic media. It was performed both in the centre of E and R cells immersed in fresh water, and at 2, 5, 10 and 20 µm away from the tip in apical cells. Hypotonic or hypertonic shocks were induced by immersing the cultures (originally in articifial sea water at 1100 mOsm L^{-1}) in half-strength ASW diluted with deionized water (~550 mOsm L^{-1}) or 2660 mOsm L^{-1} (sea water saturated with sucrose), which led to complete cell plasmolysis. One minute after medium replacement, the cell inflation / shrinking ceased, and was recorded on the same cells. Images were acquired with the Leica Application Suite software (LAS v2.2.1, Leica) and measurements were carried out using the ImageJ software. The cell axial variation appeared to be negligible (~1 µm out of 25µm total length) and was not considered further. Consequently, the 4 positions in the apical cells were considered to be the same before and after the cell inflation/shrinking. The relative radial deformation $\Delta w/w=(w_f-w_i)/w_i$, with w_f and w_i the final and initial diameter, respectively, was measured and was plotted as a function of the corresponding stress value : $\Delta w/w = f(\sigma)$ (σ calculation detailed above). It was assimilated to a “stress-strain” curve allowing to quantify the elasticity of the cell wall.

For each condition, a batch of 3 to 16 apical cells per level of osmotic stress were recorded and measured. The means ± S.D. were calculated and tested by Welch-corrected t-Student tests.

Turgor assessments by limit plasmolysis. Technique used was previously described in details in Rabillé *et al.* (in revision). Briefly, it consists in immersing filaments in a series of media with different osmotic potentials, prepared from artificial seawater in increasing concentration of sucrose. Solution in which cells stop shrinking is considered the equilibrium between the external and internal concentration. Final internal concentration is calculated by taking into account the variation in cell volume due to the shrinking. N=9 independent experiments, with n> 15 cells for each tested solution. P value = 0.407.

Scanning Electronic Microscopy (SEM). SEM was performed as described in (Le Bail *et al.*, 2011). Briefly, Ectocarpus gametes were released and grew on a polycarbonate filtration membrane (Nuclepore, diameter 13 mm, Cat N° 110406N, Whatman). After two weeks of growth, parthenosporophytes were fixed in seawater with 3% paraformaldehyde for 1 h and then washed 10 min in ASW:H_2O (3:2), ASW:H_2O (2:3) and H_2O, followed by

successively dehydration steps in 30%, 50%, 70%, 90%, 2 times 95% and 3 times 100% EtOH. They were finally dried using a critical point dryer (Baltec CPD 030, Balzer), covered with a 25 nm thick gold layer and observed with a JEOL JSM 5200 scanning electron microscope.

Transmission Electronic Microscopy (TEM). Filaments were first fixed in 4 % glutaraldehyde in 0.2 M cacodylate and 0.25 M sucrose, for 1 night at 4°C. They were rinsed 10 min in 0.2 M cacodylate, 0.25 M sucrose and 0.225 M NaCl, 10 min in 0.2 M cacodylate, 0.15 M sucrose and 0.274 M NaCl, 10 min in 0.2 M cacodylate, 0.05 M sucrose and 0.325 M NaCl, and finally 10 min in 0.2 M cacodylate and 0.35 M NaCl, at RT. Filaments were then post-fixed in 1% OsO4 in 0.2 M cacodylate and 0.33 M NaCl, 1 h in dark. After rinsing 3x10 min in 0.2 M cacodylate in 0.35 M NaCl, filaments were dehydrated in an ethanol gradient: quickly in 30% EtOH, 50 % 10 min, 70 % 3x 10 min, 90 % 3x10 min and 100 % 3x10min. Filaments were embedded in Epon resin in BEEMS capsule, directly deposited upside-down upon the microscope slide. The resin was allowed to dry one night at 37 °C then one day at 60 °C. Following longitudinal sections were performed as described in Rabillé et al. (in revision).

Atomic force microscopy. Acquisition of force curves were carried out on Ectocarpus filaments growing on glass slides, immersed in a Petri dish filled with sea water. Force indentation curves were acquired using ScanAsyst fluid cantilevers (Bruker) with a spring constant of approximately 1.5 N/m. Cantilever was calibrated by measuring deflexion sensitivity and spring constant. The deflexion sensitivity was determined by recording a force curve on a hard surface (glass slide) in seawater. The spring constant was then measured using the thermal tune method in air, which consists in the determination of the resonance frequency of the cantilever. A maximum load of 60 nN was used. Cartographies of elasticity were obtained by fitting the curves with the Sneddon model. As curves can be far from linear, their elasticity should be described as a rather complex gradient within the cell wall width. To allow a simplified view prone to comparison, we split the cell wall into slices of virtually homogeneous stiffness. Technically, each curve $\sqrt{F} = f(\Delta z)$ was optimally adjusted using R (R Core Team, 2017) to 4 straight lines, from which extremal z values were considered as region boundaries. Local average stiffness (in MPa) for each region was estimated as the square of the slope. Topography images (transverse junctions) were acquired in vivo in seawater with a SNL10, 0.32, radius = 2nm.

Wall stress calculation. The A cell profile was taken from Rabillé et al. (in revision). E, I, and R cell were assumed to have truncated ellipsoid shapes, with extremal and central radius measured on micrographies. Meridional and circumferential stresses were respectively computed using the classical Hejnowicz formulae $\sigma_s = T/(2\ \delta\ \kappa_\theta)$ and $\sigma_\theta = T/(2\ \delta\ \kappa_\theta)\ (2 - \kappa_s/\kappa_\theta)$ where T stands for Turgor, δ is the cell wall thickness and κ_θ and κ_s are respectively the circumferential and meridional curvatures (Hejnowicz et al., 1977). The global stress was then computed as $\sigma_e = [\nu(\sigma_\theta - \sigma_s)^2+(1 -\nu)(\sigma_\theta^2 + \sigma_s^2)]1/2$ where $\nu = (1- \kappa_s/\kappa_\theta)/2$ is the flow coupling factor under the assumptions of the viscoplstic model (Dumais et al., 2006).

****

Acknowledgements: We thank Paul Knox for making the antibodies available. We thank Cécile Hervé for sharing expertise on the immunolocalisation protocol.

Contribution: H.R. and B.C. performed the immunolocalisation experiments. H.R. performed the cell deformation and tip bursting experiments. B.T. performed the AFM experiments and analysed the data together with B.B. B.B. calculated the wall stresses. A.L.B.

performed the SEM experiments. S.LP. performed the TEM experiments. H.R. and E.R. prepared the *Ectocarpus* cultures. T.T prepared the antibodies. T.T. and B.C. wrote the MS.

3. Molecular underpinning of apical cell tip-growth: the role of the (actin) cytoskeleton

3.1. Background

Z. Nehr, a former PhD student of the team (2010-2013), carried out the genetic characterisation of *etoile*, an *Ectocarpus* mutant selected from UV irradiation-mediated random mutagenesis, and impaired in tip growth (Le Bail et al., 2011). Using a positional cloning approach, she identified a plausible candidate gene coding for a Rho-GTPase-Activating-Protein (Rho-GAP) coupled to a membrane binding BAR domain (Nehr, 2013). Its predicted function is to inhibit the product of the unique Rho-GTPase encoding gene present in the genome of *Ectocarpus*. Rho-GAP proteins have been involved in tip-growth regulation in the pollen tube of terrestrial plants (Klahre and Kost, 2006; Kost, 2010). The importance of Rho-GTPases in controlling tip-growth via the regulation of the dynamics of AFs in the apical or sub-apical regions have been well demonstrated in land plants and fungi hyphal fungi (Gu *et al.*, 2003; Harris and Momany, 2004; Knechtle *et al.*, 2006; Craddock *et al.*, 2012). This regulatory pathways seems well conserved across the eukaryotic tree (Vaškovičová *et al.*, 2013). In fucoid embryo, positioning of the AFs apparatus and subsequent rhizoid germination is dependent on Rac1, a Rho-GTPases protein (Muzzy and Hable, 2013; Hable, 2014).

Beside the orientation given by the identity of the causal protein involved in *etl* phenotype, the cytoskeleton and its dynamics have long been known to be essential for the functioning of tip-growth in all groups studied so far (Torralba and Heath, 2001), including prokaryotes (Fuchino *et al.*, 2013). The roles of actin filaments (AFs) and microtubules (MTs) have been studied mostly in land plants (Vidali *et al.*, 2001; Smith, 2003; Mathur, 2005), fungi (Berepiki *et al.*, 2011; Riquelme and Sánchez-León, 2014) and oomycetes (Jackson and Heath, 1989, 1990, 1993*a*; Gupta and Heath, 1997; Ketelaar *et al.*, 2012). Their involvement in cellular growth and morphogenesis has also been unravelled in brown algae (Katsaros *et al.*, 2006), especially in the polarization and rhizoid emergence in fucoid embryos (Kropf *et al.*, 1989, 1998; Hable and Kropf, 1998; Pu *et al.*, 2000; Hable *et al.*, 2003; Corellou *et al.*, 2005). In all cases, AFs were shown to play a more important role in tip-growth compared to MTs, whose role appeared generally more indirect (Kropf *et al.*, 1998).

Therefore, in order to implement the model of tip-growth in *Ectocarpus* with cellular and molecular factors, we studied the organisation and the role of MTs and AFs in the apical cell of both WT and *etl* prostrate filaments.

3.2. Organization of the microtubules (MTs) in the apical cell

The protocol used to stain the microtubule was that used by Mermelstein et al. (1998) on *Euglena gracilis*, using the tubulin was detected with an anti-tubulin antibody generated in the rat (MCA-77G, Serotec), and stained with a secondary anti-rat antibody coupled to FITC. The results obtained were usually of poor quality compared to previous staining experiments on *Ectocarpus* (see for example, Katsaros, 1992; Godfroy et al., 2017). The signal was blurred by an excessive autofluorescence of cytoplasm, and positive staining only revealed small, weakly labelled filamentous structures (probably MTs), apparently dispersed randomly into the cytoplasm (**Fig 3.1**). The MTs often looked more or less fragmented, sometimes even reduced to small patches (**Fig 3.1**), probably because of adverse effects of the fixation on the cytoplasm. However, in elongated and apical cells the MTs showed a somewhat helical or longitudinal orientation and seemed more abundant in cortical regions of the cytoplasm (**Fig 3.1 B** and **C**), while they displayed a more random orientation in ellipsoid and round cells (I and R cell types, **Fig 3.1 A**) at the centre of prostrate filaments. No difference was observed between the WT and normally-shaped apical cells of *etl* (**Fig 3.1 D**). However, in the rounded apical cells in *etl*, the MT observed the same random orientation as in the central round cells of the WT. Similar labelling was observed in the WT apical cells displaying an abnormal, round phenotype (because of ageing for example). This could suggest that the organization of MTs is dependant on cell shape rather than being controlled directly by the Rho-GAP activity. Alternatively, it might reflect different expression levels of the mutation in apical cells, due to varying environmental cues or endogenous control of gene expression.

3.3. Role of the actin cytoskeleton in tip-growth of *Ectocarpus*

Beside their role in cell wall building through the control of cell trafficking and of ionic currents (Karyophyllis *et al.*, 2000*b*; Katsaros *et al.*, 2002, 2006; Nagasato and Motomura, 2009; Nagasato *et al.*, 2010), AFs were suggested to play also a mechanical role in brown algal cell morphogenesis (Bisgrove and Kropf, 2001; Bogaert et al., 2017a,b). This mechanical function in walled cells distinct from land plants is further supported by data obtained in oomycetes, a brother group of brown algae, in which cortical AFs were shown to contribute directly to a **mechanical reinforcement** of the cell boundaries (ensemble made of the cell wall, the cell membrane and the cortical cytoplasm) with therefore a possible impact on tip growth (Jackson and Heath, 1990, 1993; Gupta and Heath, 1997).

3.3.1. Organization of the actin in the apical cell

We studied the spatial organization of AFs in the apical cell of *Ectocarpus* by staining fixed material. Several protocols have been developed for other brown algae species, for

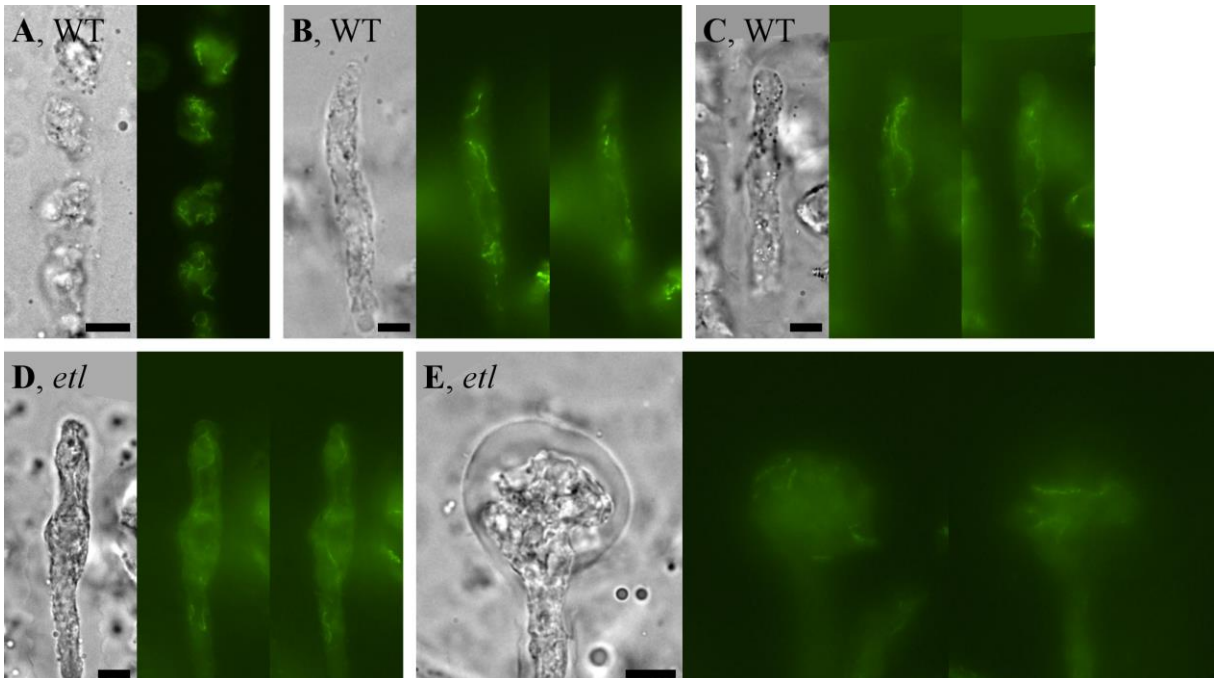

Figure 3.1 - Organization of microtubules in the apical cells of WT and *étoile*, revealed by immunofluorescence microscopy

The tubulin was detected with an anti-tubuline antibody. **A**: central, round cells of the WT showing randomly oriented MTs. **B** and **C**: WT apical cells showing helically or axially oriented MTs. **D**: a normally shaped apical cell of *etl* showing the same general orientation of MTs. **E**: an inflated apical cell of etl showing random orientation of MTs as in central, rounded cells. In each case, the left picture shows the bright-field picture of the cell, and at right several fluorescent image of the same cell taken in different focus plane. Scale bars: 5 µm.

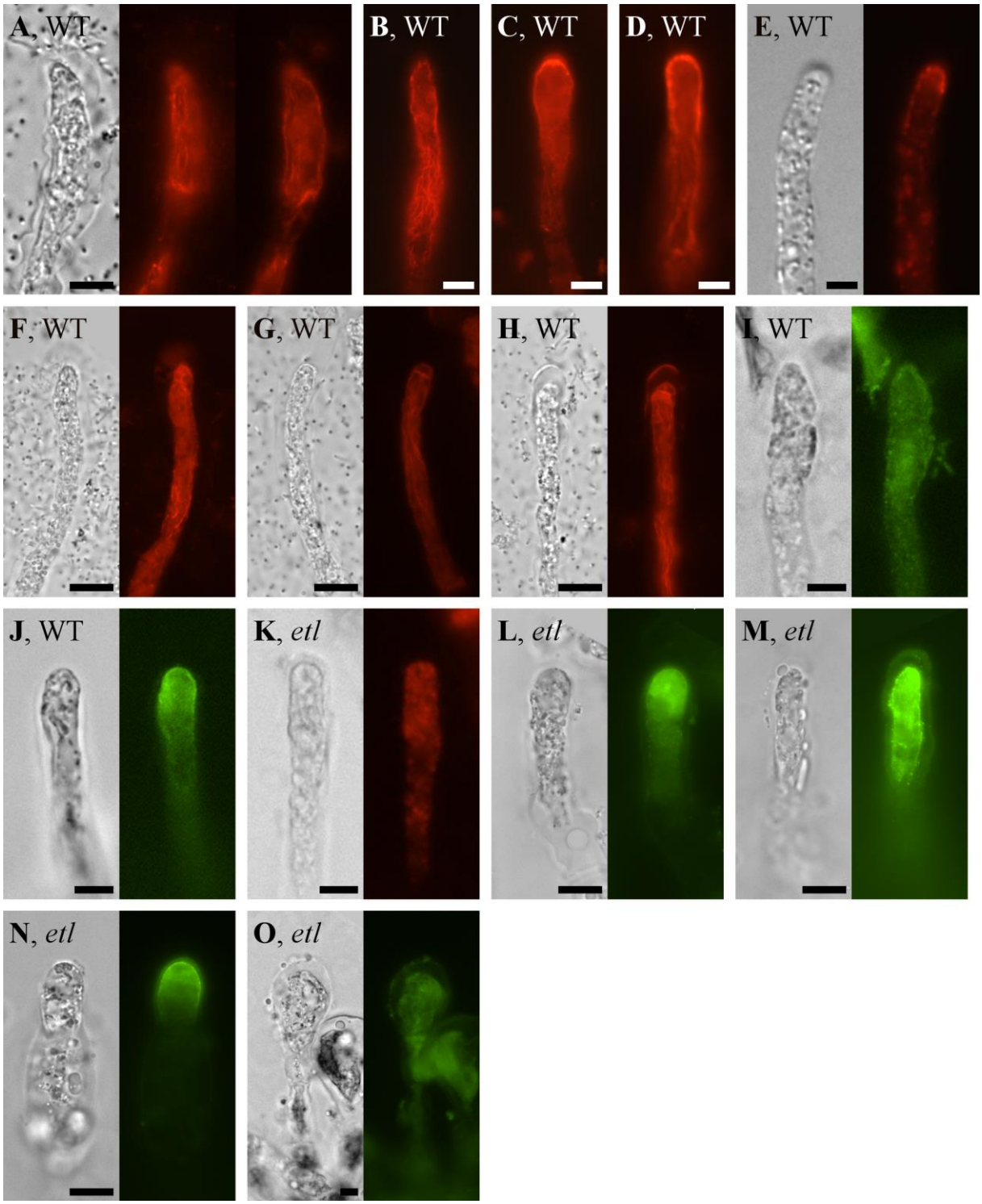

Figure 3.2 - Distribution and organization of the actin cytoskeleton in the apical cells of WT and *étoile*, revealed by (immuno)fluorescence microscopy

A to **H** and **K**: staining with AF568-Ph using the first protocol (Rabillé *et al.*, 2018). **I**, **J** and **L** to **O**: staining with the anti-actin antibody using the second protocol adapted from Mermelstein *et al.* (1998). **A**: a WT (WT) apical cell showing more or less longitudinally oriented actin cortical bundles in the shanks. Left: bf; center and right: corresponding fluorescent views, in a tangential and mid-plane focus plane, respectively. **B**: Another WT apical cell showing cortical bundles running up into the apical dome. **C** to **H**: other WT apical cells showing actin caps at their apex (see text for details). In **G** and **H**, the actin cap (arrow) is detached from the apical cell (…)

(Figure 3.2, *continued*) membrane (arrow head). In **H**, a staining is also observed at the apical cell wall (*), possibly some cortical cytoplasmic material that kept stuck to the wall (see text). **I** and **J**: WT apical cells stained with the anti-actin, showing numerous small "cortical "patch" of actin in **I** and a conspicuous apical actin cap in **J**. **K**: an *etl* apical cell showing no real staining with the AF568-Ph (red signal is only the autofluorescence of the cell). **L** and **M**. Normally shaped apical cells of *etl* showing a conspicuous actin cap at the apex. Note in **M** that the apical cap is greatly extended into the shanks. **N**: a slightly misshaped apical cell of *etl* (see the inflated shanks) still showing a clear actin cap at the apex. **O**: an inflated apical of *etl* showing a weaker, diffuse staining over the whole cytoplasm. Staining shown in B, C, D and E were made and acquired by C. Katsaros (Kapodistrian University of Athens, Greece) and are reproduced here with his kind authorization. Scale bars: 5 µm

example in *Sphacelaria* (Karyophyllis *et al.*, 2000*a,b*; Ouichou and Ducreux, 2000), in *Dictyota* (Katsaros *et al.*, 2002), in the gametophyte of *Macrocystis pyrifera* (Varvarigos *et al.*, 2004, 2007) and, obviously, in the fucoid embryos (Kropf *et al.*, 1989; Alessa and Kropf, 1999). During the current thesis project, the protocol applied on the three first species mentioned above have been adapted on *Ectocarpus* with the help of its inventor, the Pr. Christos Katsaros of the University of Athens. This protocol make use of the phalloidin-based probe, like the classic Rhodamine-Phalloidin, and is now published (Rabillé *et al.*, 2018). In our laboratory we used the AlexaFluor568-Phalloidin (AF568-Ph) as a probe. The advantage of this protocol is that phalloidin probes especially recognize the F-actin, unravelling the details of networks formed by these skeletal components.

In parallel, an alternative protocol based on Mermelstein et al. (1998) on *Euglena gracilis*, and using an anti-actin antibody, was tested together with Dr Adeel Nasir (Friedrich Alexander University of Erlangen-Nuremberg, Germany). Whether this antibody recognizes only the F-actin, or also G-actin is not clear.

3.3.1.1. Results obtained with the first protocol (AF568-Ph probe)

In all the cell types composing the prostrate filaments, an apparent random distribution of numerous thin cortical spots was observed, in addition to a weak, diffuse signal throughout the cytoplasm (**Fig. 17I**). In contrast to thick cortical bundles, a thin and dense cortical layer was clearly observed at the tip of most apical cells (**Fig 3.2 J**; **Fig 3.2 N**), with a tendency to extend in the sub-apical shanks of the apical cells. The actin cap always looked homogeneous, with no distinguishable filamentary structures. It might correspond to the same apical cap as observed on rare cells with the first protocol, but the occurrence of this cap is much more frequent here. The differences may be due to better preservation of this delicate structure with the second protocol, as the fixation of the material differs (see Rabillé *et al.*, 2018b for details about the experimental procedure). Interestingly, the same staining pattern was observed in *etl* (**Fig 3.2 L**), with the actin cap even present in apical cells that have slightly altered morphologies (**Fig 3.2 M**). The cap seemed more extended in the mutant compared to the WT (compare **Fig 3.2 N** and **J**). The apical cap was lost only in the most dramatically rounded apical cells, where it is replaced by a more diffuse, random staining that, nonetheless, remains higher compared to the other cell types (**Fig 3.2 O**). This indicates that the actin apical cap and its position are probably not dependent on the activity of ETL.

A summarized picture of the organization of actin and microtubule cytoskeleton in the apical cell of *Ectocarpus* sporophytic vegetative filaments is presented in **Fig 3.3**.

3.3.1.1. Results obtained with the second protocol (anti-actin antibody)

With the anti-actin antibody, a somewhat different pattern was obtained. A weak, diffuse staining of the cytoplasm in all the cell types composing the prostrate filaments was obtained; numerous thin cortical spots were also visible, with apparently random distribution (**Fig 3.2 I**). In contrast, thick cortical bundle was never observed with the antibody. However, a clear accumulation of actin was observed at the tip of most apical cells (**Fig 3.2 J**). This obvious structure is clearly made of a thin, dense cortical layer just below the plasma membrane (see **Fig 3.2 N**), and tend to extend in the sub-apical shanks of the apical cells. The actin cap

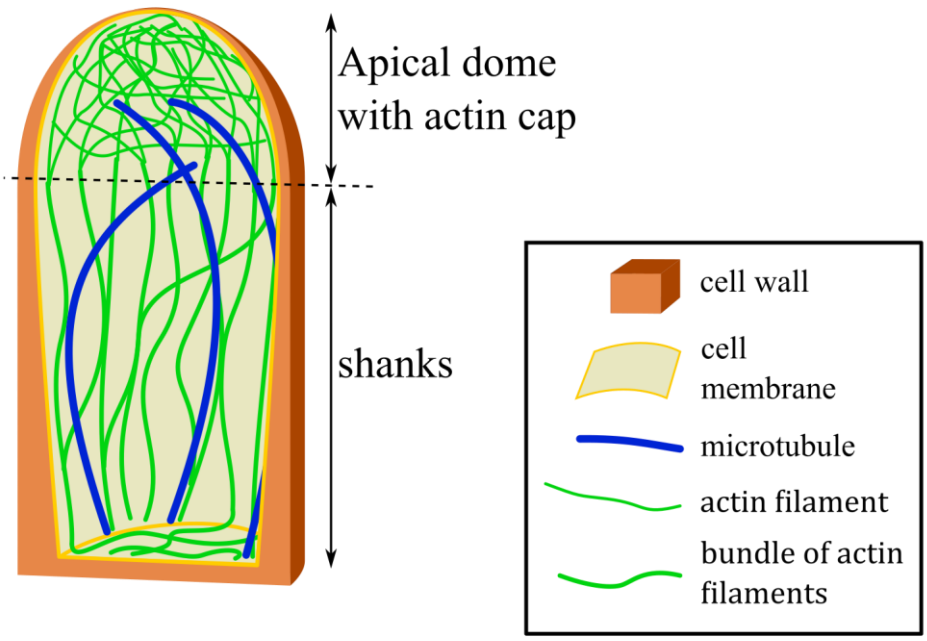

Figure 3.3 - Summary of the general organization of the actin and microtubule cytoskeleton in the *Ectocarpus* prostrate filaments of the apical cell

The general organization of the actin and microtubule cytoskeleton as observed during this thesis is sketched here. Note that the MTs probably radiate from a central centrosome next to the nucleus, as observed in other brown algal apical cells, but this has not been clearly seen in our experiments, probably because of the poor quality of the staining. The actin cap is represented as a dense meshwork of AFs radiating from the cortical actin bundle in the shanks, but such organisation is still hypothetical, as such details cannot be observed with this protocol.

always looked homogeneous, with no distinguishable filamentary structures so the exact configuration of AFs in this structure remains obscure. It is probable, though, that it corresponds to the same apical cap as observed in some apical cells with the first protocol (see above). However, the apical caps as observed with the second protocol are much more frequent than the caps observed with the first. This differences may be due to better preservation of this delicate structure with the second protocol. Interestingly, the same staining pattern was observed in *etl* (**Fig 3.2 L**), with the actin cap even present in apical cells that have slightly altered morphologies (**Fig 3.2 M**). The cap even seemed more extended in the mutant compared to the WT (compare **Fig 3.2 N** and **J**) but measures will have to be done for confirmation. The apical cap was lost only in the most dramatically rounded apical cells, where it is replaced by a more diffuse, random staining that, nonetheless, remains higher compared to other cell types (**Fig 3.2 O**). This indicate that the actin apical cap and its position are at least not dependent on the activity of ETL.

A summarized picture of the organization of actin and microtubule cytoskeleton in the apical cell of *Ectocarpus* sporophytic vegetative filaments is presented in **Fig 3.3**.

3.3.2. Impact of depolymerization of F-actin on apical cell organisation and growth

The impact of actin depolymerization was tested by subjecting *Ectocarpus* filaments to Latrunculin B (LatB), a drug derived from the sea sponge *Latrunculia magnifica* (Kasham *et al.*, 1981; Spector *et al.*, 1989), that is widely used to depolymerise AFs in many eukaryotes (Spector *et al.*, 1989; Gupta and Heath, 1997; Gibbon *et al.*, 1999; Morton *et al.*, 2000; Wakatsuki *et al.*, 2001; Chen *et al.*, 2007) including brown algae (Nagasato and Motomura, 2009).

3.3.2.1. Effect on apical growth rate and morphogenesis.

The efficiency of LatB was first verified on WT apical cells treated with 1 µM LatB for 48 h. Labelling using the AF568-Ph probe failed to display any AFs (**Fig 3.4**), supporting the fact that LatB efficiently depolymerizes AFs in Ectocarpus, at least within the first 48 hours.

Growth and morphogenesis was then investigated by time-lapse videomicroscopy on filaments growth between 5 to 7 days in normal culture medium complemented with 1 µM LatB (dissolved in 0.1% DMSO). The effect of the drug was dramatic, as tip-growth was fully stopped in less than 1 day. Instead, the apical region started to swell conspicuously, forming a large, spheroid bulge that seemed to inflate isotropically indefinitely over time (**Fig 3.5 A**). After several weeks, certain apical bulges became truly enormous in regard to the normal diameter of an apical cell (~6.5 µm), reaching an impressive diameter of 115 ± 21 µm (n = 9) after one month of culture with LatB. The surface of the tubular region, of the ellipsoid apical "bulge" and of the total cell were calculated over time and compared to the total surface gained in the control filaments grown in 0.1% DMSO during the same duration. After 48 h of treatment, the total cell surface expansion was significantly decreased in LatB-treated cells compared to DMSO-treated cells (**Fig 3.5 B**), but was still much above 0. Interestingly, the

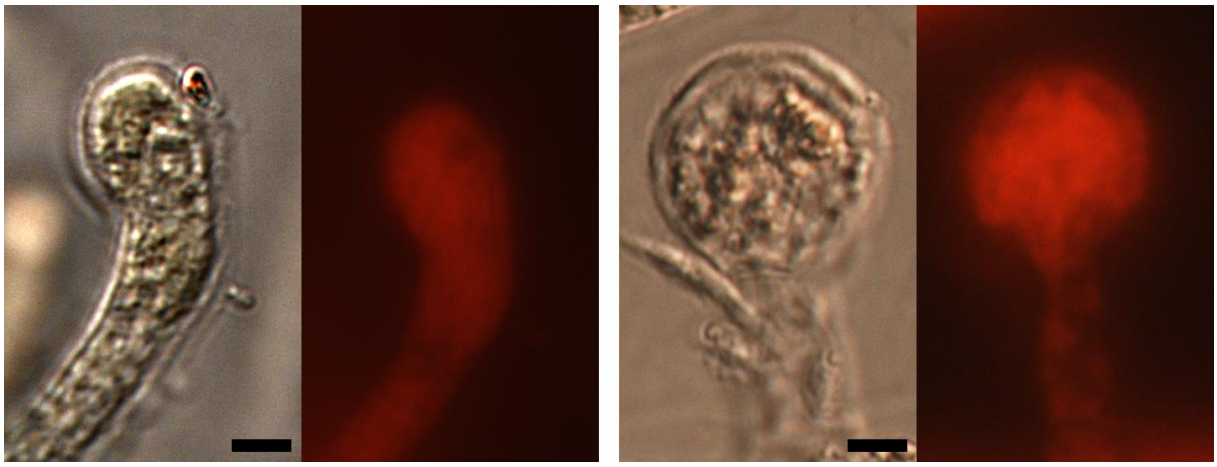

Figure 3.4 LatB effectively depolymerizes the AFs in the apical cells of *Ectocarpus* prostrate filaments

Two examples of WT apical cells treated for 48h with 1 μM LatB and then stained with AF568-Ph. For each, at left is the bright-field image and at right picture the corresponding fluorescence image. Note the swollen apical region. The treatment, staining and picture acquisition were made by C. Katsaros (Kapodistrian University of Athens, Greece) and are reproduced here with his kind authorization. Scale bars: 5 μm.

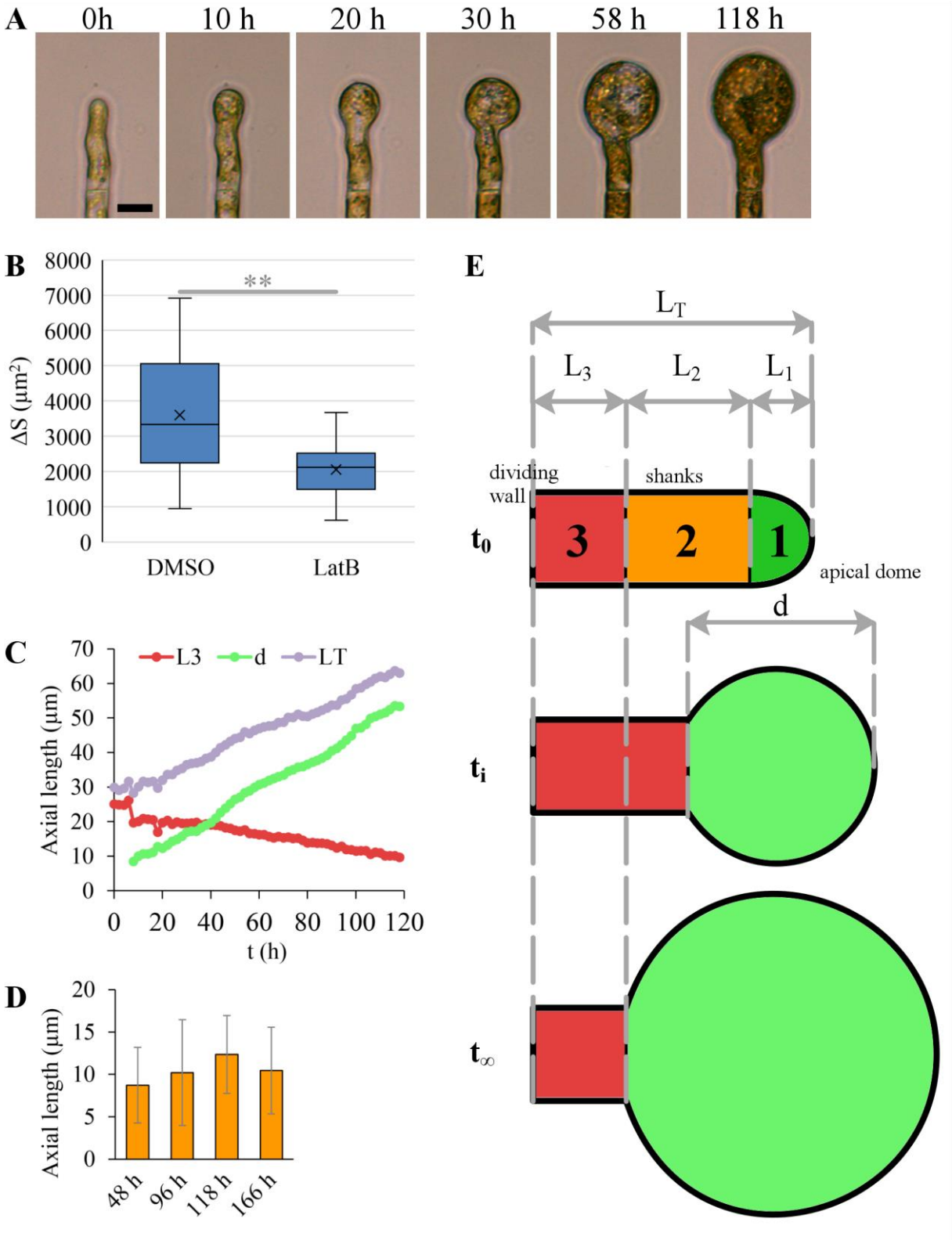

Figure 3.5 AF depolymerization of LatB abolish tip-growth but not surface expansion in apical cells, and zonal organization of the apical cells according to the dependence of the shape upon the presence of AFs

A: time series of a WT apical cells cultivated in presence of 1 µM LatB. Corresponding time after addition of the drug is indicated above each picture. Scale bar = 10 µm. **B**: total cell surface increase (*ΔS*) after 48 h of treatment, between apical cells treated with 0.1 % DMSO (control) and apical cells treated with 1 µM LatB. (…)

(Figure 3.5, *continued*) Vertical bars correspond to the standard deviation, while the lower and upper boundaries of boxes represent the first and third quartiles, respectively (n = 28 cells between each conditions). **: Welch-corrected t-Student test, $p < 0.001$. **C**: lengths of the tubular region (L_3), of the apical bulge (d) and of the whole cell (L_T) across time for an apical cell treated with LatB 1 µM. The drug was added at t = 0. **D**: Length of the initially tubular area that got incorporated into the apical bulge after 48 h, 96 h, 118 h and 166 h of treatment with 1 µM LatB. **E**: "zonation" of the apical cell into 3 sub-zone according to the dependence of the shape upon the presence of AFs. The zone 1 corresponds to the apical growing dome. The zone 2 corresponds to the sub-apical portion of the shanks which tubular shape is dependent on AFs, as measured in D. The zone 3 correspond to the part of that shanks which tubular shape is stable even in absence of AFs. The zone 2 and 3 are measured after the apical bulge stops to gain surfaces at the expanse of the tubular region of the cell, after enough time has run (t_∞). Pictures and measurements shown here were made from time-lapses done by C. Duchêne (host team intern student, 2015).

total surface expansion in LatB-treated cells appeared to result only from the surface expansion of the apical bulge, while the surface of the tubular region slowly decreased over time (n = 7 apical cells measured, not shown). This phenomenon was obvious when the length of the tubular region (L_3), the length of the apical bulge (d) and the total length of the cell (L_T) were plotted over time (see a particular case of one cell in **Fig 3.5 D**). Indeed, the expansion of the apical bulge occurred in part at the expense of a sub-apical portion of the shanks, whose tubular shape was lost and "reverted" to an ellipsoid one (defined as zone 2 in **Fig 3.5 E**). More distal regions seemed unable to revert, and conserved their cylindrical shape even after long treatments (**zone 3**). The apparent length (L_2) of this LatB-sensitive sub-apical region (**zone 2**), of axial length at t_n was calculated as $L_2 = L_{3(i)} - L_{3(n)}$, with $L_{3(i)}$ the initial length of the cylindrical shank of the cell and $L_{3(n)}$ the length of the remaining tubular region at t_n. Values of L_2 measured after 48, 96, 118 and 166 h after the beginning of LatB treatment are shown in **Fig 3.5 E**. They demonstrate that L_2 progressively increases over time but finally stagnates up to a maximum value of 12.35 ± 4.59 µm after 118 h of treatment (n = 26 cells), and thus that zone 2 has a limited size. The apical dome (**zone 1**) and **zone 2** would then correspond to an apical region of maximum 17.10 ± 4.71 µm in length, which shape would be strongly dependent on a functional actin cytoskeleton, compared to a more distal region (**zone 3**) which shape is stable (**Fig 3.5 C**). The progressive shape reversion suggests a progressive dependence upon AFs cytoskeleton in this region, to be linked to the gradient of wall thickness along the shanks (see **Paper 1**, **Part 1.2** in this report; discussed in Part IV-Discussion). These striking results provide important insight into the role of the actin cytoskeleton in *Ectocarpus* tip-growth, showing that AFs are both important for the positioning of wall expansion and the establishment and maintenance of the cylindrical shanks.

3.3.2.2. Effect on apical cell wall deformability.

The results obtained above support that AFs directly contribute to the mechanical properties of the cellular envelope. If true, then AFs depolymerisation would reduce the mechanical strength of the apical wall, thus increasing its deformability. We thus investigated the short-term impact of LatB treatment on the apparent circumferential deformability of the wall at 2, 5, 10 and 20 µm from the extreme tip of the apical cells, using the technique of cell inflation induced by hypotonic shocks described in the **Part 2**. Half-strength NSW (~550 mOsm L^{-1}) were used as the hypotonic medium. The measurements were made on apical cells treated with 1 µM LatB for 19h, or 3 µM LatB for 2h, in order to test the "immediate" effect of total and rapid AFs removal on wall mechanics, before the onset of wall "bulging". However, sign of apex bulging was already evident as early as 2 h of treatment (not shown), making uncertain the temporal relationship between the observed modifications of wall mechanics and morphological changes. This, however, indicates that the action of the drug is very rapid.

The circumferential deformability of apical cells in response to hypotonic shocks was compared to control cells treated with DMSO for one day. These cells showed a significant decrease of wall deformability at 2 and 5 µm from the tip compared to untreated cells (t-test, $p < 0.05$, **Fig 3.6**), showing that DMSO does impact the wall deformability, at least in the apical region. Indeed, when compared to DMSO-treated cells, cells treated with 3 µM of LatB **for 2 h** did not show significant differences in deformability whatever the position, indicating that the observed short-term effect may be due to the DMSO rather than to the degradation of the

AFs. In contrast, after 1 µM LatB treatment for 19 h, the circumferential deformability appeared significantly decreased at 5 µm (t-test, $p < 0.01$) and 10 and 20 µm from the tip ($p < 0.05$) compared to DMSO-treated control cells (**Fig 3.6**).

Therefore, AFs control the wall deformability. However, considering the time required for detecting any significant impact, this control might be indirect, and be mediated by wall deposition and building processes (see below). Nevertheless, when put together with the data shown in the previous section, these results strongly demonstrate that intrinsic wall stiffness is uncoupled from cell wall extensibility (see **Part 2** and the **Opinion paper** in **Part 1.3**), which is a key knowledge in the context of the understanding of biophysical mechanisms controlling cell wall growth.

3.3.2.3. Effect on the mechanical strength of the apical cell wall

During the apical cell inflation experiments on LatB–treated apical cells described above (see **Fig 3.6**), the hypotonic shocks induced the bursting of 23 % of cells treated with 3 µM LatB for 2h (n = 21), and of 50 % of cells treated with 1 µM LatB for 19h (n = 18). This phenomenon was also repeatedly observed in time-lapse experiments of filament growth in presence of LatB, although the cells were kept in full strength sea water (not shown). Consequently, while the wall become stiffer in the apical bulge (see above), the wall mechanical resistance appears lowered, indicating that these two wall parameters are uncoupled.

The direct involvement of AFs in the mechanical strength of the wall was tested by observing the impact of very short LatB treatments using the same “apex bursting experiment” as described earlier in this report (see **Chap. II**., **article 2**). In response to 3 µM LatB for 10min, 47 (±3.53) % of apical cells burst (0 % in the control). Beyond the rapidity of the drug effect, this result displays that the apical wall strength relies directly on AFs, most likely through the apical cap labelled with the actin antibody. This is reminiscent of what have been observed in the oomycetes *Saprolegnia ferax* (Jackson and Heath, 1990).

3.3.2.4. Effect on cell wall structure and cellulose content

The impact of AFs disorganisation on wall building was investigated by TEM on filaments incubated 1 week in 1 µM LatB. Pictures showed that the cytoplasm was highly disorganised, with large area of electron-lucent material (**Fig 3.7 B** to **E**). The wall structure was also slightly altered in the region of the “apical bulge”. The normal apico-basal thickness gradient was lost; instead, the characteristic internal wall layer (as observed in control cells treated with 0.1% DMSO for the same period, **Fig 3.7 A**) appeared expanded (**Fig 3.7 B**). The outer grey, denser fibrillary layer of the wall seemed unaffected, yet sometimes more expanded and “fluffier” compared to control. The total wall thickness was irregular, because the internal layer was not evenly distributed, with scarce wall material at some places and “bumps” in other places. The internal face of the cell wall was often lined with numerous large vesicles, and the boundary between the cytoplasm and the cell wall was sometimes blurred and difficult to distinguish (**Fig 3.7 E**). This wall thickening in LatB-treated cells may actually be responsible for the decrease in wall deformability described above. Indeed, for a constant turgor, a thicker wall corresponds to a lower tensile stress. Thus, in response to a

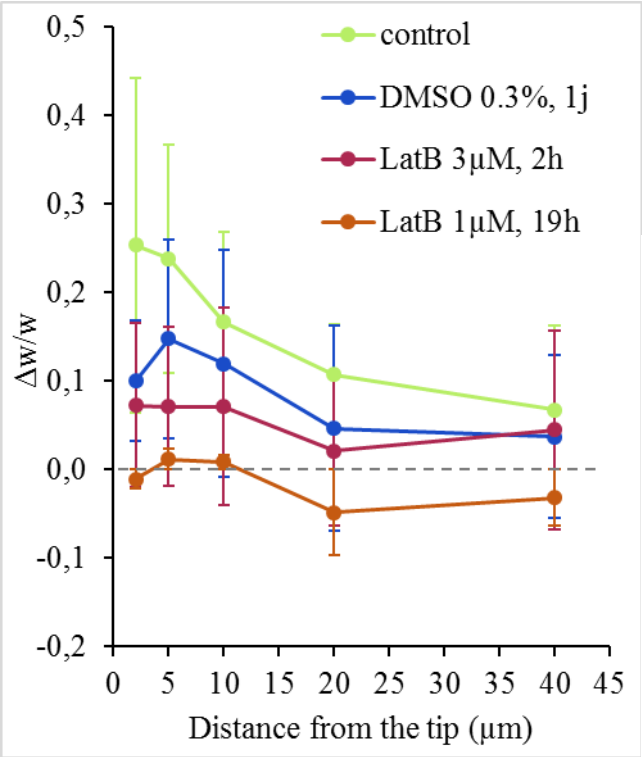

Fig. 3.6 AF depolymerization by LatB reduces cell wall deformability after ~19h of treatment

Apical cell deformability was measured by cell inflation experiments induced by hypotonic shocks. The cell diameter (*w*) at 2, 5, 10, 20 and 40 µm from the extreme tip was measured and the relative circumferential deformability (*Δw/w*) was calculated at each of these positions. The diagram represents *Δw/w* as a function of the axial distance from the tip for each condition. In all cases, algae were cultivated in NSWp in presence of the drug. Data are mean ± standard deviations (n = 11 for untreated cells, 21 for DMSO-treated cells, 16 for cells treated with 3 µM LatB for 2h and 9 for cells treated with 1 µM for 1 h). See the main text for the statistical analysis of these data.

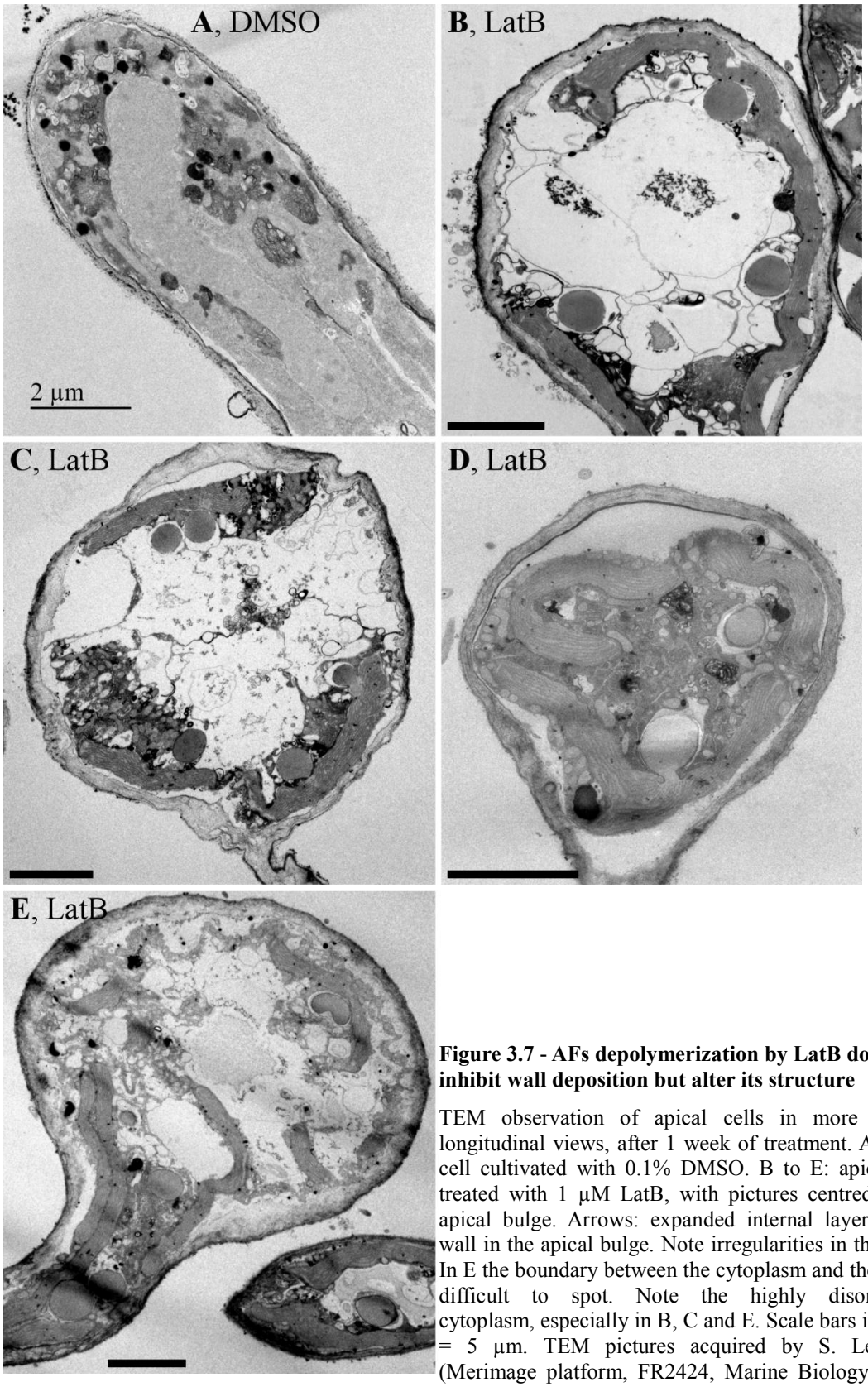

Figure 3.7 - AFs depolymerization by LatB does not inhibit wall deposition but alter its structure

TEM observation of apical cells in more or less longitudinal views, after 1 week of treatment. A: apical cell cultivated with 0.1% DMSO. B to E: apical cells treated with 1 µM LatB, with pictures centred on the apical bulge. Arrows: expanded internal layer of cell wall in the apical bulge. Note irregularities in thickness. In E the boundary between the cytoplasm and the wall is difficult to spot. Note the highly disorganized cytoplasm, especially in B, C and E. Scale bars in B to E = 5 µm. TEM pictures acquired by S. Le Panse (Merimage platform, FR2424, Marine Biology Station

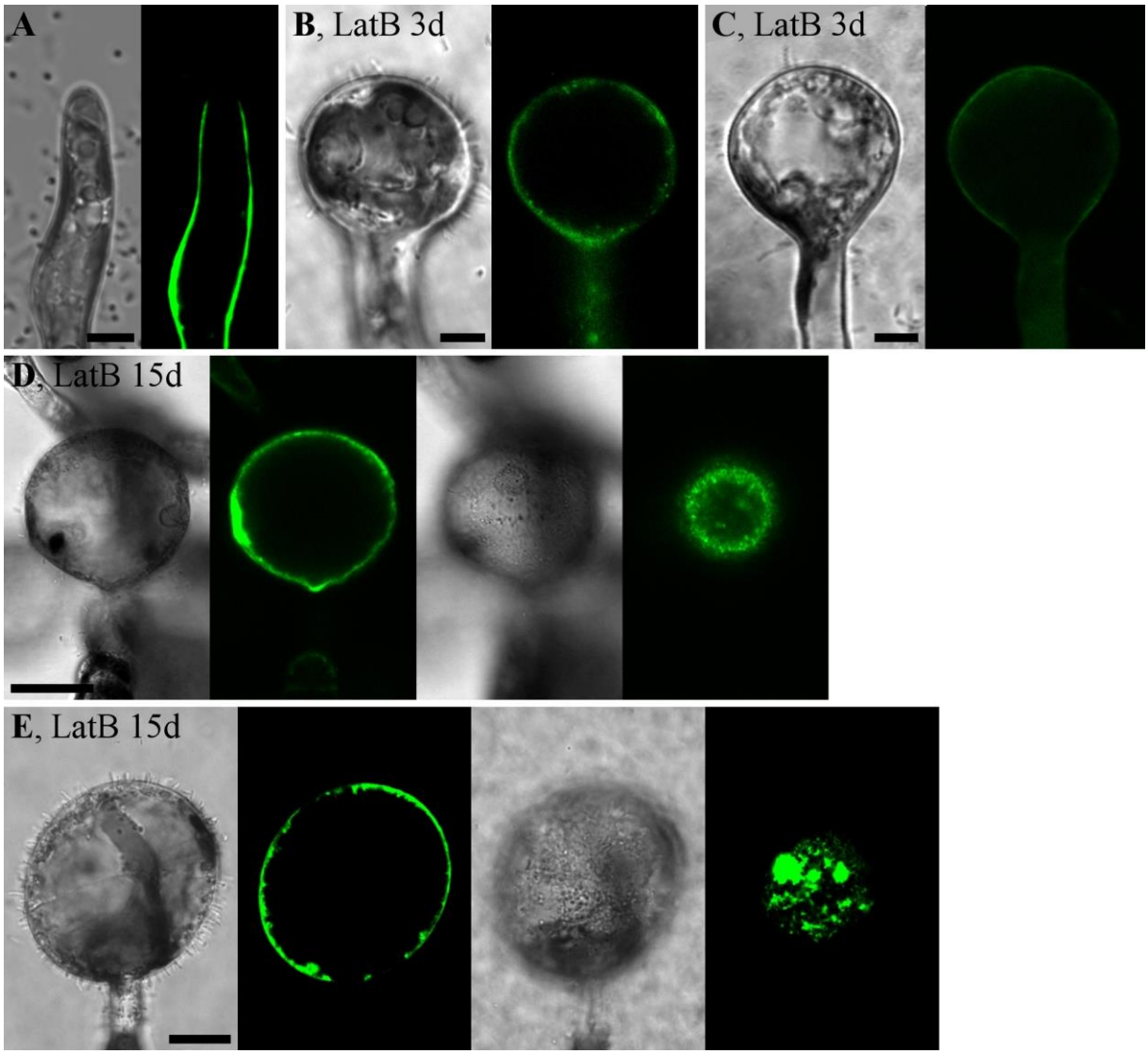

Figure 3.8 AFs depolymerization by LatB enhances cellulose deposition in the wall of the apical cell

Living cells stained with 0.003 % Calcofluor for 30 min in the culture medium. **A**: an untreated apical cell (cultivated in NSWp only). Scale bar = 5 µm. **B** and **C**: apical cells treated with 1 µM LatB for 3 days. Scale bars = 5 µm. **D** and **E**: apical cells treated for 15 days. For these two examples, a mid-plane view (left) and a tangential (right) views are shown in parallel. Note the bright patches of calcofluor staining, more evident in tangential views, denoting possible local accumulation of cellulosic material in the wall. Scale bars = 20 µm.

same hypotonic shock, the wall would expand less compared to the control because of the lower degree of stress surge.

The cellulose composition of cells treated with 1µM LatB for 3 or 15 days was assessed in living cells stained with the calcofluor-white and observed in confocal microscopy. Results showed that, contrary to the untreated apical cells (**Fig 3.8 A**), the cell wall of LatB-treated cells was enriched in cellulose in the apical bulge, already 3 days after the drug supply (**Fig 3.8 B** and **C**). Sometimes, the cellulose accumulation seemed more important in the proximal-most hemisphere of the apical bulge, but this should be verified by rigorous fluorescence quantification. In latter stage, the cellulose staining appeared more and more heterogeneous, with some intensely stained spots separated by fainter areas (**Fig 3.8 D** and **E**). For cells treated for more than 15 days, the staining appeared extremely "rugged" (**Fig 3.8 E**). However, this might be due to the progressive degradation of the wall by the numerous bacteria that systematically developed on the surface of LatB-treated *Ectocarpus* cells in absence of appropriate antibiotics in the culture medium (**Fig 3.8 D** and **E**). This extra cellulosic material might correspond to the enlarged inner wall layer observed by TEM, and the isolated "patches" of cellulose observed by Calcofluor staining may correspond to the large "bumps" of this layer. This hypothesis should be verified by immunolabelling of cellulose on TEM ultrathin sections in the future.

Overall, these results clearly demonstrate that AFs are not required to drive the deposition of cellulose into the wall. However, in their absence the deposition of cellulose seems chaotic, suggesting that AFs are required for the proper and even deposition of cellulose in the wall, as observed in normal cells.

3.4. Conclusion on the role of the cytoskeleton and its dependence on the gene *ETOILE*.

Two main structures formed by AFs in the apical cell have been revealed with our staining experiment: i) a cortical network of thick, reticulated AF bundle in the tubular shank, only revealed with the first protocol, and ii) an apical cap, easily observed with the second protocol. However, because this apical cap is not always visible, it could be a labile structure that would form and disaggregate repeatedly during growth. As we only stained fixed material, we cannot know whether it is connected to a particular state or rate of cell growth. An important result here is that the actin cap is still present in *étoile*, both in apical cells which maintained some shape polarity and in apical cells more altered morphologically, suggesting that the formation of this structure is not directly dependent on the regulatory pathway controlled by ETOILE. Reciprocally, the isotropic shape observed in the mutant does not seem to depend on the capacity to establish this actin cap. By contrast, the thick cortical bundles have not been detected in the mutant. If confirmed, this would imply that the tubular shape is stabilised by these structural elements, so that their absence in the mutant results in a reversion from the tubular shape to the spheroid shape, at least in a region of the shank which is still susceptible to such change.

4. General discussion and perspectives

During this thesis project, we built the first integrated mechanical model of tip-growth for a brown alga. Using this model, we unravelled an alternative and original mechanical principle involved in a tightly regulated gradient of cell wall thickness. This finding has important implications for the evolution of tip-growth in distantly related groups, and for the general understanding of the cellular developmental pathways that have emerged in the brown algal lineage.

In an integrated approach, we tried to unravel some of the cellular and molecular factors that control tip-growth, especially in relation with the biophysical mechanisms at play in the process. Although several parameters have tentatively been modified by various experimental approaches, our data contributed to the understanding of the role played by main factors: i) the **cell wall**: its mechanical properties and chemical composition, and their respective link to the process of the growth, and ii) the **actin cytoskeleton**, that proved essential for the functioning of tip-growth.

The discussion below is organised following the structure of the visco-plastic model, with the tensile stress on the one hand, and the cell wall mechanical properties on the other hand, as the two main components impacting cell wall expansion during growth (also named "cell wall extensibility").

4.1. Control of the tensile stress: an original biomechanical strategy of tip-growth in brown algae

4.1.1. Cell wall thickness gradient as a mechanical patterning factor in tip-growth

In the most studied of all tip-growing cell types, i.e. the pollen tube, the rapid stiffening of the cell wall after its deposition is generally thought to be the key mechanism leading to growth arrest and transition to tubular shape during tip-growth in land plants (Geitmann and Parre, 2004; Parre and Geitmann, 2005*a*; Bolduc *et al.*, 2006; Geitmann, 2006*a*; Geitmann and Steer, 2006; Zerzour *et al.*, 2009; Geitmann and Ortega, 2009). Such gradient of wall deformability along the meridional profile of the cell has also been revealed in some other tip-growing cells, the most convincing evidence being provided by Mine and colleagues for the giant-celled xanthophycean algae *Vaucheria* (Mine and Okuda, 2003). This "mechanical gradient" concept for tip-growth was embodied by numerous biophysical models (Wessels, 1988, 1990, 1993; Koch, 1994; Goriely and Tabor, 2003*b*, 2008; Dumais *et al.*, 2004, 2006; Bernal *et al.*, 2007; Goriely *et al.*, 2008, 2010; Campàs and Mahadevan, 2009; Fayant *et al.*,

2010; Eggen *et al.*, 2011). Those experimental evidences and models are explored in more details in the Revue (Rabillé and Charrier, in prep), presented in **Part 1.1**.

However, the viscoplastic model we built for the steady tip-growth of the apical cell of *Ectocarpus* parthenosporophytes revealed a biomechanical strategy for tip-growth in walled cells radically different from those described in the other organisms, that does not require any gradient of wall mechanics. Instead, integrating experimental data about the cell growth rate, the pattern of wall strain rate in the apical dome, the cell shape (curvature), the cell wall thickness, and the turgor, the model predicted that the relation between the wall strain rate and tensile stress followed a strict Lockhart's law, with a unique, constant value for the two viscoplastic properties of the wall (yield-threshold σ_y and extensibility Φ), whatever the position along the cell profile. The gradient of wall strain is thus only generated by a corresponding gradient of wall thickness. This parameter impacts the pattern of cell wall strain by significantly increasing the tensile stress in the dome, so that σ_y is locally outreached, leading to wall expansion. Gradual thickening of the wall correspondingly makes the tensile stress dwindle, generating the stable tubular shape below the apical growth area when the stress become inferior to σ_y. The continued thickening on the shanks would also be a mean to stabilize the tubular shape, by lowering further the tensile stress.

The possibility of regulating local expansion of the cell wall by local variations of the cell wall thickness has been advanced long time ago by some authors, for example by Green (1965, 1969). Two studies have evidenced gradient of wall thickness, that may also generate the typical heterogeneous pattern of wall strain in tip-growing or tip-growing-like cell types: in the regenerating apex of the stalk of the green coenocytic algae *Acetabularia acetabulum* (Von Dassow *et al.*, 2001) and in the elongating branch of leaf trichomes in *Arabidopis thaliana* (Yanagisawa *et al.*, 2015). However, in the first study, the geometrical measurements and stress calculations were very approximate, and the gradient of thickness varied greatly from one cell to the other. Moreover, the tip-growth observed corresponds actually to a healing process induced after wounding (Von Dassow *et al.*, 2001). As a consequence, the thickness gradient could be the result of the wall strain pattern rather than the cause of it. Regarding the second study, the wall thickness was conducted on longitudinal TEM pictures of the branch with a high spatial distribution. However, the measurements were made only on three branches, and the possible biases induced by askew sections have not been considered (Yanagisawa *et al.*, 2015). Moreover, the trichome branch does not elongate *via* a typical tip-growth form, but rather by an intermediate form between tip- and diffuse growth, involving a large strain anisotropy between the meridional and the circumferential axes (Yanagisawa *et al.*, 2015). Thereby, the cell wall thickness cannot, at best, be the only parameter controlling the morphogenesis of the branch.

As far as we know, our study represents the most convincing evidence of a tip-growth process entirely driven by a gradient of wall thickness. This points toward original cellular and molecular mechanisms controlling tip-growth in Phaeophyceae, at least in Ectocarpaceae, and raises interesting questions about the evolution of tip-growth in Eukaryotes.

4.1.1.1. Is thickness gradient a regular feature of brown algal tip-growing cells?

Tip-growth has barely been studied so far in brown algae, despite its occurrence in a significant proportion of families (Katsaros, 1995; Charrier *et al.*, 2012). Some data exist about the mechanism of tip-growth in the rhizoid of the fucoid embryos (Kropf *et al.*, 1989;

Bisgrove and Kropf, 2001; Coelho *et al.*, 2002; Fowler *et al.*, 2004; Corellou *et al.*, 2005; Linardić, 2018) and in the apical cells of *Sphacelaria*, a basal order only distantly related to the Ectocarpales (Silberfeld *et al.*, 2010). In regard to our results in the apical cell in *Ectocarpus*, an interesting question is whether such biomechanical strategy exists in other brown algal tip-growing cells. Interestingly, such gradient of wall thickness has been observed in the apical cells of *S. tribuloides* and *Halopteris filicina* (Katsaros, 1980, 1995; Katsaros *et al.*, 1983; Katsaros and Galatis, 1990), two species belonging to the Sphacelariales. Just as in *Ectocarpus*, the wall continues to thicken beyond the apical dome, up to the base of the cell (Katsaros *et al.*, 1983; Katsaros and Galatis, 1990). Such thickness gradient most likely impact the gradient of wall tensile stress, and thus wall expansion dynamic. However, the dynamic and biomechanics of tip-growth have yet to be explored in this brown algal order. Most importantly, it is not clear if growth occurs only at the tip or also on the shanks (Katsaros, 1995), so the link between wall thickness and expansion cannot accurately measured. Therefore, more investigations, on several species belonging to various orders, are necessary before concluding about the universality of the wall thickness gradient as a major mechanical factor of tip growth in brown algae.

4.1.1.2. Effectiveness and adaptive advantage of the control of cell wall thickness for tip-growth

Tip-growing cells generally develop in direct contact with the external environment, which physical and mechanical properties can generate considerable compression and frictional forces on the leading tip (Sanati Nezhad and Geitmann, 2013). In hyphal eumycetes and oomycetes, a stiff cell wall coupled to a high tensile turgor have been hypothesized to be necessary for the invasion of extremely hard media like soils or wood (Money *et al.*, 2004; Money, 2008). In flowers, the stiffness of the papilla cells is thought to control the trajectory of the growing pollen tube (Riglet *et al.*, 2018). Has the physical environment a similar impact on the biomechanical strategy described in *Ectocarpus*?

Contrary to the pollen tubes, root hairs or fungal hyphae, tip-growing cells of filamentous algae develop either in the sea water, which does not oppose large mechanical resistance to the expansion of the tip, or within tissues (for example other epiphyte and endophytic genus in Ectocarpales like *Laminarionema* and *Laminariocolax*). Apical cells of *Ectocarpus* sp., *S. tribuloides* (Katsaros *et al.*, 1983) and *Halopteris filicina* (Katsaros and Galatis, 1990) all seem to display a cell wall thickness gradient when grown in liquid media, suggesting that it could offer an adaptive advantage in these conditions, while very thin apical cell wall would be too fragile in the presence of large frictional or compressive forces. The mechanical impedance experienced by the tip of *Ectocarpus* when growing in contact to its natural substrate (rocks or other seaweeds) is not known and our current model cannot investigate this question. However, this remains an interesting topic for future studies about tip-growth biomechanics and its interaction with the physical environment in macroalgae.

4.1.2. How to generate a stable thickness gradient?

4.1.2.1. The predicted flux of wall delivery is low compared to that required for the pollen tube of Angiosperms

Our model makes the assumption that the cell wall thickness gradient is constant in the course of time along the apical cell. This implies that the cell generates and maintains a constant supply of wall material at any point of the cell surface, to compensate the local thinning due to in-plane expansion. Stochastic or induced fluctuations of this gradient could account for the variability in the final dome shape and diameter, and the irregular growth rate observed in time lapse-microscopy in living prostrate filaments of *Ectocarpus* (not shown).

We predicted a gradient of wall deposition rate with a peak at $s \approx 3.8$ µm. The cell wall deposition rate decreased only slowly in the shanks because the wall continues to thicken distally up to ~500 nm. When compared to the pollen tube, the absolute rate of delivery is extremely low. This is in accordance with the lack of accumulation of vesicles in the dome of *Ectocarpus* apical cells, as observed both in living algae labelled with the lipid membrane dye FM4-64 and by TEM in fixed samples. In tip-growing apical cells of *Sphacelaria* and *Halopteris*, the endomembranous systems and secretory vesicles were also poorly polarized, with only a slow gradient toward the apical tip (Katsaros, 1980; Katsaros *et al.*, 1983; Katsaros and Galatis, 1990). In contrast, in the fast growing pollen tube, large accumulation of vesicles, forming an inverted cone, have been observed (Derksen *et al.*, 1995, 2002; Parton *et al.*, 2001; Bove *et al.*, 2008; Chebli *et al.*, 2013).

In *Ectocarpus*, the real shape of the gradient of wall delivery rate was indirectly measured by FRAP experiments on apical cells labelled with FM4-64. Obviously, the real wall biosynthesis rate may diverge significantly from the local rate of exocytosis if an appreciable proportion of wall polymers are synthesized *in muro*. While the decreased rate of membrane renewal was confirmed in the dome, it did not decrease much with the distance from the extreme tip, as expected from the model. This accounts for the ongoing thickening of the cell wall in the shanks of this cell. However, it may also reflect the secretion of large amount of adhesive mucus observed by AFM imaging (unpublished results from C. Gaillard, BiBS plateform, INRA, Nantes, France) and TEM (Baker and Evans, 1973).

4.1.2.2. The actin cytoskeleton could generate the gradient of wall delivery

The dramatic impact on apical cell shape of a treatment with Latrunculin B demonstrated that AFs are necessary for the tip-growth in *Ectocarpus*. In their absence, morphogenesis switches to a (seemingly) complete isotropic mode and the formation of a large “bulge”. Interestingly, a short sub-apical portion of the shanks (~12 µm starting from the base of the dome, **Fig 3.5**) appeared to depend on AFs to maintain a tubular shape, as, after addition of LatB, this portion of the tube widened and was integrated in the bulge progressing downstream from the dome. AFs are thus essential for the establishment of the tubular shape and the restriction of the growth activity to the dome. Such importance of the actin cytoskeleton in the mechanism of tip-growth of *Ectocarpus* is not that surprising, as the fundamental importance of this component of the cytoskeleton has been evidenced in every tip-growing system studied so far (Steer, 1990; Jackson and Heath, 1993*b*; Torralba *et al.*,

1998; Raudaskoski *et al.*, 2001; Vidali *et al.*, 2001; Dent and Gertler, 2003; Ketelaar *et al.*, 2012; Takeshita *et al.*, 2014), including brown algae (Kropf *et al.*, 1989; Karyophyllis *et al.*, 2000*b*; Varvarigos *et al.*, 2004; Katsaros *et al.*, 2006). In several species, very similar "apical bulging" was observed when AFs were depolymerized, as in the oomycetes *Saprolegnia ferax* (Gupta and Heath, 1997) and *Phythophtora infestans* (Ketelaar *et al.*, 2012) and in the ascomycetes *Aspergillus nidulans* (Torralba *et al.*, 1998).

However, how exactly the actin cytoskeleton regulates tip-growth in *Ectocarpus* is still unknown. Actin labelling with phalloidin showed an extensive cortical network of AFs with thick bundles running parallel to the longitudinal axis in the shanks. In addition, a dense actin cap underlying the apical dome was displayed with an anti-actin antibody. This cap extended on sub-apical shanks in some cases. The presence of complex cortical networks of AFs is a regular feature of brown algal cells, in which they control the direction of the cellulose microfibrils (Karyophyllis *et al.*, 2000*b*; Katsaros *et al.*, 2002, 2006). Interestingly, LatB treatment did not result in any inhibition of the cell surface expansion during the formation of the large bulge in *Ectocarpus* (**Fig 3.5**). In addition, an over-deposition of cellulose was observed (**Fig 3.7**). Therefore, this suggests that AFs regulate somehow the location of wall deposition. Similar role has been proposed for *Saprolegnia ferax* hyphae (Heath and Kaminskyj, 1989) and the trichome of *Arabidopsis* (Yanagisawa *et al.*, 2015). Dense meshwork of fine AFs at the apex of tip-growing cells, that is probably the nature of the apical cap observed in *Ectocarpus*, have often been thought to promote local exocytosis (Wasteneys and Galway, 2003). They might even directly control the activity of terminal complexes responsible for the deposition of cellulose, as suspected in the apical cell of *Sphacelaria rigidula* (Karyophyllis *et al.*, 2000*b*) and in other brown algal cell types (Katsaros *et al.*, 2002). This hypothesis has been tested using our model by running simulations in which the global rate of wall deposition at the cell level is not reduced but made constant along the meridional profile (no peak of wall deposition on the shoulder of the apical dome). The results showed a progressive thinning of the apical wall that resulted in a progressive bulging of the apex, as observed in LatB-treated living cells. However, contrary to the live experiments, this apical bulging only occurred in neo-formed area, and not in the sub-apical shanks. Moreover, in the simulation the apical bulge expands more and more rapidly over time because of the thinning of the wall. These model predictions are inconsistent with what was observed experimentally, where the apical bulge expands at a constant rate and showed a significant thickening of the wall (see **Part 3** and further discussion below).

In summary, the effect of the AFs depolymerization cannot be accounted for by a simple destabilization of the wall deposition pattern. Rather, some physiological responses are likely triggered after the degradation of AFs, blurring possible conclusions as to the role of AFs in tip growth. In the future, quantitative correlation between the predicted or the observed rates of exocytosis on the one hand, and the observed distribution of AFs on the other hand, will allow better understanding. This will be initiated by FRAP experiments on LatB-treated cells.

4.2. The importance of wall mechanics in tip-growth of *Ectocarpus* apical cells

4.2.1. Mechanical features of the cell wall in the apical cell

4.2.1.1. Predicted constancy of the viscoplastic properties along the apical cell: lessons from the effect of IAA

We showed that the auxin indole acetic acid (IAA) increased the axial growth rate of the apical cells, while reducing the turgor and keeping the cell shape apparently unchanged. Modeling integrating these modifications inferred that the viscoplasticity parameters were largely modified, with a six–fold increase in the extensibility coefficient Φ and a three-fold decrease in the yield threshold σ_y (see **article 1**, **Part 2.1**). However, these parameters remained constant along the cell, as in the control growth conditions.

Interestingly, IAA does not seem to alter the cell morphogenesis *per se*. Therefore, it represents an ideal condition for our model to get further insights into the physiological and molecular mechanisms that regulate wall extensibility in *Ectocarpus*. Furthermore, IAA has been detected in *Ectocarpus* filaments where it seems to be mainly synthesized in the apical cells and to regulate the development of the vegetative thallus of the sporophyte (Le Bail *et al.*, 2010). Exploring the regulatory role of IAA could then give us insight into the deep molecular pathways regulating apical cell fate and tip-growth.

4.2.1.2. What is the nature of wall expansion during tip growth of the apical cell?

In brown algae, how cell wall expansion takes place at the molecular level is unknown. The yet undecipherable interactive network of the different cell wall components opens the way to many potential processes involving chemical reactions. At the biophysical level, the cell wall has so far been considered as either a visco-elastic material (this thesis) or a poro-elastic material (Jia *et al.*, 2017).

It is not known whether the viscoplastic parameters considered in our work correspond to the real mechanical behaviour of the cell wall (that would thus be analogous to a Bingham's viscous fluid; Dumais *et al.*, 2006; Guerriero *et al.*, 2014) or rather reflect *in-muro* remodelling activities that would mediate the expansion of the wall without necessarily affecting its mechanical state (Cosgrove, 1993*a*, 1996, 1997, 2016*b*,*a*), or even a subtle interplay of both. In any cases, the use of the viscoplastic model to *Ectocarpus* remains valid because wall viscosity is considered a good approximation of a cell wall being actively remodelled during stretching, giving it "chemorheological" properties (Dumais, 2013). At least, to fit the prediction of the biomechanical model, wall remodelling activities would have to be constant across the volume of the wall and along the meridian of the cell. These

activities would also have to be activated only when the tensile stress is above the yield-threshold (σ_y).

In tip-growing cell, the wall mechanical deformability or remodelling at the tip would be directly correlated to the constant supply of "fresh" wall material in this area, as suggested by several authors (Harold, 2002; Rojas *et al.*, 2011; Hepler *et al.*, 2013; see also the **Review** in **Part 1.1** of this report). The wall remodelling and building induced by the delivery of wall material is called intussusception (Dumais, 2013; Hepler *et al.*, 2013). However, in *Ectocarpus* that wall building is continued on a large portion of the shanks, well beyond the apical dome where surface expansion is arrested. This indicates that wall delivery and expansion are not intrinsically linked in this species. However, some remodelling factors might be targeted and / or activated specifically in the apical wall during the delivery process, as observed for pectin-methylesterases (PMES) and PME-Inhibitors (PMEIs) involved in the progressive demethylesterification of pectins in the pollen-tube[2] (Bosch and Hepler, 2005; Bosch *et al.*, 2005; Röckel *et al.*, 2007).

The model inferred that σ_y controls the final tube diameter and the growth rate while Φ only impacts the growth rate. Thus, although those parameters are constant over the growth area, they nonetheless must be regulated somehow to maintain steady tip-growth. Again, deciphering how these two parameters are regulated requires to a better knowledge of the molecular nature of wall expansion in *Ectocarpus* apical cell, and more generally in brown algae.

4.2.1.3. Intrinsic mechanical properties of the cell wall along the apical cell

In order to test whether the cell wall intrinsic mechanical properties are correlated to the spatial growth pattern, we undertook experimental measurements of the wall deformability along the longitudinal axis of the cell. Actually, the link between the intrinsic mechanics of the wall on the one hand and growth on the other hand, is hotly debated, especially in land plants where it is far from being resolved (see for example Lockhart *et al.*, 1967; Cleland, 1971; Taiz, 1984; Ortega, 1985; Cosgrove, 1987, 1993, 1996, 1997, 1999, 2005, 2016*b*,*a*; Passioura *et al.*, 1992; Ray, 1992; Nolte and Schopfer, 1997; Proseus *et al.*, 1999; Harold, 2002; Wei and Lintilhac, 2003; Thompson, 2005; Schopfer, 2006; Schopfer *et al.*, 2008; Geitmann and Ortega, 2009; Lintilhac, 2014; Braybrook and Jönsson, 2016). In brown algae, this issue only start being tackled (Linardić and Braybrook, 2017; Linardić, 2018).

4.2.1.3.1. Cell wall deformations in *Ectocarpus* filaments are mainly elastic

In response to hypotonic or hypertonic shocks, *Ectocarpus* cells respectively swell or shrink, reaching a stable volume in a few seconds (not shown). When, after a first hypotonic shock, the cells were subjected to a hypertonic shock leading to complete plasmolysis, their volume shrunk significantly, again within a few seconds. This shows that most of those wall deformation has an elastic nature (Boudaoud, 2010; Mirabet *et al.*, 2011). The time-dependent deformation indicates that the wall does not behave as a purely elastic material, but as a

[2] Note, however, that in this case, the activity of PMEs promote wall rigidification, so they are have quite an opposite effect compared to remodelling factors

viscoelastic material (Cosgrove, 1993*a*; Goriely *et al.*, 2008). According to the definition given by Goriely *et al.*, (2008), such cell wall could be modelled as a Kelvin solid or a Maxwell fluid. When the relative rate of wall deformation was measured along the apical cell and plotted as a function of stress (**article 2** in **Part 2.2**), the curves had a sigmoid shape suggesting that the deformation was not linear, as expected for a material as complex as the brown algal wall (Deniaud-Bouët *et al.*, 2014*b*).

AFM technique was used to probe the wall elasticity in *Ectocarpus* cells before this work (Tesson and Charrier, 2014, and unpublished results). The AFM was conducted in "stiffness tomography" mode, that allows to probe stiffness at various depth into the material (Roduit *et al.*, 2009; Radotić *et al.*, 2012). In all positions along the filament, the stiffness appeared to increase from the outer face toward the inner face of the wall. These AFM data seem congruent with the data of Terauchi *et al.* (2016), who showed that the inner (most recent) layer of the wall was the most dense, while the outer layer appeared in the form of a loose and poorly organized material in TEM on *Ectocarpus* cells (note, however, that their data were acquired on erect filaments).

4.2.1.3.2. Plastic deformation is also detected, but only in the apical dome

Interestingly, plastic component is also detected, but only in the apical dome (2 and 5 µm from the tip; not shown), because the wall at these two positions retract significantly less compared to cell that have not been pre-inflated (see the Material and Method, in Part 5, for more details). Plasticity is thus detected where the overall deformability is decreased, possibly indicating a negative links between the two components of wall deformability, as suggested by Ortega (2017). However, our viscoplastic model predicts that, during the inflation of the apical cell by a hypotonic shock, the added plastic strain would only occur in the apical region because the yield-threshold can only be exceeded in this location. So, the measured "plasticity" could be a confirmation of our viscoplastic model. Yet, it is possible that this "plastic" deformation corresponds in fact to a time-dependent, viscoelastic deformation. To verify this possibility, the cell retraction in plasmolysis would have to be measured several hours after transfer in the hypertonic medium.

Pooled together, these data clearly demonstrate that the intrinsic mechanical behaviour of the cell wall is complex and variable along the polarity axis of *Ectocarpus* apical cells. Better understanding of its impact in growth requires a thorough characterisation both at the biophysical and at the molecular/chemical levels, and potentially the use of mathematical tools dealing with non-linear elasticity (Goriely and Tabor, 2008), as shown in the modelling of *Ectocarpus* cell rounding (Jia *et al.*, 2017).

4.2.1.3.3. Variation of the intrinsic mechanical properties along the polarity axis and congruence with growth

Variations of the intrinsic mechanical properties were shown in different organisms other than brown algae. The experimental techniques and the nature of the mechanical properties varied in these studies. For example, in the pollen tube, the authors used the micro-indentation technique to quantify the viscoelasticity of the cell wall (Geitmann and Parre, 2004; Geitmann, 2006*a*,*b*; Zerzour *et al.*, 2009). In contrast, in *Vaucheria*, the meridional and circumferential cell wall "creep" rates were measured on wall ghosts inflated with silicone oil (Mine and Okuda, 2003). However, AFM-based techniques assess the mechanical properties

mainly in the direction normal to the cell surface, which may have few or no impact on the in-plane cell wall extensibility (Cosgrove, 2016*b*; see also the **Opinion Paper** in **Part. 1.2**). It also gives access only to a fraction of the wall, while cell inflation / shrinking experiments inform about the global deformability of the wall by averaging the mechanical properties of all cell wall layers. Finally, the lack of normality between the AFM cantilever and the surface of the dome makes data difficult to exploit. Therefore, in the context of tip growth, cell "inflation" techniques are preferable.

The most surprising feature of those stress-strain curves obtained in the *Ectocarpus* apical cell was an inverted gradient of deformability from 2 µm to 20 µm from the tip (cf **paper 2**, **Part 2.2**). On the one hand, this stiffening might be determining to prevent cell rupture where the cell wall is extremely thin; on the other hand, it cannot promote growth. Therefore, this feature shows that the immediate wall deformability is not correlated to the wall expansion, which is an important finding for the understanding of the biophysics of tip-growth in *Ectocarpus*.

Such negative gradient of deformability is unique among tip-growing cells types. Previous studies revealed a positive gradient of wall deformability from the extreme tip toward distal regions of the cell, especially in the pollen tube of some Angiosperms (Geitmann and Parre, 2004; Parre and Geitmann, 2005*a*; Geitmann, 2006*a*; Zerzour *et al.*, 2009), in *Aspergillus nidulans* hyphae (Ma *et al.*, 2005; Zhao *et al.*, 2005*b*) and in the apical cell of *Vaucheria terrestris*, a xanthophycean alga (Mine and Okuda, 2003; Mine *et al.*, 2008). A "softer" cell wall is expected in the context of tip-growth. As an example, the emergence of new growing tip was generally preceded by the local softening of the wall at the site of the protrusion (Mine *et al.*, 2007; Zerzour *et al.*, 2009).

We obtained additional data showing that growth can occur independently from the intrinsic mechanical properties. For example, treatment with the AF-depolymerizing drug LatB significantly promoted growth in the circumferential direction, while it reduced the elasticity in the same direction (see **Fig 3.5** and **3.6** in **Part 3.2.2**).

Beyond the progress in our understanding of the mechanical processes of cell wall expansion during tip growth, these data illustrate that *Ectocarpus* is a relevant model to study the relation between wall mechanics and cell morphogenesis in brown algae. In the future, it would be useful to screen for modifications of wall mechanical properties in a large range of experimental conditions altering apical cell growth and morphogenesis. To characterize more finely the wall deformability in *Ectocarpus* cells, mapping of cell deformation using fluorescent microbeads that we developed (see Rabillé *et al.*, Chapter 23 in *Protocol book for Macroalgae*, 2018) could be used in the future, allowing to "map" the wall mechanics in both meridional and circumferential directions with high spatial resolution.

4.2.2. In muro molecular determinism of wall mechanical properties

4.2.2.1. Role of cellulose and alginates

The *in-muro* molecular basis of cell wall deformability was tackled by focusing on cellulose and alginates, both thought to regulate cell wall mechanics in brown algae (Deniaud-Bouët *et al.*, 2014*b*).

We showed that cellulose, MM-blocks and GG-blocks of alginates all provide mechanical strength to the apical cell tip, as evidenced by tip bursting induced by short enzymatic treatments with cellulase, mannuronate blocks- (MM) or guluronate blocks- (GG) specific alginates lyases (AlyM and AlyG, respectively). The fact that cellulose digestion has a significant impact comparable to that of the digestion of alginates shows that this component plays similar structural and mechanical roles in the cell wall of apical cells, despite its low abundance, especially in the apical dome.

Digestion of MM alginates led to a lower rate of apex bursting compared to GG-digestion. As the MM-, MG- and GG-blocks are generally some tens of units long (Haug *et al.*, 1966), alginates chains are more probably made of series of the three kinds of blocks, and thus they all must be necessary for the structure and function of alginate gels. Interestingly, co-digestion of MM-block alginates and cellulose greatly enhanced apex bursting rate (to more than 50%), while co-digestion of GG-blocks alginates and cellulose did not increase bursting rate compared to single digestion of cellulose or GG-alginates alone. This may be the sign of differential role for the two kinds of alginate homomeric blocks.

Regarding wall expansion, immunostaining detected G-rich alginates (BAM10 antibody) and GG-blocks (using BAM11 antibody; Torode et al., 2016; not shown) up in the apex of apical cells, together with MM-blocks, suggesting that the growing wall is not associated with any higher M:G ratio. Transcriptomic analysis by Laser Capture Microdissection on individual cell types (Saint-Marcoux *et al.*, 2015) showed a strong expression for three genes coding for mannuronate-C5-epimerases (MC5E), which are enzymes involved in the conversion of M units into G units (Nyvall *et al.*, 2003; Tonon *et al.*, 2008; Fischl *et al.*, 2016) (unpublished results). This result supports a very early conversion of M-units into G-units, either in the newly made cell wall, or even inside the exocytic vesicles.

After several hours of treatments, enzymatic digestions of either cellulose or alginates had dramatic effects. Apical cell growth was entirely blocked and the wall radial deformability was drastically reduced (not shown). In addition, when M- or G- alginates were degraded, the cell accumulated a significant amount of cellulose in the dome, and wall thickness was increased (observed by TEM, unpublished results). The simultaneous growth arrest and cell wall strengthening can be explained by two alternative hypotheses. First, the degradation of cellulose or alginates impairs the integrity of the cell wall, resulting in an activation of physiological “defensive reactions” leading to wall strengthening, e.g. by over-accumulation of other wall components. This would result in an impairment of wall extensibility, ultimately blocking cell growth. This hypothesis is coherent with the observations i) that cellulose is accumulated when the cell wall is treated with alginate lyases, and ii) that alginates are over-accumulated in cells directly exposed to a hypotonic stress, especially at sites where the cell wall endure more tensile stress (see **article 2**, **Part 2.2**). Further support to this hypothesis could be obtained through alginate labelling of *Ectocarpus* filaments treated with cellulase. Other mechanisms may be responsible for wall strengthening in response to the loss of wall

integrity induced by cellulose or alginate digestion. For example, phenolic molecules contained in physodes could be discharged in the wall in some brown algae in response to stress (Pellegrini, 1980), where they would cross-links wall polymers (Deniaud-Bouët *et al.*, 2014*b*). In a more speculative scenario, wall expansion may not be linked to wall intrinsic mechanical deformability, but may be mediated by remodelling mechanisms that involved alginates and cellulose. In other words, those remodelling mechanisms responsible for the wall expansion would require the presence of these polymers, and could not work in the absence of one of them. When one kind of polymer is digested, the wall expansion would be intrinsically blocked, and tip-growth would thus stop. In such case, the continued wall deposition in the apical cell may progressively thicken the wall, resulting in an apparent reduction of wall deformability, as observed on cellulose- or alginate-lyases-treated cells.

In another set of experiments, MM- and GG-block digestion by AlyM or AlyG appeared to slow down the "growth resumption" process observed in apical cells cultivated in hypertonic conditions (1600 mOsm L^{-1}; not shown). In the first scenario, such effect would be the consequence of "reactive defence" mechanisms activated in response to the loss of cell wall integrity provoked by alginate degradation. However, in this particular case, the growth seemed not entirely blocked. If alginate main role is to mechanically reinforce the wall, they could be less essential in hypertonic conditions because of lower turgor-generated tensile stresses. Then, their abundance may be decreased in cells transferred to 1600 mOsm L^{-1}, rendering the cells less sensitive to the enzymes. In the second scenario, the wall remodelling mechanism that drives wall expansion may be less dependent on the presence of alginates.

4.2.2.2. A Golgi-dependent polymer would also be required for proper wall structures and, perhaps, mechanics

Brefeldin A (BreA) is a drug shown to block trafficking from the Endoplasmic Reticulum (ER) to the Golgi compartment in mammalian and plant cells (Staehlin and Driouich, 1997; Mishev *et al.*, 2013). In *Ectocarpus*, exposure to 10 µg mL^{-1} of BreA for several hours significantly altered the structure of the Golgi system (TEM imaging, not shown). It also completely blocked apical cell growth, while generating a slightly swollen apex with a cell wall dramatically expanded, forming a thick layer of a whitish, amorphous material. This "extra-layer" was present in both the apical bulge and the distal shanks. This is congruent with the fact that wall deposition is still very active in the shanks. The effect of this drug suggests that Golgi-dependent wall components are required for the proper wall organization, or maybe for the process of wall expansion. The same effect was observed on the forming wall during cytokinesis of the *Scytosiphon lomentaria* embryo (Nagasato et al., 2009), suggesting a conserved wall architecture and building pathway in brown algae. This essential component, which synthesis and delivery to the wall is Golgi-dependent, may be fucans. Indeed, in *Sylvetia babingtoni* embryo, a fucan compound was found to be shipped by Golgi-dependent vesicles to the membranous sacs that form the new cytokinetic wall during the first zygote division (Nagasato et al., 2010). Thus, the essential compound that is not delivered to the wall in *Ectocarpus* apical cells may simply be fucan polymers, but we did not investigate at all this complex class of polymer during this thesis.

In *Ectocarpus*, whether the growth inhibition and apex swelling in response to BreA are the result of wall thickening, or the opposite, is unknown. Indeed, the Golgi-secretory system may provide many components to the cell wall, resulting in many pleiotropic effects when impaired by BreA. However, studying the wall composition and wall mechanical properties in

BreA-treated apical cells may provide further insight into the interplay of wall molecular composition, mechanics and growth in *Ectocarpus*.

4.2.3. Cytoplasmic determinism of wall mechanical properties: direct mechanical role of the actin cytoskeleton?

4.2.3.1. Physical interactions between the actin cytoskeleton and the cell wall

The wall may not hold its mechanical properties from its own chemical composition and ultrastructure, but may also be influenced by other structural components of the cytoplasm. The cortical cytoskeleton has, indeed, often be thought to exert direct mechanical forces on the cell wall in plants, algae, fungi and oomycetes, especially in tip-growing cells (Picton and Steer, 1983; Steer and Steer, 1989; Steer, 1990; Money, 1997; Pickett-Heaps and Klein, 1998; Heath and Steinberg, 1999; Torralba and Heath, 2001). As such this component of the cytoskeleton may directly control wall deformability and / or ability to expand, and thus cell growth.

In the apical cell of *Ectocarpus*, an actin cap was observed at the apex, clearly made of a thin cortical layer just below the apical membrane. In the shanks, thick cortical bundles were displayed with a more or less longitudinal orientation, a feature very common in tip-growing cells (Steer, 1990; Kropf *et al.*, 1998; Wasteneys and Galway, 2003; Rounds and Bezanilla, 2013). The actin cap is especially interesting in relation to tip-growth mechanism. This structure has been repeatedly observed in other tip-growing species belonging to Stramenopiles, including other brown algae (Kropf *et al.*, 1989; Ouichou and Ducreux, 2000; Varvarigos *et al.*, 2004), hyphal oomycetes (Jackson and Heath, 1990, 1993*a*; Gupta and Heath, 1997; Walker *et al.*, 2006) and xanthophycean algae (*Vaucheria*, Alessa and Oliveira, 2001). Induced tip bursting in response to short term (~10 min) treatment with LatB indicate that this structure is directly involved in strengthening the thin apical wall to resist the turgor. It may be the cytoplasmic agent that strengthen the thin apical wall from its inner face, and would thus be responsible, at least in part, for the apparent inverted gradient of wall deformability observed by cell inflation / shrinking experiments (see above).

The hypothesis of wall mechanical “shielding” of the cortical actin cytoskeleton in brown algal tip-growing cells is supported by the evidence of strong physical connections between the cell wall and the cytoplasm at the growing tip of the *Pelvetia fastigiata* embryo rhizoid (Henry *et al.*, 1996). In this study, those connections were shown to depend on the presence of AFs. On the wall side, they relied on the presence of cellulose MFs and wall proteins, and are modulated by the pH and the concentration in Ca^{2+}. Some proteins involved in those connections may be homologous to proteins present in focal adhesions of animal cells. The existence of such connections is also supported by the evidence that the wall is required for stabilizing the polarity axis in the *Fucus* embryo (Kropf *et al.*, 1988). Experimental evidences and genomic data revealed the existence of α-integrin-like, talin and α-actinin proteins in *Ectocarpus* that make connections with actin in animal cells (Cock *et al.*, 2012). In the apical cells of *Sphacelaria*, an α-actinin, a β1-integrin and a wall-bound vitronectin-homologous protein were all detected by fluorescent immunostaining using antibodies raised for

heterologous proteins. All these data allow us to hypothesize the existence of integrin-containing transmembrane molecular connections, bounding the cortical AFs and the cell wall especially at the growing tip.

The potential mechanical role of the thick cortical bundles is less clear. The physical connection between the bundles in the shanks and the actin cap in the dome is unknown. The meshwork of thin AFs at the apex of tip-growing cells is sometimes considered to radiate from the thick longitudinal bundles (Wasteneys and Galway, 2003; Mathur, 2005). Works by Jackson and Heath (1990, 1993*a*) on the hyphal oomycete *Saprolegnia ferax* suggested that cortical bundles would serve in anchoring the apical cap to lateral wall allowing it to resist turgor that tends to push forward the apical tip. A similar role is possible in *Ectocarpus*.

The other long term effect of LatB on wall structure and measurable deformability (discussed in previous parts of this chapter) are also congruent with the direct mechanical involvement of AFs in strengthening the wall. As when cellulose or alginates are digested, AFs depolymerization would threaten the wall integrity, especially under the load of turgor. Thus, protective "wall reinforcement" mechanism of some sort may be activated to reinforce the wall, probably by wall thickening and over-deposition of cellulose. In the future, the direct involvement of the AFs in strengthening the apical wall may be tested by apical cell inflation / shrinking experiments or AFM on apical cells treated with LatB for very short time-scale (1 h, or even less).

4.2.3.2. Could actin filaments mechanically influence the wall strain pattern during tip-growth?

The possible direct involvement of AFs in mechanically reinforcing the wall could as well control the wall extensibility during tip growth. As mentioned earlier, the most striking effect of LatB on apical cell morphogenesis is that growth resumes in a short, sub-apical portion of the shanks, resulting in the loss of its tubular shape. This reversion in both growth activity and growth polarity underpins the role of AFs in these processes. If direct bounds exist between the wall and the cortical AFs in *Ectocarpus* cells, then the AFs could bear a part of the turgor-generated tensile stress, reducing the "effective" tensile stress born by the wall itself. Put in the context of the visco-plastic model, AFs would be a component of the yield-threshold (σ_y), together with the cell wall. AFs depolymerization by LatB would result in a decrease of σ_y and a re-initiation of growth in sub-apical areas. There is no obvious difference in the organization of the actin cytoskeleton between the sub-apical and the more distal parts of the tube in the *Ectocarpus* apical cell. Therefore, the transition between a region depending on AFs for the maintenance of its cylindrical shape to a region where AFs are no longer required would be due to the continued wall thickening along the shanks, making it more and more mechanically stable on its own.

This model is congruent with the slow, time-dependent reversion of the tubular shape because it is due to truly irreversible wall expansion rather than rapid elastic swelling of the wall.

4.2.4. Conclusion: differential role of the cytoskeleton and of the wall chemistry and mechanics in the control of growth

There must be a certain degree of functional redundancy between cellulose, alginates and AFs in contributing to the mechanical properties of the apical cell wall. All three components may reinforce the wall in some way, and their removal may mechanically weaken the wall. In all cases, the mechanical "weakening" of the wall would result in the same protective response activating a rapid thickening of the wall or any other wall modifications that may shield it again a loss of integrity. The main difference between the actin cytoskeleton and the wall polymers is that AFs are not required for wall formation and expansion *per-se*, while cellulose, alginates, and probably the other wall components including fucose-containing-polymers, seem necessary.

In conclusion, the actin cytoskeleton may play a direct mechanical patterning role, either by generating the gradient of wall delivery necessary to maintain the thickness gradient, or by direct mechanical reinforcement of the wall by transmembrane connections. These two roles are not exclusive, as the actin cytoskeleton could be multi-functional in cellular growth and morphogenesis (Kropf *et al.*, 1998; Raudaskoski *et al.*, 2001; Torralba and Heath, 2001; Katsaros *et al.*, 2006; Chebli *et al.*, 2013; Rounds and Bezanilla, 2013). On the contrary, although alginates and cellulose probably regulate the mechanical properties of the wall, there is no sign that these wall components are involved in controlling the growth pattern in tip-growing cells. This is coherent with the fact that: 1) the wall mechanical properties, or more precisely its "extensibility" need not to be regulated at a sub-cellular spatial scale; and that 2) the actual mechanical properties of the cell wall itself probably do not determine the actual extensibility of the wall, and thus could not control the profile of wall strain. Instead, tip-growing apical cells in *Ectocarpus* "make use" of the wall in a completely different way: they control the rate of wall deposition at a precise pace, controlling the local tensile stress "available" for the work of wall expansion. However, the dramatic effect of treatments that alter the wall composition suggests that a "complete", fully functional wall is absolutely required for wall expansion and cell growth.

A general overview of the results obtained during this thesis project, completed with data obtained from other studies carried out in the team or found in the literature, is presented in **Fig. 4.1**. This schema represents our current understanding of the integrated mechanism of tip-growth, from the molecular regulation to its biomechanical dynamics.

4.3. How the Rho-GAP-coding ETOILE gene controls tip-growth?

A small part of this thesis project was dedicated to the completion of the positional cloning of the *ÉTOILE* gene, most of which has been conducted by Zofia Nehr, a former doctoral student in the team (Z. Nehr, 2013). In the *étoile* mutant, tip-growth is impaired and the apical cells, first slightly polarised, become progressively isotropic (Le Bail et al., 2011; Nehr et al., 2011). This phenotype is reminiscent of the effect of AF depolymerization by

LatB, and thus suggested that this mutant was affected in the organization of the actin cytoskeleton. During this thesis, I confirmed that the gene *ÉTOILE* codes for a Rho-GTPase-Activating-Protein (Rho-GAP) containing a BAR domain probably involved in the recognition of curved lipid membranes (Z. Nehr, 2013). Rho-GAP and associated Rho-GTPase proteins have been involved in the regulation of tip-growth in tip-growing plant cells, in part by controlling the spatial arrangement of AFs, especially in the angiosperm pollen tubes and root hairs (Gu *et al.*, 2003; Šamaj *et al.*, 2004, 2006; Kost, 2008, 2010; Craddock *et al.*, 2012; Vaškovičová *et al.*, 2013). Thus, it was hypothesised that tip-growth defects in the mutant may be linked to altered architecture of the actin cytoskeleton.

However, fluorescent staining of AFs in *etl* revealed that the actin cap is still present, showing that this particular structure is not dependent on the Rho-GAP protein. The presence of the cap even in slightly misshaped apical cells of *etl* suggests that the putative "polarity cues" that define the position of this structure are not directly dependent on the local shape of the cell boundary. The thick cortical bundles, evidenced with the phalloidin-based protocol in WT cells, were not observed in the shanks of *étoile*, suggesting that their formation is under the control of the gene *ETOILE*. However, this protocol is sensitive to slight variations in the experiment conditions, and might require several repetitions before getting exploitable results. If the absence of cortical actin bundles in the shanks of the apical cells is confirmed, then it will strengthen the previous hypothesis that AFs are involved in the establishment and/or maintenance of the tubular shape.

Transcriptomics of the apical cell in *etl* showed a complete loss of genetic expression profile specific to this cell type (B. Billoud, B. Charrier, unpublished results), so ETL may also impact tip-growth by up-stream regulation of the apical cell-type fate. The putative link between ETL and the biomechanics of tip-growth in *Ectocarpus* is also integrated into **Fig 4.1**, along the cellular factor discussed above, drawing possible hypotheses to be tested for the future.

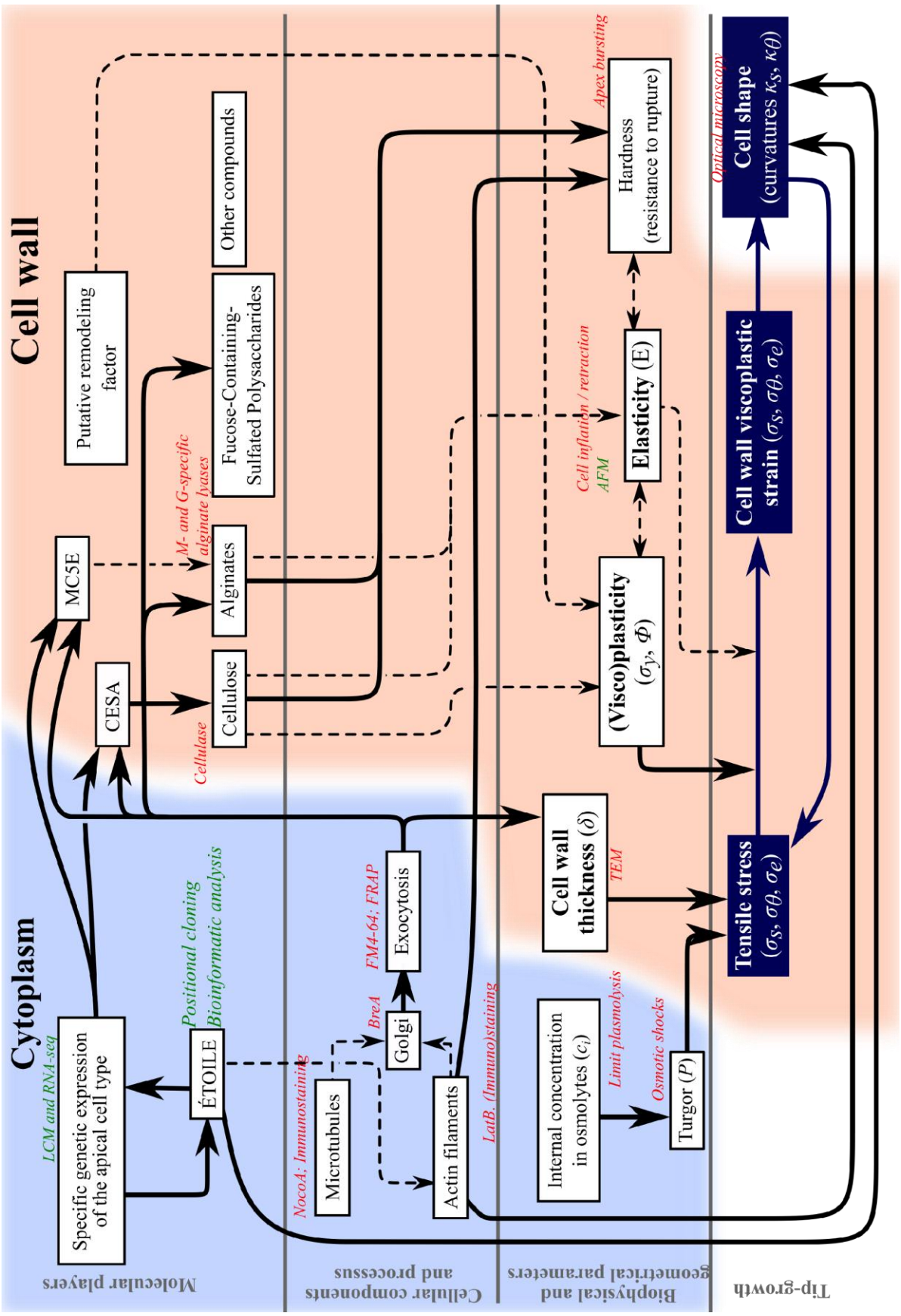

Figure 4.1 Global overview of the results on the integrated mechanism of tip-growth in the apical cell of *Ectocarpus* sporophytic vegetative filaments *(caption on the next page)*

(Figure 4.1, *continued*) This schema outlines the range of molecular, cellular and biomechanical factors and parameters that have been investigated regarding the mechanism of tip-growth, and the inferred connections with the biomechanical model (dark blue outline, bottom part of the schema, with the final output of the tip-growth process, the cell shape, at the bottom right corner). The corresponding techniques to measure or modify each parameter are indicated in italic. Most of these experiments were conducted during this thesis project (red text), but some were so during other projects (green text: transcriptomic of the apical cells of the WT and of the *étoile* mutant, positional cloning and analysis of the *ETOILE* gene, AFM measurements…). The connection between parameters outlined by thick, continuous arrows are those confirmed by experimental studies during this thesis project, from other projects in the research time or gathered from the literature. Connections in the form of thin, dotted arrows are hypothetical or suspected relationships that need to be tested or confirmed. Parameters are separated between two sub-cellular localizations, the "cytoplasm" and the "cell wall" (blue and brown background color, respectively), and also in three main categories: i) molecules (up line), ii) cellular structures and processes (second line), iii) biophysical parameters (third line) and iv) the biomechanical dynamics of cell elongation (i.e. tip-growth).

5. Material and Methods

5.1.1.1. General procedure for Ectocarpus cultivation

Gametophytes, sporophytes and parthenosporophytes (PS) of *Ectocarpus* (WT: Ec32 strain, and *étoile* mutant) are cultivated according to Le Bail and Charrier (2013). In brief, algal filaments were grown in natural sea water (NSW) completed with 10 mL L^{-1} of Provasoli Enrichment Medium (PES; Provasoli and Carlucci, 1974) in Petri dishes, at 13°C with an irradiance of about 20 µmol photon m^{-2} s^{-1} and a 14/10 h day/night cycle. Culture media are renewed every 1 or 2 weeks. For culture propagation, small tufts of filaments were transplanted individually into new dishes, under a sterile hood. All the experiments were conducted on PS that develop from unfertilized gametes released from gametophytes.

For cell wall deformability measurement and immunostaining, PS were germinated on sterile glass coverslips, while for TEM observations, they were cultivated on microscope slide, deposited at the bottom of Petri dishes. In order to make PS germinate on coverslips, gametophyte filaments bearing plurilocular sporangia were stacked in a pile at the centre of the Petri dish; some water drops were added on the edge to make a moist chamber. The pile of gametophytes was incubated at 13°C in dark for one night. It was then flooded with 500 µL of fresh NSW to induce massive gamete release from sporangia. The medium with swimming gametes was pipetted and about 20 – 50 µL (according to the density of gametes) were dropped on each sterile coverslip located individually in small Petri dishes. The gametes were allowed to settle on the coverslips surface for some hours in normal culture conditions, and then the dishes are filled with NSW and put back in culture. During the experiments, the medium was sometimes completed with 45.5 µg mL^{-1} penicillin, 22.7 µg mL^{-1} streptomycin and 4.5 µg mL^{-1} chloramphenicol in order to prevent bacteria proliferation.

5.1.1.2. Enzymatic and pharmacological treatment of filaments

The actin-depolymerizing drug Latrunculin B (LatB, from *Latrunculia magnifica*, Calbiochem) stock solution was prepared at 1 mM in DMSO. Stock-solutions were generally filter with 0.2 µm mesh-size filters (Falcon) under a laminar flux hood to sterilize them.

To treat living filaments, the culture medium of algae was replaced by fresh sea water in Petri dishes, stock solutions of enzymes or drugs were diluted into the new medium at the required concentration, and the dishes were gently shaken by hand. For long-time treatments (i.e. at least several hours), the medium was also complemented with PES and dishes were then put back in normal culture medium.

5.1.1.3. Induction of osmotic stresses

To cultivates *Ectocarpus* filaments in various level of osmotic stresses, a range of hypotonic (lower osmolarity compared to normal sea water, ~1100 mOsm L^{-1}) and hypertonic osmolarity (higher osmolarity) media was prepared, using ASW or NSW. For hypotonic

solutions, normal sea water was simply mixed with osmosed water to various proportions in order to obtain the desired final osmolarity. For hypertonic solutions, a starting solution of hyper-concentrated sea water was first prepared by diluting as much sucrose as possible, until the solution seemed close to saturation. The final osmolarity was measured with an osmometer (Osmometer Automatic, Löser, Germany), and generally ranged between 2600 and 3100 mOsm L^{-1}. Intermediate hypertonic solutions of final osmolarity c_f were prepared by mixing a volume v_{sw} of normal sea water with a volume v_h of the hypertonic mother solution, with a ratio giving the adequate final osmolarity. For long term cultivation of *Ectocarpus* PS in these media, PES was added to each (the osmotic effect of constituent of the PES was deemed negligible).

5.1.1.4. Measurement of cell wall deformability

5.1.1.4.1. Measurement of wall circumferential deformability by apical cell inflation/retraction

The deformability of a material is measured by calculating the ratio of the relative deformation in response to an applied stress (force per area, in MPa). The internal turgor pressure in cells generates a tensile stress in the cell wall. The cell wall deformability in living cells of prostrate filaments was calculated by recording the relative deformation in response to a given variation in internal turgor pressure, induced by hypotonic or hypertonic shocks. During hypotonic shocks, the turgor is increased and so is the wall tensile stress, leading to wall extension and cell inflation. Conversely, hypertonic shocks decrease turgor and tensile stress, leading to wall retraction and cell shrinking. Plotting the local change in wall tensile stress against the corresponding local change in tensile stress allows one to calculate the local deformability.

For deformability measurement experiments, *Ectocarpus* parthenosporophyte filaments grown on microscope coverslips were used. For the procedure, a coverslip was taken from its Petri dish, mounted directly on the microscope or stuck below a drilled Petri dish to form a home-made “culture chamber” that was mounted on the microscope with a small drop of culture medium on the algae. The microscope used was a DMI6000 inverted optical videomicroscope (Leica) equipped with a motorized stage and controlled by the LAS AF (v2.2.1, Leica) software. A set of positions on the surface of the coverslip were chosen, showing apical cells lying more or less parallel to the surface of the coverslip, and a first series of pictures for each position were taken (t_0). The culture medium was gently removed from the coverslip using a pipette or a piece of paper towel, and immediately replaced by a larger volume of hypotonic or hypertonic sea water (prepared as described in Part 5.2. above) making the cell swell or shrink, respectively. In all cases, the cell volume was stabilized in less than one minute after medium replacement, and a second series of pictures of the same apical cells were acquired after 1 min (t_1). Note that “hypotonic” and “hypertonic” are defined in regard of the osmolarity of the initial culture medium in which the algae were cultivated. Indeed, for filaments cultivated in sea water at 1600 mOsm L^{-1} (hypertonic stress), “hypotonic” media correspond to solutions of lower osmolarity (including normal sea water, which osmolarity is ~1100 mOsm L^{-1}), while “hypertonic” media correspond to solutions of higher osmolarity.

Using ImageJ software, the average meridional deformation was measured from pictures as the relative variation of cell length along the longitudinal axis of the filament ($\Delta L/L$), that corresponds to the length of the cell from the extreme tip (apical pole) to the dividing wall that demarcates it from the sub-apical E cell. In parallel, the circumferential deformation was measured from relative variation in cell diameter ($\frac{\Delta w}{w} = \frac{w_f - w_i}{w_i}$) (with w_f and w_i the final and initial diameter, respectively), at 2, 5, 10 and 20 µm away from the apical pole of the cell in the longitudinal direction. The cell axial length appeared to vary with very low amplitude, indicating that the meridional part of the deformation is low, at least in the shanks of in apical cells. These 4 measured positions were thus considered to be the same before and after the cell inflation/shrinking. To completely "relax" the wall, i.e. to abolish all the tensile stress, the cells were completely plasmolysed by immersion in the mother hypertonic medium (sea water + sucrose, of final concentration at least ~2600 mOsm L^{-1}). The mean ± S.D. of the relative deformation was calculated for each cell type and positions on each cell types, and significance of differences between two conditions was tested by Welch-corrected t-Student tests.

5.1.1.4.2. Estimation of wall plasticity: apical cell inflation followed by retraction

For plasticity measurement, the cell wall was first stretched by inducing a hypotonic shock (step 1), and shortly after was completely relaxed by plasmolysis in response to a strong hypertonic shock (step 2). The "pre-stretching" of the wall by cell inflation represented an extra deformation with potentially plastic (irreversible) component in addition to the elastic (reversible) stretching component. The plastic part of the deformation would result with a lower level of wall retraction during cell plasmolysis compared to the control cells that are directly shrunk by plasmolysis without "preinflation". Note, however, that this technic cannot allow to quantify the "proportion" of plastic over elastic deformation.

The protocol used was the same than that described in the previous section. Simply, apical cells were imaged after 1 min of inflation in the hypotonic medium (step 1), then the hypotonic medium was itself sucked up and replaced by the hypertonic medium to induce plasmolysis (step 2), and pictures of the same cells were taken after 1 min of immersion. The relative variation of cell length and diameter ($\Delta w/w$) at 2, 5, 10 and 20 µm from the extreme tip was calculated for the both steps as described above, relatively to the dimension of the cell in the original medium. For control, only cell dilation (by hypotonic shock) or cell shrinking (by hypertonic shock) was applied to cells, and the differences of $\Delta w/w$ between the control and cells subjected to the plasticity test were compared. Plasticity was detected at a given position of the apical cell when $\Delta w/w$ in shrunk cells was significantly higher in those cells that were "preinflated" compared to control cells.

5.1.1.4.3. Calculation of the correcting factor to properly measure cell turgor

In order to compute the final turgor value, and then tensile stresses (see previous section)., in inflated or shrunk cells by hypo- or hypertonic conditions, respectively, the calculation of the coefficient of volume variation (x) was required. Cell volume (V) was calculated from

appropriate cell dimensions measured on ImageJ. The x factor was then simply calculated as $x = \frac{V_f}{V_i}$, V_i and V_f being the cell volume before and after osmotic shock, respectively.

5.1.1.4.4. Calculation of stress-strain curves

For untreated apical cell, the local wall tensile stress could have been measured at the four positions at which the relative circumferential deformation of the wall ($\Delta w/w$, corresponding to an "elastic" strain, see **Part 5.4.1** above) was measured, for each level of osmotic shock applied. The tensile stress was calculated as described in the **Paper 1** (cf **Part 2.1**). Local stress-strain curves for the 4 positions can then be calculated, that characterize the local mechanical deformability of the wall, an approximation of its elasticity, if the plastic part of the deformation is neglected.

5.1.1.5. Measurement of apical cell wall strength

Small tufts of PS were taken off the culture and placed in 500 µl of sea water completed or not with a particular drug or enzymes at the appropriate concentration, in a multi-well culture plate. Filaments were incubated for 10 min, then the rate of apex bursting were counted manually under an inverted microscope, directly from the culture plate or after mounting between a microscope slide and a coverslip. Several sea water media were tested: ASW or NSW, completed or not with (PES), and with varying degree of dilution with pure water, to apply various level of hypotonic shocks. However, apex bursting increased rapidly when the external osmolarity decreased, and differences between control and treated sample were diminished. On the contrary, addition of PES dramatically reduced the apex bursting. So only results with full strength ASW are presented. The bursting rate was simply calculated as the ratio of burst cells over the total number of counted cells. Results from several independent counting (at least 4) were gathered for each condition. Differences between conditions were tested by applying χ^2 test between each pair of condition.

5.1.1.6. Measurement or calculus of turgor pressure

5.1.1.6.1. Measurement of turgor by limit-plasmolysis

The turgor in apical cells of various genotype or grown in various (including osmotic) conditions was measured by limit-plasmolysis and corrected for cell volume shrinking, according to a previously described protocol (Wright and Reed, 1988*a*). In short, *Ectocarpus* PS were immersed in more or less hypertonic sea water solutions (prepared as described in section V.3), for at least one minute. Then the tuft of filaments was mounted with the same medium between a microscope slide and a coverslip, and the proportion of plasmolysed apical cells was measured by counting at least 100 apical cells under an optic microscope. The counting was made as quick as possible to avoid potential artefacts due to evaporation or osmotic adjustment by the cells. The rate of plasmolysis was plotted against the external osmolarity (c_e). The limit plasmolysis (c_{pl}) corresponds to the value of c_e for which 50 % of

apical cells were plasmolysed (Wright and Reed, 1988*a*). Sometimes, independent experiments were carried out and the mean c_{pl} value was calculated. The exact osmolarity of solutions used were occasionnally verified with an osmometer.

The c_{pl} value would normally correspond to the internal osmolarity of cells (c_i) that is then used to calculate the turgor (P). However, during limit plasmolysis experiments, the volume of *Ectocarpus* cells is significantly decreased because the cell wall is very elastic (Tesson and Charrier, 2014*b*). This shrinking must be taken into account to calculate the real internal osmolarity (c_i) of the cells in their cultivation medium, and so to calculate the real P (Wright and Reed, 1988*a*). To do so, the coefficient of apical cell volume shrinking (x) was calculated as explained before (see section V.2.c), for apical cells shrunk by complete plasmolysis. The real internal osmolarity was then calculated as $c_i = x.c_{pl}$, the real difference between internal and external osmolarity as $\Delta c = c_i - c_e$, c_e being the osmolarity of the culture medium, and finally the turgor as $P = \frac{\Delta c}{410}$, in MPa.

5.1.1.6.2. Prediction of turgor value just after cell volume changes induced by an osmotic shock

In various apical cell inflation and shrinking experiments, the final turgor in the apical cell immediately after the cell volume stabilization was estimated knowing the initial internal osmolarity (c_{ii}), before the cell inflation or shrinking. Predicting the final turgor was necessary, for example, to calculate the tensile stress in the final conditions (see section V.2.d). To do so, the x factor was calculated for apical cells for each condition of inflation or shrinking (for example, for apical cells of Ec32 cultivated in normal sea water at 1100 mOsm L^{-1} and inflated by hypo-osmosis in 550 mOsm L^{-1}), as described above. The final internal osmolarity (c_{if}) was then calculated as $c_{if} = \frac{c_{ii}}{x}$ and the final turgor as $P = \frac{c_{ii}.x - c_e}{410}$, where c_e is the osmolarity of the final external medium.

5.1.1.7. Measurement of apical cell surface curvature

Apical cell contours were drawn manually from confocal images of meridional plans of apical cells immersed in NSW. Similar procedure was followed for tobacco pollen tubes from photos given by Greb Grebnev (B. Kost's lab, Erlangen Univ, Germany). A python3script was devised to compute the average contour for a series of images and used it on *Ectocarpus* and tobacco pollen tubes. The program starts with a hand-drawn contour for each cell, from which it computes a smoothed cubic spline curve. A set of equidistant points (we used a point-to-point distance of 50 nm) were extracted from the spline and the meridional curvature κ_s is computed at each point. To obtain average symmetrical curvatures, a pair of windows starting from the tip point and sliding in both directions was used (window width = 200 nm, sliding step = 50 nm). The discrete values of the $\kappa_s = f(s)$ function was used to iteratively compute the position of cell-wall point coordinates as values of x (the axial abscissa) and r (the distance to the axis), together with the meridional abscissa s, the curvatures κ_s and κ_θ, and φ the angle between the axis and the normal to the cell wall. In particular, the circular symmetry of the dome imposes at the tip (where $s = 0$), that $\kappa_\theta = \kappa_s$ thus $\sigma_\theta = \sigma_s$, whereas in the cylindrical part of the cell $\kappa_s = 0$ thus $\sigma_\theta = 2\sigma_s$.

5.1.1.8. Measurement of growth kinetics

5.1.1.8.1. Time-lapse videomicroscopy of filament growth

For time-lapse observations, filaments were germinated in wells of glass-bottom multi-well culture plates. After about 2 weeks of cultivation in normal condition, the multi-well plate was installed on the motorized stage of an Olympus CKX51 inverted optical microscope controlled through the ImageProPlus software (v.7.0, Media Cybernetics). Alternatively, the plate was mounted on an DMI6000 inverted videomicroscope (Leica) equipped with the same motorized stage and software. Wells were filled with a volume of sea water with the required drugs or osmolarity, and completed with PES (ASWp or NSWp). The filaments were let to grow under the microscope for several days. The transfer of filament in their final culture medium marked the beginning (t_0) of the time-lapse run. During the time-lapse, the multi-well culture plate was kept at 16 or 17°C by an air-conditioned closet that contain the microscope and illuminated with a ~50 Hz, 1.5 W LED lamp, with a 12/12 h day/night cycle. Several positions in each well were recorded, with one picture acquired regularly, with a time lag between 2 to 12 h between each acquisition. Time-lapses experiments were run up to one week.

At each position, one or two growing apical cells were followed during the whole time-lapse, with a more or less regular time-interval between subsequent pictures. By picture analysis on ImageJ, necessary cell dimensions were measured in order to calculate the apical cell length and surface at each time-step. The apical cell axial length and surface increase were plotted as a function of time. For LatB-treated cells, the cell surface of two sub-regions of apical cells (basal tubular region and apical “bulge”) were measured independently. The total cell surface was measured as the sum of both regions. Variations of surface of the two subregions and of the whole cell were then plotted over time for individual cells.

5.1.1.8.2. Mapping wall strain pattern by surface labelling using fluorescent microbeads

The protocol was adapted from Shaw et al. (2000) and is described in detail in Rabillé et al. (2018a). Young sporophyte filaments grown in glass-bottom Petri dishes were covered with sonicated 0.1 % (w:v NSW) of FluoSpheresTM amine, 0.2 µm, red (F8763, Molecular Probes), washed with NSW and mounted under a TCS SP5 AOBS inverted confocal microscope (Leica) controlled by the LASAF v2.2.1 software (Leica). The growth of 25 apical cells growing parallel to the glass surface was monitored, and bright-field and fluorescent pictures of median planes for each apical cell were acquired at several time points. Cell-wall contours were hand-drawn on time-lapse images using GIMP, together with their respective indicator points. The position of the extreme tip ($s = 0$) was fixed for each meridional contour and the drawing of cell contours and micro-sphere positions were aligned during the time course using steady micro-spheres attached on fixed positions. A spline was adjusted on each contour, and on each series of indicator points. The angle at each possible intersection between these trajectories and the cell contour splines were computed, making use of their first derivatives. Further analysis performed using R (R Core Team, 2017) consisted in (1) determining the distribution of angles, their mean and standard deviation, and (2) testing the hypothesis of dependence between the angle and the meridional abscissa.

5.1.1.9. (Immuno)fluorescent staining of cell wall polymers

5.1.1.9.1. Immunostaining of alginates

Immunolabelling of *Ectocarpus* filaments was conducted according to a protocol first developed for *Fucus* embryos (Torode *et al.*, 2016). Those monoclonal antibodies were produced at the University of Leeds by rat immunization, as described in Torode *et al.* (2016). Experiments were performed on three cover slips covered by 2-week-old *Ectocarpus* prostrate filaments growing in separate Petri dishes. Cover slip with algal filaments adhering to it was quickly washed in NSW, and fixed as described in Siméon *et al.* (2018). Briefly, filaments were fixed in 8 % paraformaldehyde and 10 % glycerol in PBS:NSW 1:1 for 30 min at room temperature (RT). Filaments were then washed twice with NSW and twice with PBS (50 mM NaCl, 2.7 mM KCl, 10 mM Na_2HPO_4 and 1.8 mM KH_2PO_4) and then incubated overnight in 5 % milk protein in PBS (MP-PBS). They were then incubated with hybridoma supernatants containing the primary anti-alginate antibody diluted 10-fold in MP-PBS, for 1h at RT. Samples were then incubated 1h with the secondary antibody, an anti-rat IgG coupled to fluorescein isothiocyanate (FITC), diluted 100-fold in MP-PBS. Samples were mounted in PBS and a small drop of Citifluor (Agar Scientific). Observations of the FITC fluorescence were carried out using an TCS SP5 AOBS inverted confocal microscope (Leica). The monoclonal antibodies BAM6, BAM7 and BAM10 were used.

5.1.1.9.2. Calcofluor staining on living cells

Treated or untreated filaments germinated on microscope coverslips were incubated in NSWp completed with 0.003 % Calcofluor FB for 30 min at RT. Coverslips were then extensively washed three time in large volume of NSW (for at least 30 min), and then mounted on an inverted confocal microscope (TCS SP5 AOBS, Leica), with a drop of culture medium on it, for picture acquisition. Reconstructed bright-field and fluorescent pictures were acquired in parallel by the software, with fluorescent pictures taken with a diode laser at 405 nm.

5.1.1.10. Observation of cell wall ultrastructure and thickness by TEM

5.1.1.10.1. TEM observations

Ectocarpus PS filaments germinated on microscope slide were cultivated for the appropriate duration with or without additional treatment (hypotonic conditions or drug / enzymatic treatments), and then prepared for TEM observation. Algal filaments were fixed with 4% glutaraldehyde and 0.25 M sucrose at room temperature and washed with 0.2 M sodium cacodylate buffer containing graded concentrations of sucrose. The samples were post-fixed in 1.5 % osmium tetroxide, dehydrated with a gradient of ethanol concentrations, and embedded in Epon-filled BEEM capsules placed on the top of the algal culture. Polymerization was performed first overnight at 37°C and then left for 2 days at 60°C. Ultrathin serial sections were cut tangentially to the surface of the capsule with a diamond knife (ultramicrotome) and were mounted on copper grids or glass slides. Two types of

sections were produced. 300 nm-thick serial sections were stained with toluidine blue to show the main cellular structures, including the cell wall, and mounted on glass slides. 70 nm thick sections were stained with 2 % uranyl acetate for 10 min and 2 % lead citrate for 3 min, mounted on copper grids (Formvar 400 mesh; Electron Microscopy Science) and examined with a Jeol 1400 transmission electron microscope. The last steps, starting from resin embedding, were conducted by Sophie Le Panse (Merimage plateform, FR2424, Station Biologique de Roscoff). Wall thickness was measured from TEM picture using the standard linear distance measurement tool on ImageJ. For more details about the mathematical modelling of the wall thickness gradient profile in apical cells, see the material and methods of the **paper 1** (**Part 2.1**)

5.1.1.11. (Immuno)fluorescent staining of cytoskeleton and vesicles

5.1.1.11.1. Fluorescent staining of actin filaments by AlexaFluor568-Phalloidin

During my thesis, a protocol of actin staining first developed for *Sphacelaria rigidula* (Karyophyllis et al., 2000a,b) was adapted to *Ectocarpus* during an short-term scientific mission in Pr. Katsaros laboratory at the University of Athens in October 2016. The protocols is now published (Rabillé *et al.*, 2018*b*). Fluorescent pictures were acquired with the epifluorescence microscope (BX60, Olympus) (see Part V.8.a), using the MSWG filter block (Ex. 480-550 / Em. >590 nm). Note that, alongside Dr Adeel Nasir (Friedrich Alexander University of Erlangen-Nuremberg, Germany), some attempts were made to fuse this protocols with the second one described below, but these did not give positive results.

5.1.1.11.2. Immunofluorescent staining of actin and tubulin

A second protocol of actin staining was tested in parallel on *Ectocarpus*, using a commercial antibody (rabbit anti-actin, AS13 2640, Agrisera) and a protocol originally developed for *Euglena gracillis* (Mermelstein *et al.*, 1998), both furnished by Dr A. Nasir. Tubulin was stained using a commercial anti-tubulin antibody generated in rat (MCA-77G, Serotec) using the same protocol. In short, PS filaments germinated on coverslips were fixed in 2% (PFA) in PBS, pH 8, for 30 min. They were then briefly washed in 0.5% Triton X-100 in PBS, and incubated with the same solution for 15 min, in order to permeabilize the cells. The algae were then extracted in 80% acetone (v:v) for 10 min, and washed 2x10 min in 0.5% Triton X-100 in PBS. The algae were then incubated in the blocking medium [3% Bovine Serum Albumin (BSA), 0.5% Triton X-100 in PBS and incubated 10 min at 37°C] 1 h at RT or overnight at 4°C. Samples were again washed 2x10 min in 0.5% Triton X-100 in PBS. Then, the algal samples were incubated with the primary antibody in the blocking solution for 1h. For actin staining, the samples were incubated with a 1:300 dilution of anti-actin antibody; for tubulin staining, the sample were incubated with a 1:200 dilution of anti-tubulin antibody. They were then washed 2x10 min with 0.5% Triton X-100 in PBS, and then incubated with the secondary antibody diluted in the blocking medium. For actin staining, the samples were incubated with a 1:200 dilution of mouse anti-rabbit IgG antibody conjugated to AF488 (Ex/Em: 495/519 nm); for tubulin staining, the samples were incubated with a 1:150 dilution of anti-rat FITC, and incubated for at least 2h, in dark, at RT (or overnight, at 4°C, in dark).

After a last wash with 0.5% Triton X-100 in PBS in dark, the coverslips bearing the filaments were mounted and sealed as described above.

All the incubations were carried out at RT unless said otherwise. For negative control, the same procedure was applied except that the primary antibody was omitted. Fluorescent pictures were acquired with the epifluorescence microscope (BX60, Olympus) (see Part V.8.a), using the MWB filter block (Ex. 480-550 / Em. >590 nm) for both the anti-actin and the anti-tubulin.

5.1.1.12. Observation of endomembrane dynamic by FM4-64 staining on living cells

FM4-64FX (F34653, Invitrogen) stock solution were diluted to 385.1 µM in DMSO, and then diluted to 7.7 µM in NSWp as working solution. The coverslip was put on ice. About 50 µL of 7.7 µM were added at the centre of the coverslips, then mounted on the stage of the spinning disk confocal microscope, and the integration of the fluorochrome was followed for a few minute. The fluorochrome was excited with a Neon laser at 561 nm wavelength, and the emission bandwidth was set to 580-630 nm.

6. Cited references

Abenza JF, Couturier E, Dodgson J, Dickmann J, Chessel A, Dumais J, Salas REC. 2015. Wall mechanics and exocytosis define the shape of growth domains in fission yeast. Nature Communications 6, 8400.

Ackland JC, West JA, Pickett-Heaps J. 2007. Actin and Myosin Regulate Pseudopodia of Porphyra pulchella (rhodophyta) Archeospores. Journal of Phycology 43, 129–138.

Adler J, Shevchuk AI, Novak P, Korchev YE, Parmryd I. 2010. Plasma membrane topography and interpretation of single-particle tracks. Nature Methods 7, 170–171.

Ahmad IL, Ahmad MR. 2014. Trends in characterizing single cell's stiffness properties. Micro and Nano Systems Letters 2, 8.

Alessa L, Kropf DL. 1999. F-actin marks the rhizoid pole in living *Pelvetia compressa* zygotes. Development (Cambridge, England) 126, 201–9.

Alessa L, Oliveira L. 2001. Aluminum toxicity studies in *Vaucheria longicaulis* var. macounii (Xanthophyta, Tribophyceae). II. Effects on the F-actin array. Environmental and Experimental Botany 45, 223–237.

Aletta JM, Greene LA. 1988. Growth cone configuration and advance: a time-lapse study using video- enhanced differential interference contrast microscopy. Journal of Neuroscience 8, 1425–1435.

Ali O, Mirabet V, Godin C, Traas J. 2014. Physical Models of Plant Development. Annual Review of Cell and Developmental Biology 30, 59–78.

Ali O, Traas J. 2016. Force-Driven Polymerization and Turgor-Induced Wall Expansion. Trends in Plant Science 21, 398–409.

Allen RD. 1973. CHAPTER 7 - Biophysical Aspects of Pseudopodium Formation and Retraction. In: Jeon KW, ed. The Biology of Amoeba. Academic Press, 201–247.

Al-Zube LA, Robertson DJ, Edwards JN, Sun W, Cook DD. 2017. Measuring the compressive modulus of elasticity of pith-filled plant stems. Plant Methods 13, 99.

Aouar L, Chebli Y, Geitmann A. 2010. Morphogenesis of complex plant cell shapes: The mechanical role of crystalline cellulose in growing pollen tubes. Sexual Plant Reproduction 23, 15–27.

Arnold TM, Targett NM. 2003. To grow and defend: lack of tradeoffs for brown algal phlorotannins. Oikos 100, 406–408.

Bachewich CL, Heath IB. 1997. Differential cytoplasm-plasma membrane-cell wall adhesion patterns and their relationships to hyphal tip growth and organelle motility. Protoplasma 200, 71–86.

Baker JRJ, Evans LV. 1973. The ship fouling algaEctocarpus. Protoplasma 77, 1–13.

Baldauf SL. 2003. The Deep Roots of Eukaryotes. Science 300, 1703–1706.

Baldauf SL. 2008. An overview of the phylogeny and diversity of eukaryotes. Journal Of Systematics And Evolution 46, 263–273.

Bartnicki-García S. 1990. Role of vesicles in apical growth and a new mathematical model of hyphal morphogenesis. In: Heath IB, ed. Tip Growth in Plant and Fungal Cells. San

Diego, New York, Boston, London, Sydney, Tokyo, Toronto: Academic Press, Harcourt Brace Jovanovich, 211–232.

Bartnicki-Garcia S, Hergert F, Gierz G. 1989. Computer simulation of fungal morphogenesis and the mathematical basis for hyphal (tip) growth. Protoplasma 153, 46–57.

Bartnicki-Garcia S, Lippman E. 1972. The Bursting Tendency of Hyphal Tips of Fungi: Presumptive Evidence for a Delicate Balance between Wall Synthesis and Wall Lysis in Apical Growth. Journal of General Microbiology 73, 487–500.

Baskin TI. 2005. Anisotropic Expansion of the Plant Cell Wall. Annual Review of Cell and Developmental Biology 21, 203–222.

Benkert R, Obermeyer G, Bentrup F-W. 1997. The turgor pressure of growing lily pollen tubes. Protoplasma 198, 1–8.

Berepiki A, Lichius A, Read ND. 2011. Actin organization and dynamics in filamentous fungi. Nature Reviews Microbiology 9, 876–887.

Bernal R, Rojas ER, Dumais J. 2007. The mechanics of tip growth morphogenesis: what we have learned from rubber balloons. Journal of Mechanics of Materials and Structures 2, 1157–1168.

Betz T, Koch D, Lim D, Käs JA. 2009. Stochastic Actin Polymerization and Steady Retrograde Flow Determine Growth Cone Advancement. Biophysical Journal 96, 5130–5138.

Betz T, Lim D, Käs JA. 2006. Neuronal Growth: A Bistable Stochastic Process. Physical Review Letters 96, 098103.

Bezanilla M, Gladfelter AS, Kovar DR, Lee WL. 2015. Cytoskeletal dynamics: A view from the membrane. Journal of Cell Biology 209, 329–337.

Bidhendi AJ, Geitmann A. 2016. Relating the mechanics of the primary plant cell wall to morphogenesis. Journal of Experimental Botany 67, 449–461.

Bidhendi AJ, Geitmann A. 2018. Finite element modeling of shape changes in plant cells. Plant Physiology, 141, 41-56.

Bigan E. 2015. Thesis report. Minimal conditions for protocell growth. École Polytechnique. 196 p

Billoud B, Le Bail A, Charrier B. 2008. A stochastic 1D nearest-neighbour automaton models early development of the brown alga *Ectocarpus siliculosus*. Functional Plant Biology 35, 1014–1024.

Bisgrove SR. 2007. Cytoskeleton and early development in fucoid algae. Journal of Integrative Plant Biology 49, 1192–1198.

Bisgrove SR, Kropf DL. 2001. Cell wall deposition during morphogenesis in fucoid algae. Planta 212, 648–658.

Bogaert KA, Arun A, Coelho SM, De Clerck O. 2013. Brown algae as a model for plant organogenesis. In: De Smet I, ed. Plant Organogenesis: Methods and Potocols. New York: Springer Science+Business Media, 97–125.

Bogaert KA, Beeckman T, Clerck OD. 2017a. Two-step cell polarization in algal zygotes. Nature Plants 3, 16221.

Bogaert KA, Beeckman T, De Clerck O. 2017b. Egg activation-triggered shape change in the *Dictyota dichotoma* (Phaeophyceae) zygote is actin–myosin and secretion dependent. Annals of Botany, 1–10.

Bolduc JF, Lewis LJ, Aubin CE, Geitmann A. 2006. Finite-element analysis of geometrical factors in micro-indentation of pollen tubes. Biomechanics and Modeling in Mechanobiology 5, 227–236.

Boller ML, Carrington E. 2006. The hydrodynamic effects of shape and size change during reconfiguration of a flexible macroalga. The Journal of Experimental Biology 209, 1894–1903.

Boller ML, Carrington E. 2007. Interspecific comparison of hydrodynamic performance and structural properties among intertidal macroalgae. Journal of Experimental Biology 210, 1874–1884.

Bolte S, Talbot C, Boutte Y, Catrice O, Read ND, Satiat-Jeunemaitre B. 2004. FM-dyes as experimental probes for dissecting vesicle trafficking in living plant cells. Journal of Microscopy 214, 159–173.

Borhan S, Hesaraki S, Behnamghader AA, Ghasemi E. 2016. Rheological evaluations and in vitro studies of injectable bioactive glass–polycaprolactone–sodium alginate composites. Journal of Materials Science: Materials in Medicine 27, 1–15.

Bosch M, Cheung AY, Hepler PK. 2005. Pectin methylesterase, a regulator of pollen tube growth. Plant Physiology 138, 1334–1346.

Bosch M, Hepler PK. 2005. Pectin methylesterases and pectin dynamics in pollen tubes. The Plant Cell 17, 3219–3226.

Bou Daher F, Braybrook SA. 2015. How to let go: pectin and plant cell adhesion. Frontiers in Plant Science 6.

Bou Daher F, Geitmann A. 2011. Actin is Involved in Pollen Tube Tropism Through Redefining the Spatial Targeting of Secretory Vesicles - Bou Daher - 2011 - Traffic - Wiley Online Library. Traffic 12, 1537–1551.

Boudaoud A. 2003. Growth of Walled Cells: From Shells to Vesicles. Physical Review Letters 91, 018104.

Boudaoud A. 2010. An introduction to the mechanics of morphogenesis for plant biologists. Trends in Plant Science 15, 353–360.

Bove J, Vaillancourt B, Kroeger J, Hepler PK, Wiseman PW, Geitmann A. 2008. Magnitude and direction of vesicle dynamics in growing pollen tubes using spatiotemporal image correlation spectroscopy and fluorescence recovery after photobleaching. Plant physiology 147, 1646–1658.

Bowman SM, Free SJ. 2006. The structure and synthesis of the fungal cell wall. BioEssays 28, 799–808.

Boyer JS. 2009. Cell wall biosynthesis and the molecular mechanism of plant enlargement. Functional Plant Biology 36, 383–394.

Boyer JS. 2016. Enzyme-Less Growth in Chara and Terrestrial Plants. Frontiers in Plant Science 7, 866.

Braccini I, Grasso RP, Pérez S. 1999. Conformational and configurational features of acidic polysaccharides and their interactions with calcium ions: a molecular modeling investigation. Carbohydrate Research 317, 119–130.

Braidwood L, Breuer C, Sugimoto K. 2014. My body is a cage: Mechanisms and modulation of plant cell growth. New Phytologist 201, 388–402.

Braun M, Wasteneys GO. 1998. Distribution and dynamics of the cytoskeleton in graviresponding protonemata and rhizoids of characean algae: Exclusion of microtubules and a convergence of actin filaments in the apex suggest an actin-mediated gravitropism. Planta 205, 39–50.

Bray D. 1973. Model for Membrane Movements in the Neural Growth Cone. Nature 244, 93–96.

Bray D. 1979. Mechanical tension produced by nerve cells in tissue culture. Journal of Cell Science 37, 391–410.

Bray D. 1987. Growth cones: do they pull or are they pushed? Trends in Neurosciences 10, 431–434.

Bray D, White JG. 1988. Cortical flow in animal cells. Science 239, 883–888.

Braybrook SA. 2015. Measuring the elasticity of plant cells with atomic force microscopy. In: Paluch EK, ed. Methods in Cell Biology. Biophysical Methods in Cell Biology. Elsevier Ltd, 237–254.

Braybrook SA, Jönsson H. 2016. Shifting foundations: The mechanical cell wall and development. Current Opinion in Plant Biology 29, 115–120.

Burki F. 2014. The Eukaryotic Tree of Life from a Global Phylogenomic Perspective. Cold Spring Harbor Perspectives in Biology 6, a016147.

Burki F, Shalchian-Tabrizi K, Minge M, Skjæveland Å, Nikolaev SI, Jakobsen KS, Pawlowski J. 2007. Phylogenomics Reshuffles the Eukaryotic Supergroups. PLOS ONE 2, e790.

Burström HG. 1971. Wishful thinking of turgor. Nature 234, 488.

Butterfield NJ. 2000. *Bangiomorpha pubescens* n. gen., n. sp.: implications for the evolution of sex, multicellularity, and the Mesoproterozoic/Neoproterozoic radiation of eukaryotes. Paleobiology 26, 386–404.

Buxbaum RE, Heidemann SR. 1988. A thermodynamic model for force integration and microtubule assembly during axonal elongation. Journal of Theoretical Biology 134, 379–390.

Caffall KH, Mohnen D. 2009. The structure, function, and biosynthesis of plant cell wall pectic polysaccharides - ScienceDirect. Carbohydrate Research 334, 1879–1900.

Cai G, Faleri C, Casino CD, Emons AMC, Cresti M. 2011. Distribution of Callose Synthase, Cellulose Synthase, and Sucrose Synthase in Tobacco Pollen Tube Is Controlled in Dissimilar Ways by Actin Filaments and Microtubules. Plant Physiology 155, 1169–1190.

Cameron TA, Zupan JR, Zambryski PC. 2015. The essential features and modes of bacterial polar growth. Trends in Microbiology 23, 347–353.

Campàs O, Mahadevan L. 2009. Shape and dynamics of tip-growing cells. Current Biology 19, 2102–2107.

Campàs O, Rojas E, Dumais J, Mahadevan L. 2012. Strategies for cell shape control in tip-growing cells. American Journal of Botany 99, 1577–1582.

Carpita N, MCann M. 2000. Chapter 2 - The Cell Wall. In: Buchanan B, Gruissem W, In: Jones R, eds. Biochemistry and Molecular Biology of Pants.292.

Carrington E, Grace SP, Chopin T. 2001. Life History Phases and the Biomechanical Properties of the Red Alga *Chondrus crispus* (Rhodophyta). Journal of Phycology 37, 699–704.

Castle ES. 1937. Membrane tension and orientation of structure in the plant cell wall. Journal of Cellular and Comparative Physiology 10, 113–121.

Castle ES. 1958. The topography of tip growth in a plant cell. The Journal of General Physiology 41, 377–383.

Cava F, Kuru E, Brun YV, de Pedro MA. 2013. Modes of cell wall growth differentiation in rod-shaped bacteria. Current Opinion in Microbiology 16, 731–737.

Chapman VJ. 1962. Euphycophyta, Phaeophyceae. Macmillan and Co LTD ed. The algae. London: New York - St Martin's Press, 122–215.

Charras GT, Mitchison TJ, Mahadevan L. 2009. Animal cell hydraulics. Journal of Cell Science 122, 3233–41.

Charras GT, Yarrow JC, Horton MA, Mahadevan L, Mitchison TJ. 2005. Non-equilibration of hydrostatic pressure in blebbing cells. Nature 435, 365–369.

Charrier B, Coelho SM, Le Bail A, Tonon T, Michel G, Potin P, Kloareg B, Boyen C, Peters AF, Cock JM. 2008. Development and physiology of the brown alga Ectocarpus siliculosus two centuries of research. New Phytologist 177, 319–32.

Charrier B, Le Bail A, de Reviers B, Bail AL, Reviers BD. 2012. Plant Proteus: Brown algal morphological plasticity and underlying developmental mechanisms. Trends in Plant Science 17, 468–77.

Chebli Y, Geitmann A. 2017. Cellular growth in plants requires regulation of cell wall biochemistry. Current Opinion in Cell Biology 44, 28–35.

Chebli Y, Kaneda M, Zerzour R, Geitmann A. 2012. The cell wall of the *Arabidopsis* pollen tube–spatial distribution, recycling, and network formation of polysaccharides. Plant Physiology 160, 1940–55.

Chebli Y, Kroeger J, Geitmann A. 2013. Transport logistics in pollen tubes. Molecular Plant 6, 1037–1052.

Chen JCW. 1973. The kinetics of tip growth in the *Nitella* rhizoid. Plant Cell Physiol. 14, 631–640.

Chen X, Ebbole DJ, Wang Z. 2015. The exocyst complex: Delivery hub for morphogenesis and pathogenesis in filamentous fungi. Current Opinion in Plant Biology 28, 48–54.

Chen T, Teng N, Wu X, Wang Y, Tang W, Šamaj J, Baluška F, Lin J. 2007. Disruption of actin filaments by latrunculin B affects cell wall construction in *Picea meyeri* pollen tube by disturbing vesicle trafficking. Plant and Cell Physiology 48, 19–30.

Chengappa P, Sao K, Jones TM, Petrie RJ. 2018. Chapter Seven - Intracellular Pressure: A driver of cell morphology and movement. In: Galluzzi L, ed. International Review of Cell and Molecular Biology. Academic Press, 185–211.

Cheshire AC, Hallam ND. 1985. The environmental role of alginates in *Durvillaea potatorum* (Fucales, Phaeophyta). Phycologia 24, 147–153.

Cheung AY, Wu HM. 2008. Structural and Signaling Networks for the Polar Cell Growth Machinery in Pollen Tubes. Annual Review of Plant Biology, Vol 61 59, 547–572.

Cho H-T, Cosgrove DJ. 2002. Regulation of Root Hair Initiation and Expansin Gene Expression in Arabidopsis. The Plant Cell 14, 3237–3253.

Choi EY, Jeon KW. 1989. A spectrin-like protein present on membranes of Amoeba proteus as studied with monoclonal antibodies. Experimental Cell Research 185, 154–165.

Choi EY, Jeon KW. 1992. Role of spectrin in *Amoeba proteus*, as studied by microinjection of anti-spectrin monoclonal antibodies. Experimental Cell Research 199, 174–178.

Clarke JT, Warnock RCM, Donoghue PCJ. 2011. Establishing a time-scale for plant evolution. New Phytologist 192, 266–301.

Clayton MN. 1985. A critical investigation of the vegetative anatomy, growth and taxonomic affinities of *Adenocystis*, *Scytothamnus*, and *Splachnidium* (Phaeophyta). British Phycological Journal 20, 285–296.

Cleland R. 1971. Cell Wall Extension. Annual Review of Plant Physiology 22, 197–222.

Cock JM, Sterck L, Ahmed S, et al. 2012. The *Ectocarpus* Genome and Brown Algal Genomics. The Ectocarpus Genome Consortium. In: Piganeau G, ed. Advances in Botanical Research. Elsevier Ltd., 141–184.

Cock JM, Sterck L, Rouzé P, et al. 2010. The *Ectocarpus* genome and the independent evolution of multicellularity in brown algae. Nature 465, 617–21.

Coelho SM, Scornet D, Rousvoal S, Peters NT, Dartevelle L, Peters AF, Cock JM. 2012a. *Ectocarpus*: a model organism for the brown algae. Cold Spring Harbor Protocols 2012, 193–8.

Coelho SM, Scornet D, Rousvoal S, Peters NT, Dartevelle L, Peters AF, Cock JM. 2012b. How to cultivate *Ectocarpus*. Cold Spring Harbor Protocols 2012, 258–61.

Coelho SM, Scornet D, Rousvoal S, Peters N, Dartevelle L, Peters AF, Cock JM. 2012c. Genetic crosses between *Ectocarpus* strains. Cold Spring Harbor Protocols 2012, 262–5.

Coelho SM, Scornet D, Rousvoal S, Peters N, Dartevelle L, Peters AF, Cock JM. 2012d. Extraction of high-quality genomic DNA from Ectocarpus. Cold Spring Harbor Protocols 2012, 365–8.

Coelho SM, Scornet D, Rousvoal S, Peters N, Dartevelle L, Peters AF, Mark Cock J. 2012e. Isolation and regeneration of protoplasts from *Ectocarpus*. Cold Spring Harbor Protocols 7, 361–364.

Coelho SM, Scornet D, Rousvoal S, Peters N, Dartevelle L, Peters AF, Mark Cock J. 2012f. Immunostaining of *Ectocarpus* cells. Cold Spring Harbor Protocols 7, 369–372.

Coelho SM, Taylor AR, Ryan KP, Sousa-Pinto I, Brown MT, Brownlee C. 2002. Spatiotemporal patterning of reactive oxygen production and Ca^{2+} wave propagation in fucus rhizoid cells. The Plant Cell 14, 2369–2381.

Cole RA, Fowler JE. 2006. Polarized growth: maintaining focus on the tip. Current Opinion in Plant Biology 9, 579–588.

Condeelis J. 1993. Life at the Leading Edge: The Formation of Cell Protrusions. Annual Review of Cell Biology 9, 411–444.

Corellou F, Coelho SMB, Bouget F-Y, Brownlee C. 2005. Spatial re-organisation of cortical microtubules in vivo during polarisation and asymmetric division of *Fucus* zygotes. Journal of Cell Science 118, 2723–34.

Cormier A, Avia K, Sterck L, et al. 2017. Re-annotation, improved large-scale assembly and establishment of a catalogue of noncoding loci for the genome of the model brown alga Ectocarpus. New Phytologist 214, 219–232.

Cosgrove DJ. 1986. Biophysical control of plant cell growth. Annual Review of Plant Physiology 37, 377–405.

Cosgrove DJ. 1987. Wall relaxation and the driving forces for cell expansive growth. Plant Physiology 84, 561–4.

Cosgrove DJ. 1993a. Wall extensibility: its nature, measurement and relationship to plant cell growth. New Phytologist 124, 1–23.

Cosgrove DJ. 1993b. Water Uptake by Growing Cells: An Assessment of the Controlling Roles of Wall Relaxation, Solute Uptake, and Hydraulic Conductance. International Journal of Plant Sciences 154, 10–21.

Cosgrove DJ. 1993c. How Do Plant Cell Walls Extend? Plant Physiology 102, 1–6.

Cosgrove DJ. 1996. Plant cell enlargement and the action of expansins. BioEssays 18, 533–40.

Cosgrove DJ. 1997. Relaxation in a high-stress environment: the molecular bases of extensible cell walls and cell enlargement. The Plant Cell 9, 1031–1041.

Cosgrove DJ. 1999. Enzymes and other agents that enhance cell wall extensibility. Annual Review of Plant Physiology and Plant Molecular Biology 50, 391–417.

Cosgrove DJ. 2005. Growth of the plant cell wall. Nature reviews. Molecular Cell Biology 6, 850–861.

Cosgrove DJ. 2016a. Plant cell wall extensibility: connecting plant cell growth with cell wall structure, mechanics, and the action of wall- modifying enzymes. Journal of Experimental Botany 67, 463–476.

Cosgrove DJ. 2016b. Catalysts of plant cell wall loosening. F1000Research 5, 1–13.

Cosgrove DJ. 2018. Diffuse Growth of Plant Cell Walls. Plant Physiology 176, 16–27.

Craddock C, Lavagi I, Yang Z. 2012. New insights into Rho signaling from plant ROP/Rac GTPases. Trends in Cell Biology 22, 492–501.

Craigie JS, Morris ER, Rees DA, Thom D. 1984. Alginate block structure in phaeophyceae from Nova Scotia: Variation with species, environment and tissue-type. Carbohydrate Polymers 4, 237–252.

Cuadros TR, Skurtys O, Aguilera JM. 2012. Mechanical properties of calcium alginate fibers produced with a microfluidic device. Carbohydrate Polymers 89, 1198–1206.

Dardelle F, Lehner A, Ramdani Y, Bardor M, Lerouge P, Driouich A, Mollet J-C. 2010. Biochemical and Immunocytological Characterizations of *Arabidopsis* Pollen Tube Cell Wall. Plant Physiology 153, 1563–1576.

Davì V, Minc N. 2015. Mechanics and morphogenesis of fission yeast cells. Current Opinion in Microbiology 28, 36–45.

Davì V, Tanimoto H, Ershov D, Haupt A, De Belly H, Le Borgne R, Couturier E, Boudaoud A, Minc N. 2018. Mechanosensation Dynamically Coordinates Polar Growth and Cell Wall Assembly to Promote Cell Survival. Developmental Cell 45, 170-182.e7.

Davidson LA. 2017. Mechanical design in embryos: mechanical signalling, robustness and developmental defects. Philosophical Transactions of the Royal Society B: Biological Sciences 372, 20150516.

De Reviers B. 2003. *Biologie et phylogénie des algues*, Tome 2. Belin, Paris, 256 p.

Deniaud-Bouët E, Hardouin K, Potin P, Kloareg B, Hervé C. 2017. A review about brown algal cell walls and fucose-containing sulfated polysaccharides: Cell wall context, biomedical properties and key research challenges. Carbohydrate Polymers 175, 395–408.

Deniaud-Bouët E, Kervarec N, Michel G, Tonon T, Kloareg B, Hervé C. 2014a. Chemical and enzymatic fractionation of cell walls from Fucales: insights into the structure of the extracellular matrix of brown algae. Annals of botany 114, 1203–16.

Deniaud-Bouët E, Kervarec N, Michel G, Tonon T, Kloareg B, Hervé C. 2014b. Chemical and enzymatic fractionation of cell walls from Fucales: insights into the structure of the extracellular matrix of brown algae. Annals of Botany 114, 1203–16.

Dennerll TJ, Joshi HC, Steel VL, Buxbaum RE, Heidemann SR. 1988. Tension and compression in the cytoskeleton of PC-12 neurites. II: Quantitative measurements. The Journal of Cell Biology 107, 665–674.

Dennerll TJ, Lamoureux P, Buxbaum RE, Heidemann SR. 1989. The cytomechanics of axonal elongation and retraction. The Journal of Cell Biology 109, 3073–3083.

Denny M, Cowen B. 1997. Flow and flexibility. II. The roles of size and shape in determining wave forces on the bull kelp *Nereocystis luetkeana*. Journal of Experimental Biology 200, 3165–3183.

Denny M, Gaylord B. 2002. The mechanics of wave-swept algae. Journal of Experimental Biology 205, 1355–1362.

Dent EW, Gertler FB. 2003. Cytoskeletal dynamics and transport in growth cone motility and axon guidance. Neuron 40, 209–227.

Derksen J, Emons AM. 1990. Microtubules in tip growth systems. In: Heath IB, ed. Tip Growth in Plant and Fungal Cells. San Diego, New York, Boston, London, Sydney, Tokyo, Toronto: Academic Press, Harcourt Brace Jovanovich, 147–181.

Derksen J, Knuiman B, Hoedemaekers K, Guyon A, Bonhomme S, Pierson ES. 2002. Growth and cellular organization of *Arabidopsis* pollen tubes in vitro. Sexual Plant Reproduction 15, 133–139.

Derksen J, Rutten T, Lichtscheidl IK, Win AHN de, Pierson ES, Rongen G. 1995. Quantitative analysis of the distribution of organelles in tobacco pollen tubes: implications for exocytosis and endocytosis. Protoplasma 188, 267–276.

Diz-Muñoz A, Fletcher DA, Weiner OD. 2013. Use the force: membrane tension as an organizer of cell shape and motility. Trends in Cell Biology 23, 47–53.

Domozych DS, Fujimoto C, LaRue T. 2013. Polar Expansion Dynamics in the Plant Kingdom: A Diverse and Multifunctional Journey on the Path to Pollen Tubes. Plants 2, 148–173.

Donati I, Holtan S, Mørch YA, Borgogna M, Dentini M. 2005. New Hypothesis on the Role of Alternating Sequences in Calcium−Alginate Gels. Biomacromolecules 6, 1031–1040.

Draget KI, Skjåk Bræk G, Smidsrød O. 1994. Alginic acid gels: the effect of alginate chemical composition and molecular weight. Carbohydrate Polymers 25, 31–38.

Draget KI, Taylor C. 2011. Chemical, physical and biological properties of alginates and their biomedical implications. Food Hydrocolloids 25, 251–256.

Drake T, Vavylonis D. 2013. Model of fission yeast cell shape driven by membrane-bound growth factors and the cytoskeleton. PLoS Computational Biology 9, e1003287.

Dumais J. 2013. Modes of deformation of walled cells. Journal of Experimental Botany 64, 4684–4695.

Dumais J, Harrison LG. 2000. Whorl morphogenesis in the dasycladalean algae: the pattern formation viewpoint. Philosophical Transactions of the Royal Society B: Biological Sciences 355, 281–305.

Dumais J, Long SR, Shaw SL. 2004. The mechanics of surface expansion anisotropy in *Medicago truncatula* root hairs. Plant physiology 136, 3266–3275.

Dumais J, Shaw SL, Steele CR, Long SR, Ray PM. 2006. An anisotropic-viscoplastic model of plant cell morphogenesis by tip growth. International Journal of Developmental Biology 50, 209–222.

Dunn CW, Giribet G, Edgecombe GD, Hejnol A. 2014. Animal phylogeny and its evolutionary implications. Annual Review of Ecology, Evolution, and Systematics 45, 371–395.

Durand-Smet P, Chastrette N, Guiroy A, et al. 2014. A comparative mechanical analysis of plant and animal cells reveals convergence across kingdoms. Biophysical Journal 107, 2237–2244.

Eggen E, Niels de Keijzer M, Mulder BM, de Keijzer MN, Mulder BM, Niels de Keijzer M, Mulder BM. 2011. Self-regulation in tip-growth: The role of cell wall ageing. Journal of Theoretical Biology 283, 113–121.

Eklöf JM, Brumer H. 2010. The XTH Gene Family: An Update on Enzyme Structure, Function, and Phylogeny in Xyloglucan Remodeling. Plant Physiology 153, 456–466.

Ertesvåg H. 2015. Alginate-modifying enzymes: Biological roles and biotechnological uses. Frontiers in Microbiology 6, 1–10.

Fayant P, Girlanda O, Chebli Y, Aubin C-E, Villemure I, Geitmann A. 2010. Finite element model of polar growth in pollen tubes. The Plant cell 22, 2579–2593.

Fernandes AN, Chen X, Scotchford CA, Walker J, Wells DM, Roberts CJ, Everitt NM. 2012. Mechanical properties of epidermal cells of whole living roots of *Arabidopsis thaliana*: An atomic force microscopy study. Physical Review E - Statistical, Nonlinear, and Soft Matter Physics 85, 1–8.

Ficko-Blean E, Hervé C, Michel G. 2015. Sweet and sour sugars from the sea: the biosynthesis and remodeling of sulfated cell wall polysaccharides from marine macroalgae. Perspectives in Phycology, 51–64.

Fischl R, Bertelsen K, Gaillard F, Coelho S, Michel G, Klinger M, Boyen C, Czjzek M, Hervé C. 2016. The cell-wall active mannuronan C5-epimerases in the model brown alga *Ectocarpus*: From gene context to recombinant protein. Glycobiology 26, 973–983.

Flärdh K. 2003. Growth polarity and cell division in *Streptomyces*. Current Opinion in Microbiology 6, 564–571.

Flärdh K. 2010. Cell polarity and the control of apical growth in *Streptomyces*. Current Opinion in Microbiology 13, 758–765.

Flärdh K, Richards DM, Hempel AM, Howard M, Buttner MJ. 2012. Regulation of apical growth and hyphal branching in *Streptomyces*. Current Opinion in Microbiology 15, 737–743.

Forbes MA, Hallam ND. 1979. Embryogenesis and substratum adhesion in the brown alga *Hormosira banksii* (Turner) Decaisne. British Phycological Journal 14, 69–81.

Fowler JE, Quatrano RS. 1997. Plant cell morphogenesis: plasma membrane interactions with the cytoskeleton and cell wall. Annual Review of Cell and Developmental Biology 13, 697–743.

Fowler JE, Vejlupkova Z, Goodner BW, Lu G, Quatrano RS. 2004. Localization to the rhizoid tip implicates a *Fucus distichus* Rho family GTPase in a conserved cell polarity pathway. Planta 219, 856–866.

Franze K, Guck J. 2010. The biophysics of neuronal growth. Reports on Progress in Physics 73, 094601.

Frei E, Preston RD. 1962. Configuration of alginic acid in marine brown algae. Nature 196, 130–134.

Fritsch FE, Salisbury EJ. 1920. An introduction to the structure and reproduction of plants. London, Bell: G. Bell and Sons Ltd, 668 p.

Fuchino K, Bagchi S, Cantlay S, Sandblad L, Wu D, Bergman J, Kamali-Moghaddam M, Flärdh K, Ausmees N. 2013. Dynamic gradients of an intermediate filament-like cytoskeleton are recruited by a polarity landmark during apical growth. Proceedings of the National Academy of Sciences of the United States of America 110, E1889–97.

Fukui Y. 1993. Toward a New Concept of Cell Motility: Cytoskeletal Dynamics in Amoeboid Movement and Cell Division. In: Jeon KW & Jarvik J, eds. International Review of Cytology. Academic Press, 85–127.

Garrill A, Jackson SL, Lew RR, Heath IB. 1993. Ion channel activity and tip growth: tip-localized stretch-activated channels generate an essential Ca^{2+} gradient in the oomycete *Saprolegnia ferax*. European Journal of Cell Biology 60, 358–365.

Gavrilova OV, Rudanova EE. 2000. Apical Growth in Algae. Russian Journal of Plant Physiology 47, 789–795.

Gaylord B, Denny M. 1997. Flow and flexibility. I. Effects Of size, shape and stiffness in determining wave forces on the stipitate kelps *Eisenia arborea* and *Pterygophora californica*. Journal of Experimental Biology 200, 3141–3164.

Geitmann A. 2006a. Experimental approaches used to quantify physical parameters at cellular and subcellular levels. American Journal of Botany 93, 1380–1390.

Geitmann A. 2006b. Plant and fungal cytomechanics: quantifying and modeling cellular architecture. Canadian Journal of Botany 84, 581–593.

Geitmann A, Dumais J. 2009. Not-so-tip-growth. Plant Signaling & Behavior 4, 136–138.

Geitmann A, Ortega JKE. 2009. Mechanics and modeling of plant cell growth. Trends in Plant Science 14, 467–478.

Geitmann A, Parre E. 2004. The local cytomechanical properties of growing pollen tubes correspond to the axial distribution of structural cellular elements. Sexual Plant Reproduction 17, 9–16.

Geitmann A, Steer M. 2006. The Architecture and properties of the pollen tube cell wall. In: Malhó R, ed. Plant Cell Monographs. The Pollen Tube: A Cellular and Molecular Perspective. Berlin, Heidelberg: Springer Berlin Heidelberg, 177–200.

Gerard VA. 1987. Hydrodynamic streamlining of *Laminaria saccharina* Lamour. in response to mechanical stress. Journal of Experimental Marine Biology and Ecology 107, 237–244.

Gibbon BC, Kovar DR, Staiger CJ. 1999. Latrunculin B Has Different Effects on Pollen Germination and Tube Growth. The Plant Cell 11, 2349–2363.

Gierz G, Bartnicki-Garcia S. 2001. A three-dimensional model of fungal morphogenesis based on the vesicle supply center concept. Journal of theoretical biology 208, 151–164.

Gilroy S, Jones DL. 2000. Through form to function: Root hair development and nutrient uptake. Trends in Plant Science 5, 56–60.

Godfroy O, Uji T, Nagasato C, et al. 2017. DISTAG/TBCCd1 Is Required for Basal Cell Fate Determination in *Ectocarpus*. Plant Cell Advanced Publication.

Goldenbogen B, Giese W, Hemmen M, Uhlendorf J, Herrmann A, Klipp E. 2016. Dynamics of cell wall elasticity pattern shapes the cell during yeast mating morphogenesis. Open Biology 6, 160136.

Goriely A, Robertson-Tessi M, Tabor M, Vandiver R. 2008. Elastic Growth Models. In: Mondaini RP. In: Pardalos PM, eds. Applied Optimization. Mathematical Modelling of Biosystems. Berlin, Heidelberg: Springer Berlin Heidelberg, 1–44.

Goriely A, Tabor M. 2003a. Self-Similar Tip Growth in Filamentary Organisms. Physical Review Letters 90, 108101.

Goriely A, Tabor M. 2003b. Biomechanical models of hyphal growth in actinomycetes. Journal of Theoretical Biology 222, 211–218.

Goriely A, Tabor M. 2008. Mathematical modeling of hyphal tip growth. Fungal Biology Reviews 22, 77–83.

Goriely A, Tabor M, Tongen A. 2010. A Morpho-Elastic Model of Hyphal Tip Growth in Filamentous Organisms. IUATM Bookseries. IUATM Symposium on Cellular, Molecular and Tissue Mechanics.215–225.

Gossot O, Geitmann A. 2007. Pollen tube growth: Coping with mechanical obstacles involves the cytoskeleton. Planta 226, 405–416.

Grant GT, Morris ER, Rees DA, Smith PJC, Thom D. 1973. Biological interactions between polysaccharides and divalent cations: The egg-box model. FEBS Letters 32, 195–198.

Gray DI, Gooday GW, Prosser JI. 1990. Apical hyphal extension in *Streptomyces coelicolor* A3(2). Microbiology 136, 1077–1084.

Grębecki A. 1984. Relative motion in A*moeba proteus* in respect to the adhesion sites. I. Behavior of monotactic forms and the mechanism of fountain phenomenon. Protoplasma 123, 116–134.

Grębecki A. 1994. Membrane and cytoskeleton flow in motile cells with emphasis on the contribution of free-living amoebae. In: Jeon KW, Jarvik J, eds. International Review of Cytology. Academic Press, 37–80.

Green PB. 1962. Mechanism for Plant Cellular Morphogenesis. Science (New York, N.Y.) 138, 1404–1405.

Green PB. 1965. Pathways of cellular morphogenesis. A diversity in *Nitella*. Journal of Cell Biology 27, 343–363.

Green PB. 1969. Cell Morphogenesis. Annual Review of Plant Physiology 20, 365–394.

Green JJ, Cordero Cervantes D, Peters NT, Logan KO, Kropf DL. 2013. Dynamic microtubules and endomembrane cycling contribute to polarity establishment and early development of *Ectocarpus* mitospores. Protoplasma 250, 1035–1043.

Gu F, Nielsen E. 2013. Targeting and regulation of cell wall synthesis during tip growth in plants. Journal of Integrative Plant Biology 55, 835–846.

Gu Y, Vernoud V, Fu Y, Yang Z. 2003. ROP GTPase regulation of pollen tube growth through the dynamics of tip-localized F-actin. Journal of Experimental Botany 54, 93–101.

Guan Y, Guo J, Li H, Yang Z. 2013. Signaling in pollen tube growth: Crosstalk, feedback, and missing links. Molecular Plant 6, 1053–1064.

Guerriero G, Hausman JF, Cai G. 2014. No stress! relax! mechanisms governing growth and shape in plant cells. International Journal of Molecular Sciences 15, 5094–5114.

Guiry MD. 2012. How many species of algae are there? Journal of Phycology 48, 1057–1063.

Guiry MD, Guiry GM. 2018. Algaebase. World-Wide electronic publication. National University of Ireland, Galeway. AlgaeBase.

Gupta GD, Heath IB. 1997. Actin disruption by latrunculin B causes turgor-related changes in tip growth of *Saprolegnia ferax* hyphae. Fungal Genetics and Biology 21, 64–75.

Hable WE. 2014. Rac1 signaling in the establishment of the fucoid algal body plan. Frontiers in Plant Science 5, 1–6.

Hable WE, Kropf DL. 1998. Roles of secretion and the cytoskeleton in cell adhesion and polarity establishment in *Pelvetia compressa* zygotes. Developmental Biology 198, 45–56.

Hable WE, Kropf DL. 2005. The Arp2/3 complex nucleates actin arrays during zygote polarity establishment and growth. Cell Motility and the Cytoskeleton 61, 9–20.

Hable WE, Miller NR, Kropf DL. 2003. Polarity establishment requires dynamic actin in fucoid zygotes. Protoplasma 221, 193–204.

Hale BB. 2001. Macroalgal materials: Foiling fracture and fatigue from fluid forces.

Hamant O, Haswell ES. 2017. Life behind the wall: sensing mechanical cues in plants. BMC Biology 15, 59.

Hamant O, Traas J. 2010. The mechanics behind plant development. New Phytologist 185, 369–385.

Haneef M, Ceseracciu L, Canale C, Bayer IS, Heredia-Guerrero JA, Athanassiou A. 2017. Advanced Materials From Fungal Mycelium: Fabrication and Tuning of Physical Properties. Scientific Reports 7, 41292.

Harder DL, Hurd CL, Speck T. 2006. Comparison of mechanical properties of four large, wave-exposed seaweeds. American Journal of Botany 93, 1426–1432.

Harmer S, Orford S, Timmis J. 2002. Characterisation of six α-expansin genes in *Gossypium hirsutum* (upland cotton). Molecular Genetics and Genomics 268, 1–9.

Harold FM. 1990. To shape a cell: an inquiry into the causes of morphogenesis of microorganisms. Microbiological Reviews 54, 381–431.

Harold FM. 1997. How hyphae grow: morphogenesis explained? Protoplasma 197, 137–147.

Harold FM. 2002. Force and compliance: Rethinking morphogenesis in walled cells. Fungal Genetics and Biology 37, 271–282.

Harold FM, Harold RL, Money NP. 1995. What forces drive cell wall expansion? Canadian Journal of Botany 73, 379–383.

Harold RL, Money NP, Harold FM. 1996. Growth and morphogenesis in *Saprolegnia ferax*: is turgor required? Protoplasma 191, 105–114.

Harris SD. 2011. Hyphal morphogenesis: an evolutionary perspective. Fungal Biology 115, 475–484.

Harris SD, Momany M. 2004. Polarity in filamentous fungi: Moving beyond the yeast paradigm. Fungal Genetics and Biology 41, 391–400.

Harris SD, Read ND, Roberson RW, Shaw B, Seiler S, Plamann M, Momany M. 2005. Polarisome Meets Spitzenkörper: Microscopy , Genetics , and Genomics Converge. Eukaryotic Cell 4, 225–229.

Haug A, Larsen B. 1969a. Biosynthesis of alginate. Epimerisation of D-mannuronic to L-guluronic acid residues in the polymer chain. Biochimica et biophysica acta 192, 557–559.

Haug A, Larsen B. 1969b. Biosynthesis of alginate. Epimerisation of D-mannuronic to L-guluronic acid residues in the polymer chain. Biochimica et Biophysica Acta 192, 557–559.

Haug A, Larsen B, Smidsrød O. 1966. A study of the constitution of alginic acid by partial acid hydrolysis. Acta Chemica Scandinavica 20, 183–190.

Haug A, Larsen B, Smidsrød O. 1974. Uronic acid sequence in alginate form different sources. Carbohydrate Research 32, 217–225.

Heath IB. 1987. Preservation of a labile cortical array of actin filaments in growing hyphal tips of the fungus *Saprolegnia ferax*. European Journal of Cell Biology 44, 10–16.

Heath IB (Ed.). 1990. Tip Growth in Plant and Fungal Cells. San Diego, New York, Boston, London, Sydney, Tokyo, Toronto: Harcourt Brace Jovanocich.

Heath IB, Gupta G, Bai S. 2000. Plasma membrane-adjacent actin filaments, but not microtubules, are essential for both polarization and hyphal tip morphogenesis in *Saprolegnia ferax* and *Neurospora crassa*. Fungal Genetics and Biology 30, 45–62.

Heath IB, Kaminskyj SGW. 1989. The organization of tip-growth-related organelles and microtubules revealed by quantitative analysis of freeze-substituted oomycete hyphae. Journal of Cell Science 93, 41–52.

Heath IB, Steinberg G. 1999. Mechanisms of hyphal tip growth: tube dwelling amebae revisited. Fungal Genetics and Biology 28, 79–93.

Heesch S, Cho GY, Peters AF, et al. 2010. A sequence-tagged genetic map for the brown alga *Ectocarpus siliculosus* provides large-scale assembly of the genome sequence. New Phytologist 188, 42–51.

Heidemann SR. 1990. Neuronal tip-growth. In: Heath IB, ed. Tip Growth in Plant and Fungal Cells. San Diego, New York, Boston, London, Sydney, Tokyo, Toronto: Harcourt Brace Jovanocich, 285–316.

Heidemann SR. 1996. Cytoplasmic Mechanisms of Axonal and Dendritic Growth in Neurons. In: Jeon KW, ed. International Review of Cytology. Academic Press, 235–296.

Heidemann SR, Buxbaum RE. 1998. Cell Crawling: First the Motor, Now the Transmission. The Journal of Cell Biology 141, 1–4.

Hejnowicz Z, Heinemann B, Sievers A. 1977. Tip growth: Patterns of growth rate and stress in the *Chara* rhizoid. Zeitschrift für Pflanzenphysiologie 81, 409–424.

Hellewell SB, Taylor DL. 1979. The solation-contraction coupling hypothesis of cell movement. University of Tokyo. Press.

Henry CA, Jordan JR, Kropf DL. 1996. Localized membrane-wall adhesions in Pelvetia zygotes. Protoplasma 190, 39–52.

Hepler PK, Kunkel JG, Rounds CM, Winship LJ. 2012. Calcium entry into pollen tubes. Trends in Plant Science 17, 32–38.

Hepler PK, Rounds CM, Winship LJ. 2013. Control of cell wall extensibility during pollen tube growth. Molecular Plant 6, 998–1017.

Hervé C, Siméon A, Jam M, et al. 2016a. Arabinogalactan proteins have deep roots in eukaryotes identification of genes and epitopes in brown algae and their role in *Fucus serratus* embryo development.pdf. New Phytologist 209, 1428–1441.

Hervé C, Siméon A, Jam M, et al. 2016b. Arabinogalactan proteins have deep roots in eukaryotes. Identification of genes and epitopes in brown algae and their role in *Fucus serratus* embryo development. New Phytologist 209, 1428–1441.

Hill R. 1998. The mathematical theory of plasticity. Clarendon Press.

Honkanen S, Dolan L. 2016. Growth regulation in tip-growing cells that develop on the epidermis. Current Opinion in Plant Biology 34, 77–83.

Honkanen S, Jones VAS, Morieri G, Champion C, Hetherington AJ, Kelly S, Proust H, Saint-Marcoux D, Prescott H, Dolan L. 2016. The mechanism forming the cell

surface of tip-growing rooting cells is conserved among land plants. Current Biology 26, 3238–3244.

Houk AR, Jilkine A, Mejean CO, Boltyanskiy R, Dufresne ER, Angenent SB, Altschuler SJ, Wu LF, Weiner OD. 2012. Membrane tension maintains cell polarity by confining signals to the leading edge during neutrophil migration. Cell 148, 175–188.

Hu H, Zhang R, Feng S, et al. 2018. Three AtCesA6-like members enhance biomass production by distinctively promoting cell growth in *Arabidopsis*. Plant Biotechnology Journal 16, 976–988.

Ingber DE. 1997. Tensegrity: The Architectural Basis of Cellular Mechanotransduction. Annual Review of Physiology 59, 575–599.

Insall RH, Machesky LM. 2009. Actin Dynamics at the Leading Edge: From Simple Machinery to Complex Networks. Developmental Cell 17, 310–322.

Ishikawa M, Nisizawa K. 1981. Polymannuronic Acid 5-Epimerase Activities in Several Brown Algae and its localisation in Frond. Bulletin of the Japan Society of Fishering Science 47, 889–893.

Ivakov AA, Flis A, Apelt F, Fuenfgeld M, Scherer U, Stitt M, Kragler F, Vissenberg K, Persson S, Suslov D. 2017. Cellulose synthesis and cell expansion are regulated by different mechanisms in growing *Arabidopsis* hypocotyls. The Plant Cell.

Jackson SL, Heath IB. 1989. Effects of exogenous calcium ions on tip growth, intracellular Ca^{2+} concentration, and actin arrays in hyphae of the fungus *Saprolegnia ferax*. Experimental Mycology 13, 1–12.

Jackson SL, Heath IB. 1990. Evidence that actin reinforces the extensible hyphal apex of the oomycete *Saprolegnia ferax*. Protoplasma 157, 144–153.

Jackson SL, Heath IB. 1993a. UV microirradiation implicates F-actin in reinforcing growing hyphal tips. Protoplasma 175, 67–74.

Jackson SL, Heath IB. 1993b. The dynamic behavior of cytoplasmic F-actin in growing hyphae. Protoplasma 173, 23–34.

Janmey P. 1995. Cell Membranes and the Cytoskeleton. In: Lipowsky, R., Sackmann E, eds. Handbook of Biological Physics: Structure and Dynamics of Membranes From Cells to Vesicles. Elsevier Science, 805–849.

Janson LW, Taylor DL. 1993. In vitro models of tail contraction and cytoplasmic streaming in amoeboid cells. The Journal of Cell Biology 123, 345–356.

Jia F, Ben Amar M, Billoud B, Charrier B. 2017. Morphoelasticity in the development of brown alga *Ectocarpus siliculosus*: from cell rounding to branching. Journal of The Royal Society Interface 14, 20160596.

Johnson A, Koehl M. 1994. Maintenance of dynamic strain similarity and environmental stress factor in different flow habitats: thallus allometry and material properties of a giant kelp. Journal of Experimental Biology 195, 381–410.

Jothisaraswathi S, Babu B, Rengasamy R. 2006. Seasonal studies on alginate and its composition II: *Turbinaria conoides* (J.Ag.) Kütz. (Fucales, Phaeophyceae). Journal of Applied Phycology 18, 161.

Julien J-D, Boudaoud A. 2018. Elongation and shape changes in organisms with cell walls: a dialogue between experiments and models. The Cell Surface 1, 34–42.

Kaminskyj SG, Heath IB. 1995. Integrin and spectrin homologues, and cytoplasm-wall adhesion in tip growth. Journal of Cell Science 108, 849–856.

Karyophyllis D, Galatis B, Katsaros C. 1997. Centrosome and microtubule dynamics in apical cells of *Sphacelaria rigidula* (Phaeophyceae) treated with nocodazole. Protoplasma 199, 161–172.

Karyophyllis D, Katsaros C, Dimitriadis I, Galatis B. 2000a. F-Actin organization during the cell cycle of *Sphacelaria rigidula* (Phaeophyceae). European Journal of Phycology 35, 25–33.

Karyophyllis D, Katsaros C, Galatis B. 2000b. F-actin involvement in apical cell morphogenesis of *Sphacelaria rigidula* (Phaeophyceae): mutual alignment between cortical actin filaments and cellulose microfibrils. European Journal of Phycology 35, 195–203.

Kasham Y, Groweiss A, Shmueli U. 1981. Latrunculin, a new 2-thiazolidinone macrolide from the marine sponge *Latrunculia magnifica.* Toxicon 19, 437.

Kataoka H. 1982. Colchicine-induced expansion of Vaucheria cell apex. Alteration from isotropic to transversally anisotropic growth. The Botanical Magazine Tokyo 95, 317–330.

Katsaros CI. 1980. Thesis report. An ultrastructural study of the morphogenesis of the thallus of five brown algal species. University of Athens, 298 p.

Katsaros CI. 1992. Immunofluorescence Study of Microtubule Organization in Some Polarized Cell-Types of Selected Brown-Algae. Botanica Acta 105, 400–406.

Katsaros CI. 1995. Apical cells of brown algae with particular reference to Sphacelariales, Dictyotales and Fucales. Phycological Research 43, 43–59.

Katsaros C, Galatis B. 1985. Ultrastructural studies on thallus development in *Dictyota dichotoma* (Phaeophyta, Dictyotales). British Phycological Journal 20, 263–276.

Katsaros C, Galatis B. 1988. Thallus development in *Dictyopteris membranacea* (Phaeophyta, Dictyotales). British Phycological Journal 23, 71–88.

Katsaros C, Galatis B. 1990. Thallus development in *Halopteris filicina* (Phaeophyceae, Sphacelariales). British Phycological Journal 25, 63–74.

Katsaros C, Galatis B. 1992. Immunofluorescence and electron-microscopic studies of microtubule organization during the cell-cycle of *Dictyota dichotoma* (Phaeophyta, Dictyotales). Protoplasma 169, 75–84.

Katsaros C, Galatis B, Mitrakos K. 1983. Fine Structural Studies on the Interphase and Dividing Apical Cells of *Sphacelaria Tribuloides* (Phaeophyta). Journal of Phycology 19, 16–30.

Katsaros C, Karyophyllis DA, Galatis BD. 2002. Cortical F-actin underlies cellulose microfibril patterning in brown algal cells. Phycologia 41, 178–183.

Katsaros C, Karyophyllis D, Galatis B. 2003. F-actin cytoskeleton and cell wall morphogenesis in brown algae. Cell Biology International 27, 209–210.

Katsaros C, Karyophyllis D, Galatis B. 2006. Cytoskeleton and morphogenesis in brown algae. Annals of Botany 97, 679–693.

Katsaros C, Kreimer G, Melkonian M. 1991. Localization of tubulin and a centrin-homologue in vegetative cells and developing gametangia of *Ectocarpus siliculosus* (Dillw.) Lyngb. (Phaeophyceae, Ectocarpales). Botanica Acta 104, 87–92.

Katsaros C, Reiss HD, Schnepf E. 1996. Freeze-fracture studies in brown algae: putative cellulose-synthesizing complexes on the plasma membrane. European Journal of Phycology 31, 41–48.

Kenrick P, Crane PR. 1997. The origin and early evolution of plants on land. Nature 389, 33–39.

Ketelaar T. 2002. Thesis report. Spatial organisation of cell expansion by the cytoskeleton. Wageningen University, 137 p.

Ketelaar T, Meijer HJG, Spiekerman M, Weide R, Govers F. 2012. Effects of latrunculin B on the actin cytoskeleton and hyphal growth in *Phytophthora infestans*. Fungal Genetics and Biology 49, 1014–1022.

Kierzkowski D, Nakayama N, Routier-Kierzkowska A-L, Weber A, Bayer E, Schorderet M, Reinhardt D, Kuhlemeier C, Smith RS. 2012. Elastic domains regulate growth and organogenesis in the plant shoot apical meristem. Science 335, 1096–1099.

Kim JH, Ren Y, Ng WP, et al. 2015. Mechanical tension drives cell membrane fusion. Developmental Cell 32, 561–573.

Kitzes JA, Denny MW. 2005. Red algae respond to waves: morphological and mechanical variation in *Mastocarpus papillatus* along a gradient of force. The Biological Bulletin 208, 114–119.

Klahre U, Kost B. 2006. Tobacco RhoGTPase ACTIVATING PROTEIN1 spatially restricts signaling of RAC/Rop to the apex of pollen tubes. Plant Cell 18, 3033–3046.

Kloareg B, Quatrano RS. 1988. Structure of the cell walls of marine algae and ecophysiological functions of the matrix polysaccharides. Oceanography and Marine Biology - An Annual Review. Oceanography and Marine Biology: An Annual Review, Volume 26. Margaret Barnes, 296–315.

Knechtle P, Wendland J, Philippsen P. 2006. The SH3/PH domain protein AgBoi1/2 collaborates with the Rho-type GTPase AgRho3 to prevent nonpolar growth at hyphal tips of Ashbya gossypii. Eukaryotic Cell 5, 1635–1647.

Knoblauch J, Tepler Drobnitch S, Peters WS, Knoblauch M, Drobnitch ST, Peters WS, Knoblauch M, Tepler Drobnitch S, Peters WS, Knoblauch M. 2016. In situ microscopy reveals reversible cell wall swelling in kelp sieve tubes: one mechanism for turgor generation and flow control? Plant, Cell and Environment 39, 1727–1736.

Knox JP. 2008. Revealing the structural and functional diversity of plant cell walls. Current Opinion in Plant Biology 11, 308–313.

Koch AL. 1983. The Surface Stress Theory of Microbial Morphogenesis. In: Rose AH, Morris JG, Tempest DW, eds. Advances in Microbial Physiology. Academic Press, 301–366.

Koch AL. 1994. The problem of hyphal growth in Streptomyces and Fungi. Journal of Theoretical Biology, 137–150.

Koehl MAR. 1984. How Do Benthic Organisms Withstand Moving Water? Integrative and Comparative Biology 24, 57–70.

Koehl MAR, Silk WK, Liang H, Mahadevan L. 2008. How kelp produce blade shapes suited to different flow regimes: A new wrinkle. Integrative and Comparative Biology 48, 834–851.

Koehl MAR, Wainwright SA. 1977. Mechanical adaptations of a giant kelp. Limnology and Oceanography 22, 1067–1071.

Kost B. 2008. Spatial control of Rho (Rac-Rop) signaling in tip-growing plant cells. Trends in Cell Biology 18, 119–127.

Kost B. 2010. Regulatory and Cellular Functions of Plant RhoGAPs and RhoGDIs. Signaling and Communication in Plants. Integrated G Proteins Signaling in Plants. Springer, Berlin, Heidelberg, 27–48.

Kost B, Lemichez E, Spielhofer P, Hong Y, Tolias K, Carpenter C, Chua N. 1999. Rac homologues and compartmentalized phosphatidylinositol 4,5-biphosphate act in a common pathway to regulate polar pollen tube growth. The Journal of cell biology 145, 317–330.

Kots K, Meijer HJG, Bouwmeester K, Govers F, Ketelaar T. 2017. Filamentous actin accumulates during plant cell penetration and cell wall plug formation in *Phytophthora infestans*. Cellular and Molecular Life Science 74, 909–920.

Krause M, Gautreau A. 2014. Steering cell migration: lamellipodium dynamics and the regulation of directional persistence. Nature Reviews Molecular Cell Biology 15, 577–590.

Kroeger J, Geitmann A. 2012a. The pollen tube paradigm revisited. Current Opinion in Plant Biology 15, 618–624.

Kroeger JH, Geitmann A. 2012b. Pollen tube growth: Getting a grip on cell biology through modeling. Mechanics Research Communications 42, 32–39.

Kropf DL. 1992. Establishment and expression of cellular polarity in fucoid zygotes. Microbiological Reviews 56, 316–39.

Kropf DL, Berge SK, Quatrano RS. 1989. Actin Localization during Fucus Embryogenesis. The Plant cell 1, 191–200.

Kropf DL, Bisgrove SR, Hable WE. 1998. Cytoskeletal control of polar growth in plant cells. Current Opinion in Cell Biology 10, 117–122.

Kropf DL, Kloareg B, Quatrano RS. 1988. Cell wall is required for fixation of the embryonic axis in *Fucus* zygotes. Science 239, 187–190.

La Barre S, Potin P, Leblanc C, Delage L. 2010. The halogenated metabolism of brown algae (Phaeophyta), its biological importance and its environmental significance. Marine Drugs 8, 988–1010.

Lamoureux P, Buxbaum RE, Heidemann SR. 1989. Direct evidence that growth cones pull. Nature 340, 159–162.

Lancelle SA, Hepler PK. 1992. Ultrastructure of freeze-substituted pollen tubes of *Lilium longiflorum*. Protoplasma 167, 215–230.

Landis SC. 1983. Neuronal growth cones. Annual Review of Physiology 45, 567–580.

Larsen BE, Bjørnstad J, Pettersen EO, Tønnesen HH, Melvik JE. 2015. Rheological characterization of an injectable alginate gel system. BMC Biotechnology 15, 29.

Lauffenburger DA, Horwitz AF. 1996. Cell migration: a physically integrated molecular process. Cell 84, 359–369.

Lazzaro MD, Donohue JM, Soodavar FM. 2003. Disruption of cellulose synthesis by isoxaben causes tip swelling and disorganizes cortical microtubules in elongating conifer pollen tubes. Protoplasma 220, 201–207.

Le Bail A. 2010. Thesis report. Morphogenèse précoce de l'algue brune *Ectocarpus*. Université Pierre et Marie Curie, 222p.

Le Bail A, Billoud B, Kowalczyk N, et al. 2010. Auxin metabolism and function in the multicellular brown alga *Ectocarpus siliculosus*. Plant Physiology 153, 128–144.

Le Bail A, Billoud B, Le Panse S, Chenivesse S, Charrier B. 2011. ETOILE regulates developmental patterning in the filamentous brown alga *Ectocarpus siliculosus*. The Plant cell 23, 1666–78.

Le Bail A, Billoud B, Maisonneuve C, Peters AF, Mark Cock J, Charrier B. 2008. Early development pattern of the brown alga *Ectocarpus siliculosus* (Ectocarpales, Phaeophyceae) sporophyte. Journal of Phycology 44, 1269–1281.

Le Bail A, Charrier B. 2013. Culture Methods and Mutant Generation in the Filamentous Brown Algae *Ectocarpus siliculosus*. Methods in Molecular Biology. Plant Organogenesis: Methods and Protocols. Ive de Smet, 323–332.

Lecuit T, Lenne P-F, Munro E. 2011. Force generation, transmission, and integration during vell and tissue morphogenesis. Annual Review of Cell and Developmental Biology 27, 157–184.

Lee YJ, Yang Z. 2008. Tip growth: signaling in the apical dome. Current Opinion in Plant Biology 11, 662–671.

Leliaert F, Clerck OD. 2017. Refining species boundaries in algae. Journal of Phycology 53, 12–16.

Leliaert F, Smith DR, Moreau H, Herron MD, Verbruggen H, Delwiche CF, De Clerck O. 2012. Phylogeny and molecular evolution of the green algae. Critical Reviews in Plant Sciences 31, 1–46.

Levental I, Veatch SL. 2016. The continuing mystery of lipid rafts. Journal of Molecular Biology 428, 4749–4764.

Levesque-Tremblay G, Pelloux J, Braybrook SA, Müller K. 2015. Tuning of pectin methylesterification: consequences for cell wall biomechanics and development. Planta 242, 791–811.

Lew RR. 2005. Mass flow and pressure-driven hyphal extension in *Neurospora crassa*. Microbiology 151, 2685–2692.

Lew RR. 2011. How does a hypha grow? The biophysics of pressurized growth in fungi. Nature Reviews Microbiology 9, 509–518.

Li L, Saga N, Mikami K. 2008. Phosphatidylinositol 3-kinase activity and asymmetrical accumulation of F-actin are necessary for establishment of cell polarity in the early development of monospores from the marine red alga *Porphyra yezoensis*. Journal of Experimental Botany 59, 3575–3586.

Lieber AD, Yehudai-Resheff S, Barnhart EL, Theriot JA, Keren K. 2013. Membrane tension in rapidly moving cells is determined by cytoskeletal forces. Current Biology 23, 1409–1417.

Linardić M. 2018. The role of brown algal cell walls in morphogenesis and development.

Linardić M, Braybrook SA. 2017. Towards an understanding of spiral patterning in the *Sargassum muticum* shoot apex. Scientific Reports 7, 13887.

Lintilhac PM. 2014. The problem of morphogenesis: Unscripted biophysical control systems in plants. Protoplasma 251, 25–36.

Lockhart JA. 1965. An analysis of irreversible plant cell elongation. Journal of theoretical biology 8, 264–275.

Lockhart JA, Bretz C, Kenner R. 1967. An analysis of cell wall extension. Annals of the New York Academy of Sciences 144, 19–33.

Lovy-Wheeler A, Wilsen KL, Baskin TI, Hepler PK. 2005. Enhanced fixation reveals the apical cortical fringe of actin filaments as a consistent feature of the pollen tube. Planta 221, 95–104.

Lubsch A, Timmermans K. 2017. Texture analysis of *Laminaria digitata* (Phaeophyceae) thallus reveals trade-off between tissue tensile strength and toughness along lamina. Botanica Marina 60, 229–237.

Lüder UH, Clayton MN. 2004. Induction of phlorotannins in the brown macroalga *Ecklonia radiata* (Laminariales, Phaeophyta) in response to simulated herbivory—the first microscopic study. Planta 218, 928–937.

Ma H, Snook LA, Kaminskyj SGW, Dahms TES. 2005. Surface ultrastructure and elasticity in growing tips and mature regions of *Aspergillus* hyphae describe wall maturation. Microbiology 151, 3679–3688.

Mabeau S, Kloareg B. 1987. Isolation and analysis of the cell walls of brown algae: *Fucus spiralis*, *F. ceranoides*, *F. vesiculosus*, *F. serratus*, *Bifurcaria bifurcata* and *Laminaria digitata*. Journal of Experimental Botany 38, 1573–1580.

Madgwick J, Haug A, Larsen B. 1973. Polymannuronic acid 5-epimerase from the marine alga *Pelvetia canaliculata* (L.) Dcne. et Thur.. Acta Chemica Scandinavica 27, 3592–3594.

Martin C, Bhatt K, Baumann K. 2001. Shaping in plant cells. Current Opinion in Plant Biology 4, 540–549.

Martone PT, Kost L, Boller M. 2012. Drag reduction in wave-swept macroalgae: Alternative strategies and new predictions. American Journal of Botany 99, 806–815.

Mathur J. 2005. Conservation of boundary extension mechanisms between plants and animals. The Journal of Cell Biology 168, 679–682.

Mathur J. 2006. Local interactions shape plant cells. Current Opinion in Cell Biology 18, 40–46.

Mathur J, Spielhofer P, Kost B, Chua N. 1999. The actin cytoskeleton is required to elaborate and maintain spatial patterning during trichome cell morphogenesis in *Arabidopsis thaliana*. Development 126, 5559–5568.

McHugh DJ. 2003. A guide to the seaweed industry. Rome: Food and Agriculture Organization of the United Nations.

McKee JWA, Kavalieris L, Brasch DJ, Brown MT, Melton LD. 1992. Alginate content and composition of *Macrocystis pyrifera* from New Zealand. Journal of Applied Phycology 4, 357–369.

McKenna ST, Kunkel JG, Bosch M, Rounds CM, Vidali L, Winship LJ, Hepler PK. 2009. Exocytosis precedes and predicts the increase in growth in oscillating pollen tubes. The Plant Cell 21, 3026–3040.

Meijer HJG, Hua C, Kots K, Ketelaar T, Govers F. 2014. Actin dynamics in *Phytophthora infestans*; rapidly reorganizing cables and immobile, long-lived plaques. Cellular Microbiology 16, 948–961.

Menand B, Calder G, Dolan L. 2007. Both chloronemal and caulonemal cells expand by tip growth in the moss Physcomitrella patens. Journal of Experimental Botany 58, 1843–1849.

Menzel D. 1996. The role of the cytoskeleton in polarity and rnorphogenesis of algal cells. Current Opinion in Cell Biology 8, 38–42.

Mermelstein CS, Rodrigues APM, Einicker-Lamas M, Navarrete RE de B, Farina M, Costa ML. 1998. Distribution of F-actin, α-actinin, tropomyosin, tubulin and organelles in Euglena gracilis by immunofluorescence microscopy. Tissue and Cell 30, 545–553.

Meyers MA, Chawla KK. 2008. *Mechanical behavior of materials*. Cambridge; New York: Cambridge University Press.

Michel G, Tonon T, Scornet D, Cock JM, Kloareg B. 2010a. The cell wall polysaccharide metabolism of the brown alga *Ectocarpus siliculosus*. Insights into the evolution of extracellular matrix polysaccharides in Eukaryotes. New Phytologist 188, 82–97.

Milani P, Braybrook SA, Boudaoud A. 2013. Shrinking the hammer: Micromechanical approaches to morphogenesis. Journal of Experimental Botany 64, 4651–4662.

Miller IJ. 1996. Alginate composition of some New Zealand brown seaweeds. Phytochemistry 41, 1315–1317.

Minc N, Boudaoud A, Chang F. 2009. Mechanical forces of fission yeast growth. Current Biology 19, 1096–1101.

Mine I, Menzel D, Okuda K. 2008. Morphogenesis in giant-celled algae. International Review of Cell and Molecular Biology 266, 37–83.

Mine I, Okuda K. 2003. Extensibility of isolated cell walls in the giant tip-growing cells of the xanthophycean alga *Vaucheria terrestris*. Planta 217, 425–435.

Mine I, Takezaki N, Sekida S, Okuda K. 2007. Cell wall extensibility during branch formation in the xanthophycean alga *Vaucheria terrestris*. Planta 226, 971–979.

Mirabet V, Das P, Boudaoud A, Hamant O. 2011. The role of mechanical forces in plant morphogenesis. Annual Review of Plant Biology 62, 365–385.

Mishev K, Dejonghe W, Russinova E. 2013. Small molecules for dissecting endomembrane trafficking: A Cross-Systems View. Chemistry & Biology 20, 475–486.

Mitchison TJ, Cramer LP. 1996. Actin-based cell motility and cell locomotion. Cell 84, 371–379.

Mogilner A, Oster G. 1996. Cell motility driven by actin polymerization. Biophysical Journal 71, 3030–3045.

Mohnen D. 2008. Pectin structure and biosynthesis. Current Opinion in Plant Biology 11, 266–277.

Mollet J-C, Leroux C, Dardelle F, Lehner A. 2013. Cell wall composition, biosynthesis and remodeling during pollen tube growth. Plants 2, 107–147.

Money N. 1997. Wishful thinking of turgor revisited: the mechanics of fungal growth. Fungal Genetics and Biology 21, 173–187.

Money NP. 1999. On the origin and functions of hyphal walls and turgor pressure. Mycological Research 103, 1360.

Money NP. 2008. Insights on the mechanics of hyphal growth. Fungal Biology Reviews 22, 71–76.

Money NP, Davis CM, Ravishankar J. P. 2004. Biomechanical evidence for convergent evolution of the invasive growth process among fungi and oomycete water molds. Fungal Genetics and Biology 41, 872–876.

Money NP, Harold FM. 1992. Extension growth of the water mold Achlya: interplay of turgor and wall strength. Proceedings of the National Academy of Sciences of the United States of America 89, 4245–4249.

Money NP, Harold FM. 1993. Two water molds can grow without measurable turgor pressure. Planta 190, 426–430.

Money NP, Hill TW. 1997. Correlation between endoglucanase secretion and cell wall strength in oomycete hyphae: implications for growth and morphogenesis. Mycologia 89, 777–785.

Monshausen GB, Bibikova TN, Messerli MA, Shi C, Gilroy S. 2007. Oscillations in extracellular pH and reactive oxygen species modulate tip growth of *Arabidopsis* root hairs. Proceedings of the National Academy of Sciences of the United States of America 104, 20996–21001.

Montecinos AE, Couceiro L, Peters AF, Desrut A, Valero M, Guillemin M-L. 2017. Species delimitation and phylogeographic analyses in the *Ectocarpus* subgroup *siliculosi* (Ectocarpales, Phaeophyceae). Journal of Phycology 53, 17–31.

Mørch ÝA, Holtan S, Donati I, Strand BL, Skjåk-Bræk G. 2008. Mechanical Properties of C-5 Epimerized Alginates. Biomacromolecules 9, 2360–2368.

Morton WM, Ayscough KR, McLaughlin PJ. 2000. Latrunculin alters the actin-monomer subunit interface to prevent polymerization. Nature Cell Biology 2, 376–378.

Muzzy R, Hable W. 2013. RAC1 regulates actin arrays during polarity establishment in the brown alga, *Silvetia compressa*. Developmental Biology 383, 28–38.

Nagasato C, Inoue A, Mizuno M, Kanazawa K, Ojima T, Okuda K, Motomura T. 2010. Membrane fusion process and assembly of cell wall during cytokinesis in the brown alga, *Silvetia babingtonii* (Fucales, Phaeophyceae). Planta 232, 287–298.

Nagasato C, Motomura T. 2009. Effect of latrunculin b and brefeldin a on cytokinesis in the brown alga *Scytosiphon lomentaria* (Scytosiphonales, Phaeophyceae). Journal of Phycology 45, 404–412.

Nakahori K, Katou K, Okamoto H. 1991. Auxin changes both the extensibility and the yield threshold of the cell wall of *Vigna* hypocotyls. Plant and Cell Physiology 32, 121–129.

Nakata MT, Takahara M, Sakamoto S, Yoshida K, Mitsuda N. 2018. High-Throughput Analysis of Arabidopsis Stem Vibrations to Identify Mutants With Altered Mechanical Properties. Frontiers in Plant Science 9.

Nardi CF, Villarreal NM, Rossi FR, Martínez S, Martínez GA, Civello PM. 2015. Overexpression of the carbohydrate binding module of strawberry expansin2 in *Arabidopsis thaliana* modifies plant growth and cell wall metabolism. Plant Molecular Biology 88, 101–117.

Nehr Z. 2013. Thesis report. Analyse génétique et fonctionnelle du mutant de morphogenèse étoile de l'algue brune *Ectocarpus siliculosus*. Université Pierre et Marie Curie, 191 p.

Nehr Z, Billoud B, Le Bail A, Charrier B. 2011. Space-time decoupling in the branching process in the mutant étoile of the filamentous brown alga *Ectocarpus siliculosus*. Plant Signaling & Behavior 6, 1889–1892.

Newcomb EH, Bonnet HT. 1965. Cytoplasmic microtubules and wall microfibril orientation in root hairs orientation of radish. The Journal of Cell Biology, 575–589.

Niklas K. 2000. The evolution of plant body plans—A Biomechanical Perspective. Annals of Botany 85, 411–438.

Niklas KJ. 2014. The evolutionary-developmental origins of multicellularity. American Journal of Botany 101, 6–25.

Niu R, Qin Z, Ji F, Xu M, Tian X, Li J, Yao F. 2017. Hybrid pectin–Fe 3+ /polyacrylamide double network hydrogels with excellent strength, high stiffness, superior toughness and notch-insensitivity. Soft Matter 13, 9237–9245.

Nolte T, Schopfer P. 1997. Viscoelastic versus plastic cell wall extensibility in growing seedling organs: a contribution to avoid some misconceptions. Journal of Experimental Botany 48, 2103–2107.

Nyvall P, Corre E, Boisset C, Barbeyron T, Rousvoal S, Scornet D, Kloareg B, Boyen C. 2003. Characterization of mannuronan C-5-epimerase genes from the brown alga *Laminaria digitata*. Plant physiology 133, 726–735.

Oliveira L, Bisalputra T. 1973. Studies in the brown alga *Ectocarpus* in culture. I. General ultrastructure of the sporophytic vegetative cells. Journal of Submicroscopic Cytology 5, 107–120.

Ortega JK. 1985. Augmented growth equation for cell wall expansion. Plant physiology 79, 318–320.

Ortega JKE. 2017. Dimensionless number is central to stress relaxation and expansive growth of the cell wall. Scientific Reports 7, 3016.

Ortega JKE, Smith ME, Erazo AJ, Espinosa MA, Bell SA, Zehr EG. 1991. A comparison of cell-wall-yielding properties for two developmental stages of *Phycomyces* sporangiophores - Determination by in-vivo creep experiments. Planta 183, 613–619.

Ortega JK, Smith ME, Espinosa MA. 1995. Cell wall extension behavior of *Phycomyces* sporangiophores during the pressure response. Biophysical Journal 68, 702–707.

Ortega JKE, Zehr EG, Keanini RG. 1989. In vivo creep and stress relaxation experiments to determine the wall extensibility and yield threshold for the sporangiophores of *Phycomyces*. Biophysical Journal 56, 465–475.

O'Toole M, Lamoureux P, Miller KE. 2008. A physical model of axonal elongation: force, viscosity, and adhesions govern the mode of outgrowth. Biophysical Journal 94, 2610–2620.

Ouichou A, Ducreux G. 2000. Connexions cortex–paroi chez la cellule apicale de *Sphacelaria*. Comptes Rendus de l'Académie des Sciences - Series III - Sciences de la Vie 323, 727–733.

Palanivelu R, Preuss D. 2000. Pollen tube targeting and axon guidance: parallels in tip growth mechanisms. Trends in Cell Biology 10, 517–524.

Parfrey LW, Lahr DJG, Knoll AH, Katz LA. 2011. Estimating the timing of early eukaryotic diversification with multigene molecular clocks. Proceedings of the National Academy of Sciences 108, 13624–13629.

Park YB, Cosgrove DJ. 2012a. A revised architecture of primary cell calls based on biomechanical changes induced by substrate-specific endoglucanases. Plant Physiology 158, 1933–1943.

Park YB, Cosgrove DJ. 2012b. Changes in cell wall biomechanical properties in the xyloglucan-deficient xxt1/xxt2 mutant of *Arabidopsis*. Plant Physiology 158, 465–475.

Park D, Robinson PM. 1966. Internal pressure of hyphal tips of fungi, and its significance in morphogenesis. Annals of Botany 30, 425–439.

Parre E, Geitmann A. 2005a. Pectin and the role of the physical properties of the cell wall in pollen tube growth of *Solanum chacoense*. Planta 220, 582–592.

Parre E, Geitmann A. 2005b. More than a leak sealant. The mechanical properties of callose in pollen tubes. Plant physiology 137, 274–286.

Parton RM, Fischer-Parton S, Watahiki MK, Trewavas AJ. 2001. Dynamics of the apical vesicle accumulation and the rate of growth are related in individual pollen tubes. Journal of Cell Science 114, 2685–2695.

Passioura J, Fry S, Passioura J, Fry S. 1992. Turgor and Cell Expansion: Beyond the Lockhart Equation. Australian Journal of Plant Physiology 19, 565.

Peaucelle A, Braybrook SA, Le Guillou L, Bron E, Kuhlemeier C, Höfte H. 2011. Pectin-induced changes in cell wall mechanics underlie organ initiation in Arabidopsis. Current Biology 21, 1720–1726.

Peaucelle A, Louvet R, Johansen JN, Höfte H, Laufs P, Pelloux J, Mouille G. 2008. Arabidopsis phyllotaxis is controlled by the methyl-esterification status of cell-wall pectins. Current Biology 18, 1943–1948.

Pellegrini L. 1980. Cytological studies on physodes in the vegetative cells of *Cystoseira stricta* Sauvageau (Phaeophyta, Fucales). Journal of Cell Science 231, 209–231.

Peskin CS, Odell GM, Oster GF. 1993. Cellular motions and thermal fluctuations: the Brownian ratchet. Biophysical Journal 65, 316–324.

Peters NT, Kropf DL. 2010. Asymmetric microtubule arrays organize the endoplasmic reticulum during polarity establishment in the brown alga Silvetia compressa. Cytoskeleton 67, 102–111.

Peters AF, Marie D, Scornet D, Kloareg B, Cock JM. 2004. Proposal of *Ectocarpus siliculosus* (Ectocarpales, Phaeophyceae) as a model organism for brown algal genetics and genomics. Journal of Phycology 40, 1079–1088.

Phair RD, Gorski SA, Misteli T. 2003. Measurement of dynamic protein binding to chromatin in vivo, using photobleaching microscopy. Chromatin and Chromatin Remodeling Enzymes, Part A. Methods in Enzymology. Academic Press, 393–414.

Pickett-Heaps JD. 1998. Cell division and morphogenesis of the centric diatom *Chaetoceros Decipiens* (Bacillariophyceae) II. Electron Microscopy and a New Paradigm for Tip Growth. Journal of Phycology 34, 995–1004.

Pickett-Heaps JD, Klein AG. 1998. Tip growth in plant cells may be amoeboid and not generated by turgor pressure. Proceedings of the Royal Society B: Biological Sciences 265, 1453–1459.

Pickett-Heaps JD, West JA, Wilson SM, McBbride DL. 2001. Time-lapse videomicroscopy of cell (spore) movement in red algae. European Journal of Phycology 36, 9–22.

Picton JM, Steer MW. 1982. A model for the mechanism of tip extension in pollen tubes. Journal of Theoretical Biology 98, 15–20.

Picton JM, Steer MW. 1983. Membrane recycling and the control of secretory activity in pollen tubes. Journal of Cell Science 63, 303–310.

Pierson ES. 1988. Rhodamine-phalloidin staining of F-actin in pollen after dimethylsulphoxide permeabilization - A comparison with the conventional formaldehyde preparation. Sexual Plant Reproduction 1, 83–87.

Pietruszka M. 2013. Special solutions to the ortega equation. Journal of Plant Growth Regulation 32, 102–107.

Pollard TD. 1984. Purification of a high molecular weight actin filament gelation protein from *Acanthamoeba* that shares antigenic determinants with vertebrate spectrins. The Journal of Cell Biology 99, 1970–1980.

Pollard TD, Borisy GG. 2003. Cellular motility driven by assembly and disassembly of actin filaments. Cell 112, 453–465.

Ponce NMA, Leonard PI, Flores ML, Stortz CA, Rodriguez MC. 2007. Polysaccharide localization in the sporophyte cell wall of *Adenocystis utricularis* (Ectocarpales s.l., Phaeophyceae). Phycologia 46, 675–679.

Popper ZA, Michel G, Herve C, Domozych DS, Willats WG, Tuohy MG, Kloareg B, Stengel DB. 2011a. Evolution and diversity of plant cell walls: from algae to flowering plants. Annual Review of Plant Biology 62, 567–590.

Proseus TE, Boyer JS. 2005. Turgor pressure moves polysaccharides into growing cell walls of *Chara corallina*. Annals of Botany 95, 967–979.

Proseus TE, Boyer JS. 2006a. Calcium pectate chemistry controls growth rate of *Chara corallina*. Journal of Experimental Botany 57, 3989–4002.

Proseus TE, Boyer JS. 2006b. Periplasm turgor pressure controls wall deposition and assembly in growing *Chara corallina* Cells. Annals of Botany 98, 93–105.

Proseus TE, Boyer JS. 2006c. Identifying cytoplasmic input to the cell wall of growing *Chara corallina*. Journal of Experimental Botany 57, 3231–3242.

Proseus TE, Boyer JS. 2007. Tension required for pectate chemistry to control growth in *Chara corallina*. Journal of Experimental Botany, 4283–4292.

Proseus TE, Ortega JKE, Boyer JS. 1999. Separating growth form elastic deformation during cell enlargement. Plant Physiology 119, 775–784.

Proseus TE, Zhu GL, Boyer JS. 2000. Turgor, temperature and the growth of plant cells: using *Chara corallina* as a model system. Journal of experimental botany 51, 1481–1494.

Prosser JL. 1990. Comparizon of tip growth in prokaryotic and eukaryotic filamentous microorganisms. In: Heath IB, ed. Tip Growth in Plant and Fungal Cells. San Diego, New York, Boston, London, Sydney, Tokyo, Toronto: Academic Press, Harcourt Brace Jovanovich, 233–259.

Provasoli L, Carlucci AF. 1974. Vitamins and growth regulators. Algal Physiology and Biochemistry. Oxford: Blackwell, 741–787.

Pu R, Wozniak M, Robinson KR. 2000. Cortical actin filaments form rapidly during photopolarization and are required for the development of calcium gradients in *Pelvetia compressa* zygotes. Developmental biology 222, 440–9.

Quatrano RS, Brian L, Aldridge J, Schultz T. 1991. Polar axis fixation in Fucus zygotes: components of the cytoskeleton and extracellular matrix. Development Supplement 1, 11–16.

Quatrano RS, Crayton MA. 1973. Sulfation of fucoidan in *Fucus* embryos. I. Possible role in localization. Developmental Biology 30, 29–41.

Quatrano RS, Shaw SL. 1997. Role of the cell wall in the determination of cell polarity and the plane of cell division in *Fucus* embryos. Trends in Plant Science 2, 15–21.

R Core Team. 2017. R: A Language and Environment for Statistical Computing. Vienna, Austria: R Foundation for Statistical Computing.

Rabillé H, Billoud B, Rolland E, Charrier B. 2018a. Dynamic and microscale mapping of cell growth: case of *Ectocarpus* filament cells. In: Charrier B, Wichard T & Reddy CRK, eds. Protocols for Macroalgae Research. Boca Raton: CRC Press, 349–364.

Rabillé H, Koutalianou M, Charrier B, Katsaros CI, Charrier B, Wichard T, Reddy CRK. 2018b. Actin fluorescent staining in the filamentous brown alga *Ectocarpus siliculosus*. In: Charrier B, Wichard T & Reddy CRK, eds. Protocols for Macroalgae Research. Boca Raton: CRC Press, 365–380.

Radotić K, Roduit C, Simonović J, Hornitschek P, Fankhauser C, Mutavdžić D, Steinbach G, Dietler G, Kasas S. 2012. Atomic force microscopy stiffness tomography on living arabidopsis thaliana cells reveals the mechanical properties of surface and deep cell-wall layers during growth. Biophysical Journal 103, 386–394.

Raimundo SC, Avci U, Hopper C, Pattathil S, Hahn MG, Popper ZA. 2016. Immunolocalization of cell wall carbohydrate epitopes in seaweeds: presence of land plant epitopes in *Fucus vesiculosus* L. (Phaeophyceae). Planta 243, 337–354.

Raimundo SC, Pattathil S, Eberhard S, Hahn MG, Popper ZA. 2017. β-1,3-Glucans are components of brown seaweed (Phaeophyceae) cell walls. Protoplasma 254, 997–1016.

Raudaskoski M, Åström H, Laitiainen E. 2001. Pollen tube cytoskeleton: structure and function. Journal of Plant Growth Regulation 20, 113–130.

Raven JA, Edwards D. 2001. Roots: evolutionary origins and biogeochemical significance. Journal of Experimental Botany 52, 381–401.

Ray PM. 1992. Mechanism of wall loosening for cell growth. Current Topics in Plant Biochemistry and Physiology 11, 18–41.

Reinhardt MO. 1892. Das wachsthum der Pilzhyphen. Jahrbucher fur wissenschaftliche botanik 23, 479–566.

Rensing SA. 2016. Plant Evo–Devo: How Tip Growth Evolved. Current Biology 26, R1228–R1230.

Reynaga-Peña CG, Bartnicki-García S, Reynaga-pen CG, Reynaga-Peña CG, Bartnicki-García S. 2005. Cytoplasmic contractions in growing fungal hyphae and their morphogenetic consequences. Archives of Microbiology 183, 292–300.

Riglet L, Rozier F, Kodera C, Fobis-Loisy I, Gaude T. 2018. KATANIN-dependent mechanical properties of the stigmatic cell wall regulate pollen tube pathfinding. bioRxiv, 384321.

Riquelme M. 2013. Tip Growth in filamentous fungi: a road trip to the apex. Annual Review of Microbiology 67, 587–609.

Riquelme M, Sánchez-León E. 2014. The Spitzenkörper: a choreographer of fungal growth and morphogenesis. Current Opinion in Microbiology 20, 27–33.

Riquelme M, Yarden O, Bartnicki-Garcia S, et al. 2011. Architecture and development of the *Neurospora crassa* hypha - a model cell for polarized growth. Fungal Biology 115, 446–474.

Roberson NF, Rizvi SRH. 1968. Some observation on the water-relations of the hyphae of *Neurospora crassa.* Annals of Botany 32, 279–291.

Roberts AW, Lahnstein J, Hsieh YSY, et al. 2018. Functional characterization of a glycosyltransferase from the moss *Physcomitrella patens* involved in the biosynthesis of a novel cell wall arabinoglucan. The Plant Cell, tpc.00082.2018.

Robinson S, Huflejt M, Reuille PB de, Braybrook SA, Schorderet M, Reinhardt D, Kuhlemeier C. 2017. An automated confocal micro-extensometer enables in vivo quantification of mechanical properties with cellular resolution. The Plant Cell 29, 2959–2973.

Röckel N, Wolf S, Kost B, Rausch T, Greiner S. 2007. Elaborate spatial patterning of cell-wall PME and PMEI at the pollen tube tip involves PMEI endocytosis, and reflects the distribution of esterified and de-esterified pectins. The Plant Journal 53, 133–143.

Roduit C, Sekatski S, Dietler G, Catsicas S, Lafont F, Kasas S. 2009. Stiffness tomography by atomic force microscopy. Biophysical Journal 97, 674–677.

Rojas ER, Hotton S, Dumais J. 2011. Chemically mediated mechanical expansion of the pollen tube cell wall. Biophysical Journal 101, 1844–1853.

Rosenbluth MJ, Crow A, Shaevitz JW, Fletcher DA. 2008. Slow Stress Propagation in Adherent Cells. Biophysical Journal 95, 6052–6059.

Rounds CM, Bezanilla M. 2013. Growth mechanisms in tip-growing plant cells. Annual Review of Plant Biology 64, 243–65.

Routier-Kierzkowska AL, Smith RS. 2013. Measuring the mechanics of morphogenesis. Current Opinion in Plant Biology 16, 25–32.

Ruan Y-L, Llewellyn DJ, Furbank RT. 2001. The control of single-celled cotton fiber elongation by developmentally reversible gating of plasmodesmata and coordinated expression of sucrose and K^+ transporters and expansin. The Plant Cell 13, 47–60.

Saint-Marcoux D, Billoud B, Langdale JA, Charrier B. 2015. Laser capture microdissection in Ectocarpus siliculosus: the pathway to cell-specific transcriptomics in brown algae. Frontiers in Plant Science 6, 54.

Salgado LT, Cinelli LP, Viana NB, Carvalho RT de, Mourão PADS, Teixeira VL, Farina M, Filho AGMA. 2009. A vanadium bromoperoxidase catalyzes the formation of high-molecular-weight complexes between brown algal phenolic substances and alginates. Journal of Phycology 45, 193–202.

Salmeán AA, Duffieux D, Harholt J, Qin F, Michel G, Czjzek M, Willats WGT, Hervé C. 2017. Insoluble (1 → 3), (1 → 4)-β-D-glucan is a component of cell walls in brown algae (Phaeophyceae) and is masked by alginates in tissues. Scientific Reports 7, 2880.

Šamaj J, Baluska F, Menzel D. 2004. New signalling molecules regulating root hair tip growth. Trends in Plant Science 9, 217–220.

Šamaj J, Müller J, Beck M, Böhm N, Menzel D. 2006. Vesicular trafficking, cytoskeleton and signalling in root hairs and pollen tubes. Trends in Plant Science 11, 594–600.

Sanati Nezhad A, Geitmann A. 2013. The cellular mechanics of an invasive lifestyle. Journal of Experimental Botany 64, 4709–28.

Sato ACK, Oliveira PR, Cunha RL. 2008. Rheology of Mixed Pectin Solutions. Food Biophysics 3, 100–109.

Schindelin J, Arganda-Carreras I, Frise E, et al. 2012. Fiji - an Open Source platform for biological image analysis. Nature methods 9.

Schoenwaelder M, Clayton M. 1998. Secretion of phenolic substances into the zygote wall and cell plate in embryos of *Hormosira* and *Acrocarpia* (Fucales, Phaeophyceae). Journal of Physiology 34, 969–980.

Schopfer P. 2006. Biomechanics of plant growth. American Journal of Botany 93, 1415–1425.

Schopfer P, Wei C, Lintilhac PM. 2008. Is the loss of stability theory a realistic concept for stress relaxation-mediated cell wall expansion during plant growth? Plant Physiology 147, 935–938.

Serikawa KA, Mandoli DF. 1998. An analysis of morphogenesis of the reproductive whorl of Acetabularia acetabulum. Planta 207, 96–104.

Shamsudhin N, Laeubli N, Atakan HB, Vogler H, Hu C, Haeberle W, Sebastian A, Grossniklaus U, Nelson BJ. 2016. Massively parallelized pollen tube guidance and mechanical measurements on a Lab-on-a-Chip platform. PLoS ONE 11, e0168138.

Sharova EI. 2007. Expansins: proteins involved in cell wall softening during plant growth and morphogenesis. Russian Journal of Plant Physiology 54, 713–727.

Shaw G, Bray D. 1977. Movement and extension of isolated growth cones. Experimental Cell Research 104, 55–62.

Shaw SL, Dumais J, Long SR. 2000. Cell surface expansion in polarly growing root hairs of *Medicago truncatula*. Plant Physiology 124, 959–970.

Shtein I, Bar-On B, Popper ZA. 2018. Plant and algal structure: from cell walls to biomechanical function. Physiologia Plantarum 164, 56–66.

Silberfeld T, Leigh JW, Verbruggen H, Cruaud C, de Reviers B, Rousseau F. 2010. A multi-locus time-calibrated phylogeny of the brown algae (Heterokonta, Ochrophyta, Phaeophyceae): Investigating the evolutionary nature of the 'brown algal crown radiation'. Molecular Phylogenetics and Evolution 56, 659–674.

Silberfeld T, Rousseau F, de Reviers B. 2014. An Updated Classification of Brown Algae (Ochrophyta, Phaeophyceae). Cryptogamie, Algologie 35, 117–156.

Siméon A, Duffieux D, Hervé C, Le Panse S, Knox JP, Torode TA, Charrier B, Wichard T, Reddy CRK. 2018. The immunodetection and in-situ imaging of cell wall polysaccharides in brown algae. Protocols for Macroalgae Research. Boca Raton: CRC Press, 323–334.

Smidsrød O. 1973. The relative extension of alginates having different chemical composition. Carbohydrate Research 27, 107–118.

Smidsrød O, Haug A, Whittington SG. 1972. The molecular basis for some physical properties of poly-uronides. Acta Chemica Scandinavica 26, 2563–2566.

Smith LG. 2003. Cytoskeletal control of plant cell shape: Getting the fine points. Current Opinion in Plant Biology 6, 63–73.

Spector I, Shochet NR, Blasberger D, Kashman Y. 1989. Latrunculins—novel marine macrolides that disrupt microfilament organization and affect cell growth: I. Comparison with cytochalasin D. Cytoskeleton 13, 127–144.

Staebell M, Soll DR. 1985. Temporal and spatial differences in cell wall expansion during bud and mycelium formation in *Candida albicans*. Journal of general microbiology 131, 1467–80.

Staehlin A, Driouich A. 1997. Brefeldin A Effects in Plants. Plant physiology 114, 401–403.

Steer MW. 1990. Role of actin in tip growth. In: Heath IB, ed. Tip Growth in Plant and Fungal Cells. San Diego, New York, Boston, London, Sydney, Tokyo, Toronto: Academic Press, Harcourt Brace Jovanovich, 119–145.

Steer MW, Steer JM. 1989. Pollen tube tip growth. New Phytologist 111, 323–358.

Steinberg G. 2007. Hyphal growth: a tale of motors, lipids, and the Spitzenkörper. Eukaryotic Cell 6, 351–360.

Stiller JW, Schreiber J, Yue J, Guo H, Ding Q, Huang J. 2014. The evolution of photosynthesis in chromist algae through serial endosymbioses. Nature Communications 5, 5764.

Stossel TP. 1982. The structure of cortical cytoplasm. Phil. Trans. R. Soc. Lond. B 299, 275–289.

Sudbery PE. 2008. Regulation of polarised growth in fungi. Fungal Biology Reviews 22, 44–55.

Suter DM, Errante LD, Belotserkovsky V, Forscher P. 1998. The Ig superfamily cell adhesion molecule, apCAM, mediates growth cone steering by substrate–cytoskeletal coupling. The Journal of Cell Biology 141, 227–240.

Suter DM, Forscher P. 2000. Substrate–cytoskeletal coupling as a mechanism for the regulation of growth cone motility and guidance. Journal of Neurobiology 44, 97–113.

Szymanski DB, Cosgrove DJ. 2009. Dynamic Coordination of Cytoskeletal and Cell Wall Systems during Plant Cell Morphogenesis. Current Biology 19, 800–811.

Taiz L. 1984. Plant cell expansion: regulation of cell wall mechanical properties. Annual Review of Plant Physiology 35, 585–657.

Takeshita N, Manck R, Gru N, Vega SHD, Fischer R. 2014. Interdependence of the actin and the microtubule cytoskeleton during fungal growth. Current Opinion in Microbiology, 34–41.

Tamura H, Mine I, Okuda K. 1996. Cellulose-synthesizing terminal complexes and microfibril structure in the brown alga *Sphacelaria rigidula* (Sphacelariales, Phaeophyceae). Phycological Research 44, 63–68.

Taylor DL, Condeelis JS. 1979. Cytoplasmic structure and contractility in amoeboid cells. In: Bourne GH, In: Danielli JF, eds. International Review of Cytology. Academic Press, 57–144.

Taylor DL, Fechheimer M. 1982. Cytoplasmic structure and contractility: the solation-contraction coupling hypothesis. Philosophical Transactions of the Royal Society B: Biological Sciences 299, 185–197.

Terauchi M, Nagasato C, Inoue A, Ito T, Motomura T. 2016. Distribution of alginate and cellulose and regulatory role of calcium in the cell wall of the brown alga *Ectocarpus siliculosus* (Ectocarpales, Phaeophyceae). Planta 244, 361–377.

Terauchi M, Yamagishi T, Hanyuda T, Kawai H. 2017. Genome-wide computational analysis of the secretome of brown algae (Phaeophyceae). Marine Genomics 32, 49–59.

Tesson B, Charrier B. 2014. Brown algal morphogenesis: atomic force microscopy as a tool to study the role of mechanical forces. Frontiers in plant science 5, 471.

Thomas F, Lundqvist LCE, Jam M, Jeudy A, Barbeyron T, Sandström C, Michel G, Czjzek M. 2013. Comparative characterization of two marine alginate lyases from zobellia galactanivorans reveals distinct modes of action and exquisite adaptation to their natural substrate. Journal of Biological Chemistry 288, 23021–23037.

Thompson DS. 2005. How do cell walls regulate plant growth? Journal of Experimental Botany 56, 2275–2285.

Tonon T, Rousvoal S, Roeder V, Boyen C. 2008. Expression profiling of the mannuronan C5-epimerase multigenic family in the brown alga *Laminaria digitata* (phaeophyceae) under biotic stress conditions. Journal of Phycology 44, 1250–1256.

Torode TA, Marcus SE, Jam M, Tonon T, Blackburn RS, Hervé C, Knox JP. 2015. Monoclonal antibodies directed to fucoidan preparations from brown algae. PloS One 10, e0118366.

Torode TA, O'Neill R, Marcus SE, et al. 2018. Branched Pectic Galactan in Phloem-Sieve-Element Cell Walls: Implications for Cell Mechanics. Plant Physiology 176, 1547–1558.

Torode TA, Siméon A, Marcus SE, Jam M, Le Moigne MA, Duffieux D, Knox JP, Hervé C. 2016. Dynamics of cell wall assembly during early embryogenesis in the brown alga *Fucus*. Journal of Experimental Botany 67, 6089–6100.

Torralba S, Heath IB. 2001. Cytoskeletal and Ca^{2+} regulation of hyphal tip growth and initiation. Current Topics in Developmental Biology. Academic Press, 135–187.

Torralba S, Raudaskoski M, Pedregosa AM, Laborda F. 1998. Effect of cytochalasin A on apical growth, actin cytoskeleton organization and enzyme secretion in *Aspergillus nidulans*. Microbiology 144, 45–53.

Tovey DJ, Moss BL. 1978. Attachment of the haptera of *Laminaria digitata* (Huds.) Lamour. Phycologia 17, 17–22.

Toyooka K, Goto Y, Asatsuma S, Koizumi M, Mitsui T, Matsuoka K. 2009. A Mobile secretory vesicle cluster involved in mass transport from the Golgi to the plant cell exterior. Plant Cell 21, 1212–1229.

Trevithick JR, Galsworthy PR. 1977. Morphology of slime variants of *Neurospora crassa* growing on a glass surface in liquid medium. Archives of Microbiology 115, 109–118.

Trinci APJ, Collinge AJ. 1975. Hyphal wall growth in *Neurospora crassa* and *Geotrichum candidum*. Microbiology 91, 355–361.

Tsekos I. 1999. The sites of cellulose synthesis in algae: diversity and evolution of cellulose-synthesizing enzyme complexes. Journal of Phycology 35, 635–655.

Uchiyama H, Iwai A, Dohra H, Ohnishi T, Kato T, Park EY. 2018. The effects of gene disruption of Kre6-like proteins on the phenotype of β-glucan-producing *Aureobasidium pullulans*. Applied Microbiology and Biotechnology 102, 4467–4475.

Varvarigos V, Galatis B, Katsaros C. 2007. Radial endoplasmic reticulum arrays co-localize with radial F-actin in polarizing cells of brown algae. European Journal of Phycology 42, 253–262.

Varvarigos V, Katsaros C, Galatis B. 2004. Radial F-actin configurations are involved in polarization during protoplast germination and thallus branching of *Macrocystis pyrifera* (Phaeophyceae, Laminariales). Phycologia 43, 693–702.

Vaškovičová K, Žárský V, Rösel D, Nikolič M, Buccione R, Cvrčková F, Brábek J. 2013. Invasive cells in animals and plants: searching for LECA machineries in later eukaryotic life. Biology Direct 8, 8.

Vian B, Roland J-C, Reis D. 1993. Primary cell wall texture and its relation to surface expansion. International Journal of Plant Sciences 154, 1–9.

Vidali L, Mckenna ST, Hepler PK. 2001. Actin polymerization is essential for pollen tube growth. Molecular Biology of the Cell 12, 2534–2545.

Virag A, Griffiths AJF. 2004. A mutation in the *Neurospora crassa* actin gene results in multiple defects in tip growth and branching. Fungal Genetics and Biology 41, 213–225.

Virag A, Harris SD. 2006. The Spitzenkörper: a molecular perspective. Mycological Research 110, 4–13.

Vogler H, Felekis D, Nelson B, Grossniklaus U, Vogler H, Felekis D, Nelson BJ, Grossniklaus U. 2015. Measuring the Mechanical Properties of Plant Cell Walls. Plants 4, 167–182.

V**on Dassow M, Odell GM, Mandoli DF.** 2001. Relationships between growth, morphology and wall stress in the stalk of *Acetabularia acetabulum*. Planta 213, 659–666.

Wagner VT, Brian L, Quatrano RS. 1992. Role of a vitronectin-like molecule in embryo adhesion of the brown alga *Fucus*. Proceedings of the National Academy of Sciences of the United States of America 89, 3644–3648.

Wakatsuki T, Schwab B, Thompson NC, Elson EL. 2001. Effects of cytochalasin D and Latrunculin B on mechanical properties of cells. Journal of cell science 114, 1025–1036.

Walker SK, Chitcholtan K, Yu Y, Christenhusz GM, Garrill A. 2006. Invasive hyphal growth: An F-actin depleted zone is associated with invasive hyphae of the oomycetes *Achlya bisexualis* and *Phytophthora cinnamomi*. Fungal Genetic and Biology 43, 357–365.

Wallace S, Williams JH. 2017. Evolutionary origins of pectin methylesterase genes associated with novel aspects of angiosperm pollen tube walls. Biochemical and Biophysical Research Communications 487, 509–516.

Wang Y. 2007. Flux at focal adhesions: slippage clutch, mechanical gauge, or signal depot. Science Signaling 2007, pe10.

Wasteneys GO, Galway ME. 2003. Remodeling the cytoskeleton for growth and form: An overview with some new views. Annual Review of Plant Biology 54, 691–722.

Weber A, Braybrook S, Huflejt M, Mosca G, Routier-Kierzkowska AL, Smith RS. 2015. Measuring the mechanical properties of plant cells by combining micro-indentation with osmotic treatments. Journal of Experimental Botany 66, 3229–3241.

Wei C, Lintilhac PM. 2003. Loss of stability - A new model for stress relaxation in plant cell walls. Journal of Theoretical Biology 224, 305–312.

Wei C, Lintilhac PM. 2007. Loss of stability: a new look at the physics of cell wall behavior during plant cell growth. Plant physiology 145, 763–772.

Wessels JGH. 1986. Cell wall synthesis in apical hyphal growth. In: Bourne GH, ed. International Review of Cytology. Academic Press, 37–79.

Wessels JGH. 1988. A steady-state model for apical wall growth in fungi. Acta Botanica Neerlandica 37, 3–16.

Wessels JGH. 1990. Role of cell wall architecture in fungal tip growth generation. In: Heath IB, ed. Tip Growth in Plant and Fungal Cells. San Diego, New York, Boston, London, Sydney, Tokyo, Toronto: Academic Press, Harcourt Brace Jovanovich, 1–29.

Wessels JGH. 1993. Wall growth, protein excretion and morphogenesis in fungi. New Phytologist 123, 397–413.

Winship LJ, Obermeyer G, Geitmann A, Hepler PK. 2010. Under pressure, cell walls set the pace. Trends in Plant Science 15, 363–369.

Winship LJ, Obermeyer G, Geitmann A, Hepler PK. 2011. Pollen tubes and the physical world. Trends in Plant Science 16, 353–355.

Wright PJ, Reed RH. 1988. Method for determination of turgor pressure in macroalage, with particular reference to the Phaeophyta. Marine Biology 480, 473–480.

Wu JZ, Lin Y, Zhang XL, Pang DW, Zhao J. 2008. IAA stimulates pollen tube growth and mediates the modification of its wall composition and structure in Torenia fournieri. Journal of Experimental Botany 59, 2529–2543.

Yanagisawa M, Desyatova AS, Belteton SA, Mallery EL, Turner JA, Szymanski DB. 2015. Patterning mechanisms of cytoskeletal and cell wall systems during leaf trichome morphogenesis. Nature Plants 1, 15014.

Yanai M, Kenyon CM, Butler JP, Macklem PT, Kelly SM. 1996. Intracellular pressure is a motive force for cell motion in *Amoeba proteus*. Cell Motility 33, 22–29.

Ye N, Zhang X, Miao M, et al. 2015. *Saccharina* genomes provide novel insight into kelp biology. Nature Communications 6, 6986.

Zerzour R, Kroeger J, Geitmann A. 2009. Polar growth in pollen tubes is associated with spatially confined dynamic changes in cell mechanical properties. Developmental Biology 334, 437–446.

Zhang Y, Franco M, Ducret A, Mignot T. 2010. A bacterial Ras-like small GTP-binding protein and its cognate GAP establish a dynamic spatial polarity axis to control directed motility. PLoS Biology 8, e1000430.

Zhang T, Zheng Y, Cosgrove DJ. 2016. Spatial organization of cellulose microfibrils and matrix polysaccharides in primary plant cell walls as imaged by multichannel atomic force microscopy. Plant Journal 85, 179–192.

Zhao L, Schaefer D, Marten MR. 2005a. Assessment of elasticity and topography of *Aspergillus nidulans* spores via Atomic Force Microscopy. Applied Environmental Microbiology 71, 955–960.

Zhao L, Schaefer D, Xu H, Modi SJ, LaCourse WR, Marten MR. 2005b. Elastic properties of the cell wall of *Aspergillus nidulans* studied with Atomic Force Microscopy. Biotechnology Progress 21, 292–299.

Zonia L. 2010. Spatial and temporal integration of signalling networks regulating pollen tube growth. Journal of Experimental Botany 61, 1939–1957.

Zonia L, Cordeiro S, Tupý J, Feijó JA. 2002. Oscillatory chloride efflux at the pollen tube apex has a role in growth and cell volume regulation and is targeted by Inositol 3,4,5,6-Tetrakisphosphate. Plant Cell 14, 2233–2249.

Zonia L, Müller M, Munnik T. 2006. Hydrodynamics and cell volume oscillations in the pollen tube apical region are integral components of the biomechanics of *Nicotiana tabacum* pollen tube growth. Cell Biochemistry and Biophysics 46, 209–232.

Zonia L, Munnik T. 2004. Osmotically induced cell swelling versus cell shrinking elicits specific changes in phospholipid signals in tobacco pollen tubes. Plant Physiology 134, 813–823.

Zonia L, Munnik T. 2007. Life under pressure: hydrostatic pressure in cell growth and function. Trends in Plant Science 12, 13601385.

Zonia L, Munnik T. 2008a. Vesicle trafficking dynamics and visualization of zones of exocytosis and endocytosis in tobacco pollen tubes. Journal of Experimental Botany 59, 861–873.

Zonia L, Munnik T. 2008b. Still life. Pollen tube growth observed in millisecond resolution. Plant Signaling & Behavior 3, 836–838.

Zonia L, Munnik T. 2009. Uncovering hidden treasures in pollen tube growth mechanics. Trends in Plant Science 14, 318–327.

Zonia L, Munnik T. 2011. Understanding pollen tube growth: the hydrodynamic model versus the cell wall model. Trends in Plant Science 16, 347–52.

Appendices

Appendix 1 **List of oral communications and poster presentation in congress and workshops**

Appendix 2 **List of training courses pursued**

Appendix 1. List of oral communications and poster presentation in congress and workshops

The above lists include all the oral presentations and posters that I have given during my PhD.

Oral presentations

2018 H. Rabillé, B. Billoud, B. Charrier. Mapping dynamic cell expansion. *Annual meeting of the European COST Action FA1406 "Phycomorph",* 12nd – 13th October, Roscoff, FRANCE

2017 H. Rabillé, B. Billoud, B. Tesson, D. Saint-Marcoux, S. Le Panse, E. Rolland, B. Charrier. What makes an *Ectocarpus* filament grow? Enlightenment from biophysical modeling and simulation. *2ème Symposium of the System Biology Network of Sorbonne University (BioSys)*, 1st December, Sorbonne Université, FRANCE

2017 H. Rabillé, B. Billoud, B. Tesson, S. Le Panse, E. Rolland, B. Charrier. Dynamic simulations of tip-growth in the brown alga *Ectocarpus siliculosus* using a viscoplastic model. *French Phycological Society meeting*, 19th – 20th October, Roscoff, FRANCE

2017 H. Rabillé, M. Koutalianou, B. Billoud, E. Rolland, C. Katsaros, B. Charrier. Fluorescent staining of actin cytoskeleton in vegetative cells of the filamentous brown algae *Ectocarpus siliculosus. Annual meeting of the European COST Action FA1406 "Phycomorph",* 2nd – 4th October, Brussels, BELGIUM

2016 H. Rabillé, B. Billoud, E. Rolland, S. Le Panse, C. Gaillard, B. Charrier. Mécanique de la croissance apicale chez l'algue brune *Ectocarpus sp*. Microscopie à force atomique et confocale. *Gen2Bio 2016* (meeting of the French Biogenouest network), 30th March, Saint-Brieuc, FRANCE

Posters

2016 H. Rabillé, B. Billoub, E. Rolland, B. Tesson, S. le Panse and B. Charrier. The biophysics of tip-growth in the brown alga *Ectocarpus siliculosus* (Dillw.) Lyngb. *Shaping Life* (meeting of the French Society of Developmental Biology), 24th -27th March, Marseille, FRANCE.

2015 H. Rabillé, C. Hervé, É. Rolland, P. Knox, B. Charrier. Characterisation of the mutant *Ecballium* in the brown alga *Ectocarpus siliculosus. 6th European Phycological Congress*, 24th – 28th August, London, U-K.

Appendix 2. List of training courses pursued

The above list includes all the doctoral training school that I have attended to.

2018 **Unix / Linux: computing science for biology**
Paris, FRANCE. From the 5th to the 9th and from the 19th to the 22th March 2018
Organized by the "Bioinformatic workshop" of Sorbonne University

2017 **Career objectives and career management**
Roscoff, FRANCE. From the 10th to the 15th April 2018
Organized by the Doctoral Institute of Sorbonne University

2017 **International Spring School on Animal and Plant Morphogenesis**
Hameau de l'Etoile, La Caya, Saint Martin de Londres, FRANCE. From the 26th February to the 5th March 2017.
Organized by the French Society for Developmental Biology (persons in charge: Dr Patrick Lemaire and Dr Christophe Godin).

Résumé – Rabillé, 2018. Mécanismes biophysiques et cellulaires de la croissance apicale chez l'algue brune *Ectocarpus sp.*

La croissance apicale (CA) est un mode d'élongation cellulaire extrêmement polarisée, au cours duquel la croissance en surface n'a lieu qu'à un site réduit de la cellule. Elle a lieu dans de nombreux groupes taxonomiques, et représente donc un système idéal pour des études « *évo-devo* » des mécanismes fondamentaux de morphogenèse cellulaire sur tout l'arbre du vivant. Néanmoins, l'étude de la CA chez les eucaryotes s'est principalement concentrée sur les plantes terrestres et les champignons, laissant de côté les autres groupes. Pour combler ce déficit de connaissances, les macroalgues brunes sont particulièrement intéressantes du fait de leur histoire évolutive unique, des spécificités de leurs structures cellulaires et des conditions physiques de leur milieu, qui ont probablement résulté en l'acquisition de mécanismes de morphogenèse originaux. Au cours de ma thèse, j'ai entrepris de caractériser les mécanismes de la CA chez *Ectocarpus sp.*, une espèce modèle pour les algues brunes. Pour cela, j'ai mesuré le patron du taux d'expansion de la paroi à l'apex des cellules apicales, ainsi que la pression de turgescence, la courbure de surface et l'épaisseur de paroi, afin d'alimenter un modèle viscoplastique de CA. Ce modèle a permis de prédire que le patron d'extension de la paroi dans la cellule apicale n'est pas contrôlé par un gradient de propriétés mécaniques de la paroi, mais par un gradient d'épaisseur de paroi. En outre, la mesure expérimentale de la déformabilité pariétale immédiate (principalement de nature élastique) a mis en évidence un gradient inverse de déformabilité mécanique, opposé à celui qui serait attendu si cette propriété contrôlait l'aptitude de la paroi à croître. Par ailleurs, si l'abondance globale en alginates, un composant majeur de la paroi des algues brunes, semble contrôler la rigidité de la paroi où le stress de tension est élevé, les blocs mannuronates semblent aussi importants que les blocs guluronates dans cette fonction. Enfin, nous avons montré que chez *Ectocarpus*, les filaments d'actine (FAs) sont indispensables pour restreindre la croissance pariétale dans le dôme apical, et donc dans la mise en place de la forme tubulaire dans la région subapicale. Le marquage fluorescent des FAs a montré l'existence d'une « coiffe apicale » sous le dôme, une structure commune à plusieurs autres groupes, qui apparait nécessaire pour le renforcement mécanique de la fine paroi à l'apex. Ces données suggèrent donc que les FAs pourraient contrôler le patron d'expansion de la paroi le long de la cellule en exerçant une influence directement mécanique sur la paroi cellulaire. Dans leur ensemble, les résultats obtenus au cours de cette thèse démontrent que les mécanismes biophysiques de la CA chez *Ectocarpus* sont radicalement différents de ceux rencontrés chez les plantes terrestres et les champignons. À l'avenir, ils permettront la caractérisation des mécanismes moléculaires contrôlant la CA chez les algues brunes, et ouvrent ainsi la voie à de futures études *évo-devo* de ce mode particulier de morphogenèse cellulaire.

Mots-clés : actine ; algues brunes ; biomécanique ; croissance apicale ; *Ectocarpus* ; paroi cellulaire

Abstract – Rabillé, 2018. Biophysical and cellular mechanisms of tip-growth in the brown alga *Ectocarpus sp.*

Tip-growth (TG) is a universal mode of polarized cell elongation, during which the growth activity is restricted to the pole of the cell. Its wide taxonomic occurrence makes it an ideal model system for *evo-devo* studies of basic mechanisms of cell morphogenesis across the tree of life. Nevertheless, in eukaryotes, TG studies have mainly focused on land plants and True Fungi, leaving the over taxa largely underexplored. To fill in this knowledge gap, brown macroalgae are particularly appealing because of their unique evolutionary history, their particular cellular structures and their physical environment that have likely resulted in the acquisition of original morphogenetic mechanisms. During this thesis, I aimed to characterise the biophysical mechanisms of TG in *Ectocarpus sp.*, a model species for brown algae. To do so, I measured the pattern of wall strain rate at the apex as well as the turgor pressure, the cell surface curvature and the wall thickness, in order to supply a viscoplastic model of TG with biological parameters. The model predicted that the wall expansion pattern in the apical cell is not determined by a gradient of wall intrinsic mechanical properties, but instead by a gradient of wall thickness. Moreover, experimental measurements of immediate wall deformability (mainly elastic) evidenced an inverted gradient of wall deformability, opposite to that expected if this property was to control the ability of the wall to expand. While the global abundance in alginates, a major component of the wall, seems to impact the wall stiffness where the stress is high, both mannuronate and guluronate blocks appeared necessary for this function. Finally, we have demonstrated that in *Ectocarpus*, the actin filaments (AFs) are also indispensable to restrict growth at the apical tip and so in the establishment of the tubular shape in the subapical region. Fluorescent staining of AFs showed an "apical cap" under the dome, a structure common to several other groups, that seems involved in mechanically reinforcing the thin wall at the tip. These data suggest that AFs could control the wall strain pattern along the apical cell by exerting a direct mechanical influence on the wall. Overall, the results obtained during my PhD demonstrate that the biophysical mechanism of TG in *Ectocarpus* is radically different from that found in land plants and fungi. They pave the way for uncovering the molecular pathways that regulate TG in this group, and thus for future promising evo-devo studies of this particular mode of cellular morphogenesis.

Key-words: actin ; biomechanics; brown algae; cell wall; *Ectocarpus*; tip-growth